

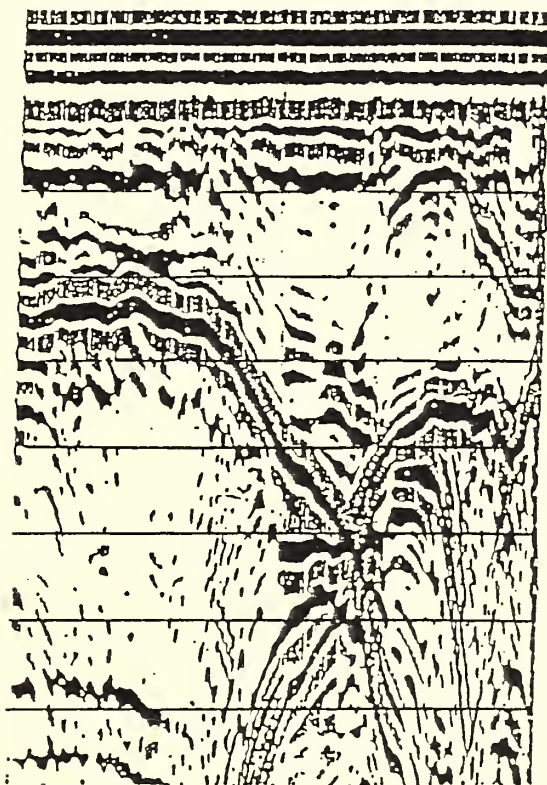
## **Historic, Archive Document**

Do not assume content reflects current scientific knowledge, policies, or practices.



aQE33  
.2  
.R33I5  
1988

# Second International Symposium on Geotechnical Applications of Ground-penetrating Radar



MARCH 6-10, 1988  
Holiday-Inn West  
Gainesville, Florida



U.S. Department of Agriculture  
Soil Conservation Service  
and  
Institute of Food and Agricultural Sciences  
University of Florida



AD-83 Bookplate  
(1-68)

NATIONAL

A  
G  
R  
I  
C  
U  
L  
T  
U  
R  
A  
L



LIBRARY



*TECHNICAL PROCEEDINGS*  
*OF THE*  
*SECOND INTERNATIONAL SYMPOSIUM*  
*ON GEOTECHNICAL APPLICATIONS OF GROUND-PENETRATING RADAR*

March 6 - 10, 1988

Holiday Inn - West

Gainesville, Florida

*Compiled by:*

Mary E. Collins  
Soil Science Dept.  
University of Florida  
Gainesville, Florida

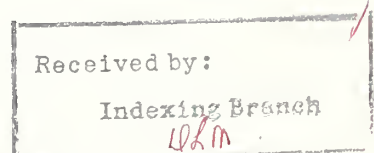
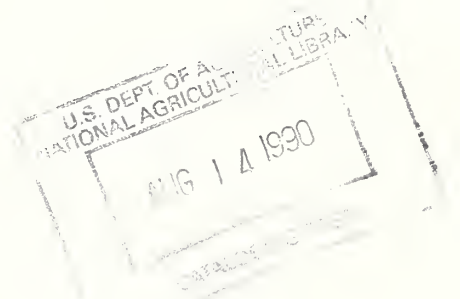
Gregg Schellentrager  
U.S.D.A. - Soil Conservation Service  
Winooski, Vermont

William E. Puckett  
U.S.D.A. - Soil Conservation Service  
Gainesville, Florida

*Sponsored by:*

Institute of Food and Agricultural Sciences  
University of Florida

U.S.D.A. - Soil Conservation Service  
Gainesville, Florida





*SYMPOSIUM PLANNING COMMITTEE*

Mary E. Collins, Ph.D.  
Associate Professor  
Soil Science Department

William E. Puckett  
GIS Coordinator  
U.S.D.A. Soil Conservation Service  
Gainesville, Florida

Gregg Schellentrager  
Assistant State Soil Scientist  
U.S.D.A. Soil Conservation Service  
Winooski, Vermont

Tony Shih, Ph.D.  
Professor  
Agricultural Engineering Department  
University of Florida  
Gainesville, Florida

Daniel Spangler, Ph.D.  
Professor  
Geology Department  
University of Florida

William Wilson  
Staff Geologist  
University of Central Florida  
Orlando, Florida



## *TABLE OF CONTENTS*

Agenda .....	v
A Geophysical Experiment to Cross-Adits Rock Investigations: Radar Tomography T. Sakayama, M. Osada and T. Kanemori .....	1
Subsurface Radar Survey of Washington Square Park, New York City: The Search for Minetta Brook J. S. Mellett, E. Karp and W. Chaisson .....	5
Electromagnetic Wave Velocity and Its Application to Civil Engineering Investigations of Soil Layers T. Sakayama, M. Osada and T. Kanemori .....	27
Propagation of Ground-Penetrating Radar Signals in Soils David V. Smith .....	31
Some Examples of Archaeological Investigations Using Ground-Penetrating Radar T. Sakayama, M. Osada and K. Tamura .....	57
Subsurface Characterization of Hazardous Waste Sites Using Ground-Penetrating Radar George Markt .....	61
Surveys of Cavities and Buried Objects by Ground-Probing Radar A. Tanaka, K. Tamura, T. Toshioka and S. Ohyo .....	111
Synthetic Aperture Processing Applied to Georadar Records T. Hara, T. Sakayama, T. Suzuki and I. Arai .....	113
Development of the Georadar System and Basic Experimentation T. Sakayama, Y. Kanezaki and T. Toshioka .....	122
Time Domain Antenna Arrays for Use in Ground-Penetrating Radar Sheldon S. Sandler .....	130
A Large Area Ground Penetrating-Radar Survey System Alan Crandall .....	139
Migration of Ground-Penetrating Radar Data: A Technique for Locating Subsurface Targets Gregory Hogan .....	164
Summary: Interpretation of Ground-Probing	

Radar: Migration Techniques D. DeBock .....	179
Ground-Penetrating Radar (GPR) Survey at Tell Halif, Israel James A. Doolittle .....	180
Airborne Surveying of Ice Covers and Water Bodies Using Short Pulse Radar K. O'Neill and S. Arcone .....	214
Investigations of the Surficial Materials of Northern Delaware C.J. Olson and J.A. Doolittle .....	255
Appendix (Abstracts) .....	257

*Agenda*  
**2nd International Symposium on Geotechnical  
Applications of Ground-Penetrating Radar  
Conference Center, Holiday Inn - West  
Gainesville, Florida U.S.A.  
March 6-10, 1988**

**Sunday, March 6th**

<b>Noon</b>	<b>Registration begins - Conference Center Lobby</b>
<b>1:30- 4:30</b>	<b>Short course:</b>  <b>Ground-Penetrating Radar: Theory and Practice</b>  Instructors:  Gary R. Olhoeft, research geophysicist, United States Geological Survey, Denver, CO.  James A. Doolittle, soil specialist (GPR), United States Soil Conservation Service, Chester, PA.
<b>6:00- 8:00</b>	<b>Poster session/reception</b>  <b>Poster #1</b>  <b>Mapping the Depth to Bedrock with Ground-Penetrating Radar.</b> J.A. Doolittle and M.E. Collins, United States Soil Conservation Service, Chester, PA and University of Florida, Gainesville, FL.  <b>Poster #2</b>  <b>Radar Signatures of Subsurface Features on Karst in West-Central Florida.</b> M.E. Collins, University of Florida, Gainesville, FL, and W.E. Puckett, G.W. Schellentrager, United States Soil Conservation Services, Gainesville, FL and Winooski, VT.

**Monday, March 7th**

<b>A.M.</b>	
<b>7:30</b>	<b>Registration continued</b>
<b>8:15</b>	<b>Opening remarks</b>  G.W. Schellentrager, assistant state soil Scientist, United States Soil Conservation Service, Winooski, VT.

James Mitchell, state conservationist, United States Soil Conservation Service, Florida.  
Dr. James Davidson, dean of research, Institute of Food and Agricultural Sciences, University of Florida, Gainesville, FL.

**ession I:**

**Geological/Hydrogeological Applications**

Moderator: Dr. S.F. Shih, University of Florida, Gainesville, FL.

- 8:40**      **Ground-Penetrating Radar Investigations of Surficial Materials in Northern Delaware.**  
C.G. Olson and J.A. Doolittle, United States Geological Survey, Reston, VA and Soil Conservation Service, Chester, PA.
- 9:00**      **A Geophysical Experiment to Cross-Adits Rock Investigation: Radar Tomography.** T. Sakayama, M. Osada and T. Kanamori, OYO Corporation, Tokyo, Japan.
- 9:20**      **A Ground-Penetrating Radar Survey of Quaternary Sediments In and Near Washington Square Park, New York, NY.** J.S. Mellett, E. Karp and R.E. Loeb, New York University, NY and Pennsylvania State University, Altoona, PA.
- 9:40**      **Using Ground-Penetrating Radar in Water Table Investigations.** S.F. Shih, D.L. Myhre, J.A. Doolittle and G.W. Schellentrager, University of Florida, Gainesville, FL and United States Soil Conservation Service, Chester, PA and Winooski, VT.
- 10:00**      **Break/discussion**
- 10:30**      **Application of Ground-Penetrating Radar in a Karst Terrain, Central Pasco County, Florida.**  
(Not Presented) D. Hearn, Michael D. Sims and Associates, Inc., Orlando, FL.
- 10:50**      **Synthetic GPR Profiles Generated by Ray-trace Analysis and Applications for Interpreting Karst Features.** B.F. Beck and W.L. Wilson, Florida Sinkhole Research Institute, University of Central Florida, Orlando, FL.
- 11:10**      **Capabilities of Ground-Penetrating Radar for Studying Sinkhole Cavities in Florida.** S.S. Kuo, University of Central Florida, Orlando, FL.
- 11:30**      **Lunch**



## **Session II:**

### **Soils Investigations**

Moderator: Dr. Mary E. Collins, University of Florida, Gainesville, FL.

**P.M.  
1:00**

**Electromagnetic Wave Velocity and Its Application to Civil Engineering Investigations of Soil Layers.** (Not Presented) T. Sakayama, M. Osada, T. Kanamori and S. Ohya, OYO Corporation, Tokyo, Japan and U.S.A.

**1:20**

**Propagation of Ground-Penetrating Radar Signals in Soils.** D.V. Smith, Geo-Centers Inc., Newton Centre, MA.

**1:40**

**Application of Ground-Penetrating Radar to Coastal Plain Soils with Variable Texture and Clay Mineralogy.** R.K. Hubbard, L.E. Anderson H.F. Perkins and H.L. Allison, United States Agricultural Research Service, Tifton, GA.

**2:00**

**Sampling Design for Ground-Penetrating Radar Application.** S.F. Shih, J.A. Doolittle and G.W. Schellentrager, University of Florida, Gainesville, FL and United States Soil Conservation Service, Chester, PA and Winooski, VT.

**2:20**

**Break/discussion**

**2:40**

**A Comparison of Two Geophysical Techniques for Soils Investigations in Steep Terrain.** C.G. Olson, United States Geological Survey, Reston, VA.

**3:00**

**Comparison of Subsurface Cavity Investigations Using Ground-Penetrating Radar, Electric Resistivity and Seismograph.** D. Filler and S.S. Kuo, University of Central Florida, Orlando, FL.

**3:20**

**Ground-Penetrating Radar Applications in Northeastern Palm Beach County, Florida.** G.M. Russell, W.L. Miller and C.J. Peterson, United States Geological Survey, Stuart, FL.

**3:40**

**Applications of Ground-Penetrating Radar to Soil Variability Investigations in a Citrus Grove.** D.L. Myhre, S.F. Shih, and S.T. Ploetz, University of Florida, Gainesville, FL and Soil Conservation Service, Sebring, FL.

- 4:00      **Application of Ground-Penetrating Radar to Archaeological Studies.** J.A. Doolittle, United States Soil Conservation Service, Chester, PA.
- 4:20      **Some Examples of Archaeological Investigations Using Ground-Probing Radar.** T. Sakayama, M. Osada, and K. Tamura, OYO Corporation, Tokyo, Japan.
- 4:40      **Application of GPR at the Solar Boat Chamber, Pyramid of Cheops, Giza, Egypt.** T. Fenner, M. Blackey, and V.J. Murphy, Geophysical Survey Systems, Inc., Hudson, NH and Weston Geophysics, Westboro, MA.

**Tuesday, March 8th**

**A.M.  
7:30**

**Registration continues**

**Session III**

**Environmental Damage Assessment**

Moderator: James A. Doolittle, United States Soil Conservation Service, Chester, PA.

- 8:30      **Use of Ground-Penetrating Radar Techniques to Aid in Site Selection for Land Application Sites.** H.G. Strangland and S.S. Kuo, Ardaman and Associates, Inc., and University of Central Florida, Orlando, FL.
- 8:50      **Subsurface Characterization of Hazardous Waste Sites Using Ground-Penetrating Radar.** G. Markt, Geo-Centers, Inc., Newton Centre, MA.
- 9:10      **Surveys of Cavities and Buried Objects by Ground-probing Radar.** A. Tanaka, K. Tamura, and S. Ohyo, OYO Corporation, Tokyo, Japan and U.S.A.
- 9:30      **Break/discussion**
- 9:50      **A Rapid Evaluation of Concrete Pavements Using Ground-Penetrating Radar.** S.S. Kuo, University of Central Florida, Orlando, FL.
- 10:10      **Ground-Penetrating Radar Investigations in the Tri-State Mining District, Kansas. (Not Presented)** R Lahti and P. Hoekstra, Blackhawk Geosciences, Inc., Golden, CO.

**10:50**            **Detection and Stabilization of Potential Sinkhole Sites at a Landfill in Alachua County, Florida.** W.L. Wilson, Florida Sinkhole Research Institute, University of Central Florida, Orlando, FL.

**11:10**            **Airborne Subsurface Exploration and Detection of Thin Layers Using Short Pulse Radar.** K. O'Neill, S. Arcone, Cold Regions Research and Engineering Laboratory, Hanover, NH.

**11:30**            **Lunch**

**Session IV:**

**New Techniques, Applications, and Equipment**  
Moderator: Dr. Carolyn G. Olson, United States Geological Survey, Reston, VA.

**P.M.**  
**1:00**

**Applications and Limitations of Computer-processed Ground-Penetrating Radar Data.** G.R. Olhoeft, United States Geological Survey, Denver, CO.

**1:20**            **Synthetic Aperture Processing Applied to Georadar Records.** (Not Presented) T. Sakayama, T. Suzuki, and I. Arai, OYO Corporation, Tokyo, Japan.

**1:40**            **Development of the Georadar System and Basic Experimentation.** T Sakayama, Y. Kanezaki, and T. Toshioka, OYO Corporation, Tokyo, Japan.

**2:00**            **A Large Area Ground-Penetrating Radar Survey System.** A. Crandall, Geo-Centers, Inc., Newton Centre, MA.

**2:20**            **Break/discussion**

**2:40**            **Time Domain Antenna Arrays for Use in Ground-Penetrating Radar.** S.S. Sandler, Geo-Centers, Newton Centre, MA.

**3:00**            **Migration of Ground-Penetrating Radar Data: A Technique for Locating Subsurface Targets; and, Real Time Kirchhoff Migration of Ground-Penetrating Radar Data.** G. Hogan and J. MacArthur, Geo-Centers, Newton Centre, MA.

**3:40**            **Variability of Radar Velocity in a Plio-Pleistocene Dune Sand, Polk County, Florida.** W.L. Wilson, Florida Sinkhole Research Institute, University of Central Florida, Orlando, FL.

**4:00**            **Interpretation of Ground-Probing Radar:  
Migration Techniques.** D. DeBock, Bles, Inc.,  
Belgium.

**6:30-9:30**        **Social and Gala Banquet**  
Keynote speaker: George E. Mosakowski  
Manager of Commercial Programs, NASA  
Kennedy Space Center, FL.

**Wednesday, March 9th**

**A.M.**  
**7:30**            **Field Trip: Ground-Penetrating Radar  
Applications in Florida.**

**Tour Guides:**

William Puckett, soil scientist, University of  
Florida, Gainesville, Florida.

Dr. Mary E. Collins, associate professor of  
soil science, University of Florida,  
Gainesville, Florida.

Dr. Dan Spangler, associate professor of  
geology, University of Florida, Gainesville,  
Florida.

James A. Doolittle, soil specialist (GPR),  
United States Soil Conservation Service,  
Chester, Pennsylvania.

William Wilson, staff geologist, Florida  
Sinkhole Research Institute, University of  
Central Florida, Orlando, Florida.

**5:00**            **Return**

**Thursday, March 10th**

**A.M.**  
**8:30**            **Session V:**

**Round Table Forum**

Moderator: Gregg W. Schellentrager, United  
States Soil Conservation Service, Winooski, VT.

General topics to discuss:

1. GPR and ground-truthing: how much is  
enough?
2. GPR: skepticism in the community!
3. GPR: where do we go from here?
4. General question/answer period

<b>10:30</b>	<b>Break/discussion</b>
<b>11:00</b>	<b>Group discussion on future activities</b>
<b>12:00</b>	<b>Adjourn</b>



# A Geophysical Experiment to Cross-Adits Rock Investigation; Radar Tomography

Toshihiko Sakayama, Masaki Osada,  
(Geotechnical Institute, OYO Corp.  
Japan)

Takashi Kanemori  
(OYO Corporation, USA)

## 1. INTRODUCTION

It is known that electromagnetic(EM) waves are generally reflected by boundaries of different dielectric constants. EM waves used in exploration are usually of very high frequencies, in the tens or hundreds of MHz, and having wavelengths from tens centimeters to a few meters, making it possible to explore in detail the structure of the ground.

Research and development of radar technique are being conducted, with hopes of realizing this effectiveness in highly resistive rock ground, to determine boundaries of rock facies, faults, fracture zones, etc. Radar tomography is one of the new geotomography techniques. There are three types of radar tomography techniques from the viewpoints of data used and analyzing technique (Lager and Lytle, 1983; Olsson et al., 1987) :

- 1) Reconstructing the distribution of EM wave velocities using first arrival times.
- 2) Reconstructing the distribution of attenuation parameters using amplitudes of received waveforms.
- 3) Reconstructing the image of reflection boundaries and scattering sources using reflection and diffraction phases in the radar records.

This paper presents the third type. It discusses problems involved with the applicability and describes the results of certain numerical and practical experiments.

## 2. NUMERICAL EXPERIMENTS

### (1) Ability of Detection of Faults

Let's explain the results of numerical experiments conducted for estimation of the ability of detecting faults in radar tomography. In the numerical experiments, following situations were assumed:

- a. Two test adits of A and B, both 40 m long and 25 m apart from each other, were parallelly excavated in the granite area. There exist faults 50 cm thick within two test adits, in distribution patterns of case 1 to case 3, shown in Fig.1.
- b. Two measuring patterns were considered: one transmitter of EM waves was placed in test adit "A", while one receiver moved along the same adit (in-line measurement). One transmitter was placed at the same point in test adit "A", while one receiver moved along the test adit "B" (cross adit measurement).

EM waveforms, shown in Fig.1, were simulated for the above two measuring patterns and for the three distribution patterns of fault. The ray tracing method involving paraxial ray approximation was conducted to simulate the EM



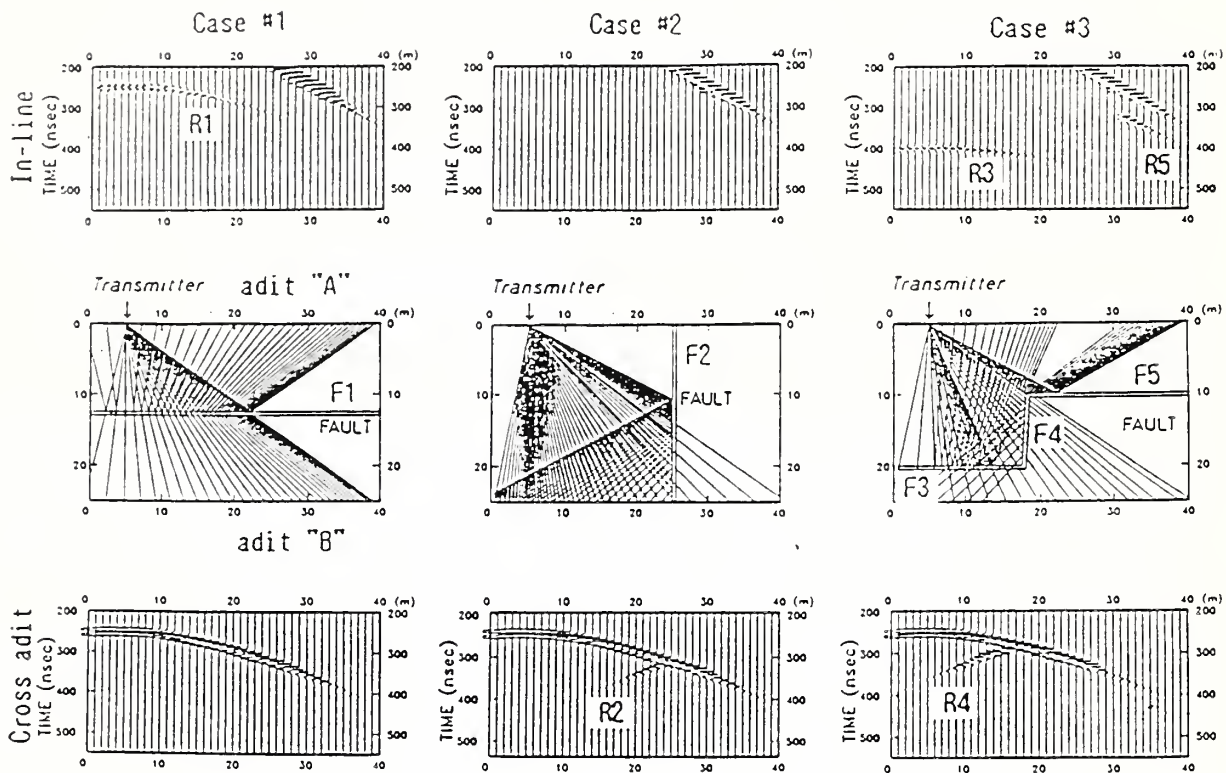


Fig.1 Theoretical Waveforms and Patterns

waveforms. Table 1 shows the physical parameters of granite and the fault, used to simulate the waveforms.

For the faults parallel to the test adits ( F1, F3 and F5 ), the reflection phases from them were appeared only in in-line records ( R1, R3 and R5 ). On the other hand, the reflection phases ( R2 and R4 ) from the faults perpendicular to the test adits ( F2 and F4 ), were appeared only in cross adit records. These results show that the combination of in-line and cross adit measurements is very important in radar tomography to obtain the accurate and detailed distribution image of faults in the objective area. The sloping phases, as seen on the upper right in in-line records, are the direct waves.

Table.1

Physical parameters  
of numerical models

	granite	fault
dielectric constant	9	18
resistivity (ohm-m)	2000	500
EM wave velocity (cm/ns)	10	7
attenuation coefficient	0.03	0.10

## (2) Reconstruction Capability for Faults

Here, the calculated waveforms mentioned above are hypothesized as measured data, to which we tried to apply reconstruction processing. The method of reconstruction processing applied is the wave front migration method.

Fig.2 shows the results of reconstruction. In each case #1 to #3, it can



be said that the characteristic patterns of the faults in the original models were successfully reconstructed, especially in places where reflection points are densely distributed.

However, there are some elliptical artifacts on some places, in the reconstructed profiles. It is considered that these artifacts were generated, because only a few records obtained by one transmitting point, were put into the reconstruction processing. If much more records, obtained by many transmitting points surrounding the objective area, were put into the analysis, this phenomenon could be avoided.

### 3. FIELD EXPERIMENTS

An example of radar tomography conducted in a sandstone area is shown in Fig.3, which is the result of migration processing. The two adits intersected at a 90 deg. angle. One transmitting point was set in one adit and six receiving points were set at 1 m intervals in another adit.

In the reconstructed profile, some continuous phases appear and the comparatively clear phases, denoted by a and b, are considered to be reflection surfaces compared with the geological information of test adits. And furthermore, there are many elliptical migration noises, those are artifacts, produced through processing. We think that it should be possible to hold them down by increasing the number of transmitting and receiving points. The capability of radar tomography to reconstruct the image of faults are explained as follows.

Faults sometimes cannot be detected, depending on their locations or the placement of measuring points. In order to correctly reconstruct underground structures, reflection points should be distributed as densely as possible. Thus, a number of measurements are necessary, and processing should be conducted using all data.

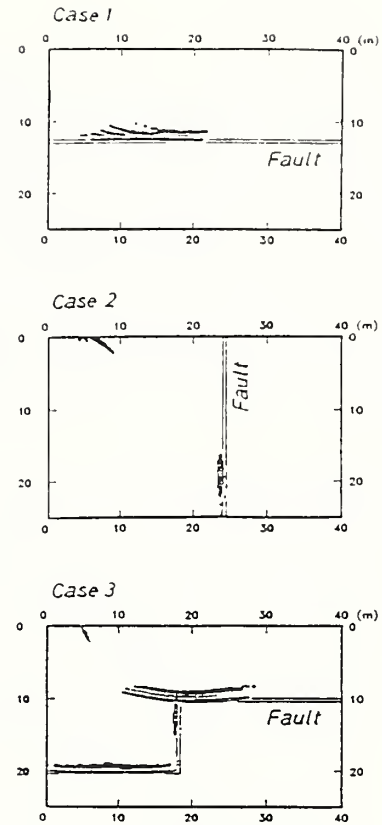


Fig.2 Results of reconstruction

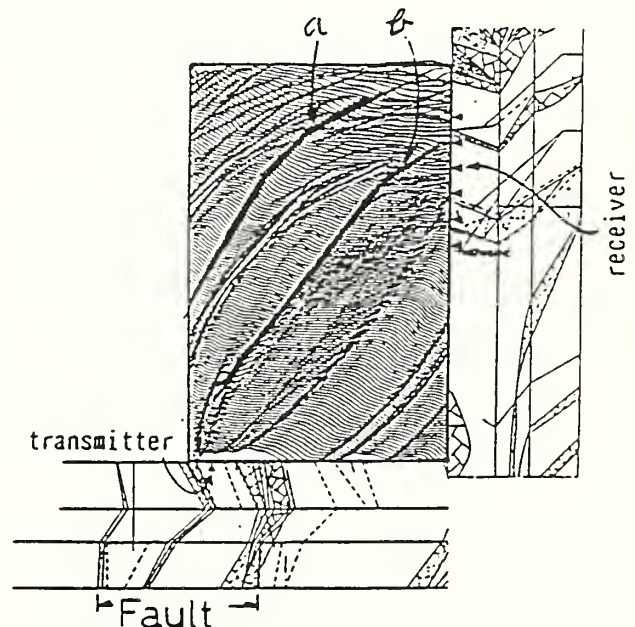


Fig.3 Example of field experiments

#### 4. AFTERWORD

This paper has described of radar tomography technique. The advantages and problems of this technique are summarized as follows. The wavelengths of EM waves used in radar tomography are very short, compared to the elastic waves used in seismic tomography. Consequently, radar tomography should theoretically give higher resolution, and should be suited for obtaining the underground structure in detail. However, there are limitations to the propagation distance of EM waves, especially in ground of low resistivity. The major area for further research of radar tomography is expansion of the range in which exploration is possible. For this purpose, development of radar system with high power and high sensitivity, is necessary.

#### REFERENCES

- Ben-Menahem, A. and W.B. Beydoun, Range of validity of seismic rays and beam methods in general inhomogeneous media - I. General theory, Geophys. J. R. astr. Soc., 82, 1985.
- Daily, W.D. and R.J. Lytle, Geophysical Tomography, J. Geomag. Geoelectr., 35, 423-442, 1983.
- Olsson, O et al., Crosshole Investigation - Results from Borehole Radar Investigations, SKB, Stockholm, Sweden, 1987.

SUBSURFACE RADAR SURVEY OF WASHINGTON SQUARE PARK,  
NEW YORK CITY: THE SEARCH FOR MINETTA BROOK  
James S. MELLETT, Edwin KARP, and William CHAISSON.  
Department of Biology, New York University, New York,  
NY 10003.

#### ABSTRACT

A ground-penetrating radar survey was carried out in a portion of Washington Square Park in New York City in order to (a) trace the subsurface extent of Quaternary stratigraphic units that had been uncovered in nearby building excavations, and (b) locate the former course of Minetta Brook, a stream that flowed through the Park until the early to mid nineteenth century. Penetration depth of an 80 MHz antenna was minimal, attaining depths of only a few meters, with very little resolution. Neither the Quaternary sediments nor the former ground surface around the brook was determined, but distinct targets, interpreted to be old culverts, were mapped. Severe attenuation of radar signal was assumed to be the result of road salt deicing, a saline ground water table, and visitation of the park by domestic dogs.

#### INTRODUCTION

Any geologist attempting to do geomorphology or stratigraphy in heavily developed urban areas lacks the fundamental data base of having outcrops available. This is especially true in downtown New York City, which has had a long history of human intervention in the landscape.

From 1797-1825, part of Washington Square Park was a Potter's Field. Once burials had stopped, the field was to be filled up and leveled. In 1826, what had been the Potter's Field was named the Washington Military Parade Ground, and proposals were made to enlarge the parade ground to the present size of Washington Square Park. By 1828, the Potter's Field had been leveled and the area was now called Washington Square (Still, MS a, b; Minutes of the NYC Common Council, 1917).

This paper describes an attempt to: (1) trace in the subsurface Quaternary stratigraphic units located in nearby building excavations; (2) determine the configuration of the former ground surface under a portion of Washington Square Park, and (3) to locate the actual course of Minetta Brook through the park, using ground-penetrating radar.

#### GROUND TRUTH FROM BORINGS AND EXCAVATIONS

Current elevations in the paved areas of the region of the Park we surveyed run from 25 to 28 feet above mean sea level. (The datum on the New York City Parks Department map is based on a datum plane 2.75 feet above mean sea level at Sandy Hook, NJ).

A number of boring records and direct excavation data (see Appendix) were examined for the area across the street, to the south of the radar survey area. Ground water elevations, bedrock elevations, and subsurface materials

were noted. All elevations are reported here with respect to the USCGS mean sea level datum at Sandy Hook, New Jersey.

Ground water data spanning some 40 years indicate an inferred, approximate elevation range for observed ground water levels of 3 to 10 feet above mean sea level.

The bedrock elevations range from 13 to 34 feet below MSL. Where reported, the bedrock was schist or quartzite. The subsurface materials above bedrock range from gravels, to sands, silts, and clays; organic material also occurs.

In an excavation for an underground university library in 1984, just across the street, to the south of the radar survey, sands, silts, clays and organic materials were sampled. The organic-bearing sediments were observed between 1 and 8 feet above MSL. Radiocarbon dating of some of the organic sediments yielded ages of about 13,000 years BP. These are the first inland, and also the oldest radiocarbon dates reported for Manhattan Island (Karp and Loeb, 1986). Harris and Pipes (MS) noted organic sediments in boring logs of the same general area, and Pickman and Rockman (MS) suggested a possible marsh environment for some sediments observed in their boring records. Only two borings have been done within Washington Square Park itself (Berkey and Fluhr, 1934). One boring about 340 feet northeast of our radar survey consists of sand down to about 2 feet below



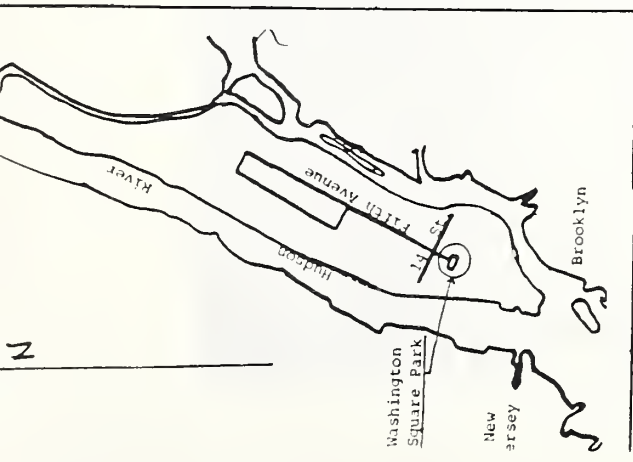
sea level; another, 520 feet to the east consisted of gravel, sand, and clay down to 6 feet below MSL.

#### MINETTA BROOK

According to historical records (Randel, 1811, Longworth, 1817, Pror and Dunning, 1817), the Minetta Brook stream channel entered the park at the north end, and flowed southwest across the park to the level of MacDougal Street and Washington Square South (West 4th Street). From there it continued in a southwesterly direction to eventually drain into a swamp on the Hudson River. The brook appeared on city maps as early as 1639, but as the surrounding area was settled, portions of the stream began to be filled, and by 1817, it had begun to disappear from maps of Greenwich Village. By 1831, no surface trace of it was mappable, and it had simply disappeared, a casualty of urbanization. Our transects (Fig. 1) were run across the axis of the brook, as shown on some of these earlier maps, in an attempt to locate the stream channel, and map the surrounding subsurface former topography.

#### RUNNING THE SURVEY

The ground-penetrating radar survey was carried out with a Geophysical Survey Systems model 3112 80 megahertz antenna, which was leased from John Fett of Austin Texas. Weather was clear on the day of the survey (13 Nov 87), with



West 4th St.

MacDougal

Washington Sq. South

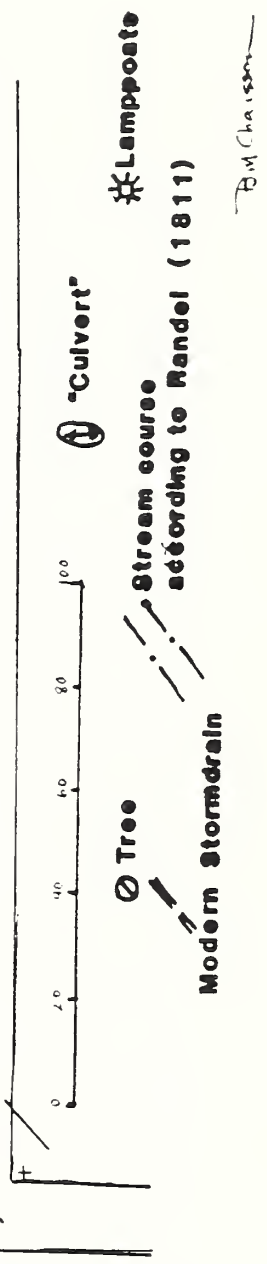
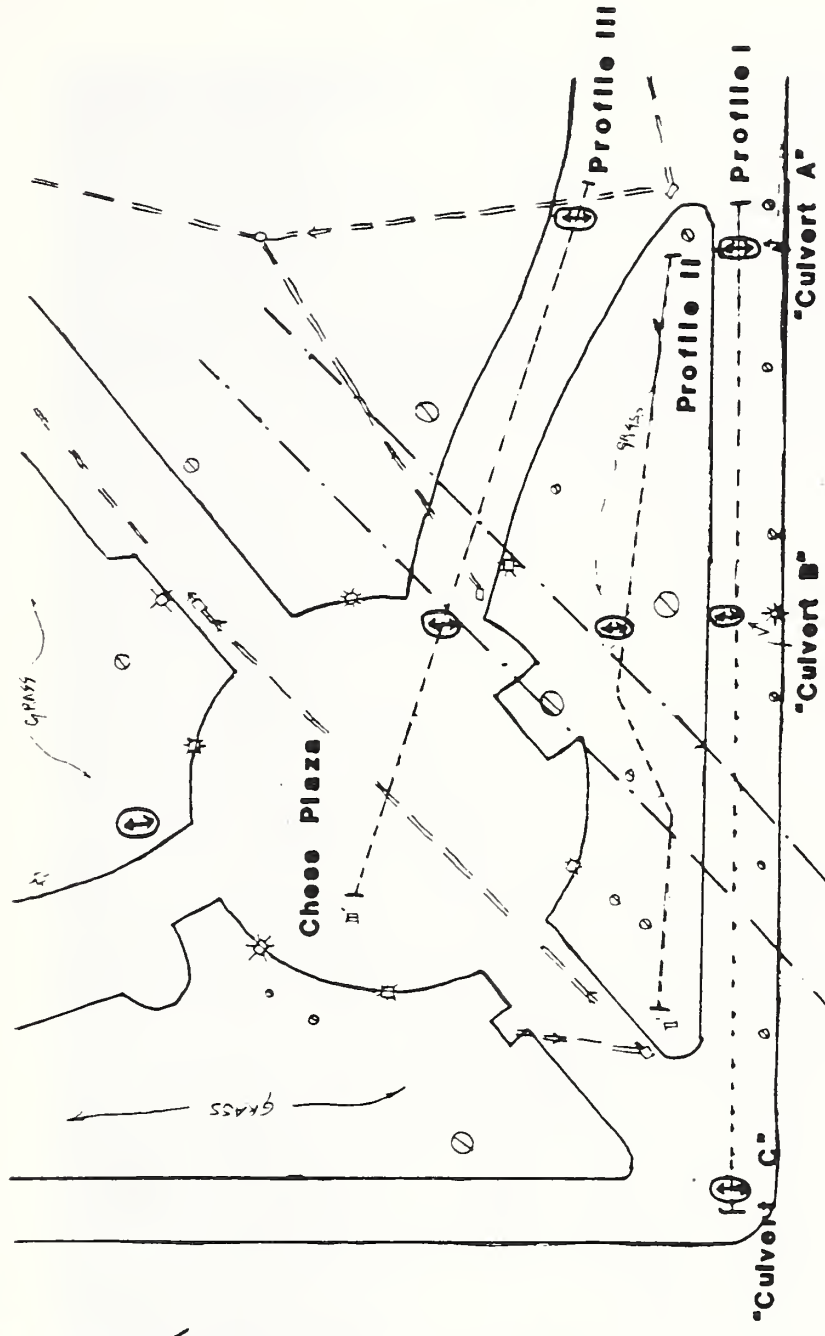


Fig. 1 Map of Survey Area

B. J. Harrison

an ambient temperature of 50 degrees F (10°C). Three days prior to the survey, New York City received a snow and ice storm, and all the paths and walkways in the park were heavily salted. Large patches of rock salt (NaCl) were visible as we ran the antenna over the surface.

A series of transects were run with ranges as high as 500 nanoseconds in an approximate east-west direction, parallel to West 4th Street. Other runs were made on grassy areas, as well as bituminous paved portions, across the presumed axis of Minetta Brook. Surprisingly, penetration depth over the paved portions of the park appeared to be about the same as those run on grassy parts.

When runs were made with a 300 MHz antenna (GSSI model 3105), the return signal petered out at a depth of 28 ns, in strong contrast to runs made with this antenna in, say, sands and gravels in southern Vermont, where the return echo would have run clear off the page. It was obvious that here in the park, something was seriously impeding the penetration depth of the signal.

The first runs (Profile I, Fig. 2) were made at the south boundary of the park on the bituminous walk parallel to Washington Square South. Three subsurface targets



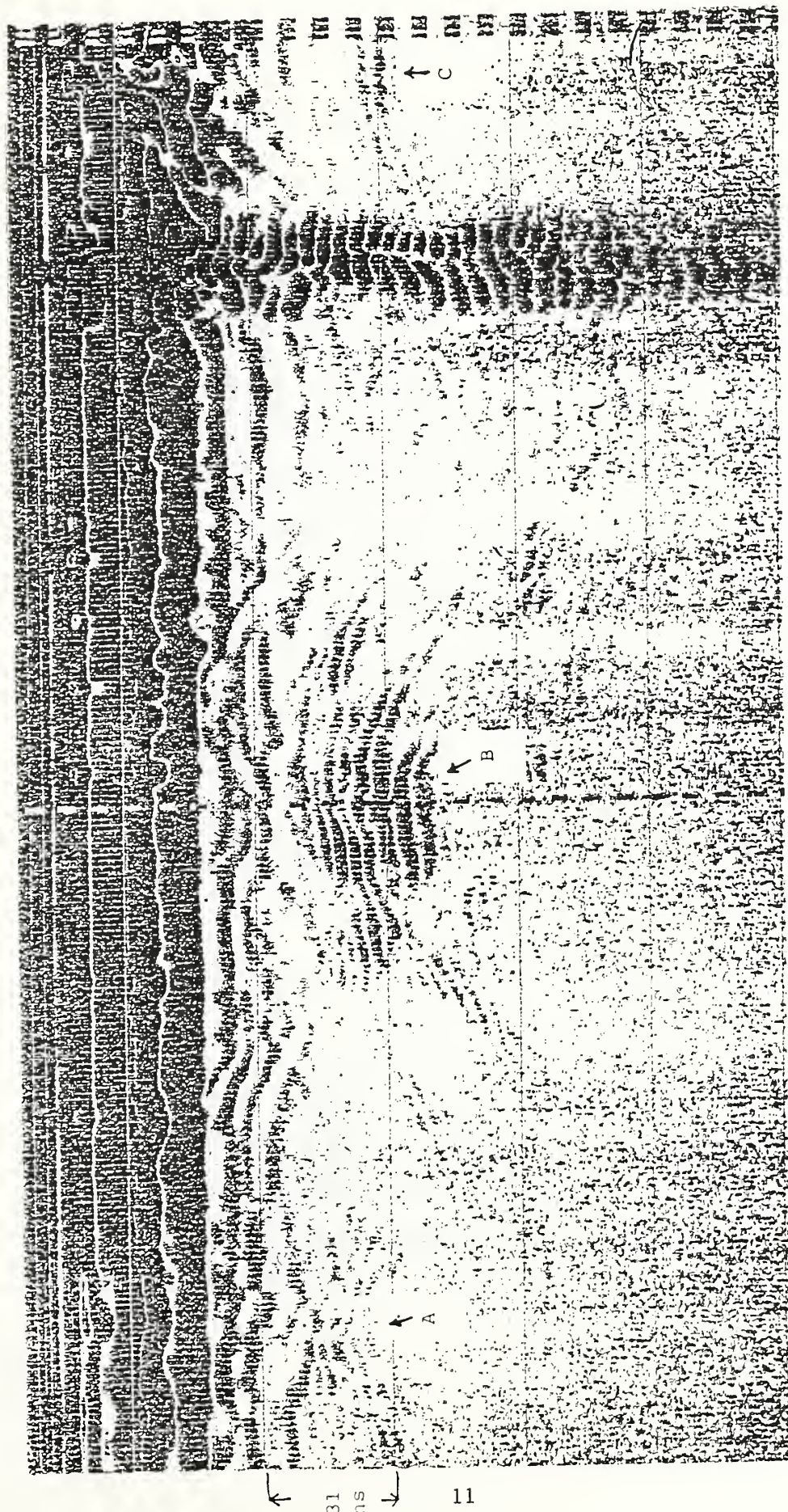


Fig. 2 Radar scan along Profile I (on pavement). 80 MHz, 300ns

Width of section: 190 ft.

Arrows indicate "culvert" targets

were seen here at depths ranging from 77 to 80 ns (The strong vertical echo at the right side of the scan is a reflection from a steel manhole cover). A second series of runs (Profile II, Fig. 3) were made on a grassy area parallel to the first profile. Although recorded penetration depth was slightly better than that on the bituminous strip, it still reached only about about 80 ns deep. One faint hyperbolic echo was seen here.

The third series (Profile III, Fig. 4) were made on a paved area at an oblique angle to the first two, in an approximate NW-SE orientation, extending along the path toward the chess plaza. A series of targets seen as hyperbolic echoes were visible here also. Subsequent runs were made wherever a space was available to tow the antenna. Some runs could not be extended because of benches, chess tables, trees, and topographic obstructions.

#### INTERPRETATION:

Before any conclusions could be drawn about what the targets were, one first must exclude artifacts that might result from overhead targets reflecting back radar waves to an unshielded antenna. Fortunately, the Parks Department map (Finley, 1981) provides detailed locations of lamp posts, and the location, size and species of every tree. We noted the location and height of all overhead branches and obstructions along the runs, as well as the position of all



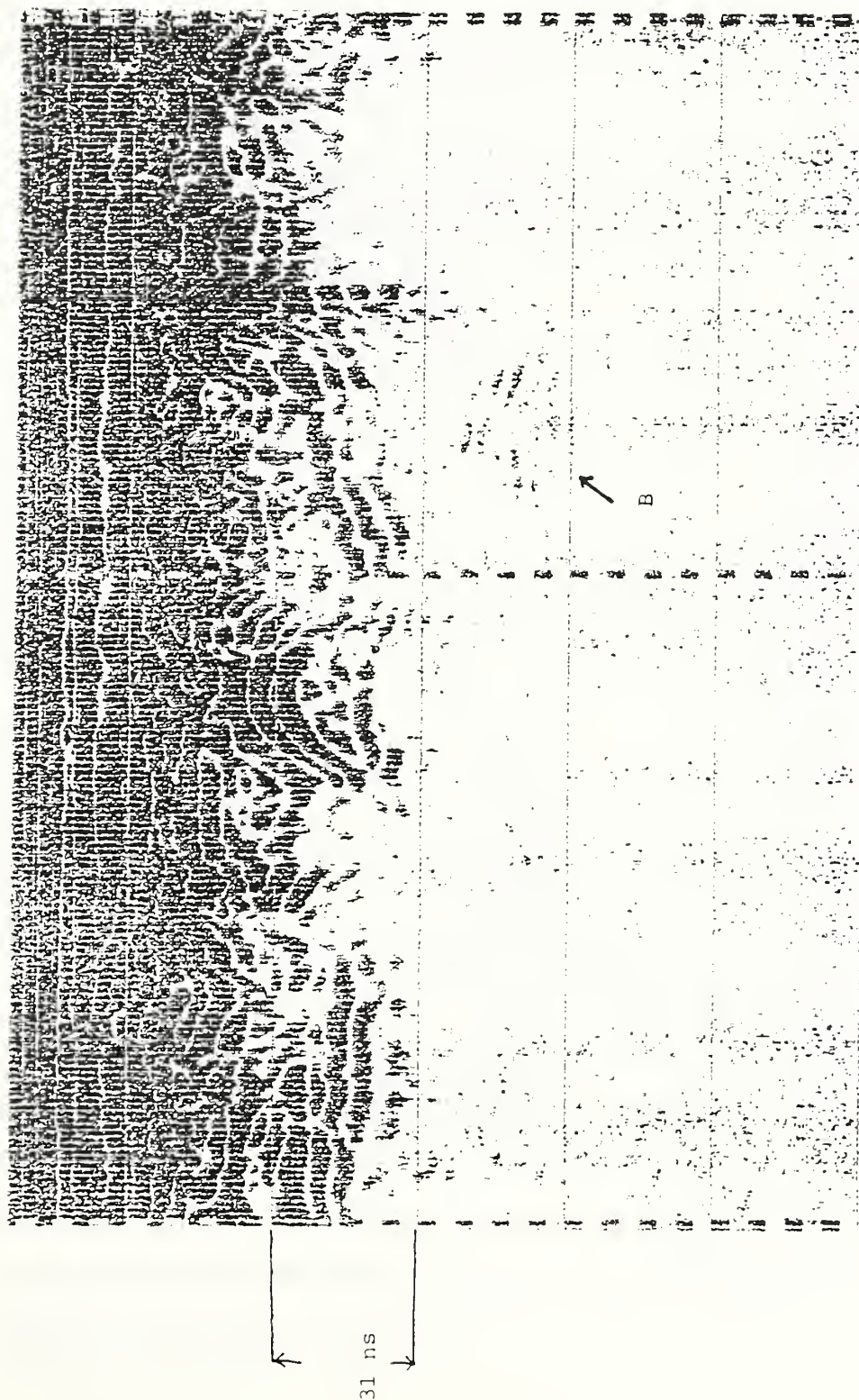


Fig. 3 Radar scan along Profile II  
(on grass). 80 MHz, 300 ns

Width of section: 150 ft.

Arrows indicate "culvert"  
targets.

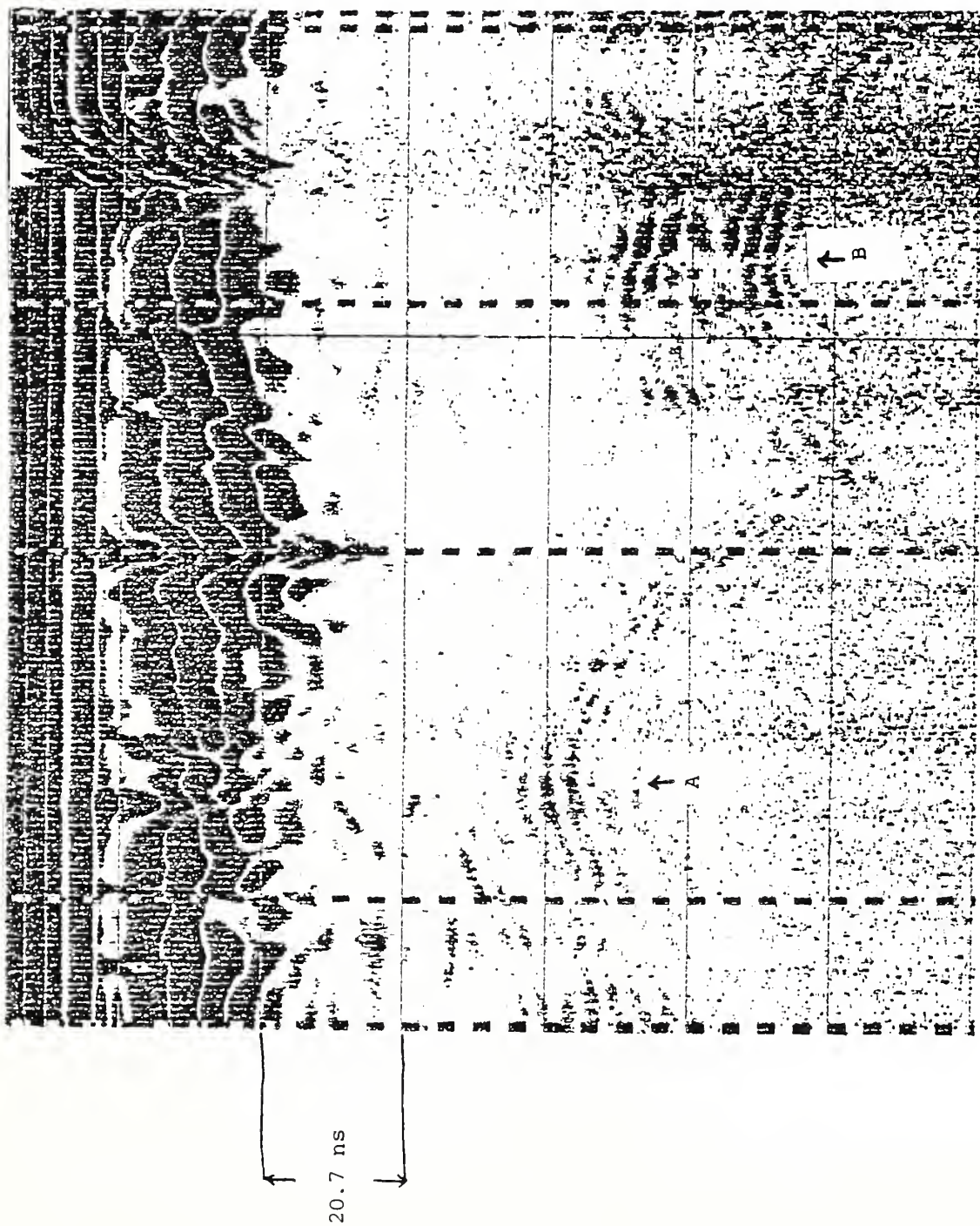


Fig. 4 Radar scan along Profile III  
(on pavement). 80MHz, 200ns

Width of Section: 145 ft.  
Arrows indicate "culvert" targets.

underground utilities. Analysis of the recorded strips showed no unequivocal correlation between the radar echoes and small or large branches. One possible correlation occurred near a tree and lamp post on runs 1 and 2, although the light itself extended over the street, and not on the sidewalk where the transect was run. The lamp post's horizontal limb was about 35 feet (70 ns) away, and the overhead tree branches, which extended from the trunk at an acute angle skyward, were 33 feet above the antenna, or 66 ns away. The targets seen on the strip were too strong to be tree branches, and these targets appeared where there were no overhead branches at all. Organic material such as wood at that distance would have a "soft", or diffuse radar echo, and would not appear as strongly as the echoes seen in runs 2-5.

All of these transects were run over the presumed course of Minetta Brook. We at first thought that we had seen some of the actual old ground surface, with these convex upward echoes presumed to be part of the clay in the B horizon of soils. We were about to prepare maps showing the presumed drainage divides and stream channels in the area around 1750, but something was amiss. One problem with the echoes is that they are too smooth and regular. In addition, where the actual locus of the stream channel was presumed to be, the echoes cross one another; they are not smoothly continuous (Fig. 4).



The radar signals suggest distinct, smoothly curved targets, much like the echoes obtained from pipes underground, rather than a continuous horizon. We now feel that these may be culverts that were installed some time in the 19th century to help drain the brook, and reduce flooding in nearby basements. The Common Council minutes of New York City (1917) are instructive here, and we quote two discussions relevant to our study.

"...on the 23d August last an ordinance was passed directing a culvert to be built in Amity Street to communicate with the Sewer intended to be built in the 6th Avenue so as to carry off the Minetta water; but in consequence of the proprietors of property between Amity and 4th streets filling up their low grounds the Committee [159] on that subject have directed the culvert to be built in 4th street." (13 March 1820, p. 19).

"Resolved that the Superintendant (sic) of Repairs construct and place a trunk of Timber and plank of sufficient dimensions to convey the waters of the Minetto (sic) brook from the present tunnel at Fourth St. until it shall intersect the Fifth Avenue at Sixth street..." (20 Dec 1824, p. 219).

We ran our survey along 4th street; the intersection of Fifth Avenue and Sixth Street (Now Waverly Place) is northeast of our survey, at the north entrance to the park.

We show the location and presumed orientation of the conduits in Figs. 1 and 5. They do not parallel the presumed course of Minetta Brook as ascertained from a consensus of historic records (Randel, 1811), and we believe these culverts may have been placed to drain a swamp that the brook flowed through in the western half of the park, on the Peter Warren farm. Unfortunately, we were unable to actually see the former ground surface, or the Quaternary sediments we were originally looking for.

We were able to determine the dielectric properties of the near subsurface material in a series of runs made with a 300 MHz antenna over a drain pipe of known depth. Round trip pulse velocities were estimated to be 6.8 ns/ft. Applying that to the culvert targets, we obtain depths of 10 to 13 feet under the ground surface (Fig. 5), well below the depth of known water mains and electric utilities in the region, as shown on the Parks Department maps.

One unanswered question was why we obtained such poor penetration depth with both the 80 MHz and 300 MHz antennas. An obvious answer was the rock salt used on the pavement after the snow storm. Although halite crystals will transmit radar waves, as soon as water enters the picture, the salt ionizes and becomes highly conductive, and most of the incident radar energy is reflected or absorbed by a thin highly conductive layer (Ulriksen, 1982, p. 82). The second answer has a historical component. The entire

20'

Elevation  
in feet

24

23

22

21

20

19

18

17

16

15

14

13

12

11

10

9

8

7

6

5

4

3

2

1

0 2.75' above mean sea level

0 20

— mean sea level —

"CULVERT A"

"CULVERT B"

"CULVERT C"

This is an inferred approximate elevation range for nearby observed ground-water levels outside the radar survey area.

40 60 80 100 120 140 160 180

Fig. 5 "Culvert" locations along Profile I showing relationship between targets and water table.



southern part of Manhattan Island is underlain by highly permeable sands and gravels, which were exploited for domestic and commercial water use as early as the 17th century. The sands and gravels are hydraulically connected to the Hudson and East Rivers, which are estuarine, and contain brackish water. As groundwater was pumped out, and as the recharge area of the city was paved over, more brackish water was taken into the aquifers, contaminating them with salt. By the early 1900's, all the wells in lower Manhattan were brackish and many were abandoned as drinking water sources (Geraghty, 1959).

We were able to obtain a water sample from a sump in a nearby building (Vanderbilt Hall), where the top of the saturated zone was at an elevation of about 18 feet below the street level, or 7 feet above mean sea level. Water in the sump flowed continuously at a light trickle, and the elevation of 7 feet at the top of the saturated zone falls within the range of groundwater elevations obtained in nearby construction sites (3-10 feet above MSL). The assay (Table 1), which was provided for us by the New York City Department of Environmental Protection Bureau of Water Supply Central Laboratory, showed high chlorinity levels. Normal freshwater chloride levels run about 10 ppm in the New York City watershed areas; here they were 300 ppm, suggesting rock salt contamination, or brackish water influx from the nearby rivers (Chlorinity of seawater is 19,000

ppm, Weast et al, 1986). Specific conductance, which is a measure of all of the ions in the water, was also quite high, and is directly relevant to the attenuation of the radar signals. Groundwater is still used in the area for cooling boilers and air conditioning units, so there continues to be a constant, but small demand for the water, and with reduced recharge areas, the chance for replacement of the brackish groundwater by fresh water is slight or non-existent.

The elevated alkalinity and hardness levels of the water sample compared to reservoir water may be the result of leaching of  $\text{CaCO}_3$  from the concrete. Occasionally,  $\text{CaCl}$  is added to concrete when it may be exposed to freezing temperatures after pouring to hasten curing (Neville, 1981), and it is possible that some of the elevated chloride level might result from leaching from the concrete. We doubt that this is the source of the elevated chlorides, but do not have any information on the composition of the concrete. Generally, floor slabs with reinforcing bars are not doped with  $\text{CaCl}$ .

In interpreting the assay, we had to discount that the water in the sump, which was flowing continually, might represent either a broken water main, or a leaking sanitary sewer line. New York City's drinking water is fluoridated, and if a leak is suspected, the City looks for fluoride in any samples. Leaks from sewer lines would have very high

fecal coliform counts, and high levels of ammonia. Our assay showed very little fluorine (although the fluoridating system on one of the reservoir sources had been down for a week or so before our survey), and yielded an almost a zero fecal bacterial count, with no trace of the microscopic organisms that are endemic in the New York City water system (Any organisms may have been filtered out by the subsoil, however). Although not conclusive, these values are consistent with our interpretation that the water we assayed is an actual sample of ground water, and not an artifact of leaking pipes.

The third element that might account for the diminished penetration of the radar waves may be the result of having a little green oasis in a large urban paved desert. One puzzling question noted earlier was why the soil did not allow radar wave penetration to any great depth, compared to the bituminous paved areas. The grassy portions of the park are not salted after snowstorms, although some rock salt may leach into the grassy regions after being dissolved in rain and soaking into the soil. But we must not forget that hundreds of dogs visit the park every day, and a little calculation demonstrates that thousands of liters of urine are deposited on the grass in every corner of the park every week adding sodium, P, N, and chloride ions. Much of the P and N would be taken up by the vegetation in the park, but other salts would remain in the soil to attenuate the energy of the radar waves.

## ACKNOWLEDGEMENTS

Thanks go to the New York University Central Administration for their support and encouragement of this project, particularly to Mssrs. Ed Bruno, Bob Rapp, Gaston Grajo, and W. Fields. Prof. Bert Salwen of the Department of Anthropology generously provided us with information collected by his students in an ongoing study of urban archaeology, and Prof. Bayrd Still and Tom Frusciano of the NYU Archives provided a great deal of accurate historical information. We thank Prof. Irving Brick, chairman of the Department of Biology for providing support for the antenna rental, to Mr. Melvin Weil and Mr. Thomas Bisogno of Subsurface Consulting, Ltd. for providing the loan of the surveying equipment. Mr. Mike Greenman and Mr. Anthony Assande of the New York City Department of General Services provided much information on borings in the Greenwich Village area, and Mr. L. Stern, of Geo-Tech Associates aided in our subsurface interpretations of boring records. We also thank the New York City Parks Department, especially Mr. Patrick Pomposello, Borough Commissioner for Manhattan for giving us permission to carry out the Park survey, and the New York City DEP Board of Water Supply for an assay of the water sample, especially Ms. Eva Chen, Dr. G. Iwan and Mr. J. Dalton. Prof. Robert E. Loeb of Penn State University made helpful comments on the first draft of this report.

## REFERENCES

Berkey, C. P. and W. Fluhr (1934) "Rock data map of Manhattan". Vol. 1, sheet 26. Civil Works Administration, Project 114.

City of New York (1917) "Minutes of the Common Council of the City of New York (1784-1831)".

Finley, E. W. (1981) "Topographical survey of portion of Washington Square Park" Map file no. M-T-98-104 (Prepared for NYC Department of Parks).

Geophysical Survey Systems, Inc. (1987) Operations Manual, Subsurface Interface Radar, SIR System-3 GSSI, Hudson, NH.

Geraghty, J. J. (1959) "Ground-Water problems in the New York City Area. Ann. NY Acad. Sci. , vol.80, art. 4, pp.1049-1059.

Harris, W. and M-L. Pipes (MS) "Historical background study: New York University Law School extension project". NYU Department of Anthropology (Revised 1985 by R. Yamin and B. Salwen).

Karp, E. and R. E. Loeb (1986) "Late glacial sediments in Greenwich Village, New York City". Amer. Quat. Assoc., Progr. Abstr. 9th Ann. Meeting, p. 141.

Longworth, (1817) "Guide through the city of New York" (map).

Neville, A. M. (1981) Properties of Concrete , 3rd ed., Pitman Publ., London, chap. 2.

Pickman, A. and D. Rockman (MS) "Archaeological boring program, New York University Law School extension". NYU Department of Anthropology.

Pror and Dunning (1817) "The city of New York" (map).

Randel, J. (1811) "Plan of the city of New York" (map).

Salwen, B. and R. Yamin (MS) "Final Report on Sullivan Street Site" (in progress), NYU Department of Anthropology.

Still, B. (MS) "Washington Square Park: Cemetery and Parade Ground" New York University Archives.

Still, B. (MS)b "Brief notes on the history of Washington Square Park" New York University Archives.

Ulriksen, C.P.F. (1982) "Applications of Impulse radar to Civil Engineering" Ph.D. Thesis, Lund University, Lund, Sweden.

Weast, R. C., M.J. Astle, and W.H. Beyer (1987) CRC Handbook of Chemistry and Physics , CRC Press Inc., Boca Raton FL, p. F-140.

TABLE 1

Chemistry of Vanderbilt Hall water sample compared to New York City Aqueduct waters. Values are in parts per million (ppm), unless otherwise indicated.

	Vanderbilt Hall	Catskill System	Croton System
Alkalinity as CaCO <sub>3</sub>	274	12	47
Hardness (CaCO <sub>3</sub> )	470	20	70
Total Chlorides	300	9.1	29.8
Fluoride	0.35	0.93	0.68
Nitrogen (as NH <sub>3</sub> )	<0.1	0.03	0.05
Nitrate	0.15	0.33	0.28
pH	7.4	6.7-7.8	6.9-7.6
Specific conductance, micro mhos/cm	1680	77	226
Fecal coliform	0	0	0

Assay provide by New York City Department of  
Environmental Protection Bureau of water resources.



## APPENDIX: Sources of Subsurface Data

Kevorkian Building (NYU) October 1969  
Borings 1, 2, 3  
Philip J. Healy, Inc.

Kevorkian Building (NYU) June 1970  
Borings 1, 2, 3  
Warren George, Inc.

Sullivan Street (NYU) January-February 1984  
Borings 1, 2, 3, 5, 6, 7, 10, 11  
Warren George, Inc.

Vanderbilt Hall (NYU) August-September 1948  
Borings 4, 5, 6, 8, 9, 10, 11  
Philip J. Healy, Inc.

Vanderbilt Hall (NYU) August 1981  
Borings 1, 2, 3, 4, 5  
N.J. Drilling Co, Inc.

Washington Square Park  
Borings 34, 35  
Berkey and Fluhr, 1934

Profiles are described in Pickman and Rockman (MS), Harris and Pipes (MS), and Salwen and Yamin (MS). A site survey map prepared by E.B. Lovell of S. P. Belcher, Inc., New York, NY (October 1983), no. 235729, 31 L. B. 541 was consulted for data on the Sullivan Street borings.



Electromagnetic Wave Velocity and its Application to  
Civil Engineering Investigations of Soil layers

Toshihiko Sakayama, Masaki Osada,  
(Geotechnical Institute, OYO Corp.  
Japan)

Takashi Kanemori, Satoru Ohya  
(OYO Corporation, USA)

## 1. INTRODUCTION

Ground probing radar is a subsurface exploration system that uses electromagnetic (EM) waves. The system is used for profiling measurement or wide-angle reflection and refraction (WARR) measurement.

In the WARR measurement, the transmitting antenna is fixed, and measurements are made while the receiving antenna is moved away. This method measures changes in the two-way travel time of reflected waves, thus providing information on EM wave velocity distribution as well as depths of reflection surfaces. In the profiling measurement, both transmitting and receiving antennas are moved simultaneously with fixed antenna-separation, to obtain the information of the shallow underground structures along a measuring line.

If WARR measurements are carried out at uniform intervals along a measuring line, both reflection profiles (common offset gathers) and the information of EM wave velocities can be obtained. This paper takes a look at EM wave velocity to investigate the potential for assuming the condition of water containing of soil.

## 2. RELATIONSHIP BETWEEN EM WAVE VELOCITY AND WATER CONTENT

Soil ground is regarded as an electric conductive media, and its characteristics are identified by velocity values and attenuation coefficient values of EM wave. EM wave velocity depends on dielectric constant which is related to degree of water saturation and volumetric water content.

Fig.1 shows the relationship between water content and EM wave velocity. In this figure, the degree of water saturation is used as a parameter. This relationship is theoretically obtained, regarding the soil as a composite media of particles, water and air. It can be seen that the greater the water content of the ground, the more the EM wave velocity decreases.

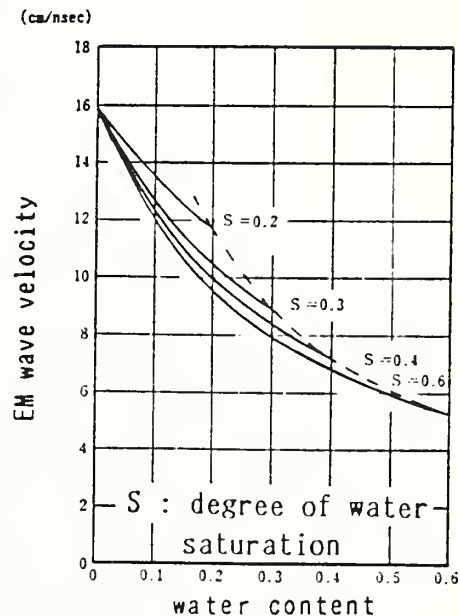


Fig.1 Relationship between water content and EM wave velocity

Consequently, by investigating in detail the distribution of EM wave velocity in the ground, it becomes possible to estimate the condition of water containing of the ground.

### 3. METHODS OF MEASUREMENT AND ANALYSIS

The investigation site was a loam embankment with 7 m height. Measuring line, on the top of the embankment, was 60 m long. In addition to profiling measurement, WARR measurements were also conducted. The WARR measurements were taken every 1 m, and the separations of transmitting and receiving antennas were varied from 60 cm to 280 cm with 20 cm intervals in each measurement.

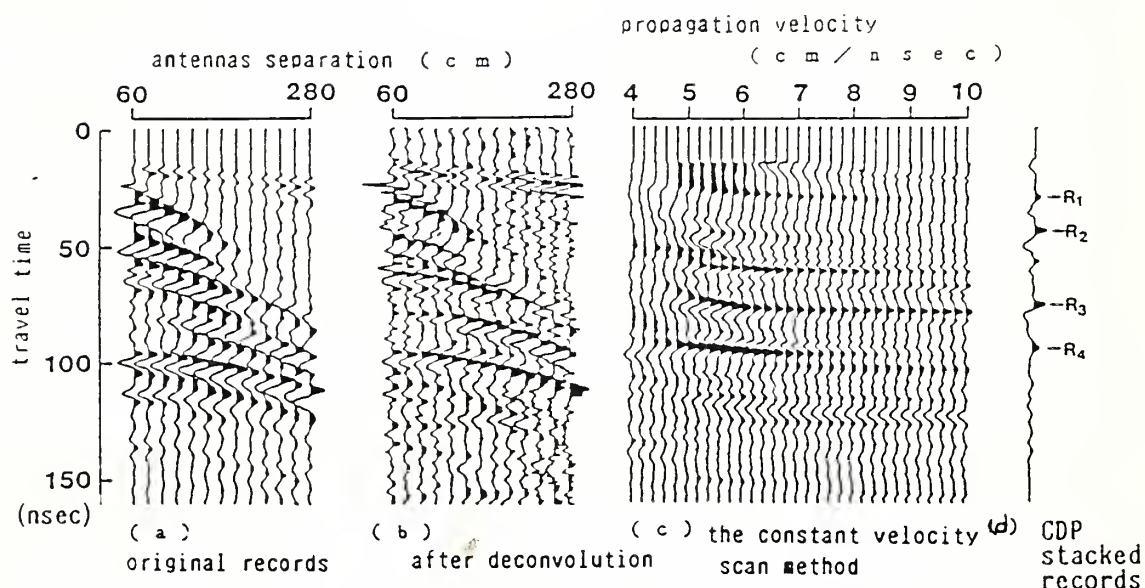


Fig.2 Outline of the processing

Fig.2 shows the changes of waveforms in the different step of processing. The first step is automatic gain control (AGC) processing (not shown in Fig.2), which generally strengthens faint signals from deep areas. The second step is called deconvolution processing (Fig.2 b). Unlike the original waveform, reflection waves are converted to more impulsive waveforms. In the third processing step, apparent EM wave velocity is determined by the constant velocity scan method (Fig.2 c). In this method, stacking velocity is progressively changed at regular intervals, as the data is repeatedly corrected and stacked. An optimal stacking velocity for a given reflection phase is obtained when the amplitude of the reflection phase is maximum. The stacking velocities for each reflection phase were determined and the CDP stacked was performed (Fig.2 d), which improves the SN ratio of the reflection profile.

#### 4. ANALYZED RESULTS

Fig.3a shows an original record taken by profile measurement. The horizontal axis is distance along the measuring line. The vertical axis is two-way travel time. The reflection surface of the concavity, that can be seen in 0-20 m on the measuring line, corresponds to the top boundary of old excavation, when soil had in the past been removed by excavation, and then returned. It was supposed that the gently sloping reflection surface in the 30-60 m on the measuring line was either a boundary between different types of soil or a boundary between soils having different degrees of compaction. Fig.3b is the CDP stacked section. Data processing has improved image resolution. Also, reflection waves from a somewhat deep region have been emphasized. Fig.3c shows distribution of EM wave velocities of each soil layer. They are the interval velocities calculated from the stacking velocities of each reflection event. The profile is characterized by a low velocity layer at 2-3 m depth along the measuring line at 25-60 m. It may

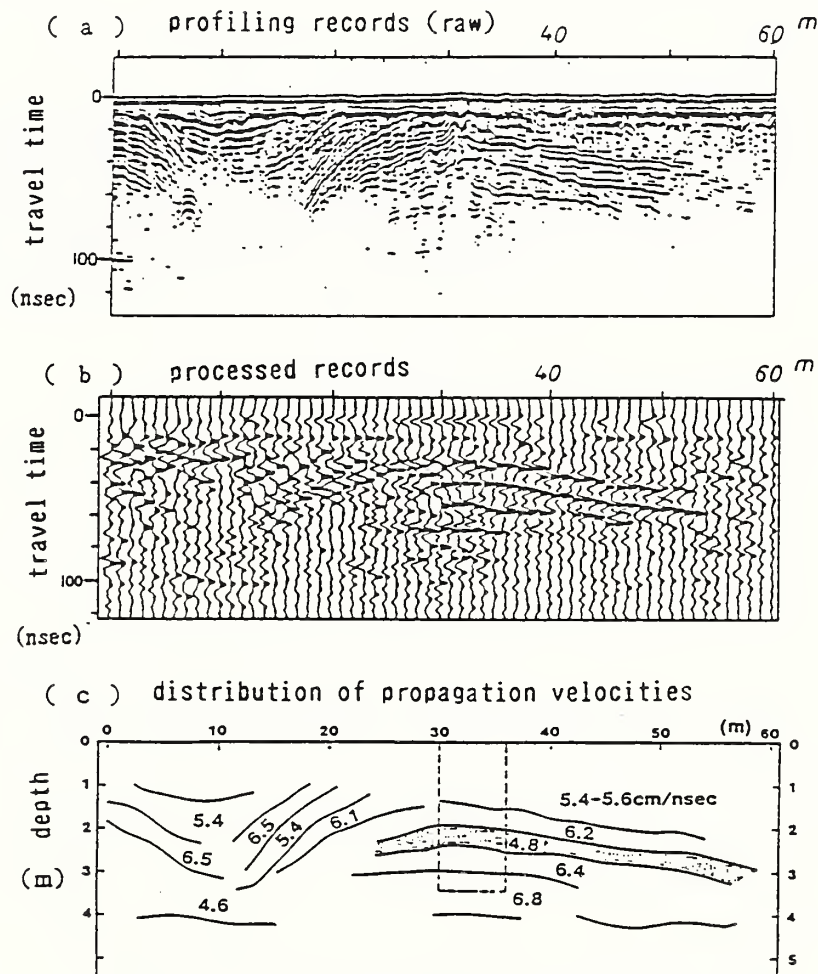


Fig.3 Results of ground probing radar measurements

be estimated that the water content of this low velocity layer is much higher than the surrounding area.

Excavation was conducted at the area within the broken line, in Fig.3c. Fig.4 is a sketch of the excavation surface. Here, we can detect the subtle differences in soil property within the embankment. There is good correspondence between the boundaries of soil layers obtained from excavation and the reflection surfaces in the EM wave velocity profile obtained by ground probing radar. It can be seen that the low velocity zone of 4.8 cm/ns corresponds to an extremely loose loam layer, having a high water content.

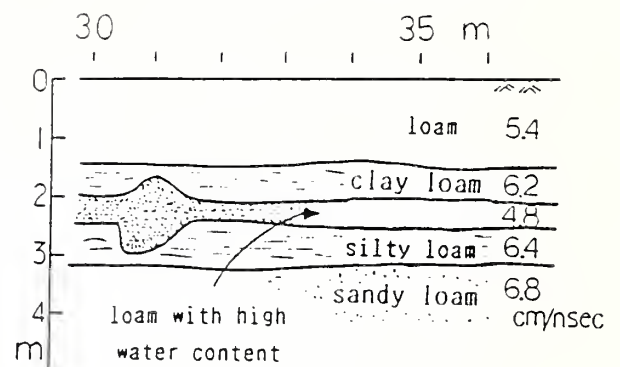


Fig.4 A sketch of the excavation surface compared with the EM wave velocities

## 5. CONCLUSION

Computer processing can improve image resolution of the records of the ground probing radar. It is clearly shown in this paper that the EM wave velocity profile (obtained by WARR measurement and the constant velocity scan method) can reveal more subtle difference in soil properties than the normal profiling measurement. And the velocity profile has a possibility to provide the estimation of water containing condition of the ground.

PROPAGATION OF GROUND PENETRATING RADAR  
SIGNALS IN SOILS

BY

DAVID V. SMITH\*

Submitted For Presentation  
At

Second International Symposium On  
Geotechnical Applications Of  
Ground Penetrating Radar

March 6-10, 1988

\* Manager, Geophysical Measurements Group  
GEO-CENTERS, INC., Newton Centre, MA 02159

# PROPAGATION OF GROUND PENETRATING RADAR SIGNALS IN SOILS

## ABSTRACT

The interpretation of ground penetrating radar (GPR) data and the development of automated data processing methods require an understanding of electromagnetic propagation through the earth. Accurate depths to subsurface reflectors can be deduced from the standard two-way travel-time output plots once the velocity of radar pulse propagation in the subsurface is determined. Easily measured soil properties provide velocity estimates and information on the maximum attainable probing depth for available antenna frequencies.

A theoretical background describing electromagnetic properties of soils and rocks is presented. Following a brief discussion of these properties on GPR pulse propagation in the earth, different soil models are examined and related to GPR data.

## INTRODUCTION

Subsurface radar detection systems have been the object of study for over a decade by both military and environmental agencies. In both applications, the objectives are to locate and identify buried or submerged objects, otherwise not detectable, and to spatially determine the structural make-up of the subsurface.

The principle of operation involves the generation of a pulse train of electromagnetic radiation in the frequency range of 10-1000 MHz. In accordance with the laws of classical elec-



tromagnetism, the wave propagates, with material dependent attenuation, through a given medium - the earth. When the wavetrain encounters a material or boundary of different dielectric properties, the wave is partially reflected. This reflected wave is then detected and the time interval between transmission and detection is recorded.

Hence, the time interval can be converted to a distance or depth. A typical system is depicted in Figure 1.

### Theoretical Background

The electromagnetic properties of all materials are described by complex media dependent parameters, with the complex electrical conductivity defined as  $\sigma^* = \sigma' - j\sigma''$ , the complex permittivity or dielectric constant defined as  $\epsilon^* = \epsilon' - j\epsilon''$  and the complex magnetic permeability defined as  $\mu^* = \mu' - j\mu''$ . Note that  $\epsilon^* = \epsilon_0 \epsilon_r^*$ , where  $\epsilon_r^*$  is the complex relative permittivity and  $\epsilon_0 = 1/36\pi \times 10^{-9}$  Farad/m, and  $\mu^* = \mu_0 \mu_r^*$ , where  $\mu_r^*$  is the complex relative permeability and  $\mu_0 = 4\pi \times 10^{-7}$  Henry/m.

The real effective parameters,  $\sigma_e$  and  $\epsilon_e$ , can be measured and are related to the complex constitutive parameters by:

$$\sigma_e = \sigma' + \omega\epsilon'' \quad (\text{Si/m}) \quad (1)$$

$$\epsilon_e = \epsilon' - \frac{\sigma''}{\omega} \approx \epsilon' \quad (\text{Farad/m}) \quad (2)$$

where  $\epsilon'$  equals the real part of the dielectric constant,  $\sigma'$  equals the zero frequency conductivity ( $\sigma_{dc}$ ). The imaginary part of the complex conductivity  $\sigma''$  equals zero at the frequencies of interest, and  $\epsilon''$  is the dielectric relaxation loss factor due to the oscillation of dipolar water molecules in a time varying electric field. From (2) the real effective permittivity ( $\epsilon_e$ ) is seen to equal the real part of the complex permittivity ( $\epsilon'$ ).

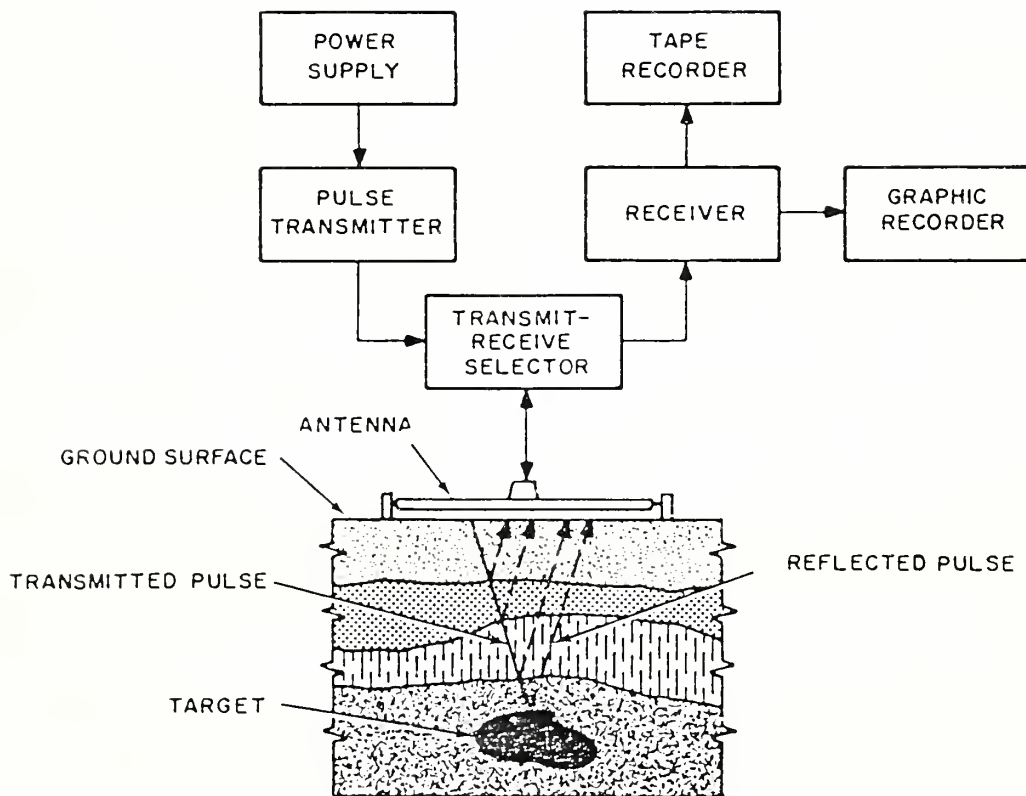


Figure 1. Ground Penetrating Radar (GPR) System, block diagram.

The magnetic permeability,  $\mu^*$ , is assumed to be real throughout such that  $\mu^* \approx \mu'$  and  $\mu_r' = 1$  for most earth materials.

Electromagnetic energy is dissipated in the form of heat and is the sum of two energy dissipation processes; namely, conduction and relaxation. Conduction in earth materials is caused by electron and ion movement in an electric field. This movement may be free or exchangeable. Clays which are ion exchangeable, exhibit higher conductivities than non-exchangeable soils. Water, which usually contains free carriers in the form of dissolved salts, increases the conductivity of soils and rocks. Relaxation losses are due to the induced oscillation of the permanent dipole moment of the water molecule in a propagating electric field.

The relative complex permittivity for water ( $\epsilon_{rw}^*$ ) is both frequency and temperature dependent and is obtained from the Debye formula (King and Smith, 1981 [1]),

$$\epsilon_{rw}^* = \epsilon_{rw}' - j\epsilon_{rw}'' = \epsilon_{r\infty} + \frac{\epsilon_{rs} - \epsilon_{r\infty}}{1 + j\omega\tau} \quad (3)$$

where:

- $\epsilon_{rs}$  = relative static permittivity (temperature dependent)
- $\epsilon_{r\infty}$  = relative optical permittivity = 5.5
- $\tau$  = relaxation time (temperature dependent)

Table 1 gives values of  $\epsilon_{rs}$  and  $\tau$  as a function of temperature. The relative real and imaginary terms are given by:

Table 1. STATIC PERMITTIVITY, RELAXATION TIME, AND  
CRITICAL WAVELENGTH OF WATER

$$(\epsilon_{r\infty} = 5.5)$$

T(°C)	$\xi$ .	$\tau$ (sec)	$i$ (cm)
0	88.2(89)	$17.8 \times 10^{-12}$	3.34
5	86.2	15.1	2.85
10	84.2	12.7	2.39
15	82.3	10.9	2.05
20	80.4	9.50	1.80
25	78.2(78.3)	8.31	1.57
30	76.7	7.36	1.39
35	75.0	6.58	1.24
40	73.1	5.95	1.12
45	71.4	5.37	1.01
50	69.8	4.87	.912
55	68.2	4.44	.837
60	66.6(65.8)	4.03	.760
65	65.0	3.72	.701
70	63.6	3.45	.650
75	62.1	3.23	.608
80	60.8		
85	59.5		
90	58.1		
95	56.8		
100	55.4(53.7)		
200	34.6(31.6)		
300	17.7(15.2)		

Source Interpolated from data of Collie et.al., Proc., Phys., Soc., London 60. 145 (1948: and Akerlöf and Oshry, J.Chem.Soc.72,2844 (1950). The values in parentheses are theoretical, calculated from Kirkwood's formula (6.17). J.G. Kirkwood, J.Chem.Phys. 7,911 (1939): and G.Oster and J.G. Kirkwood, J.Chem.Phys. 11,175 (1943) (From King and Smith, 1981).

$$\epsilon_{r\omega}' = \frac{\epsilon_{rs} + \epsilon_{r\infty} \omega^2 \tau^2}{1 + \omega^2 \tau^2} \quad (4)$$

$$\epsilon_{r\omega}'' = \frac{\omega \tau (\epsilon_{rs} - \epsilon_{r\infty})}{1 + \omega^2 \tau^2} \quad (5)$$

This frequency and temperature dependence is illustrated in Figure 2, where the maximum loss due to relaxation occurs at an approximate frequency of  $2 \times 10^{10}$  Hz for water and at  $3 \times 10^3$  Hz for ice. Therefore, the losses due to the relaxation process in unfrozen soils and rocks occur at extremely high frequencies and are only dependent on the water content.

Figure 3 shows the behavior of the relative real effective permittivity  $\epsilon_{er}$  ( $= \epsilon_r'$ ) and the effective conductivity,  $\sigma_e$ , for a typical clay-loam soil with a water content of about 10% by weight. The effective conductivity is fairly independent of frequency from very low frequencies to about  $10^6$  Hz (1 MHz), indicating that  $\sigma'$  (dc conductivity) in Equation (1) is the dominant factor in determining the propagation losses in the material at low frequencies. The loss associated with the dipolar relaxation of water, represented by  $\omega\epsilon''$  in (1), begins to dominate at frequencies above 1 MHz. For perfectly dry materials, the effective conductivity,  $\sigma_e$ , equals the dc conductivity and is independent of frequency because  $\epsilon''$  is zero. This relationship suggests that if the dc conductivity and moisture content of the soil are known, the effective conductivity over the frequency range of interest (10 to 1000 MHz) can be calculated. Also, if the moisture content is known, the relative real effective permittivity,  $\epsilon_{er}$ , can be estimated from various soil models.

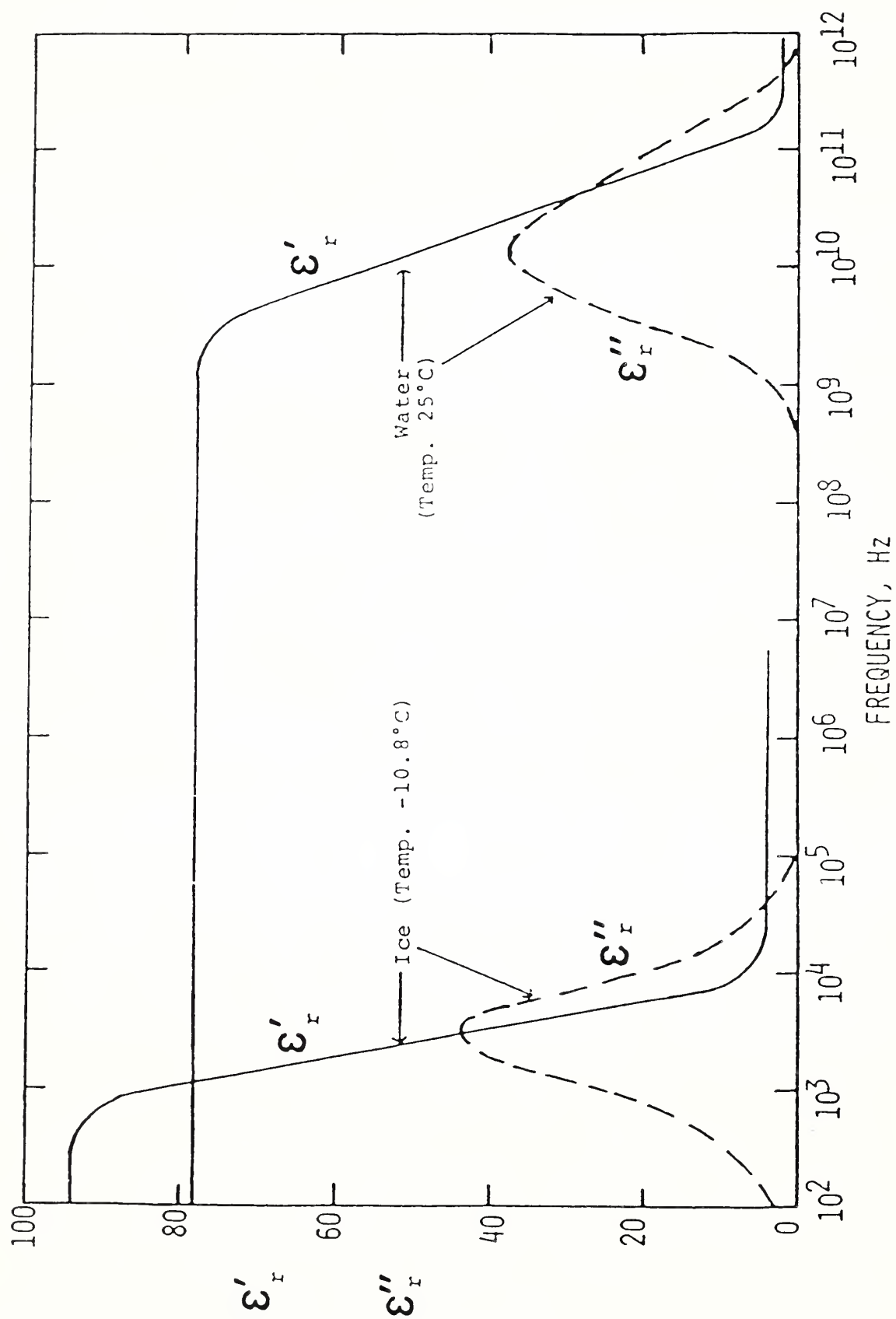
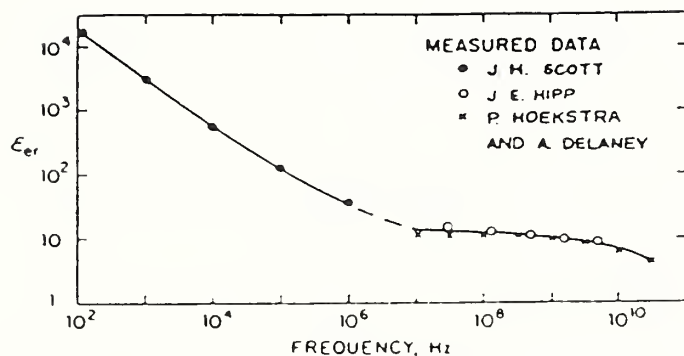


Figure 2. Dielectric behavior of water and ice.



a.



b.

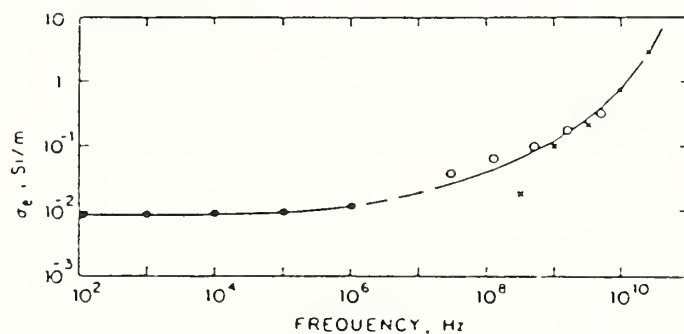


Figure 2. Relative effective permittivity  $\epsilon_{er}$  and effective conductivity  $\sigma_e$  as a function of frequency for a typical clay-loam soil with a water content of about 10% by weight. (From King and Smith, 1981)

In common earth materials there is a trade-off between probing depth and resolution. Quantitatively, the spatial resolution (or minimum discontinuity dimension detectable) is approximated by one-half the radar wavelength in the medium:

$$r = \lambda/2 = v_m/(2f) = c/(2f\sqrt{\epsilon_{er}}) \quad (7)$$

where

- $r$  = the minimum resolvable dimension,
- $\lambda$  = the radar wavelength in the medium,
- $c$  = the velocity of light,
- $f$  = the radar frequency,
- $\epsilon_{er}$  = the relative effective dielectric constant.

The probing depth is determined by the frequency of operation and the electromagnetic properties of the soil, principally the conductivity and the dielectric constant. Signal attenuation is usually given in terms of dB/meter (Morey, 1984):

$$A = (12.863 \times 10^{-8}) f \sqrt{\epsilon_{er}} (\sqrt{p^2 + 1} - 1)^{1/2} \text{ (dB/m)} \quad (8)$$

where

$$p = \text{loss tangent} = \frac{\sigma_e}{2\pi f \epsilon_o \epsilon_{er}} = \frac{1.8 \sigma_e}{f \epsilon_{er}} 10^{10}$$

with

- $f$  = frequency in Hz
- $\epsilon_o$  = dielectric constant of free space  
( $8.85 \times 10^{-12}$  farads/meter)
- $\epsilon_{er}$  = relative effective dielectric constant
- $\sigma_e$  = effective conductivity (mhos/meter)

Nominal GPR systems transmit approximately 100 volts and can readily detect 1 millivolt, giving 100 dB of usable signal; the attenuation increases with increasing frequency. Thus, by

changing the radar frequency through the use of different antennas, a range of probing depth and resolution is made available.

A summary of the physical properties of common media which affect the propagation and attenuation of electromagnetic signals is shown in Table 2. Careful analysis of the reflected pulse, combined with a knowledge of the electromagnetic properties of the soil, can reveal information such as percentage of water content, density variation, and the location and depth of buried objects.

Table 2. Approximate VHF electromagnetic parameters of typical earth materials.

Material	Approximate Conductivity $\sigma$ (mho/m)	Approximate Dielectric Constant	Depth of Penetration
Air	0	1	Max (km)
Limestone (dry)	$10^{-9}$	7	
Granite (dry)	$10^{-8}$	5	
Sand (dry)	$10^{-7}$ to $10^{-3}$	4 to 6	
Bedded Salt	$10^{-5}$ to $10^{-4}$	3 to 6	
Freshwater Ice	$10^{-5}$ to $10^{-3}$	4	
Permafrost	$10^{-4}$ to $10^{-2}$	4 to 8	
Sand, Saturated	$10^{-4}$ to $10^{-2}$	30	
Freshwater	$10^{-4}$ to $3 \times 10^{-2}$	81	
Silt, Saturated	$10^{-3}$ to $10^{-2}$	10	
Rich Agricultural Land	$10^{-2}$	15	
Clay, Saturated	$10^{-2}$ to 1	8 to 12	∇
Seawater	4	81	Min (cm)

A more quantitative picture of the penetration performance of the GPR in soils is presented in the next section.

## Soil Models

Dielectric mixing models are used to relate the electromagnetic behavior of a heterogeneous mixture to the electrical properties of the constituents. Many soil models have been developed based on theoretical considerations and empirical data to explain the variations of the constitutive parameters (permittivity, conductivity, and permeability) with changes in soil type and moisture content.

Soils consist of basically four components: mineral material, organic material, water, and air. Except in the upper few inches of a soil, the quantity of organic matter is extremely small and is considered negligible. The solid portion of a soil, e.g., minerals, and the gaseous portion are very similar in terms of the constitutive parameters,  $\epsilon^*$  and  $\sigma_e$ , and are here considered electrically indistinguishable. This approach simplifies a complex four-phase problem to that of two phases, involving only dry soil and water mixtures.

The mineral fraction of most soils consists of some combination of sand and silt, clay size particles usually composed of quartz, feldspar, mica, and various clay minerals. The minerals in the sand and silt fraction of soil are generally electrically neutral and are good insulators. Completely dry clay is also an insulator. The introduction of moisture changes both the complex dielectric constant and the conductivity of the soil. These changes, especially with respect to conductivity, are most pronounced in the clays.

Clays are micro-crystalline, sheet-structured silicates. The surface of each clay particle tends to be negatively charged and readily adsorbs cations, typically  $\text{Ca}^{+2}$ ,  $\text{Mg}^{+2}$ ,  $\text{H}^+$ ,  $\text{K}^+$ ,  $\text{Na}^+$ , and  $\text{NH}_4^+$ . These adsorbed cations are loosely held to the surface and can be exchanged for other cations or essentially go into solution when mixed with water and are, hence, called exchangeable ions. Because of the extremely small particle size of clays, the surface area per unit volume is very large and a great many ions are adsorbed. These adsorbed ions can contribute appreciably to the ionic soil conductivity. A measure of the number of ions adsorbed to the surface of clay particles is the cation exchange capacity. Typical cation exchange capacities of common clays range from about 10 milliequivalents/100 g for kaolinite to over 140 milliequivalents/100 g for montmorillonite or vermiculite.

Archie (1942) [2] empirically related the measured values of dc electrical conductivity,  $\sigma_m$ , from a wide variety of brine saturated sand formations with the water conductivity,  $\sigma_w$ , via

$$\sigma_m = \sigma_w \theta_v^n \quad (9)$$

$\theta_v$  is the porosity or fractional volume of water and  $n$  is called the cementation index. The index has been found to be close to 2, with grain shape causing variation. Archie's law in clayey soils assumes that the free ions in the clay are also present in the pore water.

Archie's law provides a means for estimating the dc conductivity of a mixture. However, as Equation (1) shows, the effective conductivity ( $\sigma_e$ ) also includes the imaginary part (relaxation) of the complex dielectric constant of the mixture. As the frequency increases, this term increases and must be included to properly estimate  $\sigma_e$ .

In the simplest case, the relative complex dielectric constant for a two-component system (soil and water) is the sum of the relative dielectric constants of each of the components weighted by their relative volumes. The formula for this simple volumetric mixing model was given by Brown (1956) [3] as

$$\epsilon_{rm}^* = \theta_v \epsilon_{rw}^* + (1 - \theta_v) \epsilon_{rs}^* \quad (10)$$

where:

$$\begin{aligned} \epsilon_{rm}^* &= \text{relative complex permittivity of the mixture} \\ \epsilon_{rw}^* &= \text{relative complex permittivity of water} \\ \epsilon_{rs}^* &= \text{relative complex permittivity of soil} \\ &= \epsilon'_{rs} \\ \theta_v &= \text{volume fraction of water} \end{aligned}$$

However, a more realistic model was proposed by Birchak et al. (1974) [4] based on the optical path length of a single electromagnetic ray. Their complex index of refraction models yields

$$\epsilon_{rm}^* = [\theta_v (\epsilon_{rw}^*)^{1/2} + (1 - \theta_v) (\epsilon_{rs}^*)^{1/2}]^2 \quad (11)$$

in which the symbols are as in (10).

The magnetic permeability,  $\mu^*$ , is assumed to be real throughout such that  $\mu^* = \mu'$  and  $\mu_r' = \mu'/\mu_0$ . The relative permeability is related to the magnetic susceptibility,  $k$ , by

$$\mu_r' = 1 + 4\pi k \quad (12)$$



where  $k$  is expressed in c.g.s. (emu) units. The susceptibility of most earth materials is usually on the order of  $10^{-6}$  to  $10^4$  c.g.s. units with a resulting  $\mu \approx \mu_0$  and  $\mu_r \approx 1$ . However, when there is a significant magnetite ( $\text{Fe}_3\text{O}_4$ ) content in the material, the susceptibility, and hence, the permeability increase. Figure 4 gives experimental data relating magnetic susceptibility to volume percent magnetite content (Lindsley, et al, 1966) [5].

From these data, susceptibility can be estimated for rocks of different magnetite content, and permeability, attenuation, velocity, and maximum depth of penetration can be calculated. These results suggest that  $\mu_r$  will be very nearly equal to one and any effects will be minimal, unless very high concentrations of magnetite are present, as in an iron ore.

#### Electromagnetic Propagation

The propagation of electromagnetic energy in a medium can be described by the parameter  $\gamma$ , the complex propagation constant of the medium, which is derived from Maxwell's equations describing the behavior of electromagnetic fields (Jackson, 1975 [6]; Kraichman, 1976 [7]). The propagation constant is defined as:

$$\gamma = \alpha + j\beta = (-\omega^2 \mu' \epsilon_e + j\omega \mu' \sigma_e)^{1/2} \quad (13)$$

where the angular frequency  $\omega=2\pi f$  ( $f$  = frequency in Hertz) and the medium, i.e., the earth, is characterized by the parameters  $\mu'$ ,  $\epsilon_e$ , and  $\sigma_e$  (Horton et al., 1982 [8]).  $\alpha$  and  $\beta$  are the real attenuation constant and real phase constant, respectively. As

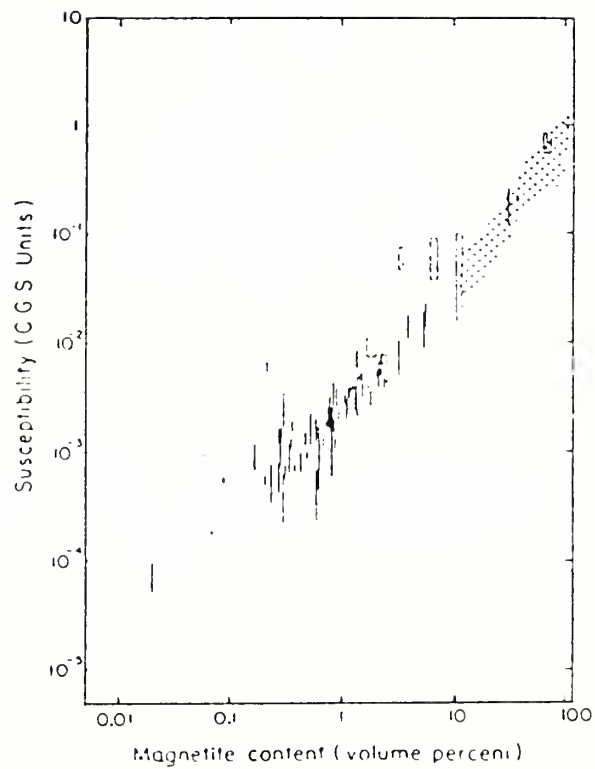


Figure 4. Empirical relationship between magnetic susceptibility and magnetite content for a variety of rocks.

the radiated electromagnetic wave propagates through the soil with a phase velocity

$$v = \frac{\omega}{\beta} \text{ (m/sec)} \quad (14)$$

it suffers an exponential attenuation, such that

$$A = 20 \log e^{\alpha} = 8.686 \alpha \text{ (dB/m)} \quad (15)$$

The reflection and transmission of incident electromagnetic energy at a boundary is a function of the impedance differences between the two materials. The characteristic complex impedance,  $\eta$ , of materials is given by

$$\eta = \frac{j\omega\mu'}{\gamma} \quad (16)$$

Table 3 lists the calculated attenuation, phase velocity, and intrinsic impedance for several typical materials at 100 MHz.

The complex reflection coefficient in the case of reflection involving a two-layer earth is given by

$$\rho = \frac{\eta_2 - \eta_1}{\eta_2 + \eta_1} \quad (17)$$

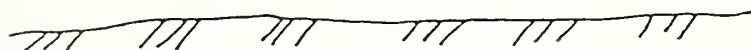
where  $\eta_1$  is the intrinsic impedance of the upper layer and  $\eta_2$  is the intrinsic impedance of the lower layer. Table 4 gives the calculated complex reflection coefficients at a smooth, flat boundary for several combinations of materials listed in Table 3 that are likely to be present in various soils. Note that the greater the impedance contrast, the greater the magnitude of the reflection coefficient. Both the magnitude and phase angle contain information indicative of the boundary conditions and relative properties of the two materials. The calculated effect of moisture content on the detection range to a rough plane reflector is shown graphically in Figure 5.

TABLE 3. TYPICAL ELECTROMAGNETIC PROPERTIES OF  
MATERIALS AT 100 MHz

<u>Material</u>	<u>A</u> <u>dB/m</u>	<u>V<sub>m</sub></u> <u>cm/ns</u>	<u>η</u> <u>ohms</u>
Air	0	30	377
Fresh water	0.18	3.33	42 + j0.046
Sea water	326	1.50	10 + j9.33
Sandy soil, dry	0.44	16.0	202 + j2.6
Loamy soil, wet	1.93	7.07	88.8 + j2.2
Clayey soil, wet	12.5	7.63	93 + j16.2
Iron	$1.7 \times 10^7$	$3.2 \times 10^{-9}$	2.0 + j2.0
Basalt	$8.2 \times 10^{-3}$	15.0	188 + j0.04
Sandstone	0.73	13.4	168 + j3.0

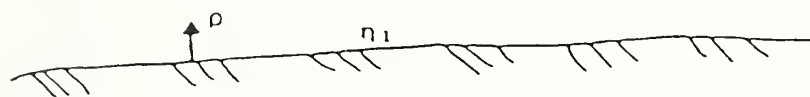
Where  $\eta$  = Characteristic Impedence of Material

TABLE 4 REFLECTION AT A BOUNDARY



Layer 1

$$\rho = \frac{\eta_2 - \eta_1}{\eta_2 + \eta_1}$$



Layer 2

$\eta_2$

	Complex Reflection Coefficient	Magnitude &	Phase Angle
<u>Sandy soil, dry</u> <u>Clayey soil, wet</u>	$-0.36 + j0.07$	37	$169^\circ$
<u>Loamy soil, wet</u> <u>Clayey soil, wet</u>	$0.03 + j0.07$	8	$67^\circ$
<u>Loamy soil, wet</u> <u>Iron</u>	$-0.95 + j0.04$	95	$177^\circ$
<u>Loamy soil, wet</u> <u>Air</u>	$0.62 - j0.008$	62	$-0.7^\circ$

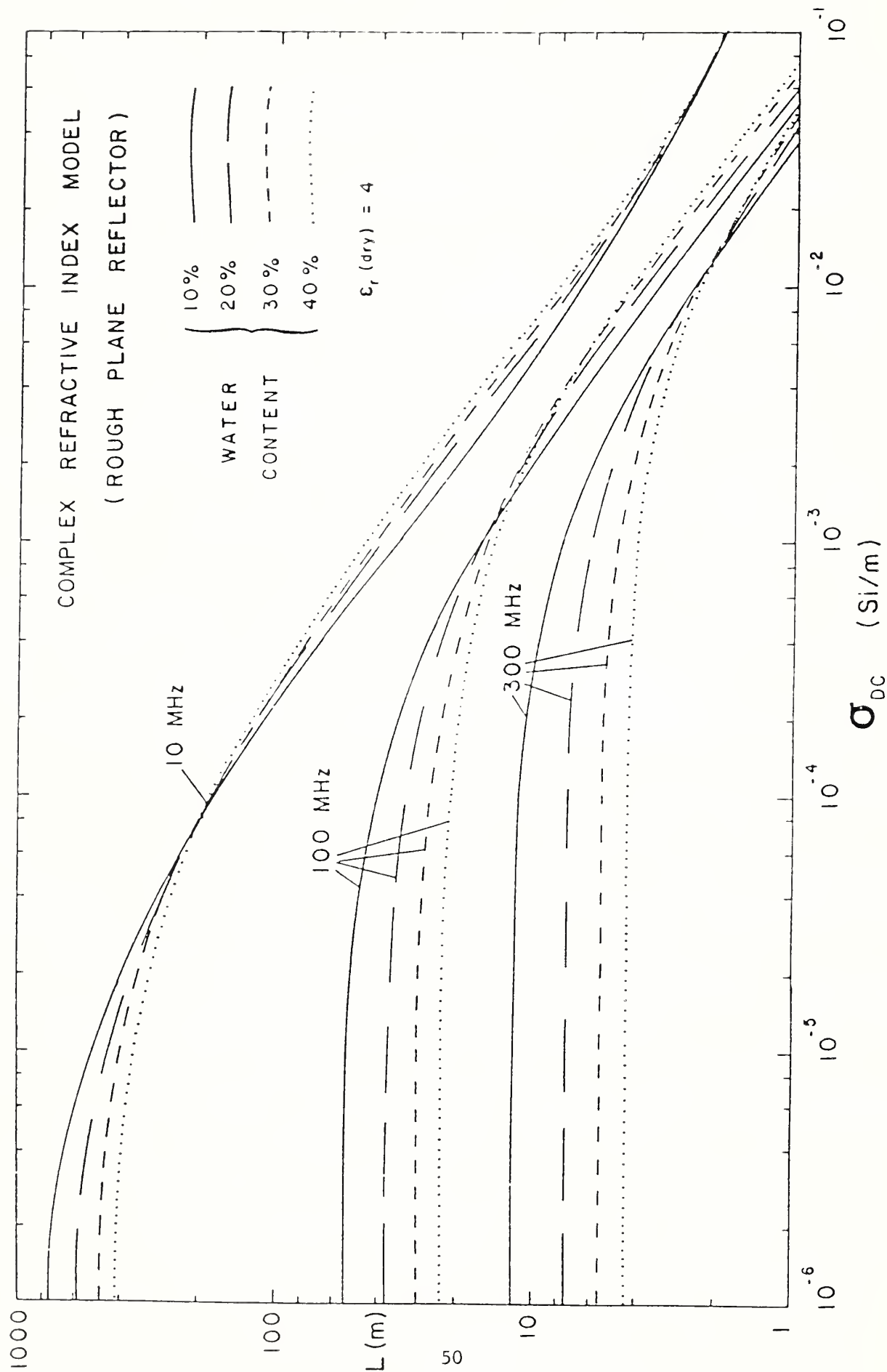


Figure 5. Radar range ( $L$ ) as a function of DC conductivity ( $\sigma_{DC}$ ) at different frequencies. Plots are based on a Complex Refractive Index Soil Model and reflection from a rough plane reflector (After Horton et al. 1981).



The maximum range for ground penetrating radar is a function of the radar system parameters, target parameters, and the electromagnetic properties of the material being probed.

At low soil attenuation, the maximum range, relatively independent of soil conductivity, is limited by geometric spreading losses and is a function of the radar system parameters.

As the attenuation increases, maximum radar range decreases and the magnitude of the range becomes dominated by soil conditions and is less dependent on the radar system. Signal attenuation in soils and rocks is primarily a function of pore water content and conductivity and, therefore, is highly variable. However, estimates of attenuation can be made for various soil and rock types. These estimates indicate that depth of penetration will be limited in clays and greatest in some granites, as shown graphically in Figure 6.

#### Radar Pulse Modeling

Actual examples of GPR data substantiates the theoretical relationship between soil dependent attenuation and maximum depth of penetration are shown in the following figures.

A 300 MHz system acquired the data shown in Figure 7 over soil which is primarily clean, well sorted fine sand of a glacial outwash deposit. The strong reflections from individual metal objects are distinct down to 20 feet. Geologic bedding is detectable at an even greater depth, showing that signal attenuation is small in this medium.

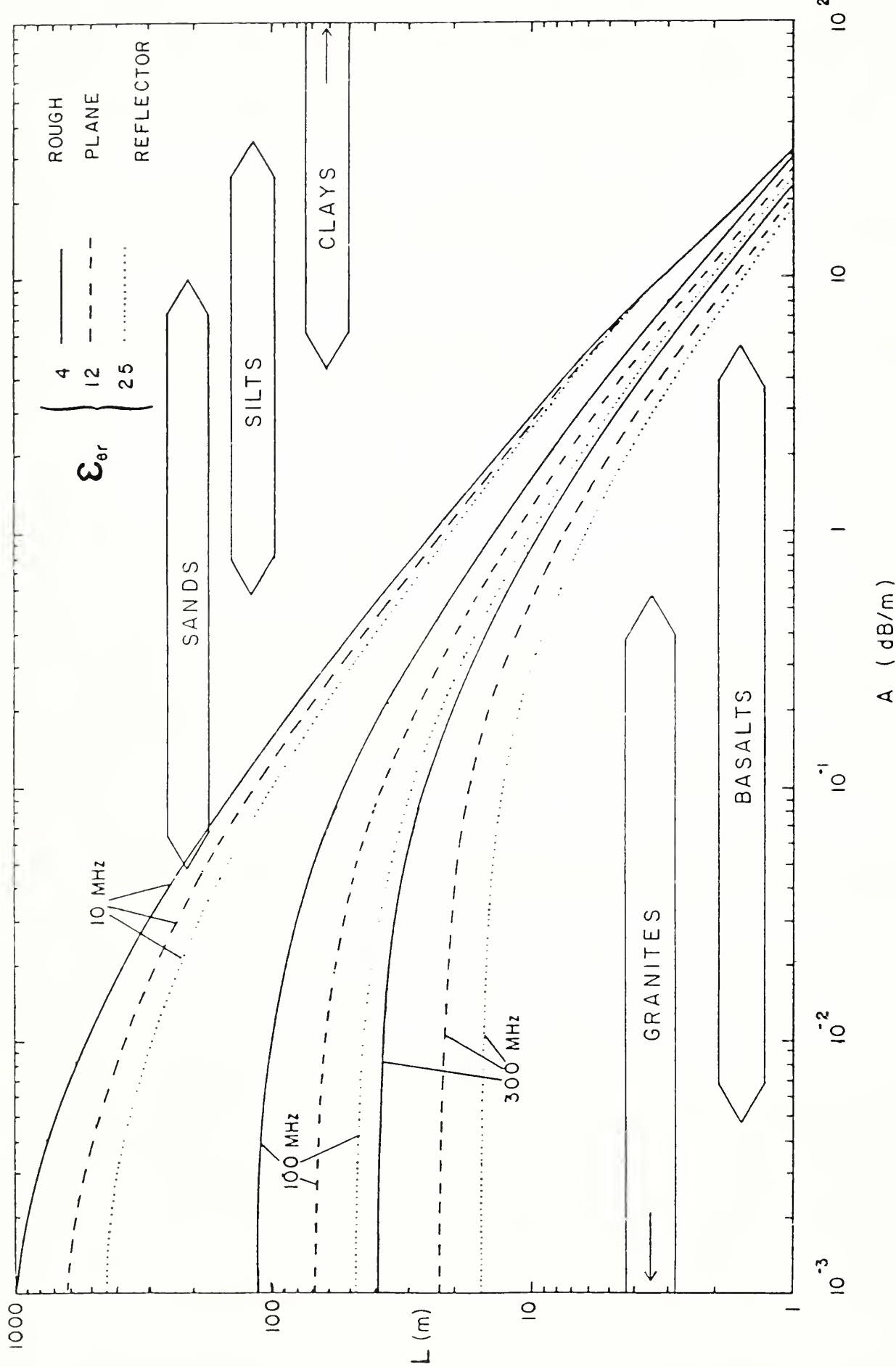


Figure 6. Variation of maximum depth of penetration ( $L$ ) as a function of attenuation ( $A$ ) for different frequencies and dielectric constants. Typical ranges of attenuation for different earth materials are also shown. (After Horton et al. 1981).

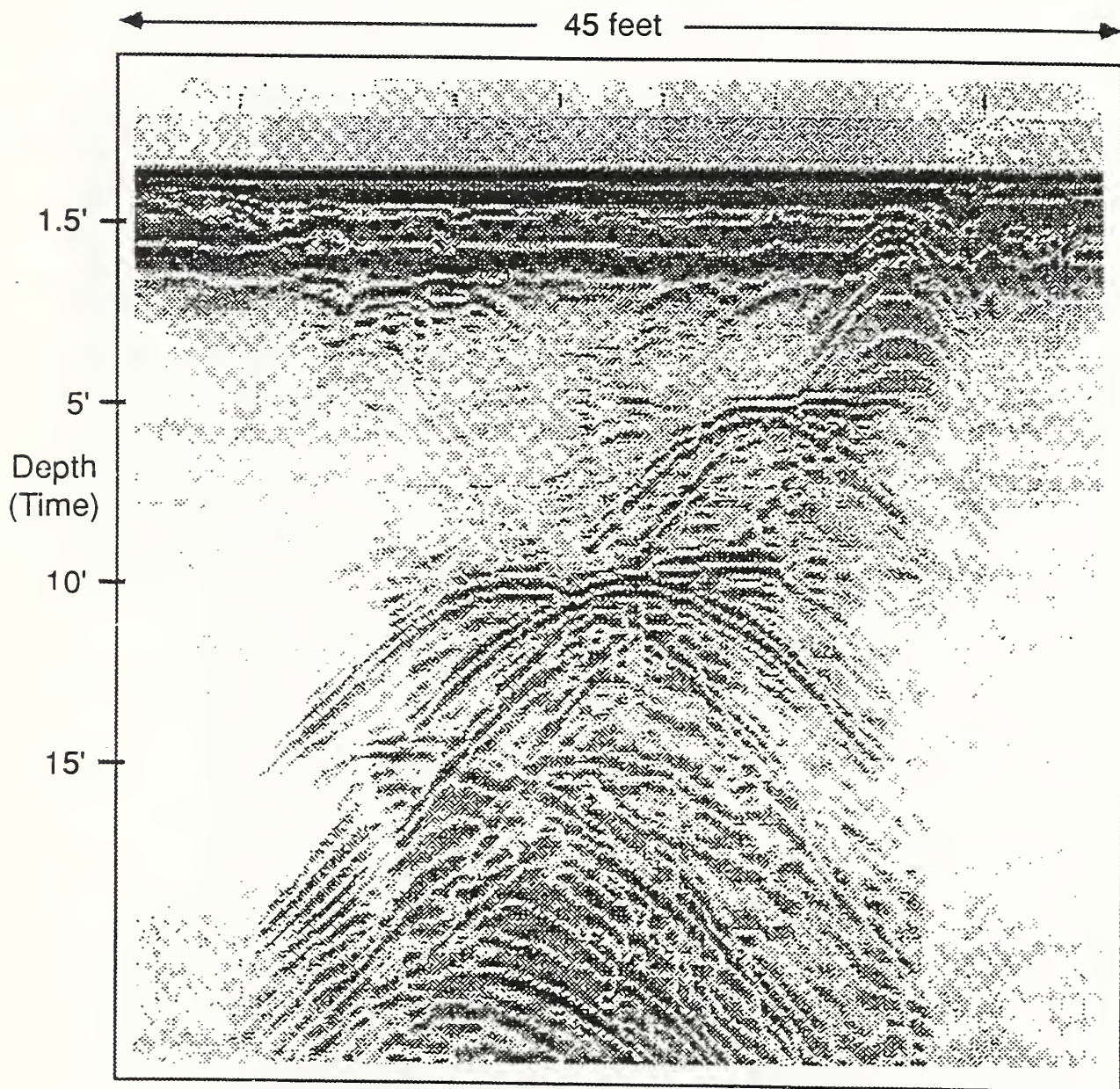


Figure 7. 300 MHz GPR reflections in sand. Hyperbolic reflections are from metal objects at various depths.



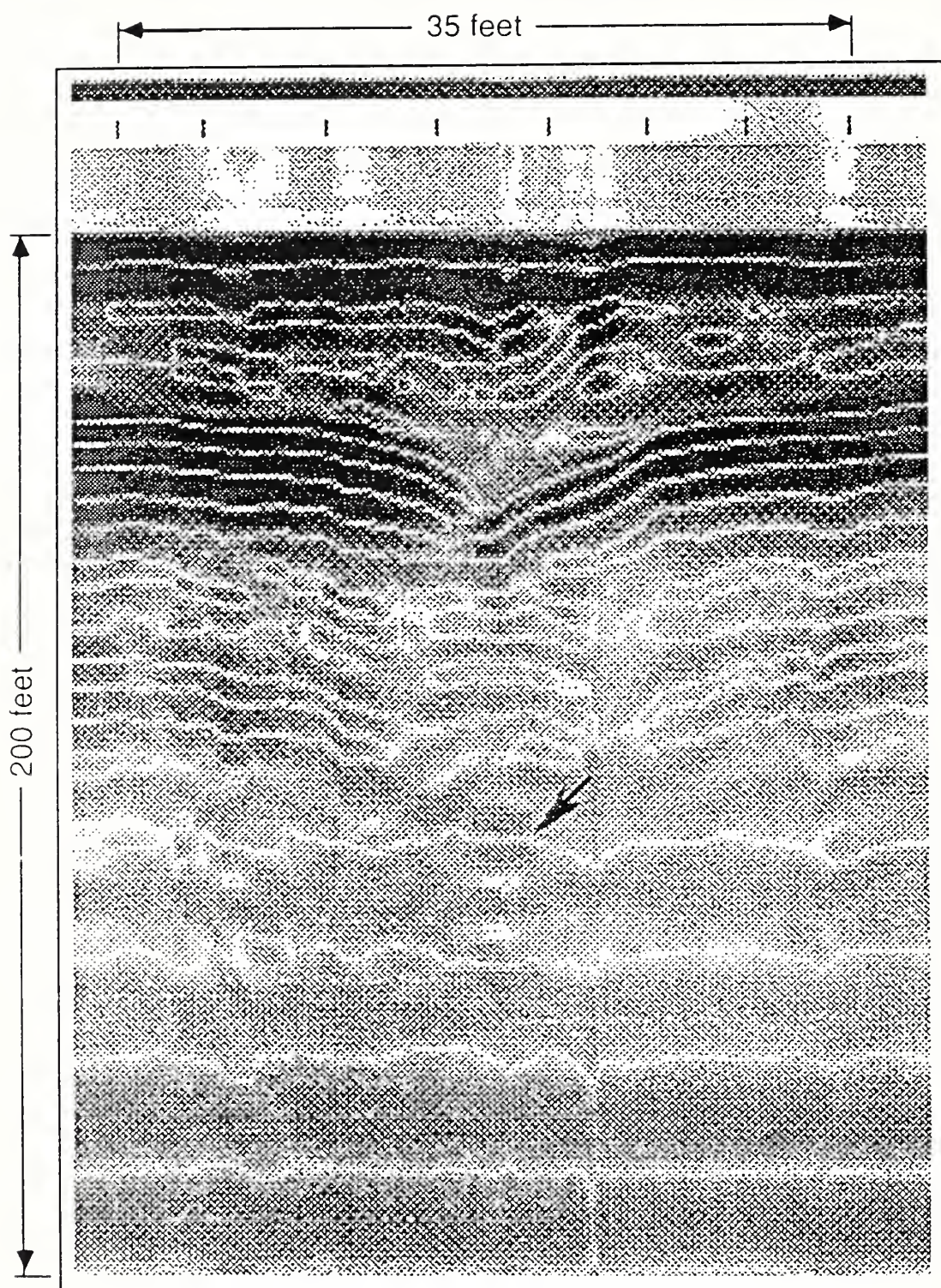


Figure 8. 80 MHz GPR scan in permafrost. Arrow shows location of metal target.



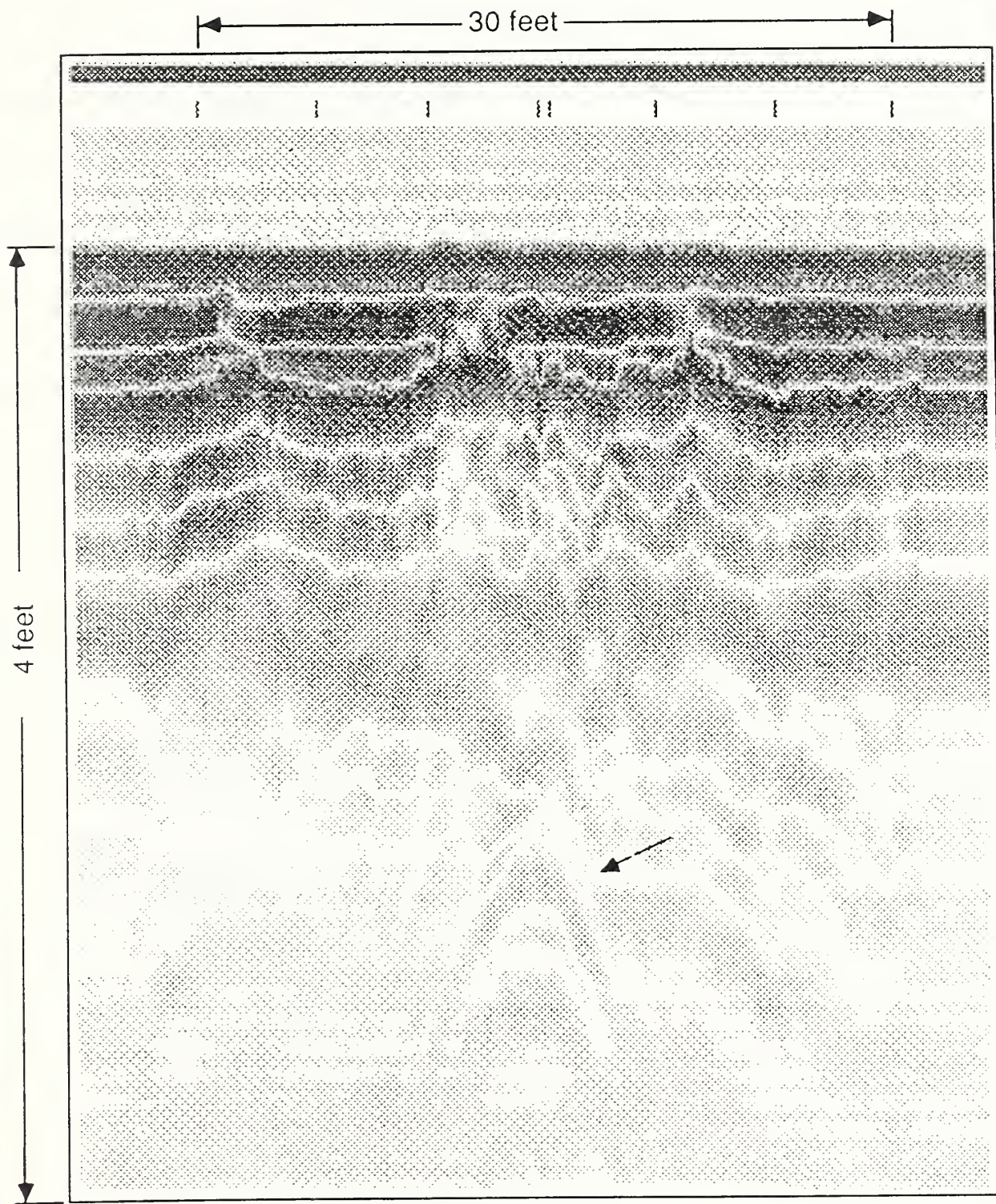


Figure 9. 80 MHz GPR scan in clay. Arrow indicates hyperbolic reflection from shallow metal object.

## References

1. King, R.W.P. and G.S. Smith, 1981, Antennas in Matter, MIT Press, Cambridge, MA.
2. Archie, G.C., 1942, "The Electrical Resistivity Log as an Aid in Determining Some Reservoir Characteristics", Trans. AIME, V. 146, p. 54-62.
3. Brown, W.F., 1956, "Dielectrics", in Encyclopedia of Physics, Vol. 17, Berlin: Springer.
4. Birchak, J.R., C.G. Garner, J.E. Hipp, and J.M. Victor, 1974, "High Dielectric Constant Microwave Probes for Sensing Soil Moisture", Proc. IEEE, Vol. 62, No. 1, p. 93-98.
5. Lindsley, D.H., G.E. Andersen, and J.R. Balsley, 1966, "Magnetic Properties of Rocks and Minerals", in S.P. Clark (ed.), Handbook of Physical Constants, Geologic Society of America, Memoir 97, P. 543-552.
6. Jackson, J.D., 1975, Classical Electrodynamics, 2nd Edition, John Wiley & Sons, New York.
7. Kraichman, M.B., 1976, Handbook of Electromagnetic Propagation in Conducting Media, Naval Material Command, NAVMAT P-2302.
8. Horton, K.A., R.M. Morey, R.H. Beers, V.J. Jordan, S.S. Sandler, and L. Isaacson, 1982, An Evaluation of Ground Penetrating Radar for Assessment of Low Level Nuclear Waste Disposal Sites, GEO-CENTERS, INC., Newton Centre, MA, rep. NUREG/CR-2212 (GC-TR-81-171).



# Some Examples of Archaeological Investigations Using Ground-probing Radar

Toshihiko Sakayama, Masaki Osada,  
Koichi Tamura  
(Geotechnical Institute, OYO Corp.  
Urawa, Saitama, Japan)

## 1. INTRODUCTION

Buried cultural properties are messages in the ground left to us from our ancestors, as well as indicators of our heritage of an unique culture built up in Japan. These cultural properties teach us historical facts, and at the same time present us with valuable suggestions concerning our future. However, these buried cultural properties are fated to be lost every year, because of land development. Excavation work for the purpose of development projects has rapidly increased in recent years. Every year, in Japan, the number of excavations is said to reach 10,000 throughout country. So that, prior to excavations, preliminary investigation methods are required to speedily explore the underground conditions. On the other hand, we should preserve important buried cultural properties with no more destruction. So that, nondestructive methods of investigations are required. In recent years, geophysical methods, especially ground-probing radar surveys, have fulfilled these requirements for many different types of archaeological remains. In this paper, we explain the use of ground-probing radar in archaeological investigations. Example of practical applications of ground-probing radar in archaeological investigations are also given.

In Japan, buried remains are often located at shallow depths, 1 to 2 m. Ancient culture layers or the upper surfaces of remains constitute boundaries of areas of differing soil properties. These boundary surfaces act as reflection surfaces that can be identified by ground-probing radar. The remains of pit dwellings, waler courses, ditches, etc. are buried by soil accumulation over the generations. Their projecting upper surfaces become reflection surfaces. Buried shell heaps or stone chambers in ancient burial mounds themselves act as reflection bodies that show up on ground-probing radar records.

## 2. DETECTION OF PIT DWELLING BURIED IN VOLCANIC ASH

Japan is well known as a country of volcanoes. There have been a number of discoveries of archaeological remains covered by volcanic ejecta. Recently, the discovery at Kuroimine site in Gunma Prefecture of the remains of an entire village drew wide spread attention. These remains were buried in a pumice layer, from the eruption of Mt. Haruna in sixth century A.D.

In order to identify the distribution of the dwelling at this site, located in a pumice layer, approximately 2.0 to 2.5 m thick, ground-probing radar was used effectively. There are marked differences in the characteristics of the pumice layer covering the former ground surface and loam layer below

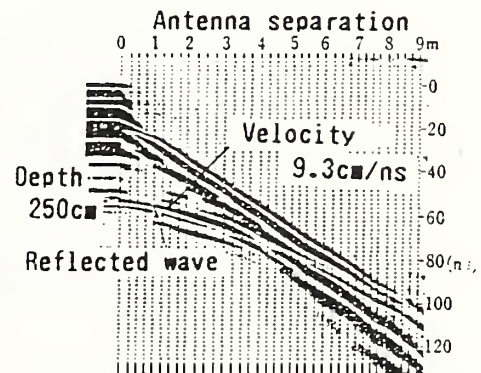


Fig. 1 A result of WARR measurement obtaining wave velocity and depth of reflection surface.

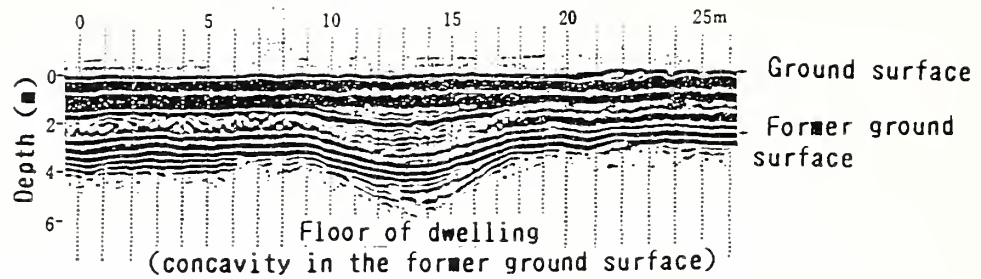


Fig. 2 Radar profile of an ancient dwelling buried in a pumice layer.

it. The boundary between the two layers is a good reflection surface.

Fig. 1 shows the results of wide-angle reflection and refraction (WARR) measurement at this site. In the WARR record, a reflection phase having the velocity of 9.3 cm/ns appears clearly. The depth of reflection boundary, estimated at 2.5 m from the velocity and the two way time, corresponds to the boundary between the pumice layer and the loam layer. The top surface of loam layer is the former ground surface before the eruption of the volcano. As shown in Fig. 2, profile measurement catches the undulations of the former ground surface. The radar profile clearly shows a concavity in the former ground surface, having a width 7 to 8 m. This kind of concavities are the remains of floor of pit dwellings.

### 3. EXPLORATION FOR MOATS REMAINS OF MIDDLE AGE CASTLES

In the Middle Ages, the environs of castles were divided by walls and moats. So it is important to investigate wall remains and moat remains which delimit the extent of castle.

Ground-probing radar was effectively used in the investigation of the remains of the Kawagoe castle in Saitama Prefecture. At this site, the scale of moats remains surrounding the environs of castle remains are comparatively large. Their locations can be effectively explored beforehand by ground-probing radar. Fig. 3 shows a record of the remains of a moat, as obtained by ground-probing radar. The Kawagoe castle is located on the left bank of Iruma river. The entire surface at this site have loam deposits 2.0 to 2.5 m thick on a sandy gravel layer. The

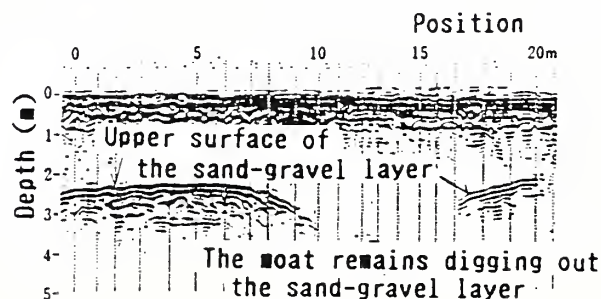


Fig. 3 Radar profile of the moat remains surrounding the environs of castle remains.

boundary between the loam layer and sandy gravel layer clearly appears on the ground-probing radar profile. Since the moat has a large concavity, the bottom of the sandy gravel layer is also concave, and therefore, the ground-probing radar record clearly shows cross section at the moat. From this record, it can be seen that the width of the moat is approximately 11 m, and the depth is approximately 3.2 m.

The Kawagoe castle remains have been designated as a national historical relic, meaning that the government policy for preservation of historical relic is applied. It is especially important to use nondestructive methods for exploring distribution of remains at this kind of buried cultural properties. Ground-probing radar can be expected to become a mainstay method in this field.

#### 4. EXPLORATION FOR JOMON AGES SHELLMOUND REMAINS

Shellmounds of the Jomon Ages in Japan have been found at a lot of places over the Kanto region. Especially, large and small shellmounds are concentrated along the coast of Tokyo Bay. Some of large shellmounds have a great academic significance. Buried shellmounds constitute a kind of anomaly in the ground that show up as strongly reflective bodies in ground-probing radar records. Consequently, ground-probing radar is extremely effective way for grasping the distribution of shellmounds buried underground.

The Kasori Shellmound Site, in Chiba Prefecture, is the largest one from 2500 to 7500 years ago. As such, it is designated as a national historical relic. It consists of a round portion to the north and a horseshoe shaped portion to the south. Their diameters ranges from 130 to 170 m. A number of investigation results show that small shell heaps and dwelling remains may be located in the vicinity of this large shellmound. Ground-probing radar has also been used in these investigations to clarify the distribution of small shell heaps and pit dwellings.

Fig. 4 shows a record of a small shell heaps as taken by ground-probing radar. Strong local reflections are evident surrounding the shell heaps. A ground layer profile around the shell heap, obtained from a test excavation, is also shown in the same figure. As is shown in this profile, it is very common that shell heaps exist in previously abandoned pit dwellings.

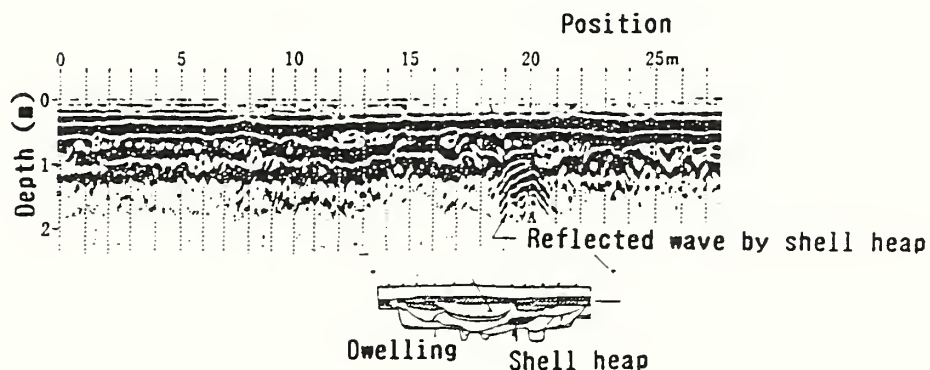


Fig. 4 Radar profile of a small shell heaps in previously abandoned dwelling and diagram showing a ground layer profile as confirmed by excavation.

## 5. CONCLUSION

It has only been the past several years that ground-probing radar has come to be used in exploration for archaeological remains. Therefore, it can be said that this field of investigation is still in the stage of research concerning clear establishment of its applicability. However, in the examples, it has already been established that, depending on the type and conditions of burial of the remains, extremely detailed exploration of some remains is possible. Exploration provides information that is important to the recovery in proper order and preservation of the buried cultural properties. In addition, the information obtained is vital to the planning of excavations. Ground-probing radar is also easier to use and more economical for preparatory investigation in comparison to trench investigations, etc.

There are many different types of buried cultural properties, and the conditions under which they are buried differ widely. It is becoming more and more important that investigations for such buried remains be conducted beforehand, to determine the situation of the ground. In order to meet this demand, it will be necessary to improve ground-probing radar and other types of exploration technology.

SUBSURFACE CHARACTERIZATION OF HAZARDOUS WASTE  
SITES USING GROUND PENETRATING RADAR

BY

GEORGE MARKT\*

Submitted For Presentation  
At

Second International Symposium On  
Geotechnical Applications Of  
Ground Penetrating Radar

March 6-10, 1988

\* Scientist, GEO-CENTERS, INC., Newton Centre, MA 02159





## TABLE OF CONTENTS

	<u>Page</u>
LIST OF FIGURES.....	ii
LIST OF TABLES.....	iv
1.0 Introduction.....	1
2.0 Ground Penetrating Radar.....	1
3.0 GPR Investigation of a Former Gasoline Station, Manchester, New Hampshire.....	4
4.0 Geophysical Investigation of the Nuclear Lake Site, Pawling, New York .....	11
5.0 Conclusions.....	38
References.....	40
Appendix A: Electromagnetic Wave Propagation Through the Common Earth Materials.....	A-1

## LIST OF FIGURES

<u>Figure</u>	<u>Page</u>
2.1 Ground Penetrating Radar System, block diagram.....	3
3.1 Two views of a former gasoline station site.....	6
3.2 GPR scan lines conducted over the site of a former gasoline station.....	7
3.3 GPR profile obtained over the three 4000 gallon fiber glass gasoline storage tanks.....	8
3.4 Map of subsurface features observed in GPR profiles obtained over the site of a former gasoline station..	9
3.5 GPR profiles obtained over pipes east of the former gasoline station.....	10
4.1 Site map of the Nuclear Lake Site; Dutchess County, New York.....	12
4.2 GPR scan lines conducted over Area A.....	14
4.3 GPR profile obtained along the 30 east line south of the plutonium storage facility.....	15
4.4 GPR profile obtained along the 12.5 south line north of the plutonium facility.....	16
4.5 Map of subsurface features observed in GPR profiles taken over Area A.....	18
4.6 GPR scan lines conducted over the gravel driveway and grassy area south of the former remote assembly building in Area B.....	20
4.7 GPR profile obtained along the 15 south line, south of the former remote assembly building in Area B.....	21
4.8 GPR profile obtained along the 0 west line, south of the former remote assembly building in Area B.....	22

# LIST OF FIGURES (CON'T)

<u>Figure</u>	<u>Page</u>
4.9 Map of subsurface features observed in GPR profiles taken over the area south of the former remote assembly building in Area B.....	23
4.10 View of Nuclear Lake taken from the earth dam area....	25
4.11 Grid system with 100 meter centers established on Nuclear Lake.....	26
4.12 Magnetometer scan lines conducted over Nuclear Lake...	27
4.13 Survey boat equipped for the magnetic survey of Nuclear Lake.....	29
4.14 Map of magnetic anomalies detected in the magnetometry survey of Nuclear Lake.....	30
4.15 Survey boat equipped for the GPR survey of Nuclear Lake.....	31
4.16 GPR scan lines conducted over Nuclear Lake.....	32
4.17 GPR profile obtained along the 10 east line on Nuclear Lake.....	34
4.18 GPR profile obtained over a reflective target placed in the lake at a depth of 13 feet.....	35
4.19 Map of prominent GPR reflectors observed in the GPR survey of Nuclear Lake.....	36
A.1 Variation of maximum depth of penetration as a function of attenuation for different frequencies and dielectric constants.....	A-5

## LIST OF TABLES

<u>Table</u>		<u>Page</u>
4-1	Estimated Coordinates, Depth, and Size of GPR Reflectors Detected in GPR survey of Nuclear Lake.....	37
A-1	Approximate VHF Electromagnetic Parameters of Typical Earth Materials.....	A-4

## 1.0 Introduction

Ground Penetrating Radar (GPR) has been successfully applied to the subsurface characterization of hazardous waste sites (HWS). The technique provides a quick, cost effective means of HWS hydrogeologic site assessment. This paper summarizes GPR field investigations conducted by GEO-CENTERS, INC. at two different and geologically distinct HWS. One GPR field investigation was conducted at the site of a former gasoline station to detect underground fiber glass gasoline storage tanks and associated subsurface pipes. The other GPR field investigation was conducted at the site of a former experimental nuclear reactor. This investigation consisted of two land based surveys to detect subsurface pipes and tanks and the search of a 50 acre lake for metal drums, believed to have been disposed of in the lake. Examples of field data are presented along with interpretive maps detailing the successful results of these investigations. A discussion of electromagnetic wave propagation through the earth is included as Appendix A.

## 2.0 Ground Penetrating Radar

The principle of ground penetrating radar (GPR) involves the generation of a wavetrain of electromagnetic radiation in the frequency range of 10 to 1000 MHz at the surface of the earth. In accordance with the laws of classical electromagnetism, the wave propagates through the subsurface with material dependent attenuation. When the wavetrain encounters interfaces between materials of different electromagnetic properties, the wave is partially reflected. This reflected energy is then detected by the surface receiver, and the travel time between transmission and detection is recorded. If the velocity of propagation is known, the time interval measured can be converted into a depth.

The equipment required in a GPR survey consists of an antenna, a transmitter and receiver, a control unit, a data output device, and a power supply. A radar antenna is a radio antenna designed to provide a high signal-to-noise ratio and either emits a radar pulse, receives a radar pulse, or does both. The transmitter, when triggered, generates a short duration pulse ranging from 1 to 6 nanoseconds. The pulse repetition rate is typically 50 KHz which is controlled by a 50 KHz clock.

The control unit consists of a transmit-receive selector, a radar signal receiver system, and an ancillary signal processing unit. The transmit-receive selector switches the antenna from the transmit mode to the receive mode and disables the pulse transmitter a few nanoseconds after the transmitter is triggered. The receiver system amplifies the reflected signal received by the antenna and transforms the signal from radio frequencies to audio frequencies so that the signal can be displayed or recorded. The reflected signals, which are sinusoidal in shape, are intensity modulated and transformed into a series of dark and light bands on the printer/plotter. The more positive or negative signal amplitudes appear as darker bands, while signal amplitudes closer to zero appear as lighter bands. The ancillary signal processing unit performs a variety of functions in order to apply various filters to the data.

A Geophysical Survey Systems, Inc. (GSSI) System 7 was used to conduct the surveys. Figure 2.1 presents a block diagram of a typical GPR system. A number of antennas are available ranging from 10 MHz (the GEO-CENTERS proprietary deep penetrating antenna) to 1000 MHz.



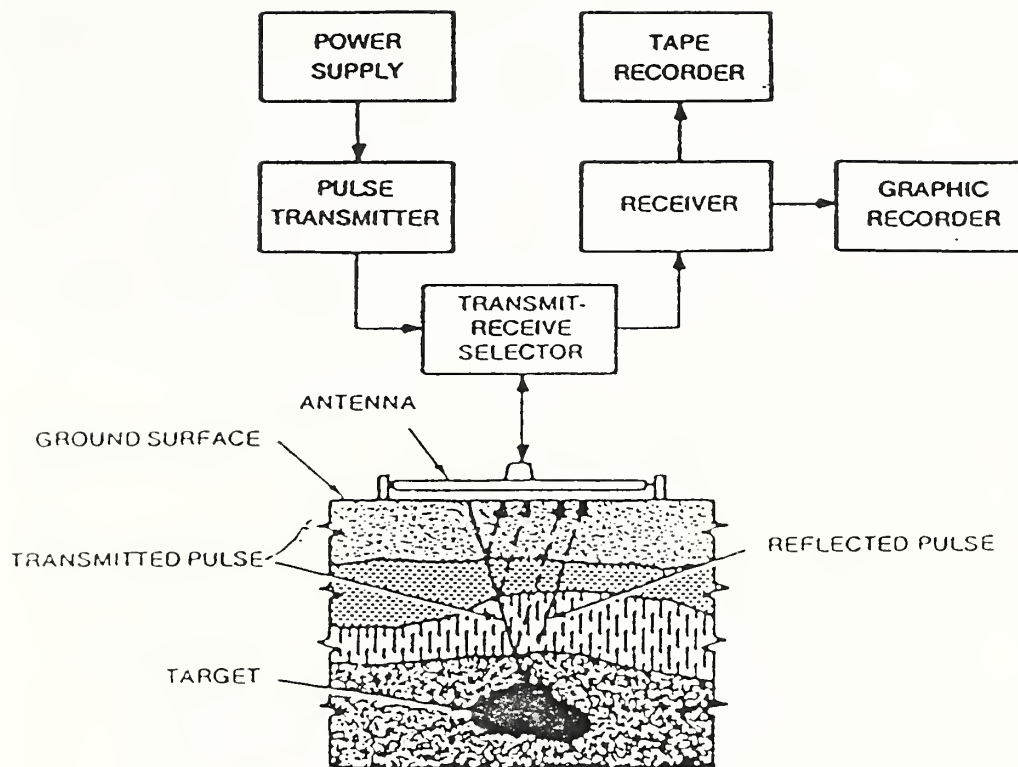


Figure 2.1. Ground penetrating radar (GPR) system, block diagram.

### 3.0 GPR Investigation of a Former Gasoline Station in Manchester, New Hampshire.

GEO-CENTERS, INC. conducted a GPR field investigation of a former gasoline station in Manchester, New Hampshire on September 3, 1987. The purpose of this investigation was to locate subsurface objects to aid in the subsequent installation of monitoring wells at the site. Of particular interest was the delineation of three 4000 gallon fiber glass storage tanks and subsurface pipes associated with them. Also of interest was the location of a municipal water main and subsurface pipes associated with a septic tank and waste oil tank behind the station.

Two views of the site are presented in Figure 3.1. A grid system with 5 foot centers was established over the 115 foot by 90 foot area and the 300 MHz antenna was manually towed over the site along the series of GPR scan lines indicated in Figure 3.2. A representative example of GPR profiles obtained over the three 4000 gallon fiber glass gasoline storage tanks is presented in Figure 3.3. These profiles were recorded over a time window of 60 nsec. An actual depth of 3.25 feet to the top center of the middle tank was measured in the field. These profiles were recorded over a time window of 60 nsec, therefore, a velocity of electromagnetic propagation of 0.11 ft/nsec was calculated for the site. This value, indicative of soil conditions at the site, was used to estimate depths to all GPR reflectors detected.

All data interpretation and analyses were performed in the field. Areas beneath which GPR reflectors were detected are indicated in Figure 3.4. Fuel transfer pipes were observed to extend from the fiber glass storage tanks to the pump island

area. Tank ventilation pipes were observed to extend from the tanks to the rear of the station. A large pipe, believed to be the municipal water main, was observed to extend from the road towards the storage tank area. Pipes or electrical conduit were observed to extend from the pump island area to the rear of the station near the waste oil treatment tank. Also observed was an area east of the station beneath which a number of deeply buried pipes were observed. A representative GPR profile over these pipes is displayed in Figure 3.5. Each of these areas was outlined on the pavement with survey paint and designated as an area within which monitoring wells should not be installed.

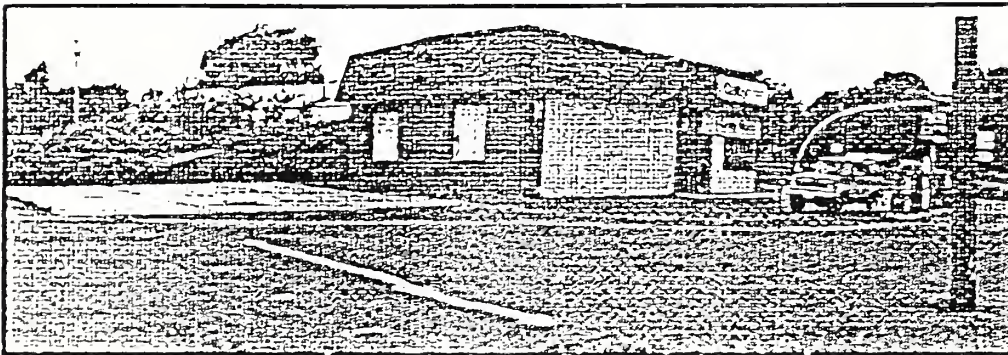
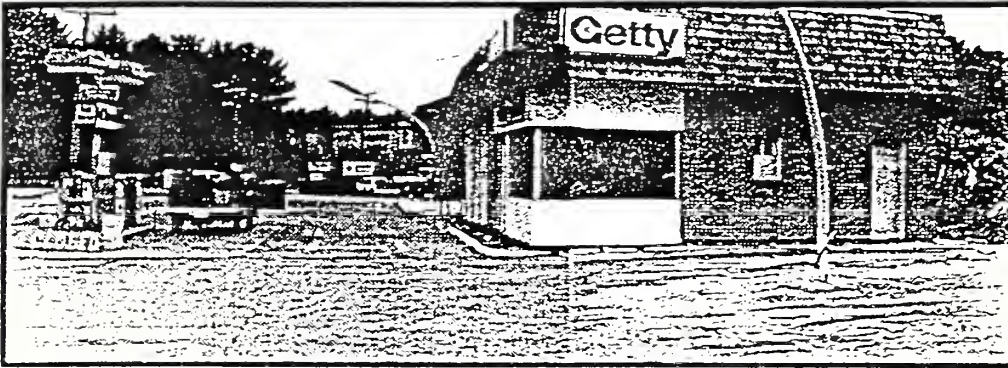


Figure 3.1. Two views of the former gasoline station.

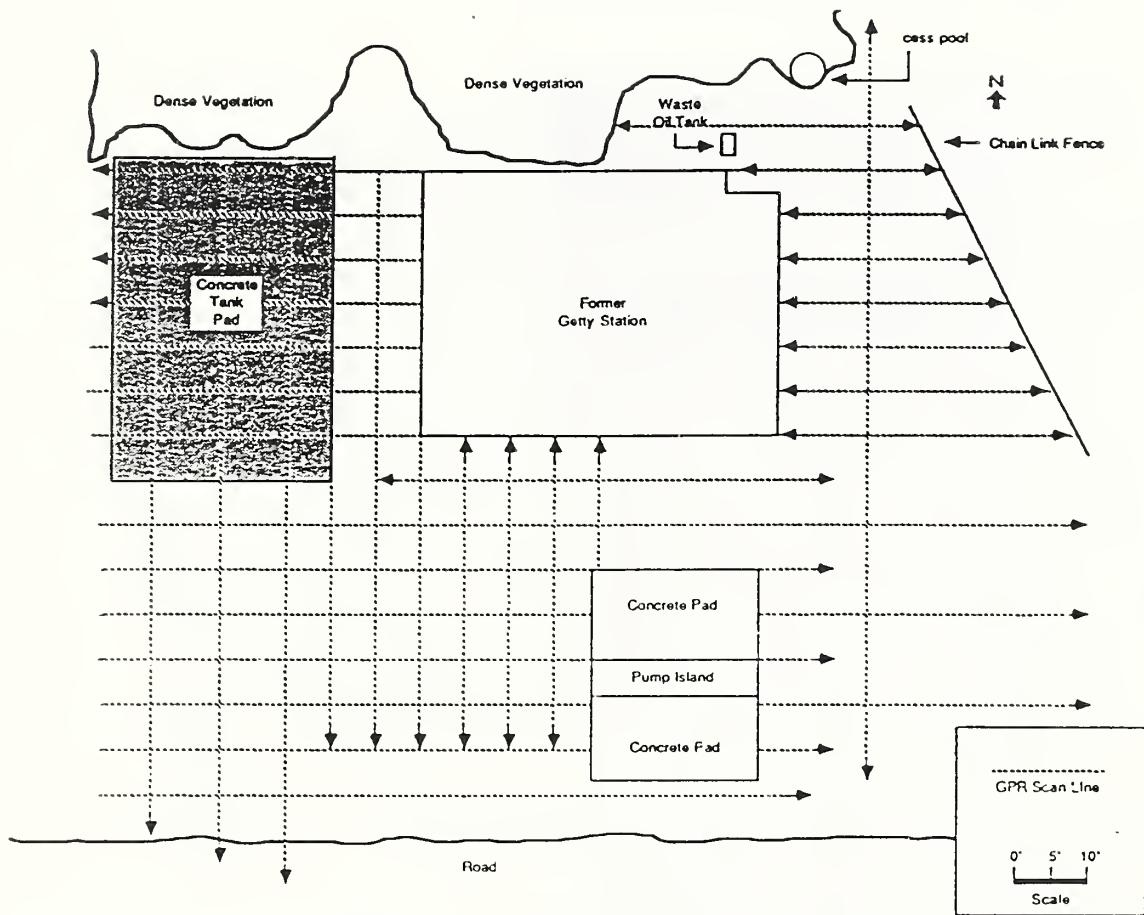


Figure 3.2. GPR scan lines conducted over the site of a former gasoline station.



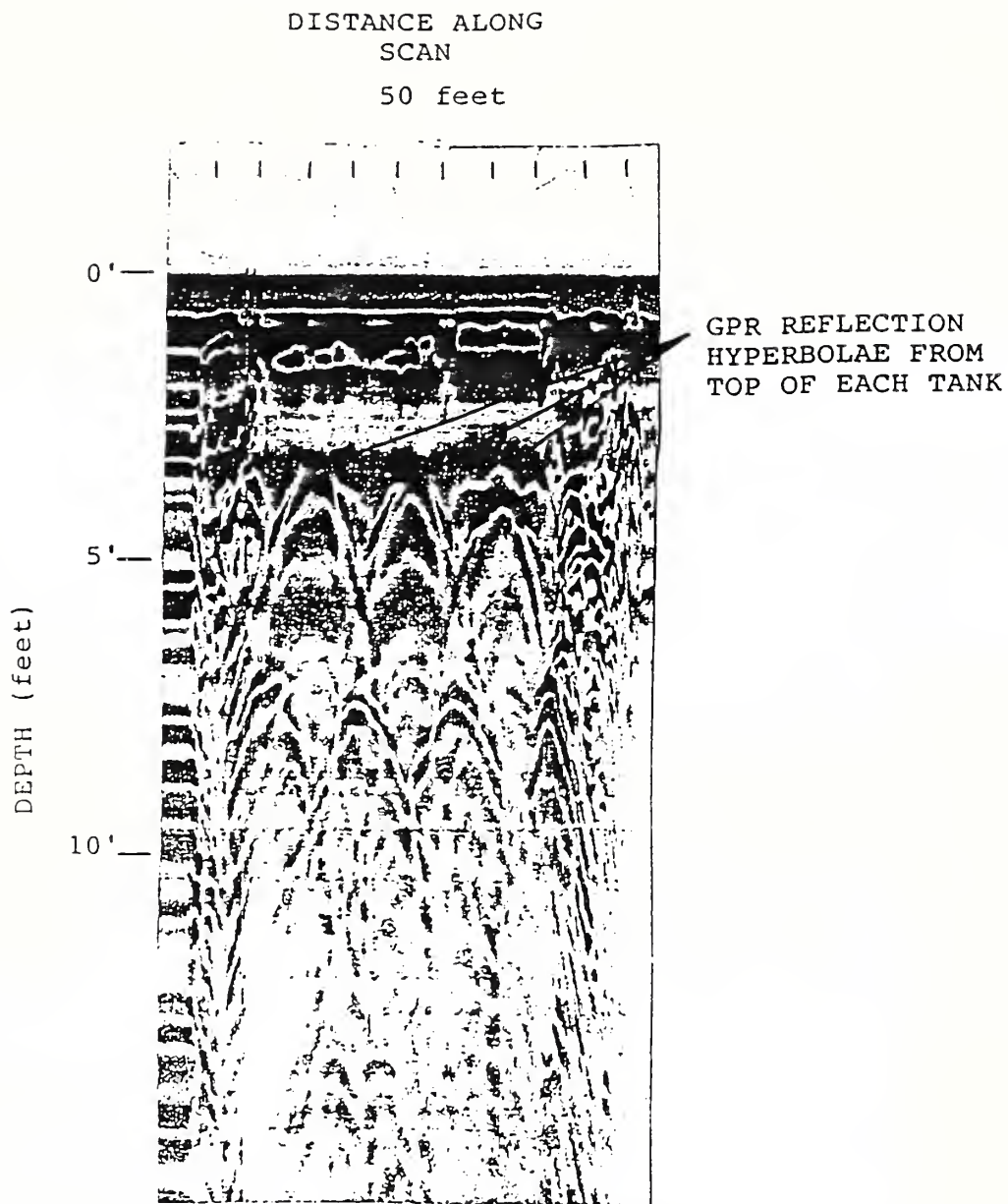


Figure 3.3 GPR profile obtained over the three 4000 gallon fiber glass gasoline storage tanks.



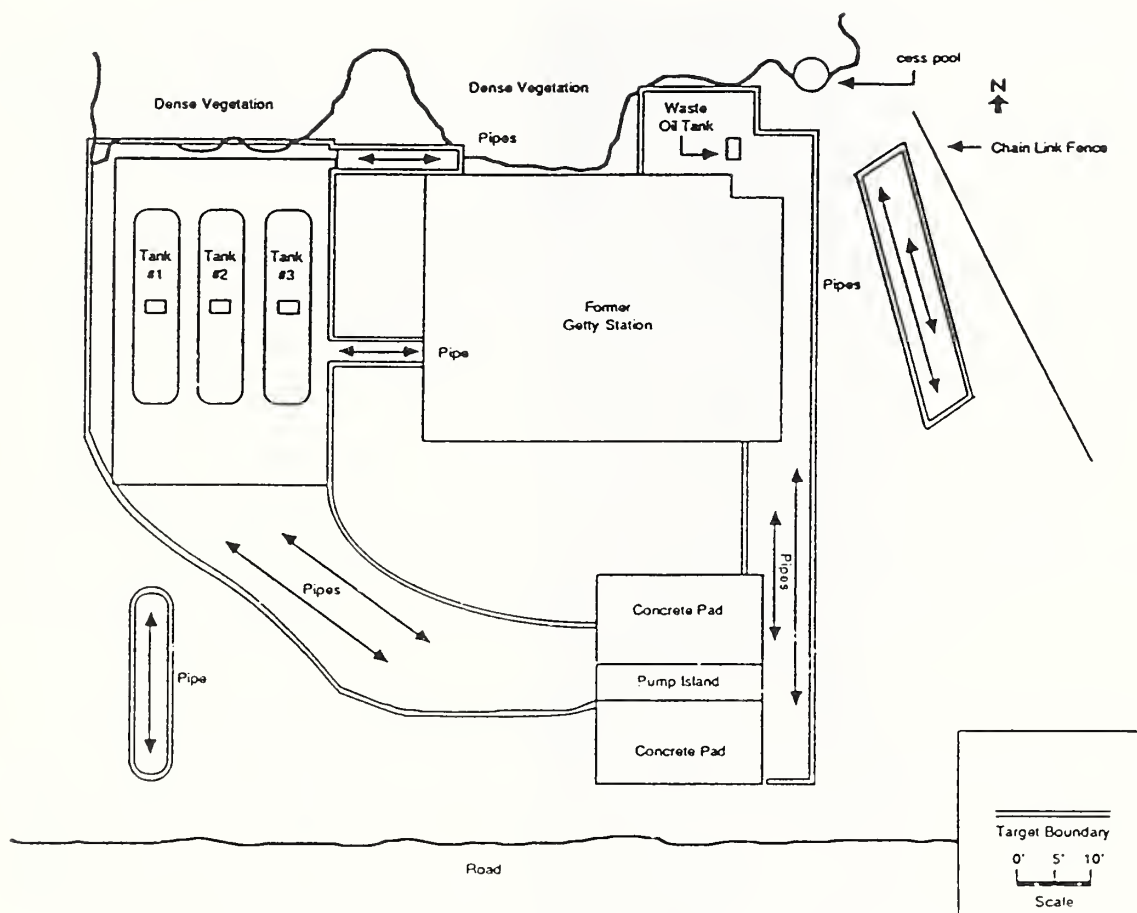


Figure 3.4. Map of subsurface features observed in GPR profiles obtained over the site of a former gasoline station.

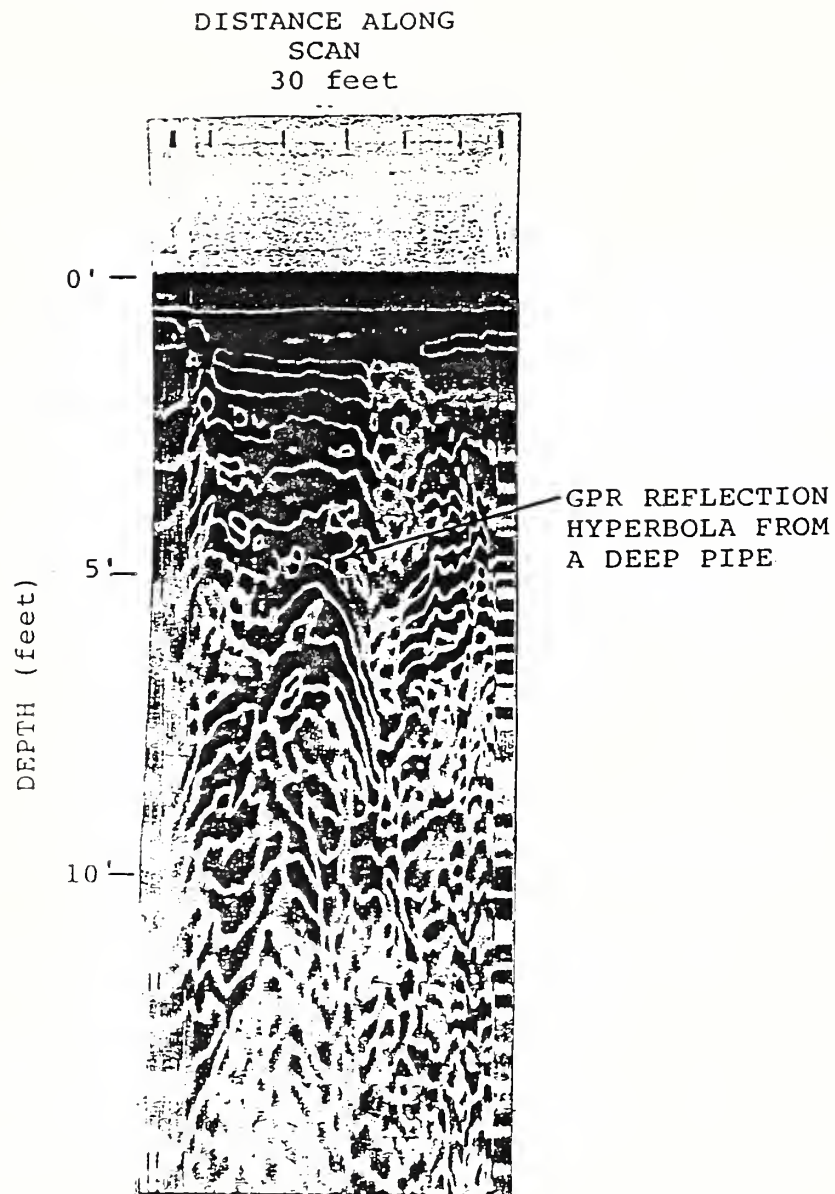


Figure 3.5. GPR profile obtained over pipes east of the former gasoline station.

#### 4.0 Geophysical Investigation of the Nuclear Lake Site Pawling, New York.

GEO-CENTERS, INC. conducted a GPR field investigation of the Nuclear Lake Site in September, 1986 under contract to the Oak Ridge Associated Universities (ORAU) in support of their radiological assessment of the site. The site, near Pawling in Dutchess County, New York, is a 1137 acre parcel consisting of a 53 acre lake, a site access road, vacant buildings, parking lots, and underground utilities (Figure 4.1). The site is heavily wooded and public access is restricted. In 1972 an explosion occurred near the plutonium storage facility in a building used for the testing of nuclear reactor fuel rods, spraying plutonium dust into the air. After an extensive clean-up effort, the contaminated buildings were closed and abandoned. The site is currently owned by the National Park Service who purchased it in 1979 with the intention of re-routing the Appalachian Trail through the area.

The first phase of the field investigation consisted of GPR surveys of the parking lot west of the plutonium storage facility (Area A) and the grassy area south of the remote assembly building (Area B) which was used for decontamination purposes by workers during the clean-up effort. These surveys were conducted in order to identify locations of subsurface leaching fields, drain pipes, and septic tanks to assist ORAU in the subsequent installation of monitoring wells at the site. The second phase of the investigation consisted of a magnetometry survey of the lake combined with a GPR survey in order to detect and locate metallic 55 gallon drums which may have been disposed of in the lake.

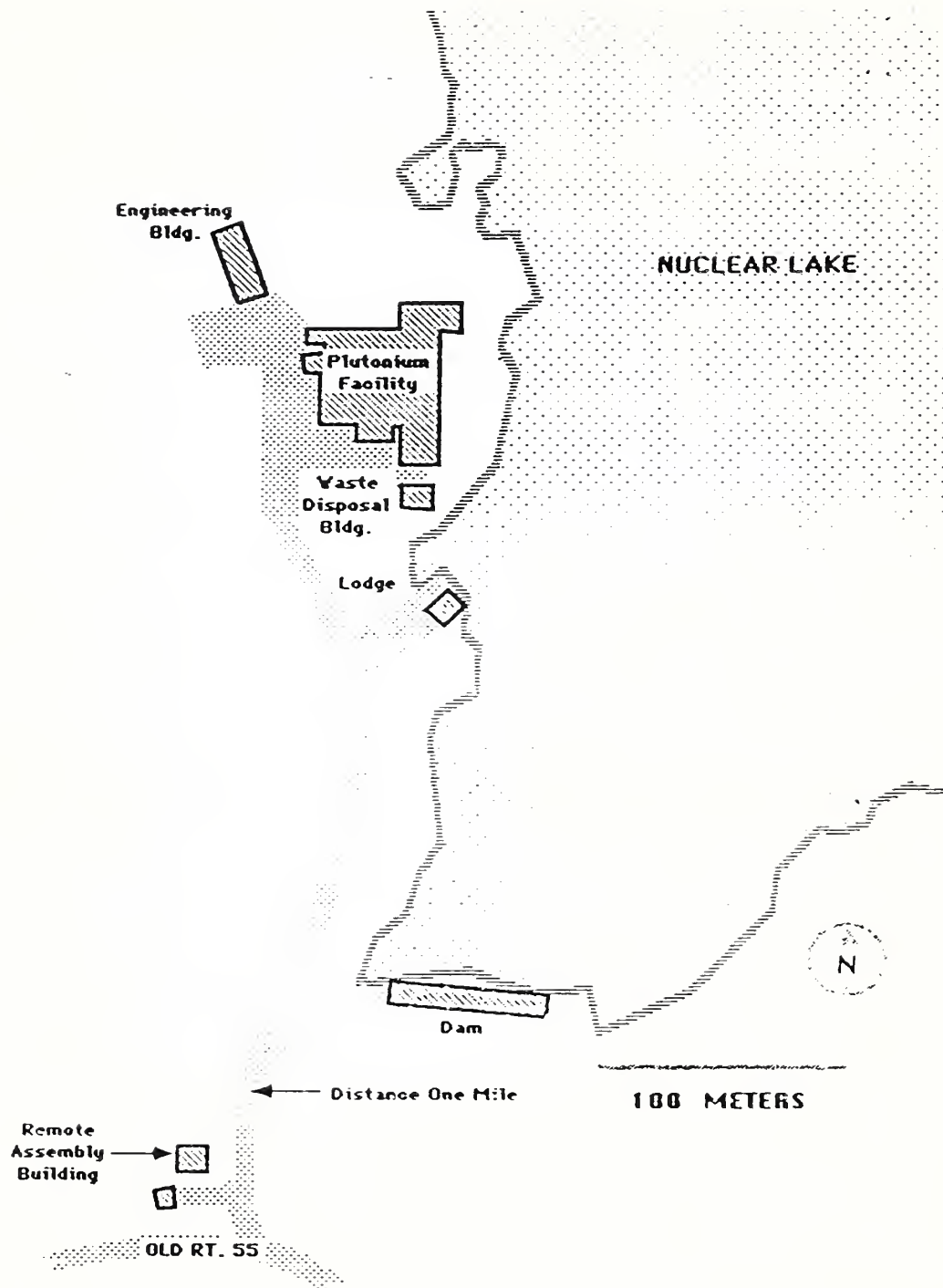


Figure 4.1. Site map of the Nuclear Lake Site;  
Dutchess County, New York.



GEO-CENTERS, INC.

Area A consists of a wooded and paved area beneath which a leaching field and associated subsurface pipes are suspected to exist. Bulk resistivity measurements using a Wenner spread with a spacing of 1 meter were obtained for the purpose of estimating the maximum possible depth of electromagnetic penetration. An average reading of 310 ohm-meters was obtained. The maximum depth of electromagnetic penetration with the 300 MHz antenna employed was estimated to be 23 feet from Figure A.1 and soil conditions at the site.

The 300 MHz antenna was manually towed over the area at a rate of about 1 ft/sec along the series of GPR scan lines indicated in Figure 4.2. The transmit-receive selector on the control unit was set so as to allow for these scans to be recorded over a time window of 100 nsec. Four GPR scan lines spaced 1 meter apart were also run from south to north over a suspected burial pit north of the plutonium storage facility. These scans were recorded over a time window of 160 nsec in an effort to obtain deeper ground penetration.

The soil in Area A was observed to be fairly sandy with high water content. The velocity of electromagnetic propagation was, therefore, estimated to be 4.35 cm/sec from Table A-1 and Equation A-1. This value was then used to obtain depth estimates to subsurface reflectors observed in radar profiles taken over this area.

Representative examples of GPR profiles obtained are displayed in Figures 4.3 and 4.4. Figure 4.3 is a GPR profile obtained over the paved area along the 20 east line south of the plutonium facility. Hyperbolae corresponding to reflections from eight underground pipes are prominently displayed in the profile.

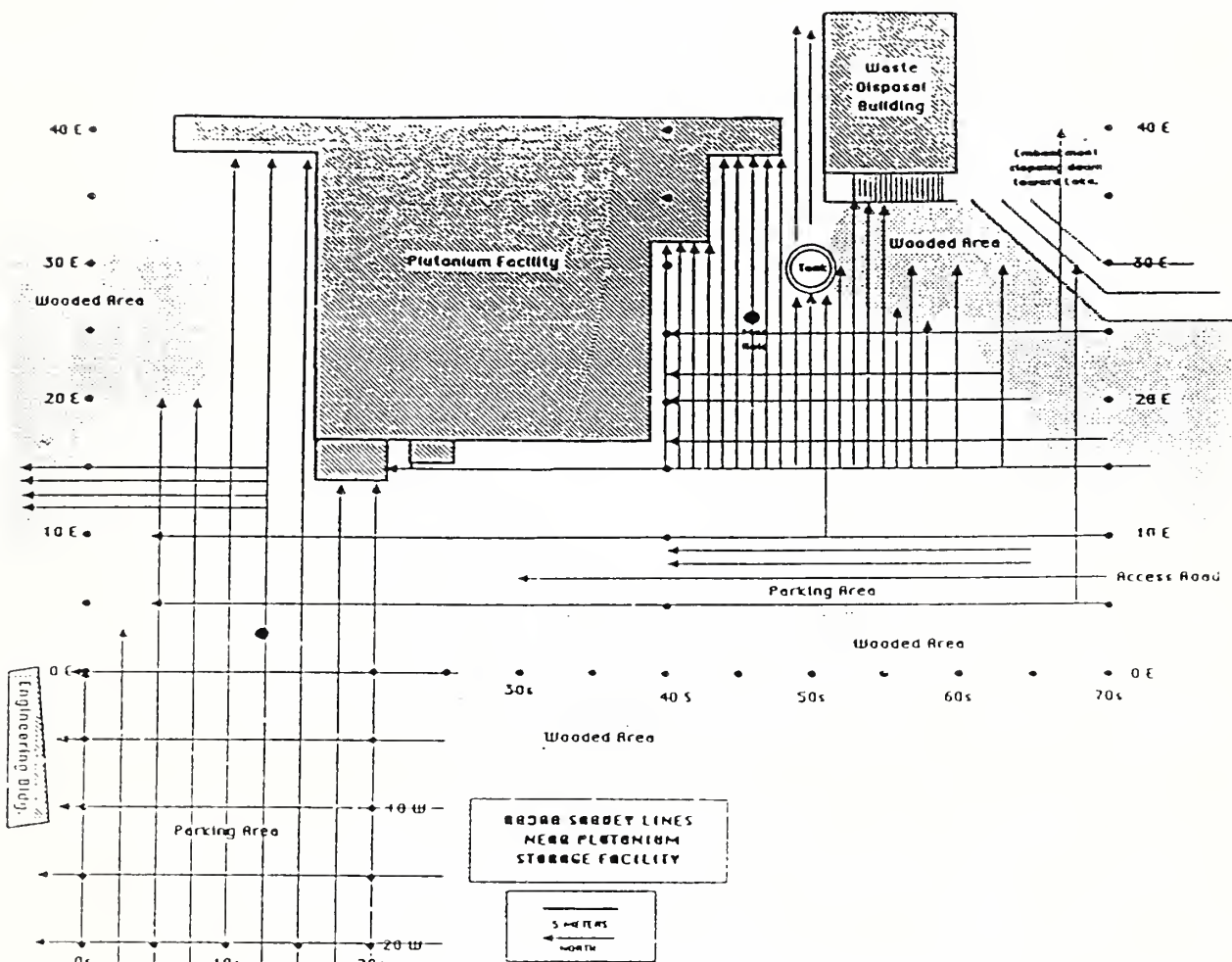


Figure 4.2. GPR scan lines conducted over Area A.



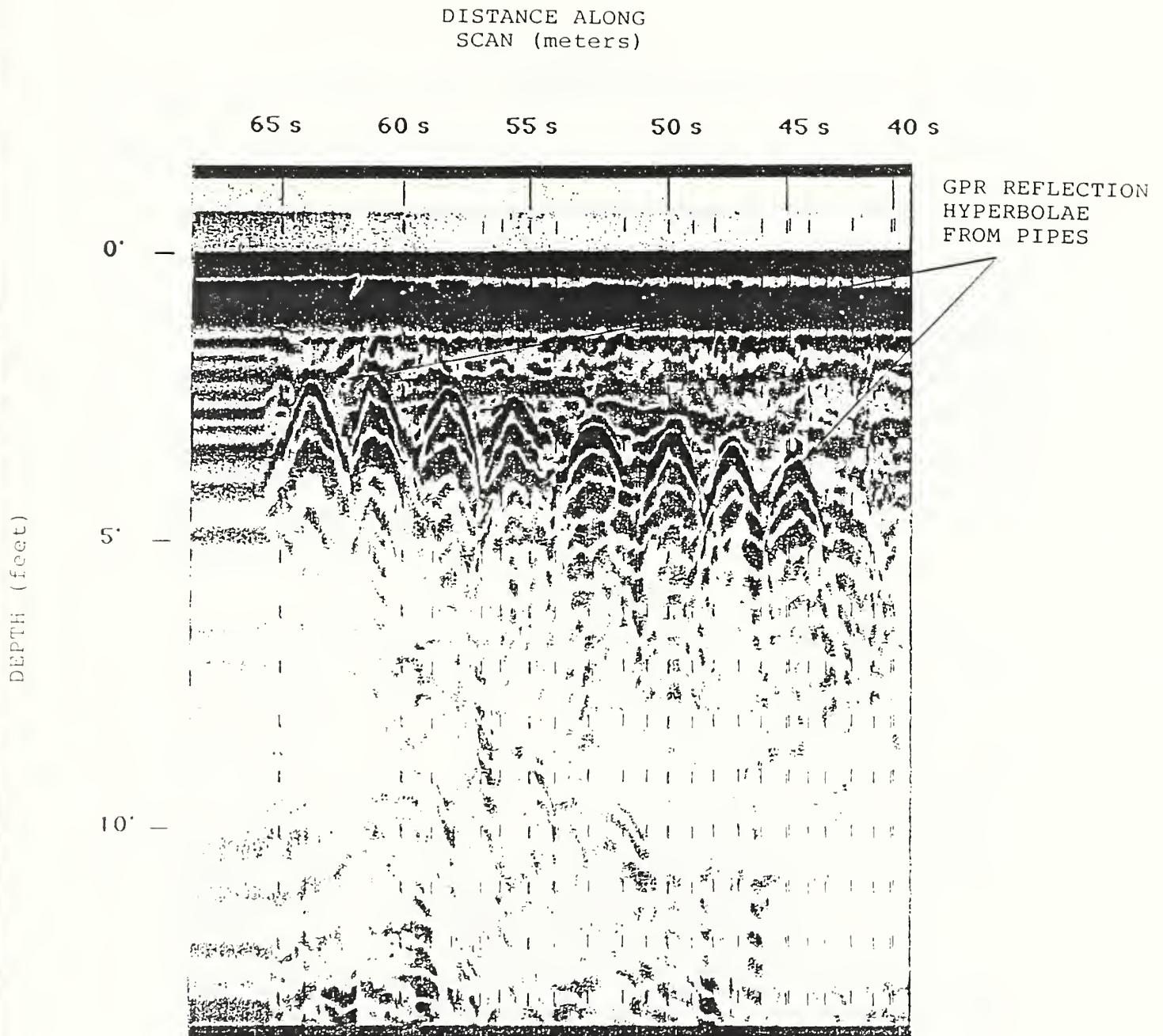


Figure 4.3. GPR profile obtained along the 30 east line south of the plutonium storage facility.

DISTANCE ALONG  
SCAN (meters)

10 E

15 E

20 E

25 E

30 E

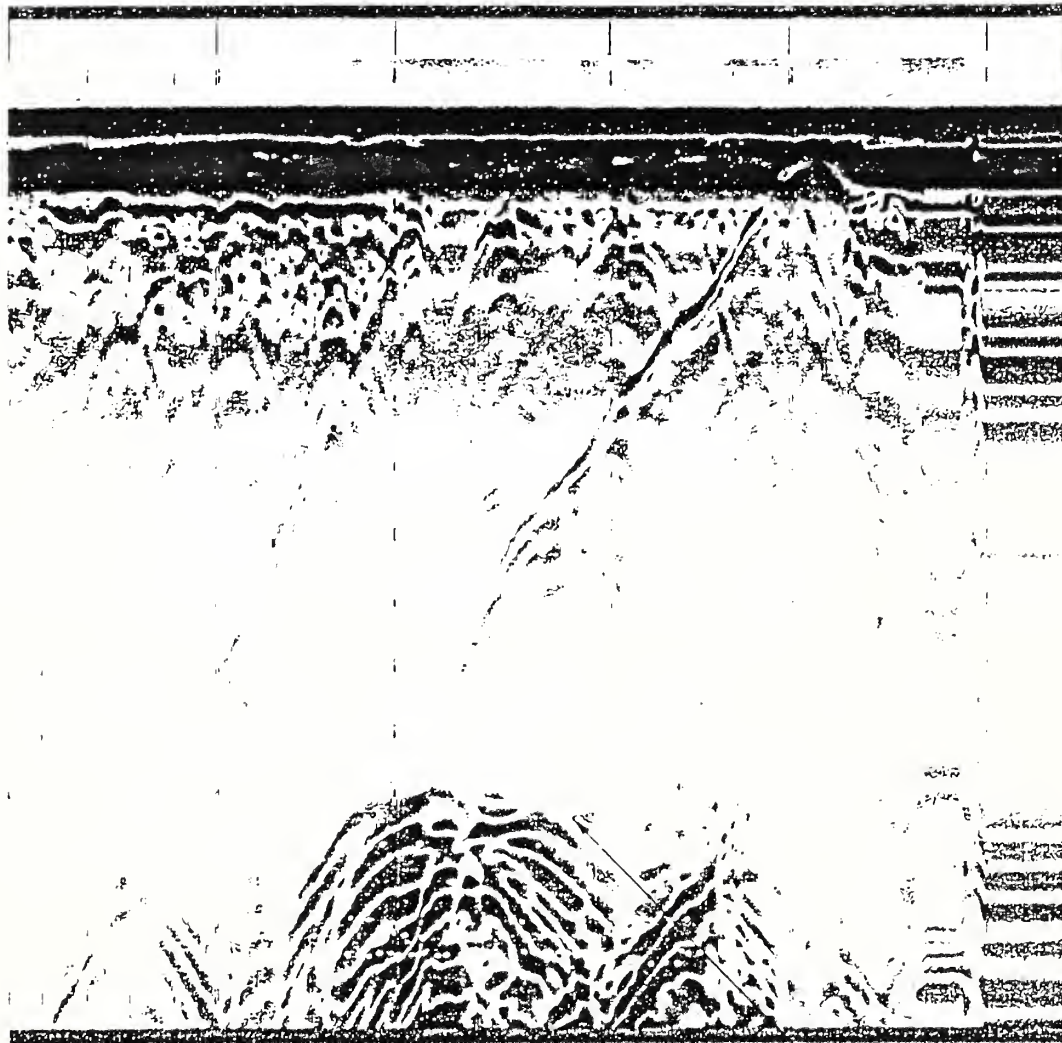
35 E

0'

5'

10'

DEPTH (feet)



REFLECTOR

Figure 4.4. GPR profile obtained along the 12.5 south line north of the plutonium facility.



Figure 4.4 is a GPR profile obtained over the grassy area along the 12.5 south line north of the plutonium facility. A deep reflective mass, approximately 11 feet deep, is observed in this profile.

A map of subsurface features observed in GPR profiles observed in Area A is presented in Figure 4.5. The location and extent of underground pipes were marked directly on the pavement with spray paint upon completion of the survey. With the exception of two pipes running from the plutonium facility to the cement retention tank, all pipes in the area south of the plutonium storage facility appear to be associated with a manhole near the center of the parking lot. The suspected leaching field is believed to exist beneath the wooded and paved area west of the waste disposal building near the access road.

A total of three shallow underground pipes were observed in the area west of the plutonium storage facility, none of which are believed to be associated with the manhole near the center of the parking lot. Other features of interest include a deep reflective mass beneath the grassy area north of the plutonium facility and an area of disturbed earth indicative of a possible trench. A weak reflection was observed to exist at an approximate depth of 9 feet beneath this area. GPR scans along lines 15 and 20 west were continued north along the western side of the engineering building. However, no features of interest were observed.

Area B consists of a gravel driveway and grassy area beneath which a septic system associated with the remote assembly building is known to exist. The 300 MHz antenna was manually





towed over this area along the series of GPR scan lines indicated in Figure 4.6. These scans were recorded over time window of 100 nsec.

The soil in Area B is fairly similar to that of Area A. The same velocity of electromagnetic propagation was, therefore, used to obtain estimations of depths to subsurface reflectors. Representative examples of GPR profiles obtained are displayed in Figures 4.7 and 4.8. Figure 4.7 is a GPR profile obtained along the 15 south line, south of the former remote assembly building. A shallow underground pipe, approximately 1.5 feet deep is observed in this profile. Figure 4.8, a GPR profile obtained along the 0 west line, displays the deep reflector observed to exist southeast of the former remote assembly building.

A map of subsurface features observed in GPR profiles taken over Area B is presented in Figure 4.9. Features of interest include three shallow underground pipes associated with a septic system currently in use at the building, a shallow reflector adjacent to the building, a deep reflector southwest of the building, and three areas of shallow metallic debris in the southern portion of the site. The location and extent of these features were marked with spray paint on the ground surface of the area upon completion of the survey.

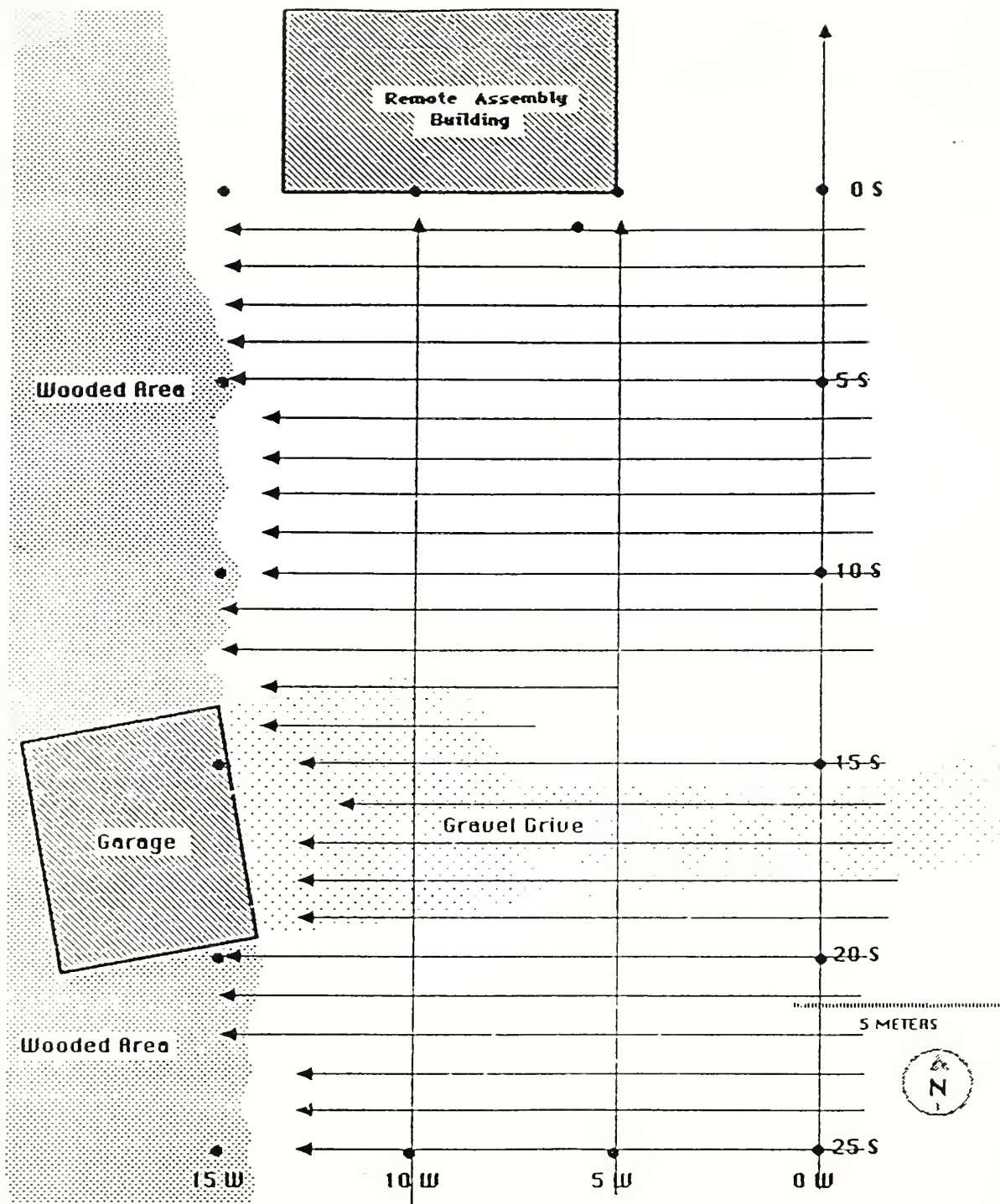


Figure 4.6. GPR scan lines conducted over the gravel driveway and the grassy area south of the remote assembly building in Area B.



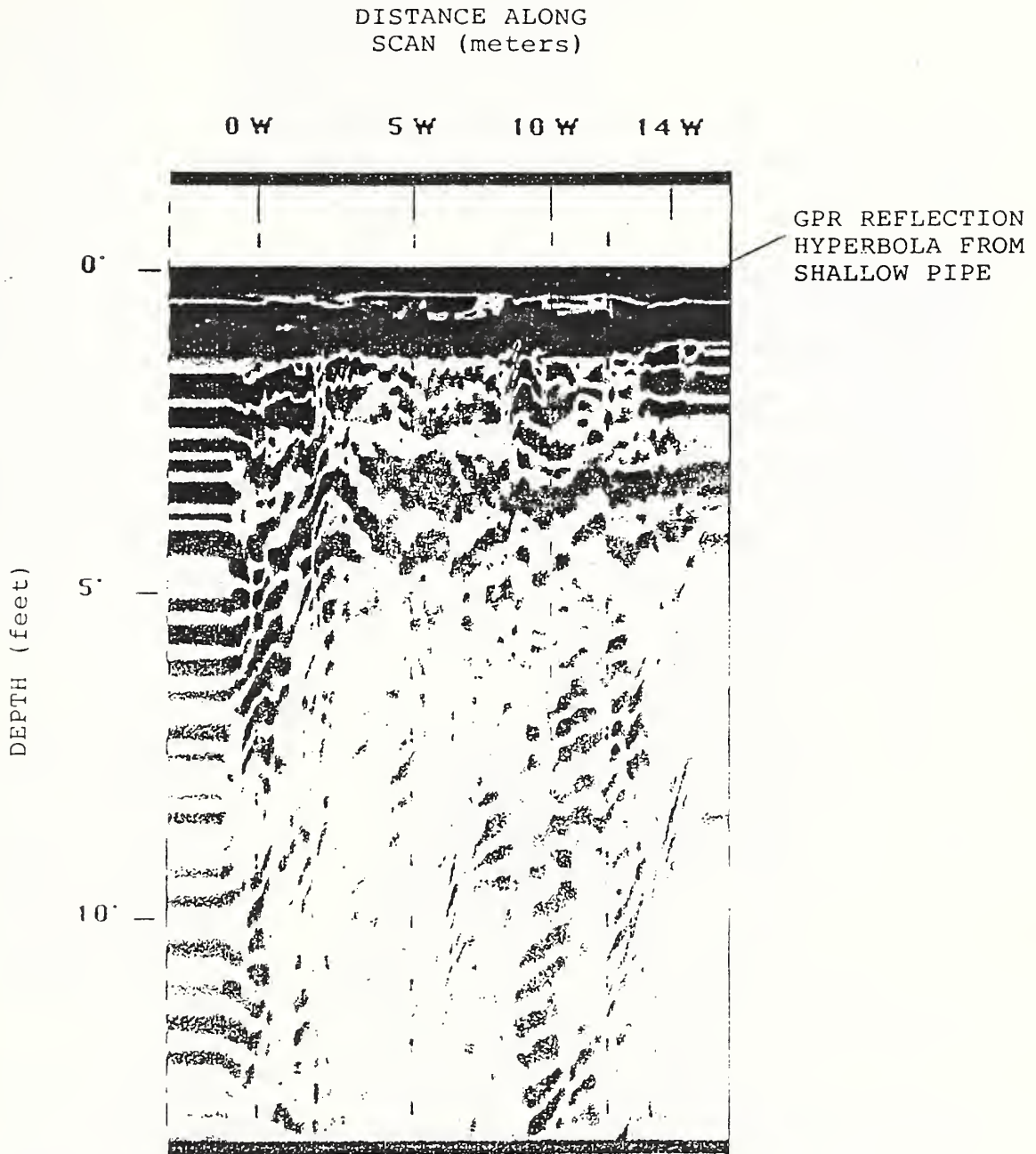


Figure 4.7. GPR profile obtained along the 15 south line, south of the former remote assembly building in Area B.

DISTANCE ALONG  
SCAN (meters)

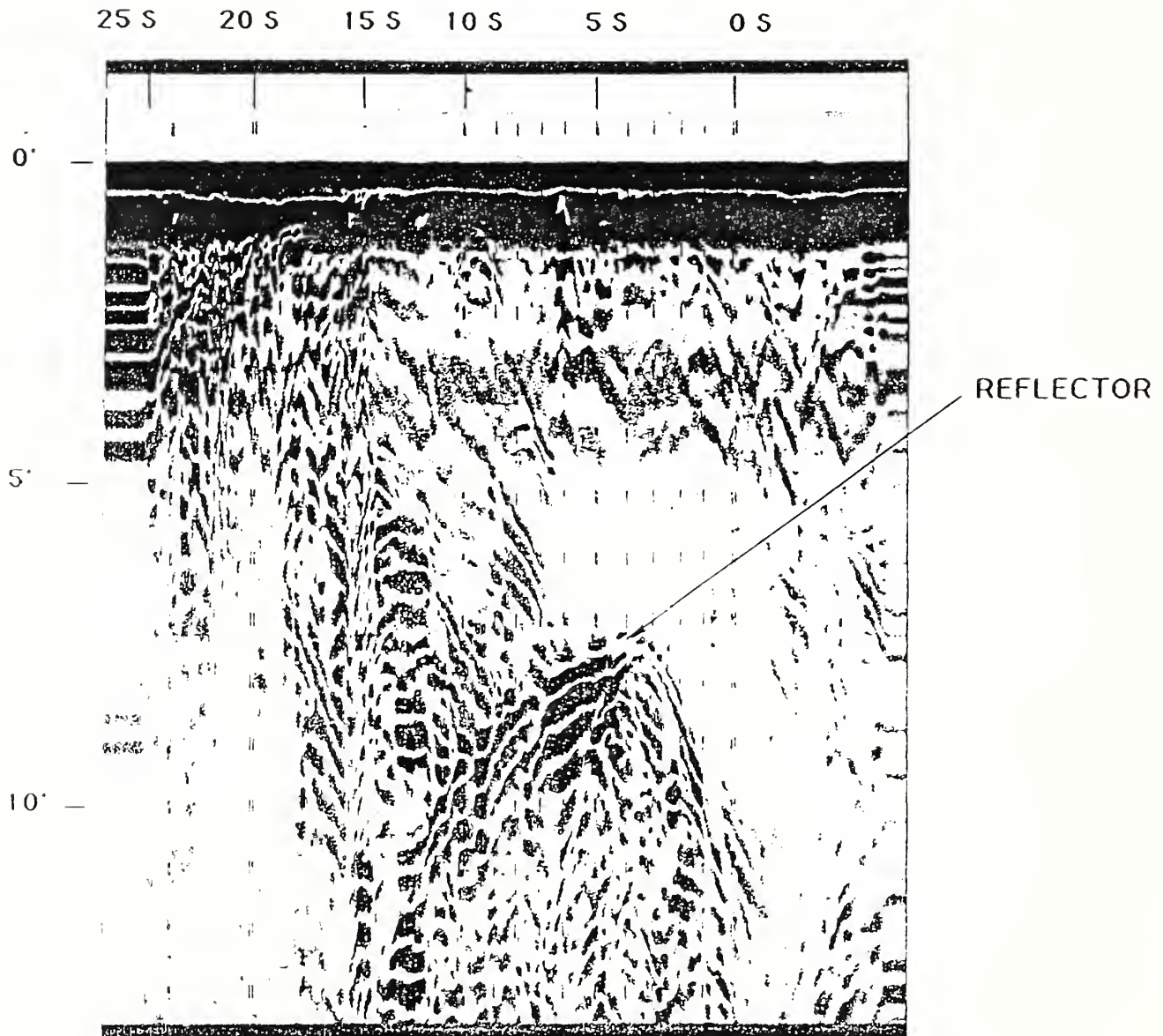


Figure 4.8. GPR profile obtained along the 0 west line, south of the former remote assembly building in Area B.



GEO-CENTERS, INC.

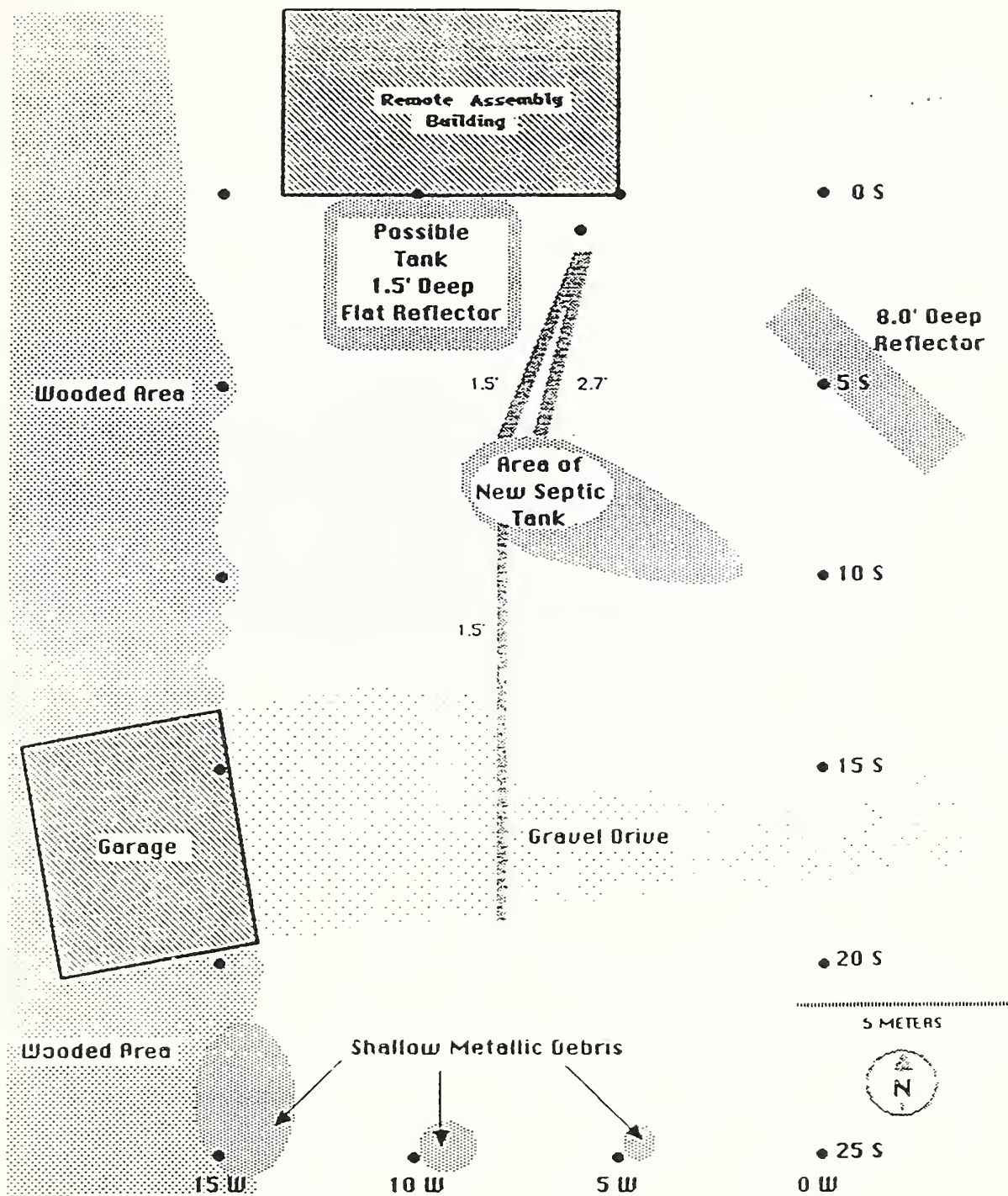


Figure 4.9. Map of subsurface features observed in GPR profiles taken over the area south of the remote assembly building in Area B.



GEO-CENTERS, INC.



A view of Nuclear Lake is presented in Figure 4.10. The lake is about 800 meters long by 300 meters wide and was a large low lying wetland area prior to the construction of the dam (Figure 4.1) in 1948. The average depth of the lake is about 4.0 meters and near shore areas are fairly steep and rocky. The lake bottom is heavily littered with fallen trees, many of which are exposed on the lake surface. A fairly thick layer of sediment was observed to blanket the lake bottom in near shore areas. A small island exists in the southern portion of the lake and an area of shallow rocks, some exposed above the lake surface exist about 100 meters north of the island. The lake water is very murky and visibility is limited. The lake surface remained fairly calm throughout the duration of the survey.

A grid system with 100 meter centers was established on Nuclear Lake. Marker buoys were located at points of intersection (Figure 4.11). A rope extended along the 0 east line across the center of the lake served as a center line and main positional reference for geophysical surveys on the lake. Marker buoys were attached at intervals of 10 meters along ropes extended along the 300 and 600 south lines from the center line to both the eastern and western shores of the lake.

A magnetometry survey of Nuclear Lake was first conducted with a Forster Ferex 4.021 fluxgate magnetometer. The magnetometer was operated in a "static difference" mode in which the difference in the magnetic field, or the vertical gradient, between the two sensors in the probe of the instrument was continuously measured. A series of north-south trending scan lines spaced 10 meters apart were conducted over the entire surface of the lake (Figure 4.12). A dead reckoning method utilizing an on-board compass and the marker buoys located along the 300 and 600 south lines was used to maintain course heading



Figure 4.10. View of Nuclear Lake.



*GEO-CENTERS, INC.*

**Nuclear Lake  
Pauling NY**

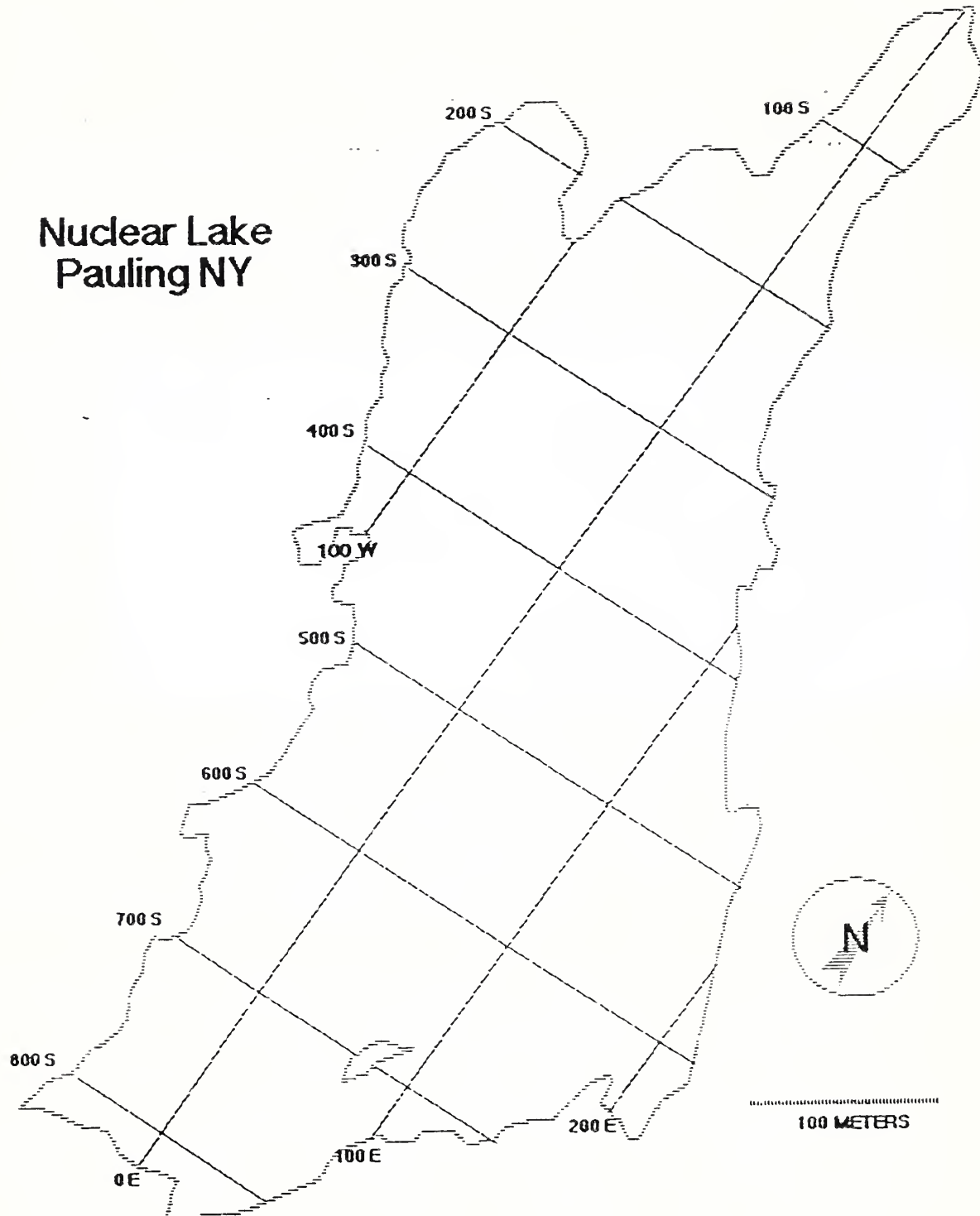


Figure 4.11. Grid system with 100 meter centers established on Nuclear Lake.



**GEO-CENTERS, INC.**



# Magnetometer Survey Lines

## Nuclear Lake Pauling NY

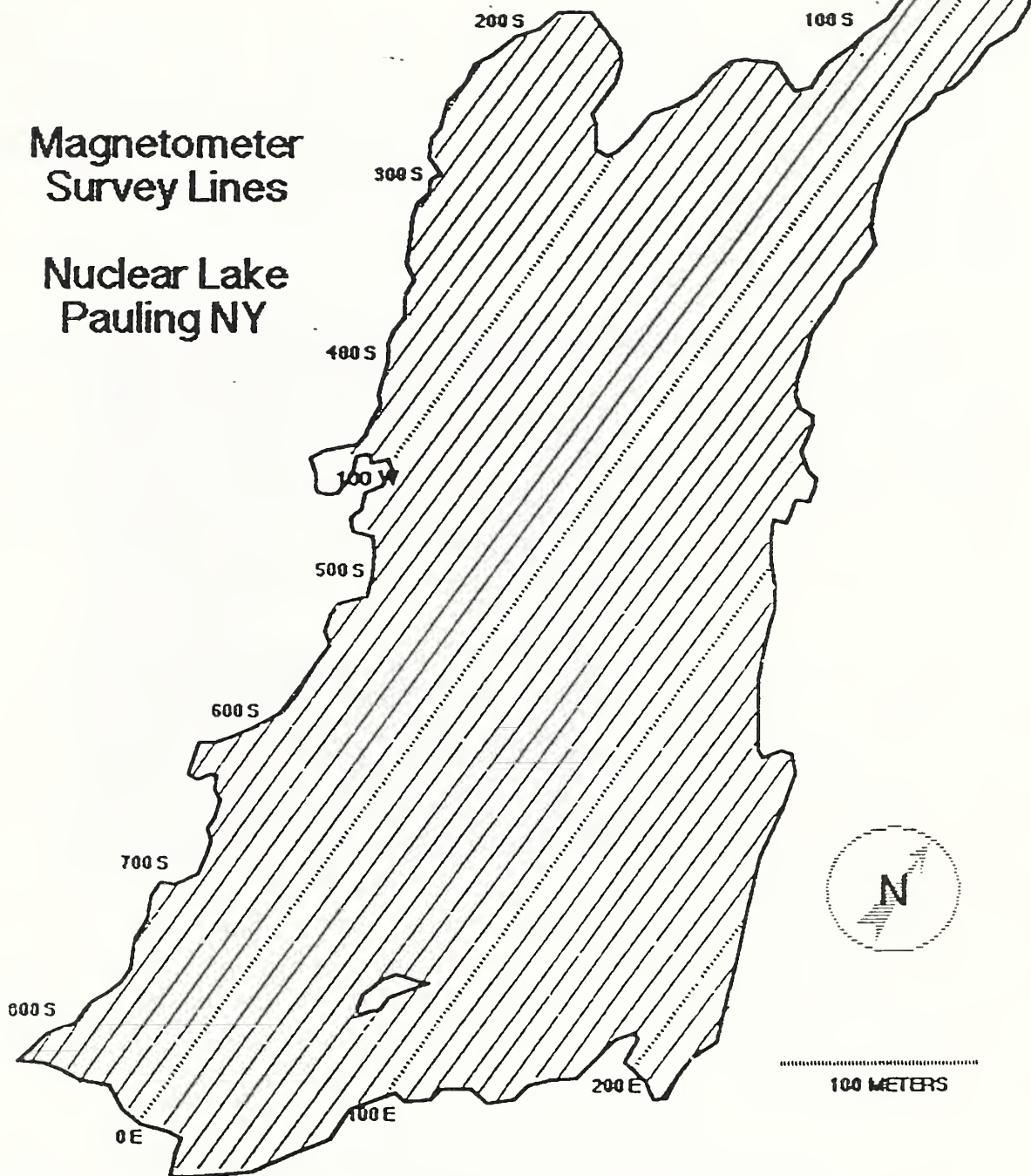


Figure 4.12. Magnetometer scan lines conducted over Nuclear Lake.



GEO-CENTERS, INC.

along each line. Each scan was conducted with the sensor probe of the magnetometer suspended from a wooden boom extended a distance of 1.5 meters from the stern of the survey boat (Figure 4.13). With the exception of shallow areas, the sensor probe was towed a distance of 4 meters below the surface of the lake. A marker buoy was dropped overboard upon the detection of an anomalous magnetic gradient.

Figure 4.14 presents a map of magnetic anomalies detected with the Forster Ferex 4.021 fluxgate gradiometer during the magnetometry survey of Nuclear Lake. The actual location of each magnetic anomaly may differ by as much as  $\pm 5$  meters from marked locations due to positioning difficulties encountered on the lake during the survey. Many of the anomalies near the shore are believed to be associated with bedrock outcroppings.

The GPR survey of Nuclear Lake was conducted with the 300 MHZ antenna suspended from a wooden platform a distance of 1.5 meters from the stern of the survey boat directly on the surface of the lake (Figure 4.15). Six parallel north-south trending GPR scans spaced 10 meters apart were run over the center of the lake between the 5 west and 60 east lines, the most suspect area of possible drum disposal. Another north-south trending scan line was also run along the 100 east line. GPR scans were then run over areas of anomalous magnetic gradient previously detected and marked in the magnetic survey of the lake (Figure 4.16) In order to further define the location, depth, and size of objects possibly associated with each anomaly.

The horizontal beam width of the Geophysical Survey Systems, Inc. (GSSI) 300 MHz antenna used in this survey is  $\pm 45^\circ$ . The width of the zone of total coverage of the lake bottom on either side of a GPR scan is, therefore, equal to the depth of the lake

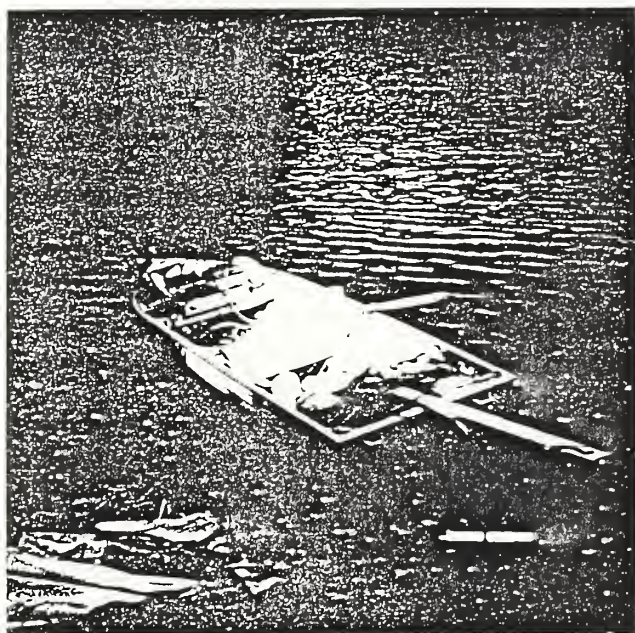


Figure 4.13. Survey boat equipped for the magnetic survey of Nuclear Lake.



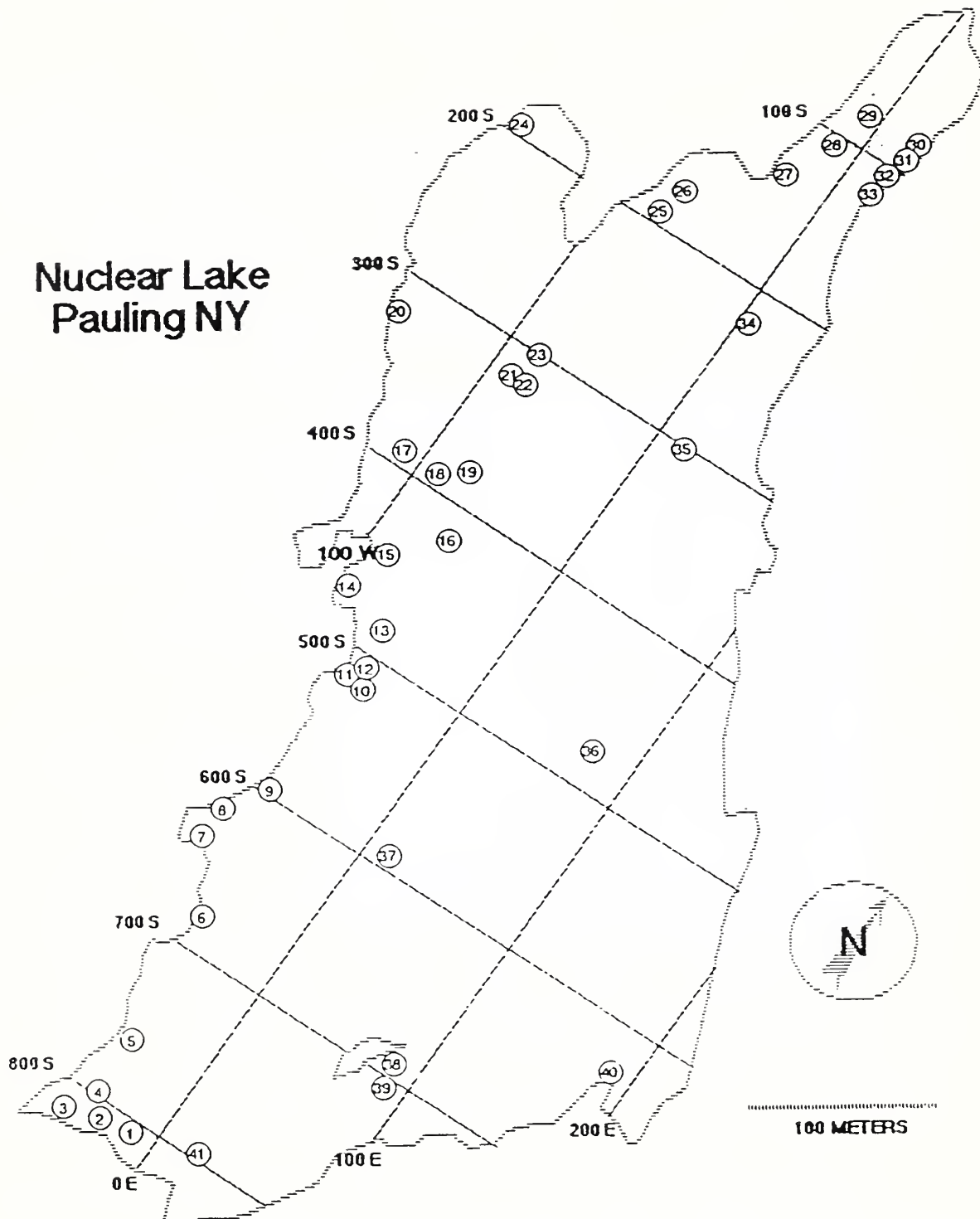


Figure 4.14. Map of magnetic anomalies detected in the magnetometry survey of Nuclear Lake.



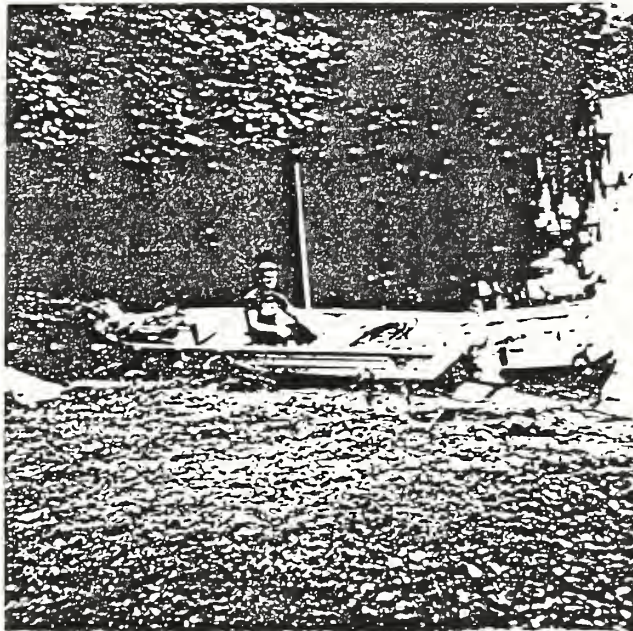
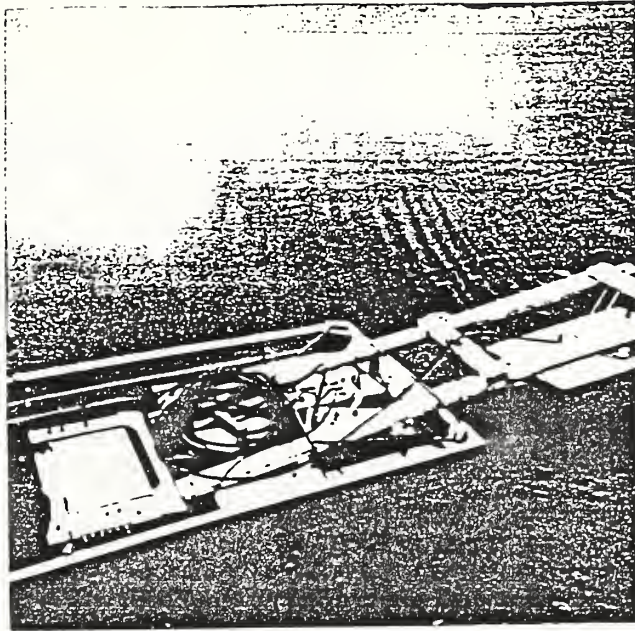


Figure 4.15. Survey boat equipped for the GPR survey of Nuclear Lake.



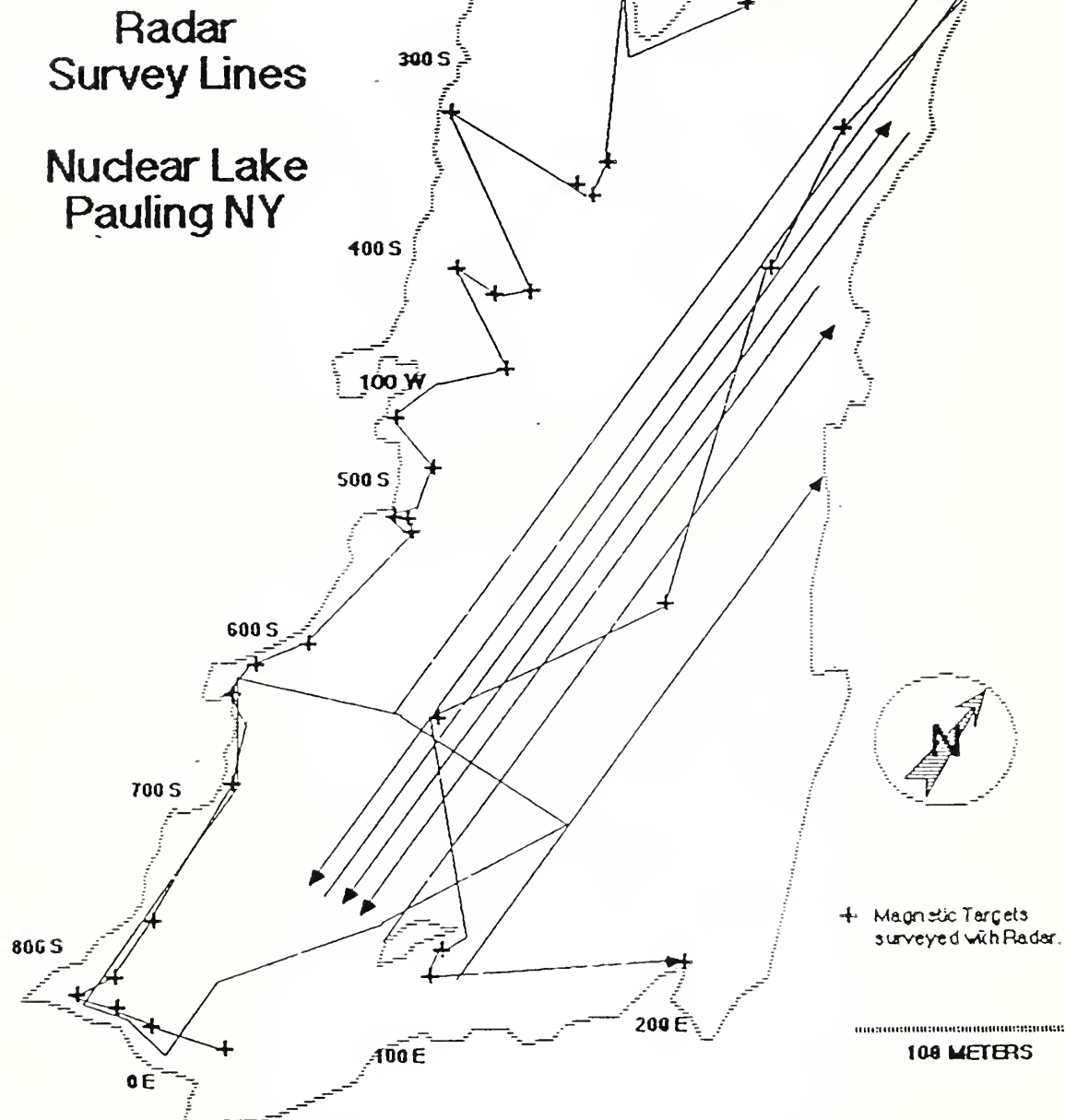


Figure 4.16. GPR scan lines conducted over Nuclear Lake.

at any particular point along the line. Nearly 100% coverage of the lake bottom was achieved with GPR in the area between the 5 west and 60 east lines over which the six parallel north-south GPR scans were conducted. This estimate is based upon an average lake depth of 4.75 meters for this area and a line spacing of 10 meters.

A representative example of GPR profiles obtained in the GPR survey of Nuclear Lake is displayed in Figure 4.17. Strong GPR reflectors, possibly associated with metallic objects on the bottom of the lake are displayed in this profile. Weaker GPR reflectors from dead trees, completely submerged and lying on the bottom of the lake are also displayed in this profile.

A reflective target was placed in the lake at a known depth of 4.0 meters and a GPR scan was run directly over it (Figure 4.18) in order to obtain an indication of the velocity of electromagnetic propagation through the lake. This value was then used to obtain depth estimates to each GPR reflector observed. A map of prominent GPR reflectors observed in profiles taken over Nuclear Lake is presented in Figure 4.19. The approximate location, depth, and size of each reflector is given in Table 4-1.

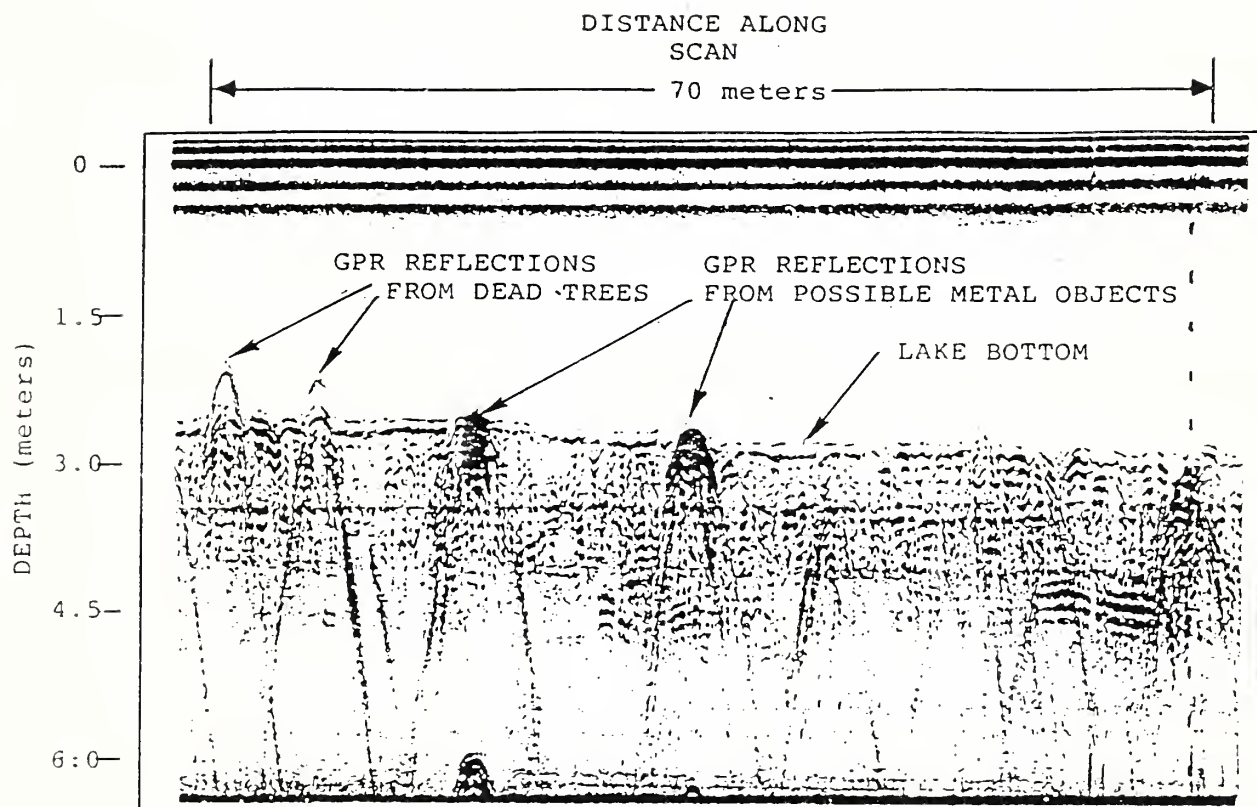


Figure 4.17. GPR profile obtained along the 10 east line on Nuclear Lake.

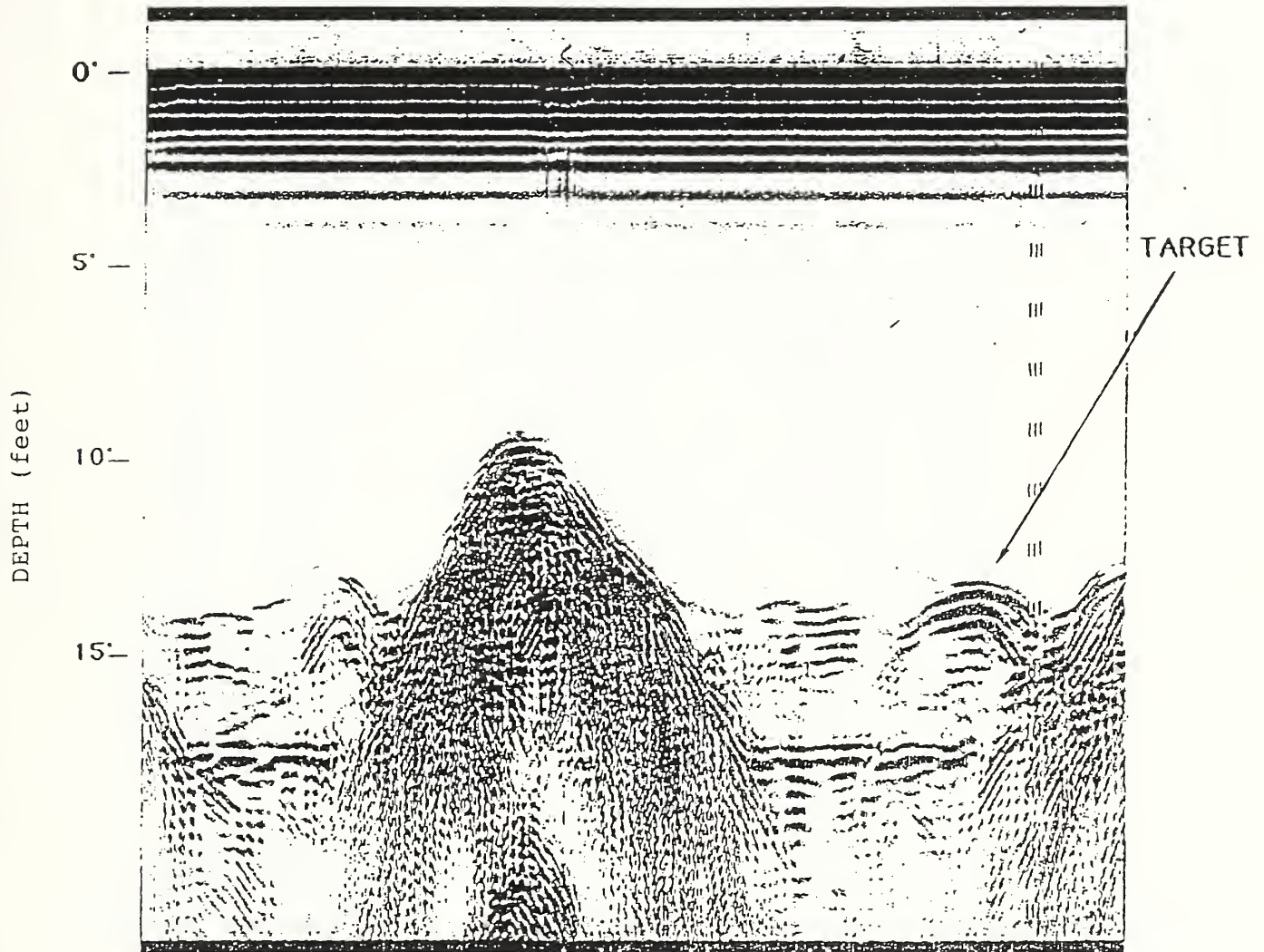


Figure 4.18. GPR profile obtained over a reflective target placed in the lake at a depth of 13 feet.

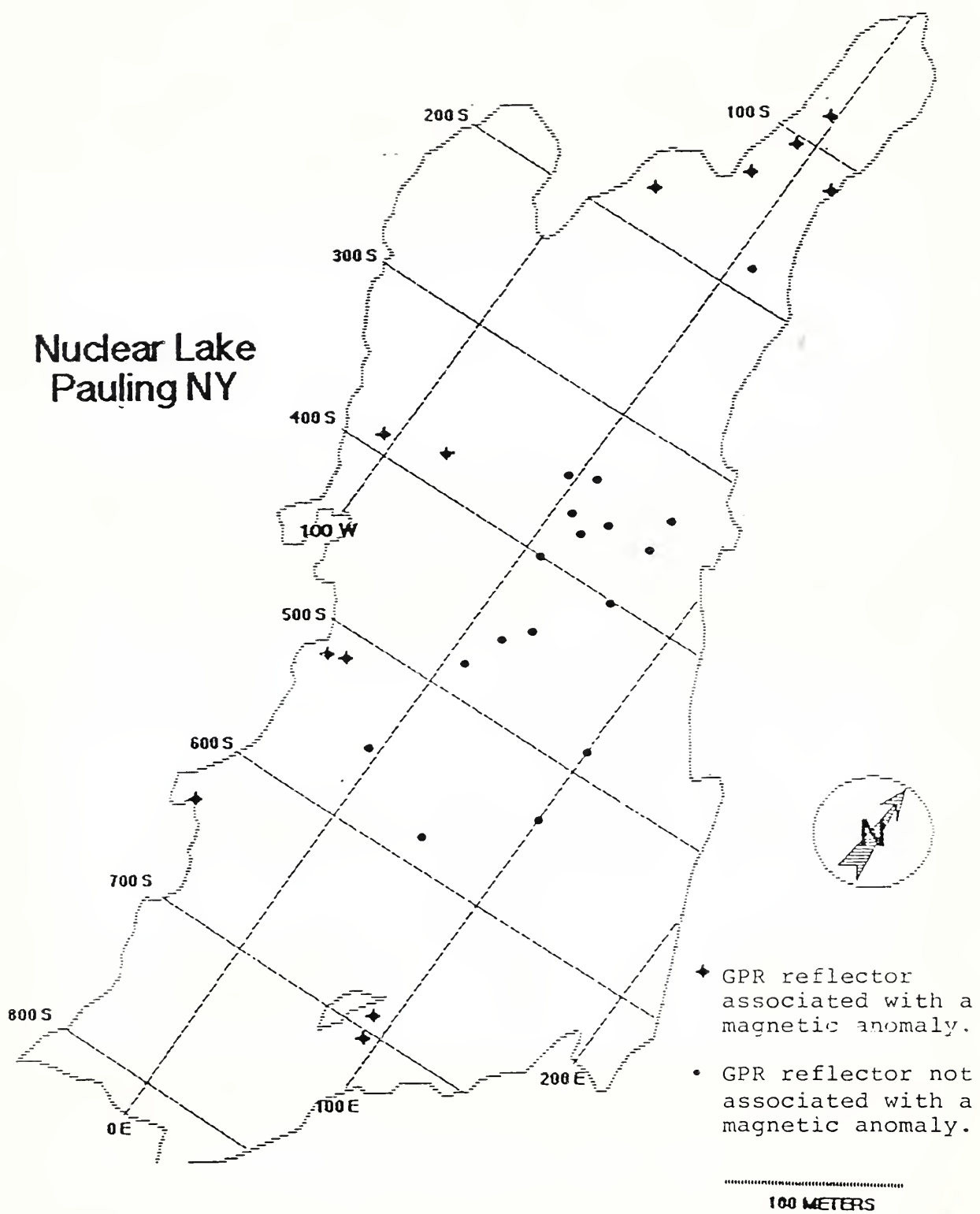


Figure 4.19. Map of prominent GPR reflectors observed in the GPR survey of Nuclear Lake.

  
GEO-CENTERS, INC.



TABLE 4-1

Estimated Coordinates, Depths and Size of GPR Reflectors  
Detected in GPR Survey of Nuclear Lake

<u>Location</u>	<u>Depth (feet)</u>	<u>Size (meters)</u>
353S, 5W	11	1.7
557S, 5W	15	1.6
180S, 10E	10	0.7
343S, 10E	11	1.3
364S, 10E	11	2.0
400S, 10E	11	0.6
473S, 10E	12	1.0
372S, 20E	11	0.8
464S, 20E	12	2.0
362S, 30E	10	1.3
442S, 30E	12	0.9
338S, 60E	9	2.5
358S, 60E	10	1.8
402S, 60E	11	1.5
485S, 100E	12	1.6
541S, 100E	12	0.6
* 663S, 77W	4	0.3
* 512S, 68W	2	0.3
* 510S, 65W	5	0.3
* 390S, 110W	6	0.3
* 390S, 70W	10	0.6
* 177S, 60W	8	0.2
* 135S, 20W	4	0.2
* 106S, 10W	3	0.1
* 80S, 5W	4	0.6
* 120S, 35E	3	0.3
* 686S, 85E	1	0.2
* 707S, 90E	7	0.2

\*GPR reflector associated with magnetic anomaly.

GPR reflectors correlated with magnetic anomalies are the most probable locations of metallic objects on the lake bottom. GPR reflections that coincide with magnetic anomalies in the extreme northern end of the lake are believed to be associated with an old barbed wire fence, running through the area that became submerged when the earthen dam was constructed and the lake level rose. GPR reflections that are not correlated with magnetic anomalies are possibly non-ferrous metallic objects on the bottom of the lake or are ferrous objects missed by the wide grid spacing of the magnetic survey. Some magnetic anomalies were found which were not associated with GPR reflections. These are not shown in Figure 4.19 and are believed to be due to rock outcroppings of high magnetite content possibly existing on the lake bottom. Each magnetic anomaly detected and GPR reflection observed was fairly isolated and no appreciable concentration of either were observed to exist in the lake.

## 5.0 Conclusions

GPR reflections observed in profiles obtained from scans run over the concrete tank pad west of the former gasoline station were used to verify the existence of the fiber glass tanks, which were installed without a permit, as well as to estimate the dimensions of each tank. The subsequent monitoring well installation program conducted at the gasoline station as well as the program conducted in areas A and B at the Nuclear Lake Site were successful. Maps of subsurface features observed in each of these GPR surveys (Figures 3.4, 4.5, and 4.9) were used to assist the contractors in the placement of these monitoring wells, thus demonstrating the applicability of GPR to HWS monitoring well installation programs.

The clean-up effort at Nuclear Lake is currently under review by the national Parks Service and arrangements are being made to further investigate prominent GPR reflectors observed in the lake. The geophysical investigation conducted on Nuclear Lake demonstrates the effectiveness of water based GPR combined with magnetometry in locating objects submerged in freshwater lakes and lagoons.

## References

1. Breiner, S., 1973, "Applications Manual for Portable Magnetometers", GeoMetrics, Inc., Sunnyvale, CA.
2. Dobrin, M.B., 1960, Introduction to Geophysical Prospecting, McGraw-Hill, New York.
3. Gendzwill, D., 1981, "Magnetic Fields of a Dipole", Manual of Geophysical Hand-Calculator Programs, Society of Exploration Geophysicists, Tulsa, Oklahoma.
4. Grant, F.S., and G.F. West, 1965, Interpretation Theory in Applied Geophysics, McGraw-Hill, New York.
5. Horton, K.A., R.M. Morey, R.H. Beers, V. Jordan, S.S. Sandler, L. Isaacson, U.S. Nuclear Regulatory Commission, "Evaluation of Ground Penetrating Radar at Low Level Nuclear Waste Disposal Sites", NUREG CR-2212, 1981.
6. Morey, R.M., "Continuous Subsurface Profiling by Impulse Radar", Proc. of Engineering Foundation Conference on Subsurface Exploration for Underground Excavation and Heavy Construction, American Society of Civil Engineers, 1974, pp. 213-232.
7. Telford, W.M., L.P. Geldart, R.E. Sheriff, and D.A. Keys, 1976, Applied Geophysics, Cambridge University Press.

## APPENDIX A

### Electromagnetic Wave Propagation Through Common Earth Materials

The velocity of propagation of the electromagnetic wave through the earth can be determined as a result of the calibration process. For earth materials with an effective relative dielectric constant,  $\epsilon_{er}$ , the velocity of propagation,  $v_m$ , of the electromagnetic wave is approximated by:

$$v_m = \frac{\omega}{\beta} = \frac{c}{\epsilon_{er}^{1/2}} \quad (A-1)$$

where:

$\omega = 2\pi f$  = angular frequency of the electromagnetic radiation

$f$  = frequency in Hertz

$c = 3 \times 10^8$  m/sec, the propagation velocity of electromagnetic energy in free space

$\beta$  = phase constant, or the imaginary part of the propagation constant of the medium through which the electromagnetic wave travels.

The phase constant,  $\beta$ , is obtained from  $\gamma$ , the complex propagation constant of the medium through which the electromagnetic wave travels. The propagation constant,  $\gamma$ , is derived from Maxwell's equations describing the behavior of electromagnetic fields and is defined as:

$$\gamma = \alpha + j\beta = (-\omega^2 \mu \epsilon + j\omega \mu \sigma)^{1/2} \quad (A-2)$$



where:

- $\alpha$  = attenuation constant of the medium
- $\mu$  = magnetic permeability of the medium
- $\epsilon$  = effective dielectric permittivity of the medium
- $\omega$  = angular frequency of the electromagnetic energy
- $\sigma$  = effective electrical conductivity of the medium

In common earth materials there is a trade-off between the depth of electromagnetic penetration and the resolution of sub-surface structure. The depth of penetration is determined by the frequency of the transmitted electromagnetic energy as well as the electromagnetic properties of the material through which the energy travels. Signal attenuation,  $A$ , is approximated by:

$$A = 20 \log e^{\alpha} = 8.68\alpha \text{ (dB/m)} \quad (\text{A-3})$$

Attenuation increases with increasing frequency. By increasing the frequency of the transmitted energy through the use of different antennas, the depth of penetration is decreased, while finer resolution of shallower structure is attained.

The amount of energy reflected at any electromagnetic interface is described by the complex reflection coefficient:

$$\rho = \frac{\eta_2 - \eta_1}{\eta_2 + \eta_1} \quad (\text{A-4})$$

where:

- $\rho$  = complex reflection
- $\eta_1$  = complex impedance of upper layer
- $\eta_2$  = complex impedance of lower layer

The complex impedance is given by:

$$\eta = \frac{j\omega\mu}{\gamma} \quad (A-5)$$

where  $\gamma$  is the electromagnetic propagation constant defined in Equation A-2.

A summary of the physical properties of common media which affect the propagation and attenuation of electromagnetic signals is shown in Table A.1. Careful analysis of reflected radar pulses, combined with a knowledge of the electromagnetic properties of the soil through which they propagate can provide information regarding location, depth, and composition of buried objects. For example, metallic objects have different electromagnetic properties than soils and will, therefore, give rise to strong reflections and a phase shift. Geologic interfaces give relatively weak reflections and no significant phase shift.

A more quantitative picture of the penetration performance of GPR is shown in Figure A.1. Here, the range (for different electromagnetic frequencies) is plotted directly as a function of attenuation in various media. The plots result from calculations assuming the return signal is from a rough plane reflector.

TABLE A-1

Approximate VHF Electromagnetic Parameters of  
Typical Earth Materials

<u>Material</u>	<u>Approximate Conductivity <math>\sigma</math> (mho/m)</u>	<u>Approximate Dielectric Constant</u>	<u>Depth of Penetration</u>
Air	0	1	Max (km)
Limestone	$10^{-9}$	7	
Granite (dry)	$10^{-8}$	5	
Sand (dry)	$10^{-7}$ to $10^{-3}$	4 to 6	
Bedded Salt	$10^{-5}$ to $10^{-4}$	3 to 6	
Freshwater Ice	$10^{-5}$ to $10^{-3}$	4	
Permafrost	$10^{-4}$ to $10^{-2}$	4 to 8	
Sand, Saturated	$10^{-4}$ to $10^{-2}$	30 to 50	
Freshwater	$10^{-4}$ to $3 \times 10^{-2}$	81	
Silt, Saturated	$10^{-3}$ to $10^{-2}$	10	
Rich Agricultural			
Land	$10^{-2}$	15	
Clay, Saturated	$10^{-2}$ to 1	8 to 12	∇
Seawater	4	81	Min (cm)

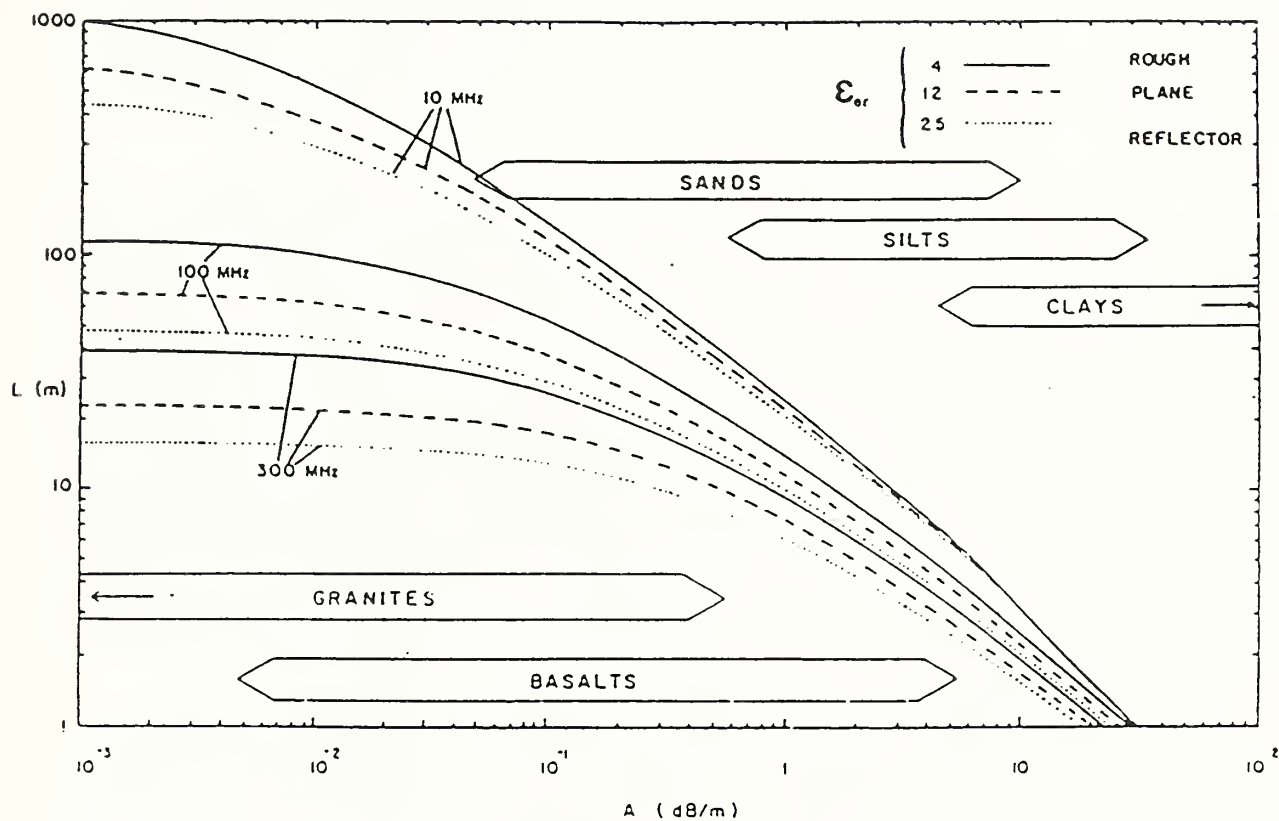


Figure A.1. Variation of maximum depth of penetration ( $L$ ) as a function of attenuation ( $A$ ) for different frequencies and dielectric constants. Typical ranges of attenuation for different earth materials are shown (after Horton et. al., 1981).

# Surveys of Cavity and Buried Object by Ground-Probing Radar

Akio Tanaka, Koichi Tamura,  
Tetsuma Toshioka  
(Geotechnical Institute,  
OYO Corporation, Japan)  
Saloru Ohya  
(OYO Corporation, USA)

## 1. INTRODUCTION

The maximum probing depth of ground-probing radar is about 3 to 5m in usual soil ground in Japan. Accordingly, in many cases, ground-probing radar has been used for high resolution survey of underground shallow range. The survey for the maintenance of structures or for detecting cavities and old buried pipes under pavements, is one of the effective surveys for ground-probing radar.

Especially, large cavities often occur and underlie the pavement along shore-line or the pavement under which water pipes have been installed by shield driving method. Such occurrence of cavities is extremely hazardous, as it tends to cause the abrupt collapse of the pavement. For the safety management of roads, whether paved or unpaved, recent trend has been indicating the increasing demand for cavity detecting.

This paper refers to some examples of surveys actually done by using ground-probing radar.

## 2. EXAMPLES OF SURVEYING CAVITIES UNDER PAVEMENTS

A collapse of a paved road surface, when it once occurred, makes us worried about other possible cavities in the vicinity. In such a case, we often drill holes in the road surface at regular intervals to see if there are any cavities or not. This conventional method, however, does not permit continuous survey of the road surface in question, and it is only at just point drilled by chance that we find cavities actually.

On the other hand, ground-probing radar permits continuous survey of roads without damaging road surfaces. These days, ground-probing radar is used first, and then the paved surface, that shows an indication of a cavity on a radar profiling record, is opened to confirm the existence of a cavity. Such are the steps for repairing and restoring the road to its former condition.

A roadbed, subgrade etc., with certain structure, are usually provided under the paved road surface. The record obtained by ground-probing radar on a normal road is shown in Fig.1. It shows a pattern of continuous stripes arranged laterally.

On the other hand, at the place where a cavity exists underground, a strong hyperbolic reflection pattern from the top surface of a cavity is obtained. Fig.2 shows a typical reflection pattern, that indicates a cavity under a paved road surface, recorded by ground-probing radar.

Fig.3 shows an example of detecting the existence and the extent of a cavity under the paved road by using ground-probing radar. A diameter of this cavity shown there is estimated about 3m. Fig.4 shows the radar record of



reflected pattern from this cavity, and the result of the excavation for confirming the existence of it. The actual shape of the top surface of the cavity and that of the reflected pattern recorded by ground-probing radar correspond to each other very well. It was confirmed that the cavity was 3.0 m wide and 1.2m thick. A water pipe is buried under this road, and the leakage of water from this pipe is considered to have caused the occurrence of the cavity.

It is strongly desired, in view of the safety maintenance of roads, to find such cavities as early as possible to repair roads.

### 3. EXAMPLES OF SURVEYING PIPES BURIED UNDERGROUND

There are many lifelines buried under roads such as waterworks, sewerage, power cables, town gas pipes, etc. The maintenance work for them often requires ground-probing radar.

The following is an example of surveying the conditions of a buried pipe. Fig.5 shows the record obtained on a measuring line across a road by ground-probing radar. There are two hyperbolic reflection patterns in an upper and a lower position of the record. These reflection patterns indicate a water pipe buried underground. The reflection appearing in the upper position is considered to have come from the upper surface of the buried pipe, and the reflection in the lower position from the lower surface of it. This buried pipe is filled with water, and the propagation velocity of electromagnetic wave in water is 3.4cm/ns. The difference in the travel time of the reflected waves from the upper and the lower position is 63ns, which means that the diameter of the buried pipe is  $(3.4 \times 63)/2=107\text{cm}$ .

Ground-probing radar thus reveals that a pipe of about 1.0m in diameter is buried underground.

Fig.6 shows the record obtained along a road by ground-probing radar. The reflection from the top surface of a buried pipe is recorded continuously. It is clearly shown that the top surface of it is gently undulating. The breaks on the continuous reflection pattern appear at intervals of 4m, which shows that the water pipe is comprised of 4m long pipes jointed together in line.

As a result of the above survey in which ground-probing radar was used, this buried pipe is considered to be comprised of 4m long huge pipes whose diameter is about 1m. And the route and burying depth of this pipe are also revealed.

### 4. CONCLUSION

Ground-probing radar is an effective method in surveying objects buried from 2 to 3m deep underground, and is used especially for surveying cavities and buried pipes under paved or unpaved road surfaces.

Many lifelines are buried under roads in Japan, and ground-probing radar is effectively used for their maintenance. Cavities generated under roads may lead to the collapses of road surfaces, which will result in fatal accidents in such places as have heavy traffic. It is very important, in view of the safety maintenance of roads, to find cavities and repair them in advance so that accidents may be prevented.

Supervisors of road maintenance have a craving for ground-probing radar which has an improved surveying capacity and higher resolution. Improvement of the radar to meet such needs is now under way.

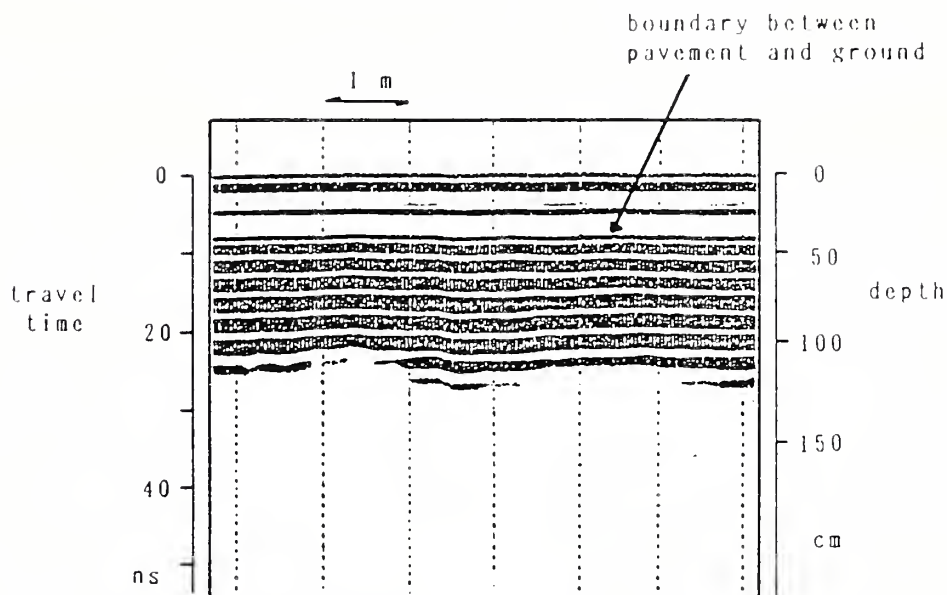


Fig.1 A sample record obtained on a normal road.

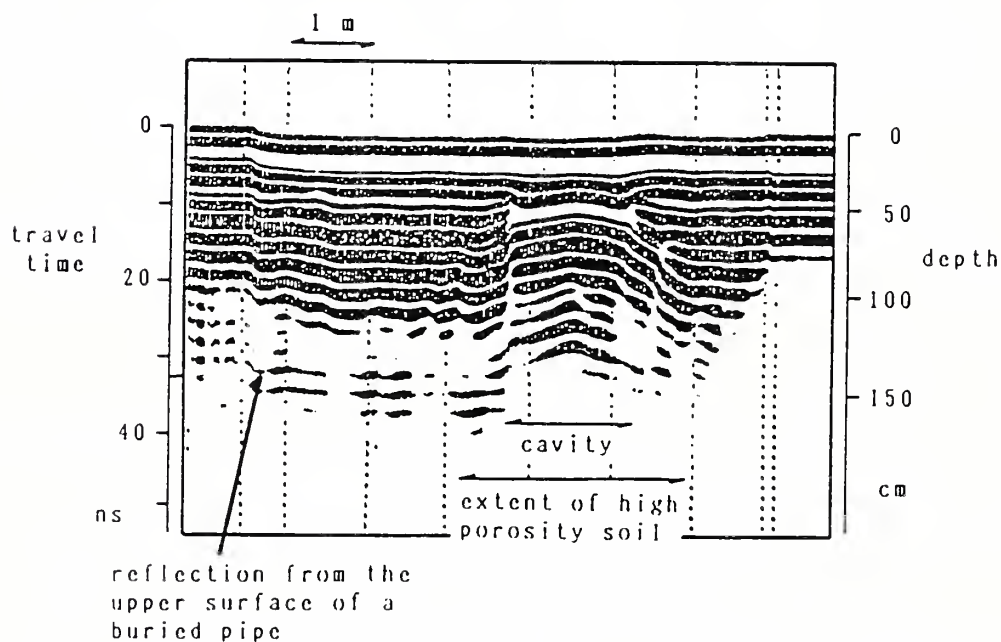


Fig.2 A typical pattern of a cavity under a paved road.

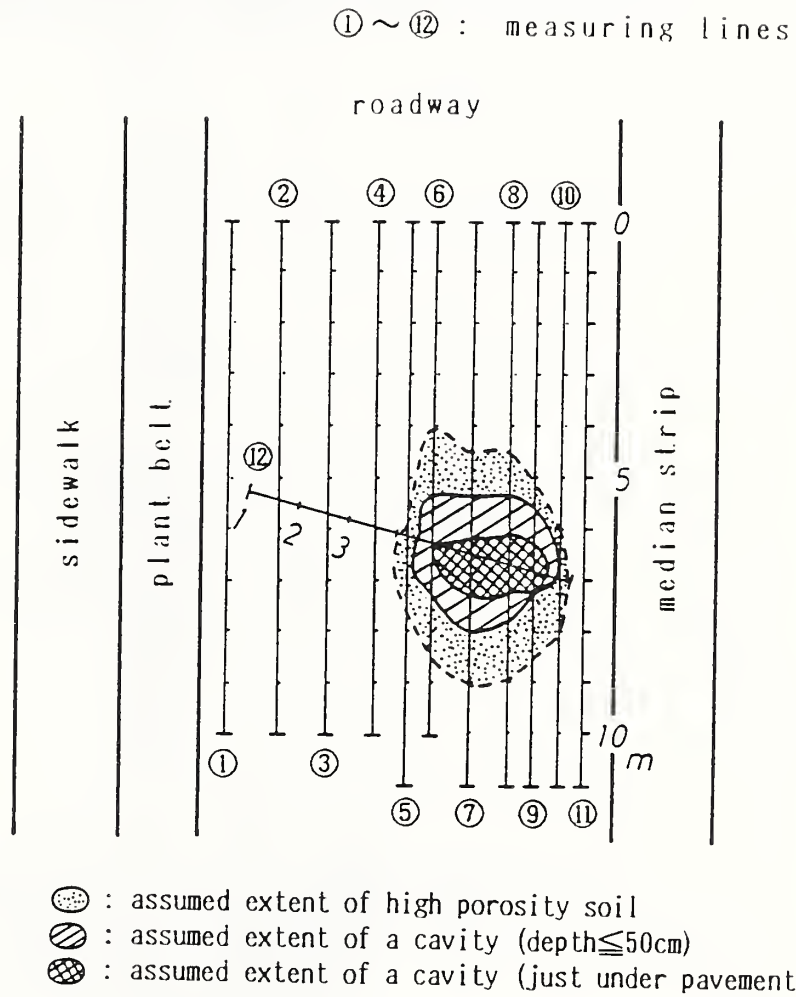
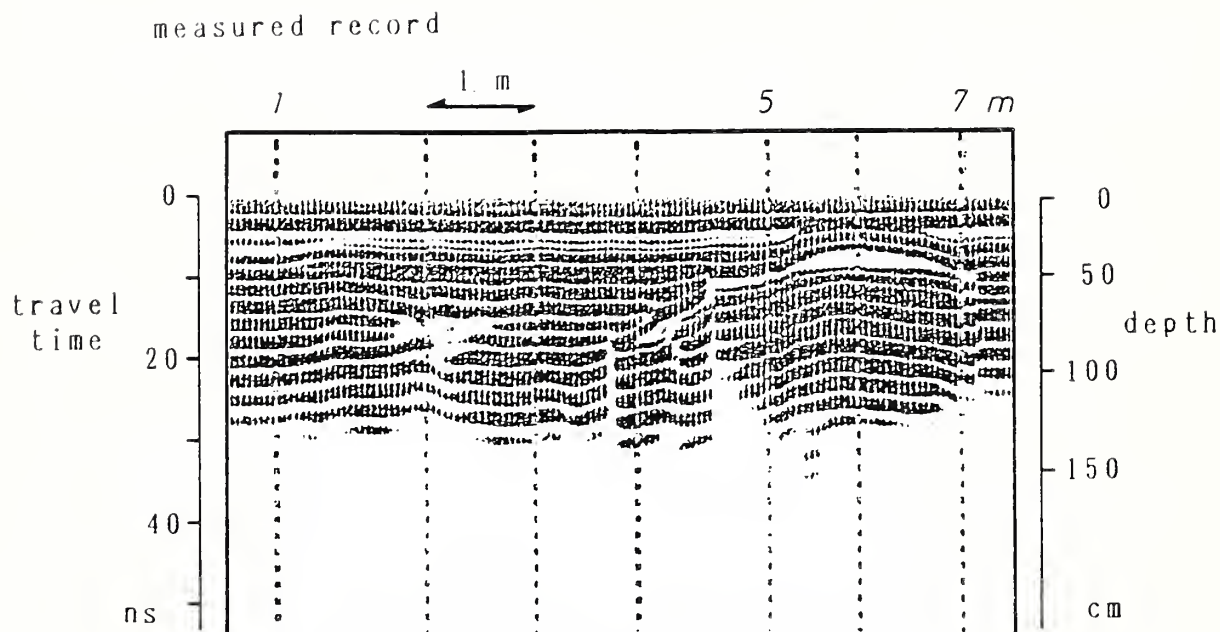
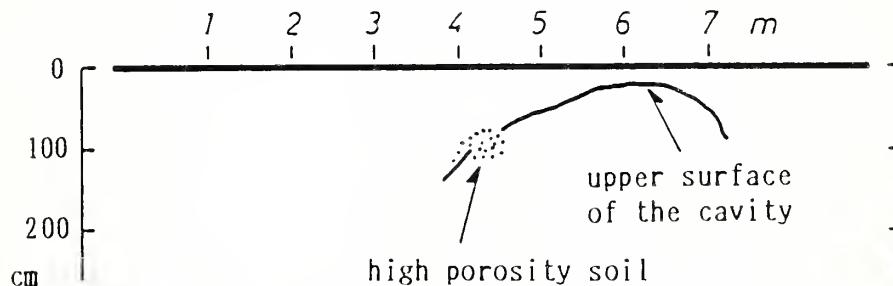


Fig.3 An example of detecting the existence and the extent of a cavity under a paved road.



assumed structure under measuring line



the result of the excavation

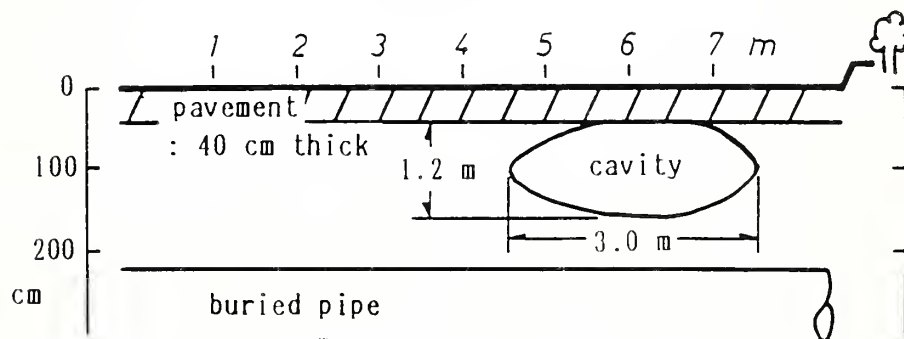


Fig.4 The radar record of a cavity and the result of the excavation.

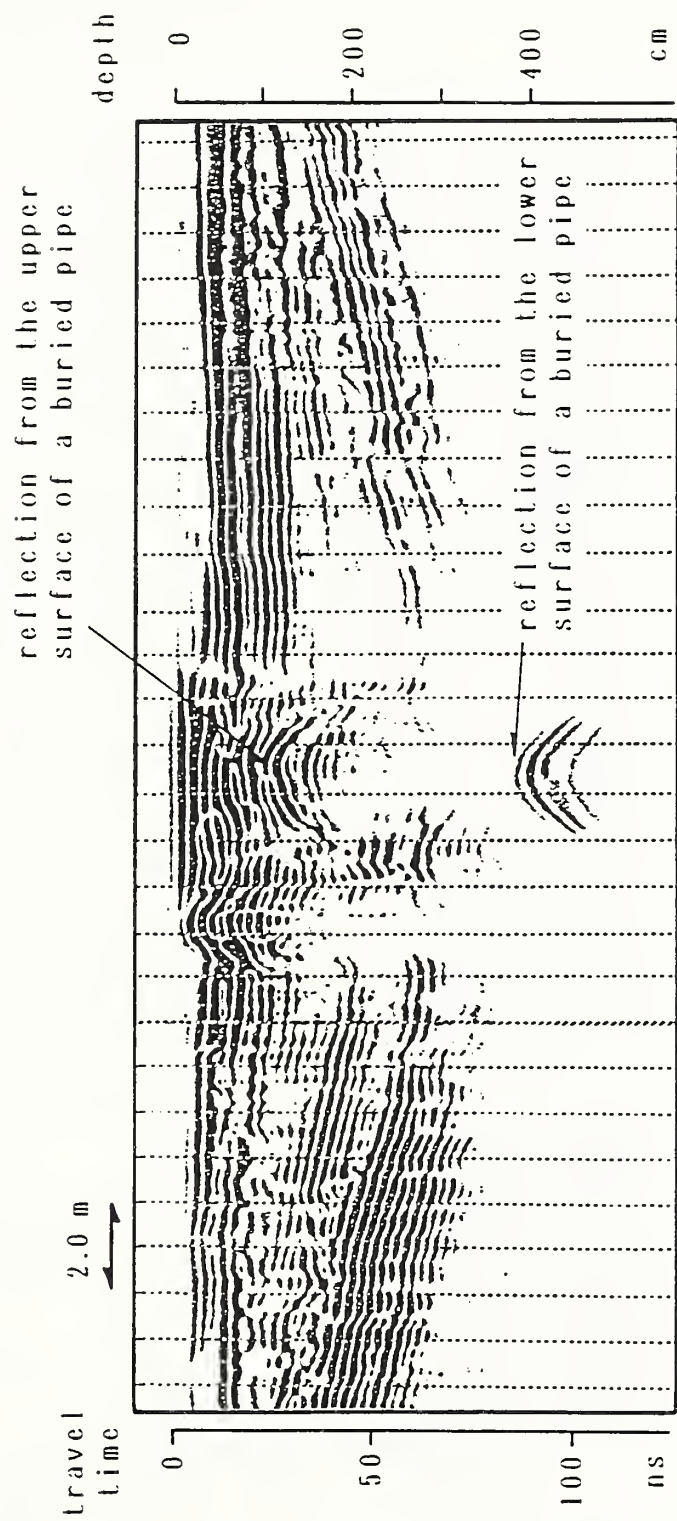


Fig.5 The record obtained on a measuring line across the road.



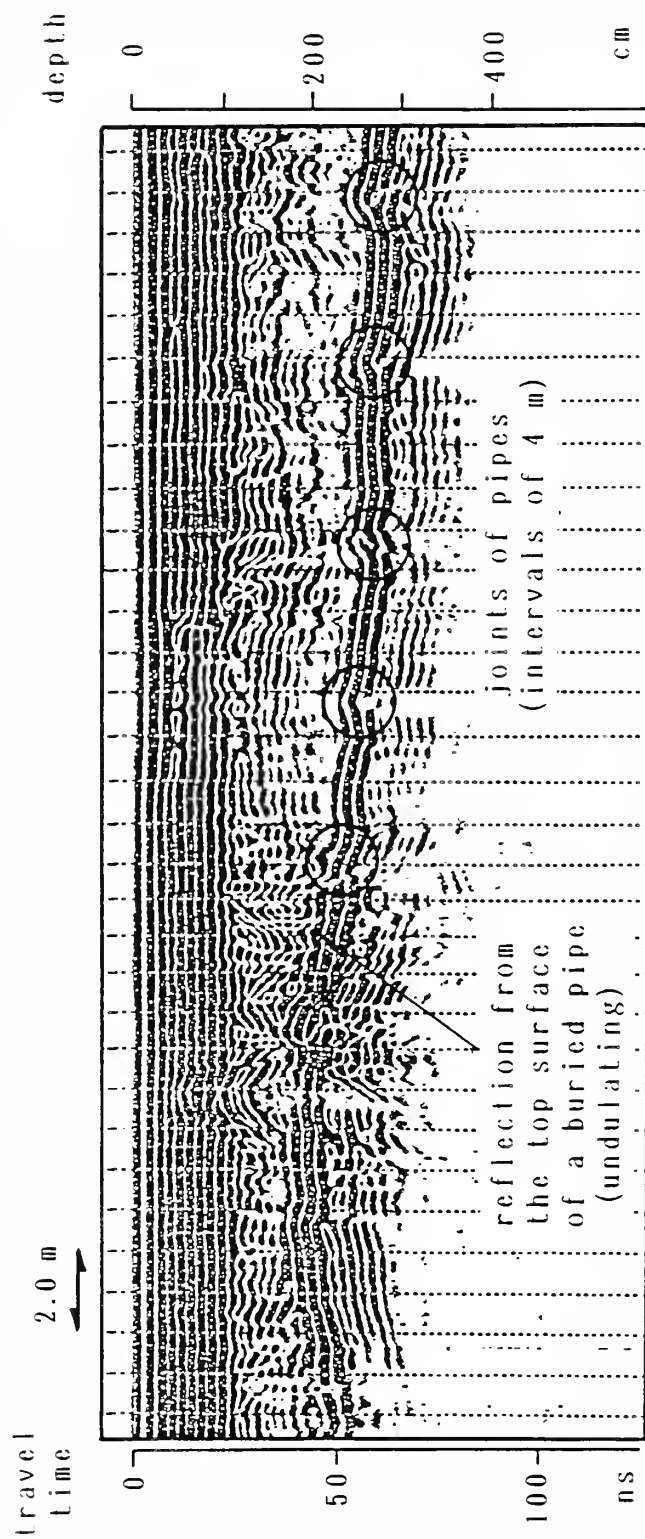


Fig. 6 The record obtained on a measuring line along the road.

Tetsuo Hara, Toshihiko Sakayama ( OYO Corporation )

Tsutomu Suzuki, Ikuo Arai (The University of Electro Communication )

## 1. Introduction

Georadar is an instrument for detecting underground structures. Georadar transmits electromagnetic pulse records towards the underground and receives reflected waves from underground reflectors. While this method is effective for the investigation of shallow underground structures, some technical improvements need to be made. These include achievement of better resolution of records, deeper penetration of the ground and methods for determining the composition and features of reflectors. To solve these problems, not only the improvement of hardware, but development of effective signal processing techniques are necessary.

This paper describes a signal processing technique, "synthetic aperture processing" for application to pulse radar records. It also demonstrates that this technique is effective for the improvement of horizontal resolution and S/N ratio of georadar profiles.

## 2. Synthetic Aperture Processing

Fig.1 shows the locus of reflected signals generated by the point reflector at pointy P ( $X_i, Y_j$ ). Here, the X axis indicates the ground surface, and the Y axis indicates depth. Formula (1) shows the locus of reflected signals generated by moving the antenna along the X axis.

$$T_L = \sqrt{(X_k - X_i)^2 + Y_j} / C \quad (1)$$

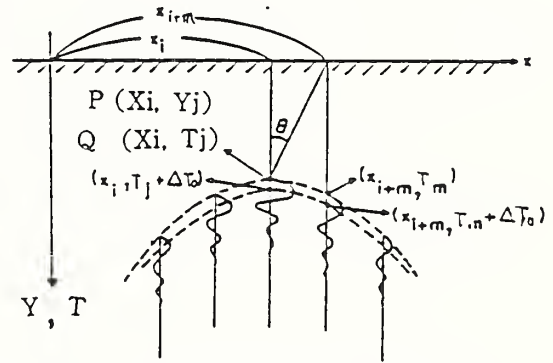


Fig.1 Distribution of Echo Signal (Suzuki 1985)

By stacking the signal  $S (X_k, T_k)$  along the locus described by Formula 1, the enhanced signal  $Q (X_i, T_j)$  can be obtained as shown in Formula (2)

$$Q (X_i, T_j) = \sum_{m=-M}^M \rho_m \cdot S (X_{i+m}, T_m) \quad (2)$$

$\rho_m$ : weighting function  $T_m = \sqrt{(X_{i+m} - X_i)^2 + Y_j} / C$

Formula (1) shows the locus of signals reflected from the point reflector placed at P ( $X_i, Y_j$ ) on the georadar profile. However, another locus should be obtained for stacking on the point ( $X_i, T + \Delta T$ ). Using these loci, stacking for each depth is carried out as shown in Formula (3)

$$Q(X_m, T_m + n \Delta T_0) = \sum_{n=1}^N \rho_m S(X_{i+m}, T_m + n \Delta T_0) \quad (3)$$

Actually, the above formula (3) is applied for the calculation with all the combination of the reflection point P (Xi, Yj).

### 3. Efficiency Synthetic Aperture Processing

As shown in Fig.2, horizontal resolution obtained through synthetic aperture processing, as represented in Formula (3), is equivalent to the resolution that is obtained when (2M+1) antennae are aligned along the X axis and are focused on target position P.

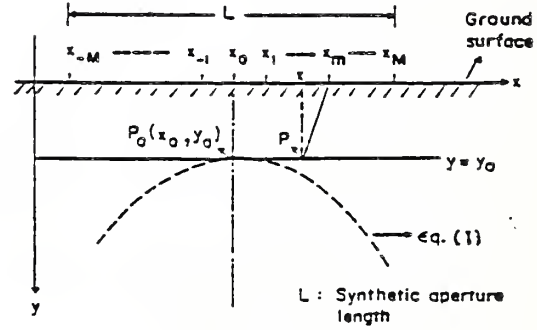


Fig.2 Equivalent Antennae Array (Suzuki 1985)

On the assumptions of the receiving pattern (both way) by an antenna being expressed by R and of the point target existing under ground at P (Xi, Yj), the receiving electric field of an antenna located at X = Xm, is in proportion to the following formula.

$$E(X_m) = R(X_m - X) e^{-i2k\sqrt{(X_m - X_i)^2 + Y_j^2}} \quad (4)$$

Then, if the phase compensation is made to align the focus with the point P, Synthetic Electric Field can be expressed by the following formula.

$$E(X_m) = \sum_{m=-M}^M \rho_m \cdot E(X_m) e^{i2k(\sqrt{(X_m - X_i)^2 + Y_j^2} - Y_0)} \quad (5)$$

Fig.3 shows the distribution of intensity values of the electric field, before and after processing. This figure shows the remarkable improvement of horizontal resolution by this processing technique. In performing the processing, as shown in Formula (1), the velocity of electromagnetic waves propagated in the ground must be estimated. The WARR (wide angle reflection and refraction) measurement can be used to estimate the velocity.

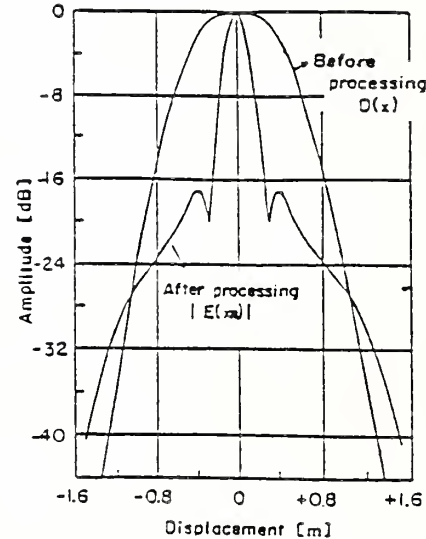


Fig.3 Pattern after Synthetic Aperture Processing (Suzuki 1985)

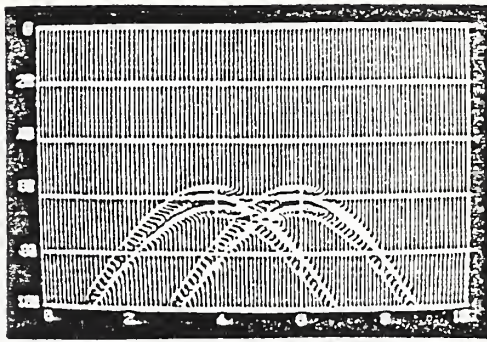


Fig. 4 Echo Distribution Chart in case of 2 targets (depth=2.25m, spacing: 2m)

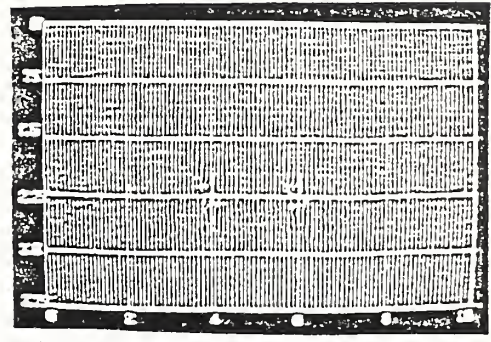


Fig. 5 Echo Distribution Chart after Aperture Processing

Fig.4 shows the simulated waveforms from the reflecting objects placed 2.25m deep and with 2m spacing, while Fig.5 shows the result after Synthetic Aperture Processing is given to Fig.4. Equivalent antenna pattern narrowed and resolution enhancement by Synthetic Aperture Processing, are obvious, from Fig.5.

#### 4. Processing Results Applied to Actual Field Data

The following records were obtained by the Georadar-1 system, manufactured by OYO Corp. Field records are printed out from the printer housed in the system. The digital data is transferred via GP-IB inter face to floppy disks, either in OYO's Field Data Logger or the NEC PC-9801 Vm personal computer. The records stored on the Field Disk Logger's floppy disks can be read out using the PC-9801 personal computer (see Fig.6)

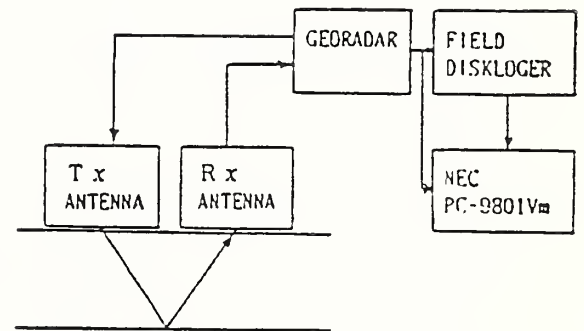


Fig.6 Data Acquisition System

Synthetic aperture processing was executed under the following software environment :

Computer	: NEC PC-9801Vm
OS	: MS-DOS
Language	: MS-FORTRAN
Processing Environment	: RAM Disk used
Data Size/Image	: 0.5Kbyte x 120 traces
Processing Time	: 15 minutes/image

Fig.7 shows profile records obtained along a measuring line laid across five pipes buried approximately 1 meter deep. A hyperbolic diffraction pattern from the buried pipes can be recognized at points denoted by A to E in the figure.

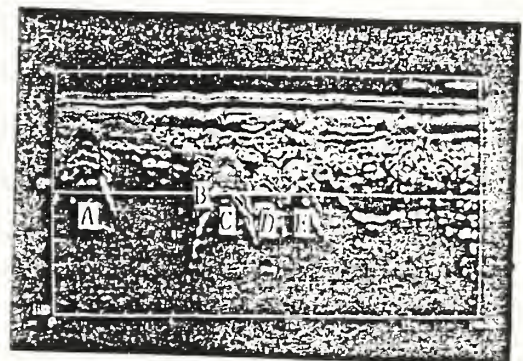


Fig.7 Radar record (before processing)



Fig.8 shows the profile obtained after data processing that included synthetic aperture processing. Propagation velocity of the electromagnetic waves in the ground, which is a parameter of data processing, was determined by WARR measurement. Data processing makes it easy to identify the buried pipes. Data processing includes such steps as deconvolution filtering, noise reduction, as well as synthetic aperture processing.

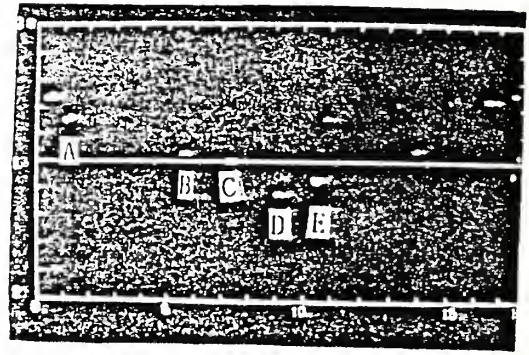


Fig.8 Radar record (after processing)

## 5. Summary

This paper has presented the enhancement of horizontal resolution feasible with the Georadar, by the application of Synthetic Aperture Processing Method to the record obtained by the Georadar. In addition to such effect, this processing brings about further effects as elimination of clutter along with enhancement of S/N ratio, as the result of adding processing conducted with the entire images.

For further improvement of this Method, the speedup of Processing Speed etc are what authors are planning to contrive in the future.

## References :

- Tsutomu Suzuki : Exploration, measurement and control, underground and underwater, by electromagnetic wave :  
vol 20, no 8, pp 762-772
- Ikuo Arai, Tsutomu Suzuki : Geo-exploration radar of compression type ( series no. 2),  
Electronic Information Communication  
Society, SANE83-8, May 1983

## Development of the Georadar System and Basic Experiments

Toshihiko Sakayama, Yukio Kanezaki,  
Tetsuma Toshioka (OYO, Corp., Japan)

### 1. INTRODUCTION

Ground probing radar, using impulsive electromagnetic waves, is an effective method for exploration of shallow underground structures. However, this technique has still not been fully developed, and many efforts by researchers and designers have been exerted. We have developed a new radar system, Georadar II, with the objectives of expanding exploration capability and improving accuracy and efficiency of exploration. Specifically, the system embodies the following development advances: (1) simultaneous observation by a multiple receiving antenna system; (2) high speed data acquisition; and (3) high S/N ratio, attained by countermeasures taken against various noise sources.

This paper explains the outline and specifications of Georadar II, with reference to its hardware. It gives the results of an actual underground investigation conducted with the system.

### 2. OUTLINE OF THE SYSTEM

As indicated in Fig. 1, Georadar II is a system composed of one transmitting antenna and a multiple receiving antenna system (up to 6 receiving antennas can be connected to the system). Fig. 2 is a block diagram of the system.

Georadar II consists of antennas, transmitting/receiving circuits, a control unit, a recording unit and a power supply unit. Table 1 shows the main specifications of the system.

### 3. FEATURES OF GEORADAR II

Development of Georadar II focused on the following three objectives:

- (1) Realization of a multiple receiving antenna system
- (2) Development of a vehicle trailer system
- (3) Realization of high quality recording

Much effort was invested, especially in the first two items, to achieve these objectives. Following are explanations of the development program.

#### (1) Multiple Receiving Antenna System

The following advantages can be expected from a multiple receiving antenna system: (a) expansion of measurement scope; (b) improvement of S/N ratio of the records, through data processing of signals from each antenna.

At the same time, disadvantages can also be expected from a multiple receiving antenna system. These include leakage of electromagnetic waves, interfering with one another and decreasing S/N ratio of the record. However, we were able to overcome such problems, i.e., reduce noise, through circuit



design and mounting techniques. The following noise reducing measures were taken:

- (a) The transmitting and receiving probes were covered with a metallic shield.
- (b) Impedances between each antenna terminal were matched.
- (c) Interference between receiving probes was reduced by adjustment of the matching between the high frequency amplification circuit and the low frequency conversion circuit in the probes.
- (d) Shielding of the antenna with a ferrite plate, which is an absorber of electromagnetic waves, or by painting the antenna with conductive carbon.

## (2) Vehicle Trailer System

In order to increase the efficiency of explorations using the vehicle trailing system, the system must have high speed acquisition capability. Specifically, this means the visual scanning rate of 100 msec must be shortened to approximately 10 msec. At the same time, a high sampling rate circuit is employed, to maintain high record quality. A high speed line scanning discharge type recorder was used.

Fig. 3 shows the examples obtained when the system was moved along a paved road at 10 km/h speed, using 4 receiving antennas. Reflection phases are evident in the right part of each record. The reflector is supposed to be a box culvert.

## (3) High Quality Recording

The most important factors in achieving enhancement of records quality are the characteristics of antennas and the quality of transmitting-receiving circuits. This system uses dipole antennas, which have wide frequency characteristics.

The transmitter used in the system uses a charge type circuit that was newly developed. There are two types of transmitter; the charge and discharge types. As shown in Table 2, comparative testing of these two types of transmitter showed that the charge type has superior features.

In addition, improvements over previously available receiving antenna circuit were made; S/N ratio was increased and the minimum receiving sensitivity was improved by 12 dB.

## 4. Application of Georadar II in Underground Investigations

Fig. 5 shows the records taken, in clay ground. They show cavities beneath the road. One transmitting antenna and four receiving antennas were placed along the profiling line (see Fig. 4). The records from the R1 and R4 antennas do not show the reflection phases of the cavities clearly because these antennas were not located above the cavities. The records from the R2 and R3 antennas, which were adjacent to the transmitting antennas, near the center of the road, clearly show diffraction patterns from the cavities. These results demonstrate that the effectiveness of the multiple receiving antenna system is that it can cover a wide range measurement at one time.

Fig. 6 shows results from an archaeological investigation. The reflection event at 2--3 meters shows up extremely clearly. It was compared with the boundary between the loam layer and the gravel layer. Excavation confirmed that the concave structure on the right side is an ancient moat, constructed in the latter half of the 12th century. Record taken by the Georadar II system indicates that the moat extends down to the gravel layer beneath the loam.

## 5. CONCLUSION

New advances achieved by the Georadar II system include a transmitting antenna mounted on a trailer and multiple (max. 6) receiving antennas. In developing the new system, the following technical advances were made:

- (1) Interference noise generated between each antenna was reduced by effective shielding of the antennas and matching the circuits installed in the probe.
- (2) A high speed scanning and sampling circuit was developed, providing high speed data recording.

By using the new system, up to 6 profile records can be taken simultaneously at speeds several times that of conventional systems, along different lines or at different offset distances. The records obtained can be processed using deconvolution filtering, CDP stacking, migration, etc., to obtain high resolution data on underground structures at greater depths.

Table 1 Specification of Georadar- II system

● Transmitter (antenna and electronics)	
pulse generation	: discharge type
center Frequency	: 350MHz
pulse width	: 3.5ns
output voltage	: 75V <sub>PP</sub> or 100V <sub>PP</sub>
● Receiver (antenna and electronics)	
center frequency	: 350MHz
amplifier gain (in raw frequency)	: 34dB
● Controlling unit	
recording time range	: 25~150ns
scanning rate	: 10~100ms
amplifier gain (at low frequency)	: -20dB~40dB
time gain amplifier	: 40dB(digital controled amplifier)
● Graphic recorder	
number of channels	: 1~6chs,(simultaneous recording)
number of tones	: 14 tones (monochrome)
recording rate	: 2.5~40 lines/sec
● data recorder	
number of chanel	: 7chs.
tape speed	: 1.2~38cm/sec
input frequency	: DC~10KHz

Table 2 Comparison of transmitting methods

Type	Advantages	Disadvantages
discharge type	<ul style="list-style-type: none"> <li>• simple transmitter circuit</li> <li>• suitable for high frequency antenna</li> </ul>	<ul style="list-style-type: none"> <li>• relatively large lateral radiation</li> <li>• unsuitable for low resistance ground</li> <li>• instability of transmisson for varying ground conditions</li> </ul>
charge type	<ul style="list-style-type: none"> <li>• suitable for low resistance ground</li> <li>• high stability for varying ground conditions</li> <li>• relatively low lateral radiation</li> </ul>	<ul style="list-style-type: none"> <li>• complicated transmitter circuit</li> <li>• unsuitable for high frequency antenna</li> </ul>

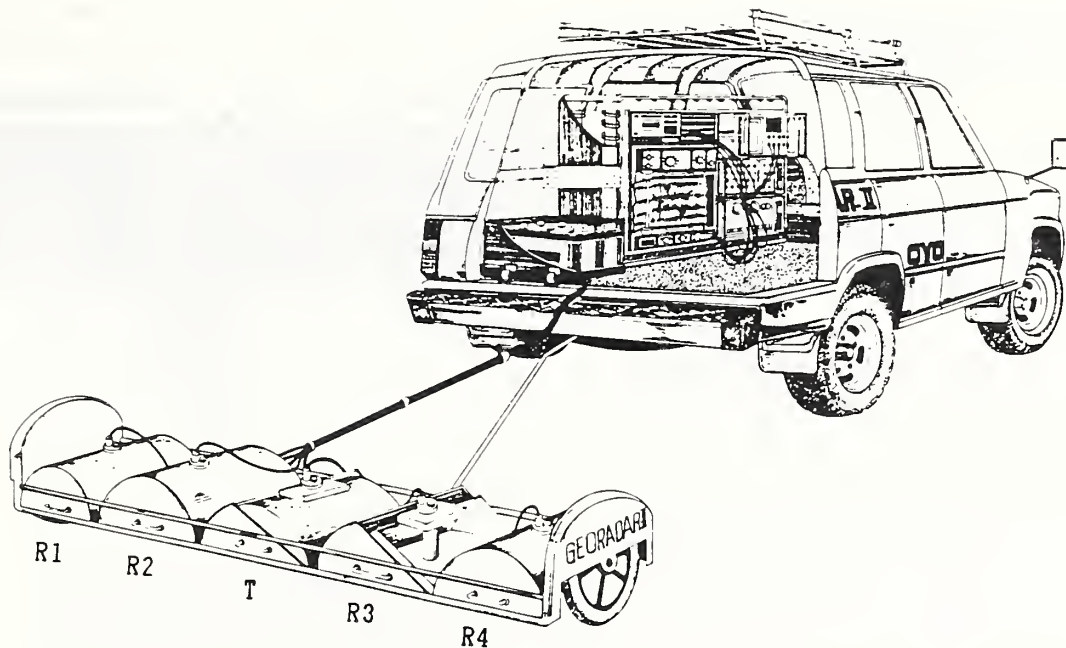


Fig.1 An illustration of Georadar-II system

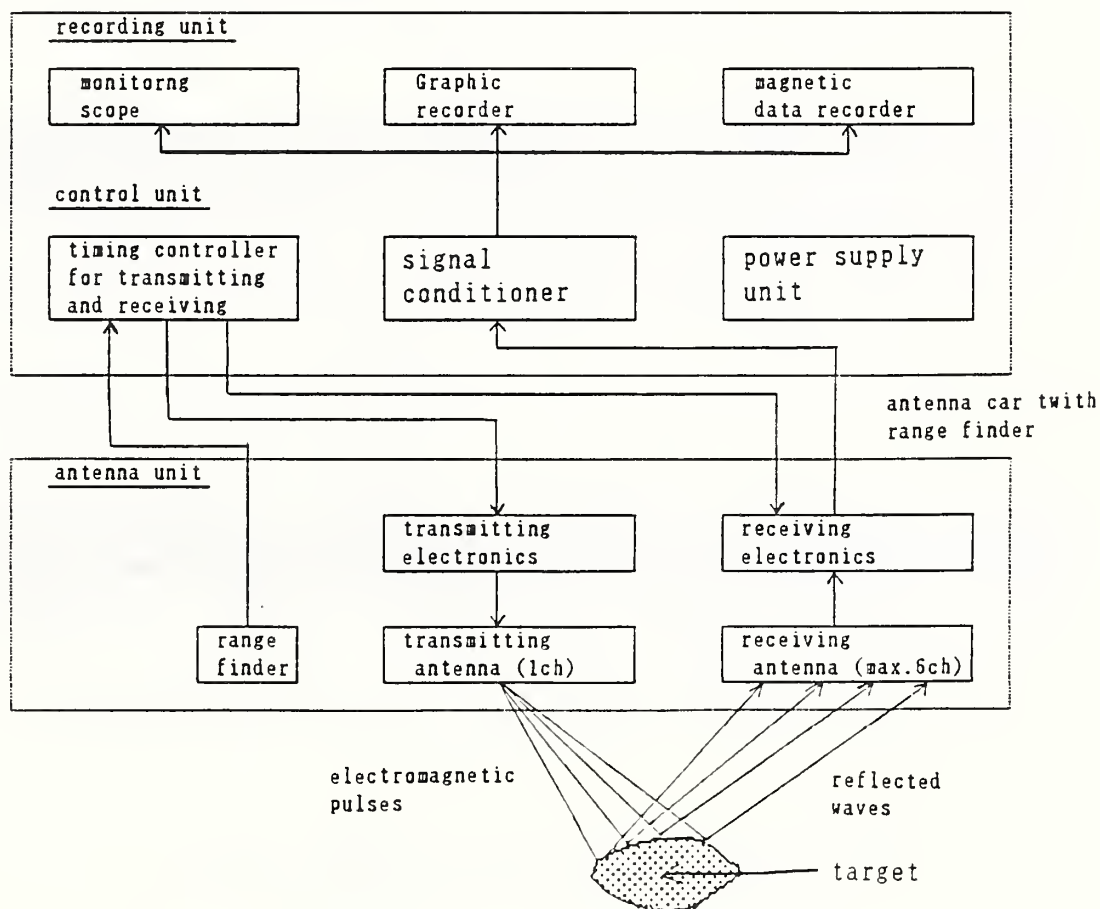
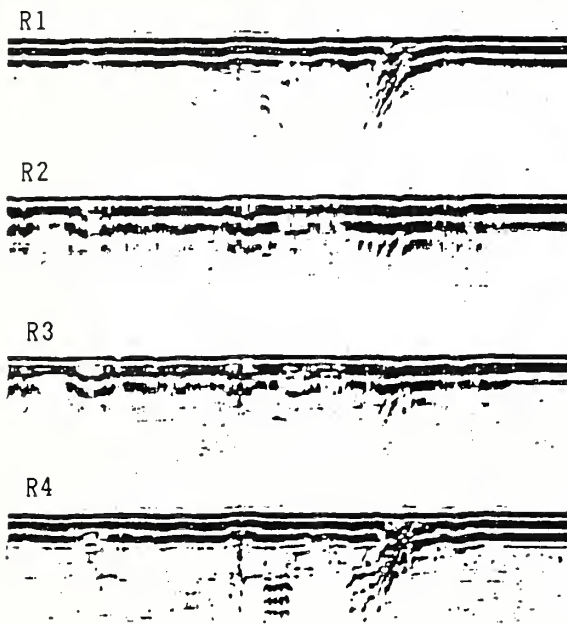


Fig.2 Block diagram of Georadar-II system



Specimen of Record On R1 receiving antenna

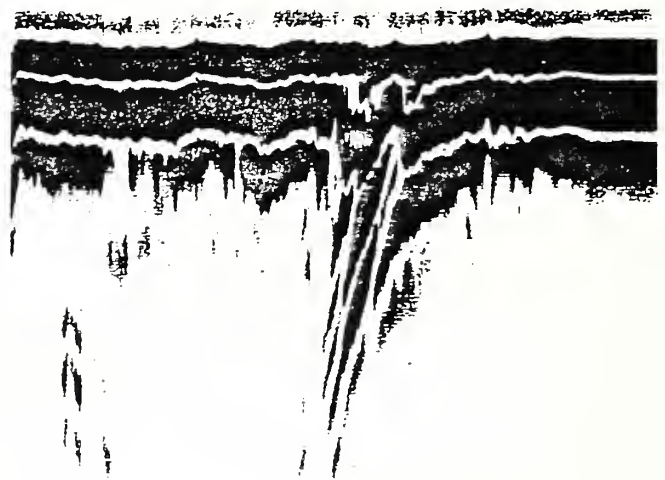


Fig.3 Records obtained by moving Georadar-II along a paved at 10 km/h speed, using 4 receiving antennas

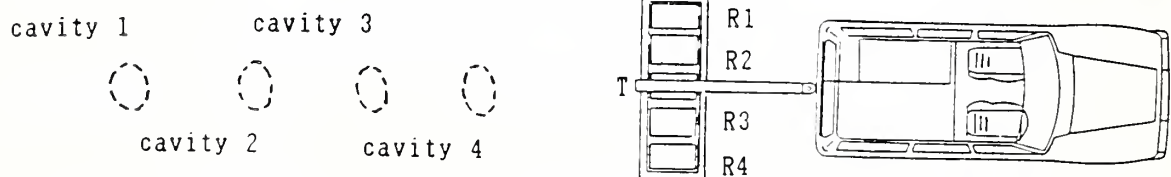


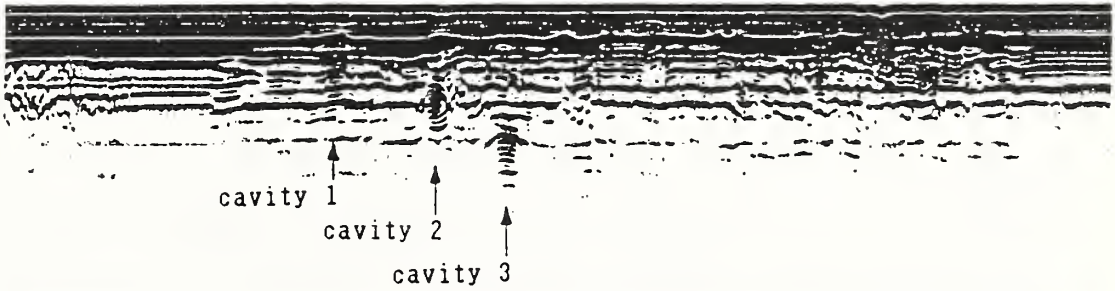
Fig.4 T shaped configuration of multiple antenna system



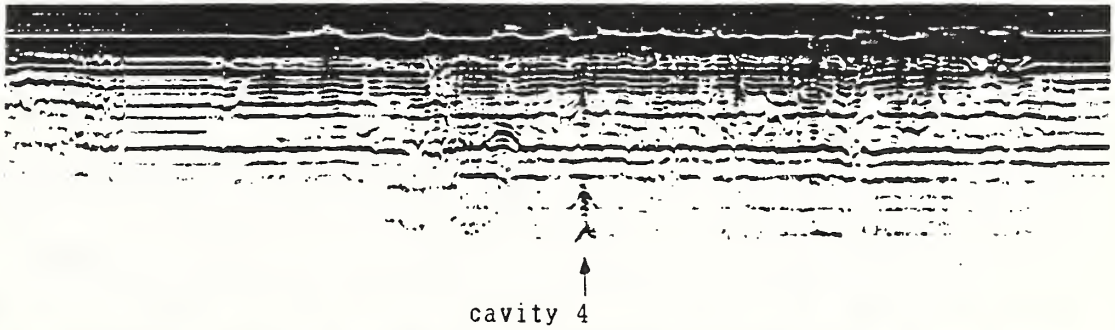
R 1



R 2



R 3



R 4

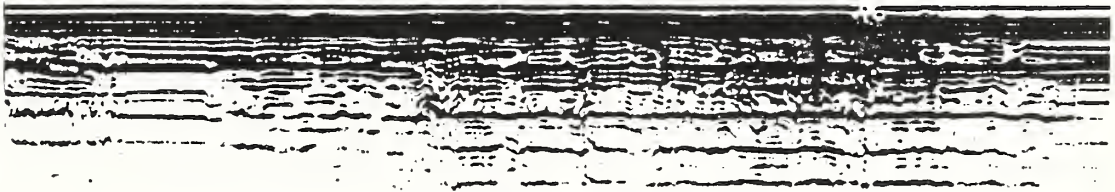


Fig.5 Records of the 4 channel recorder  
(Georadar-II, T shaped configuration)

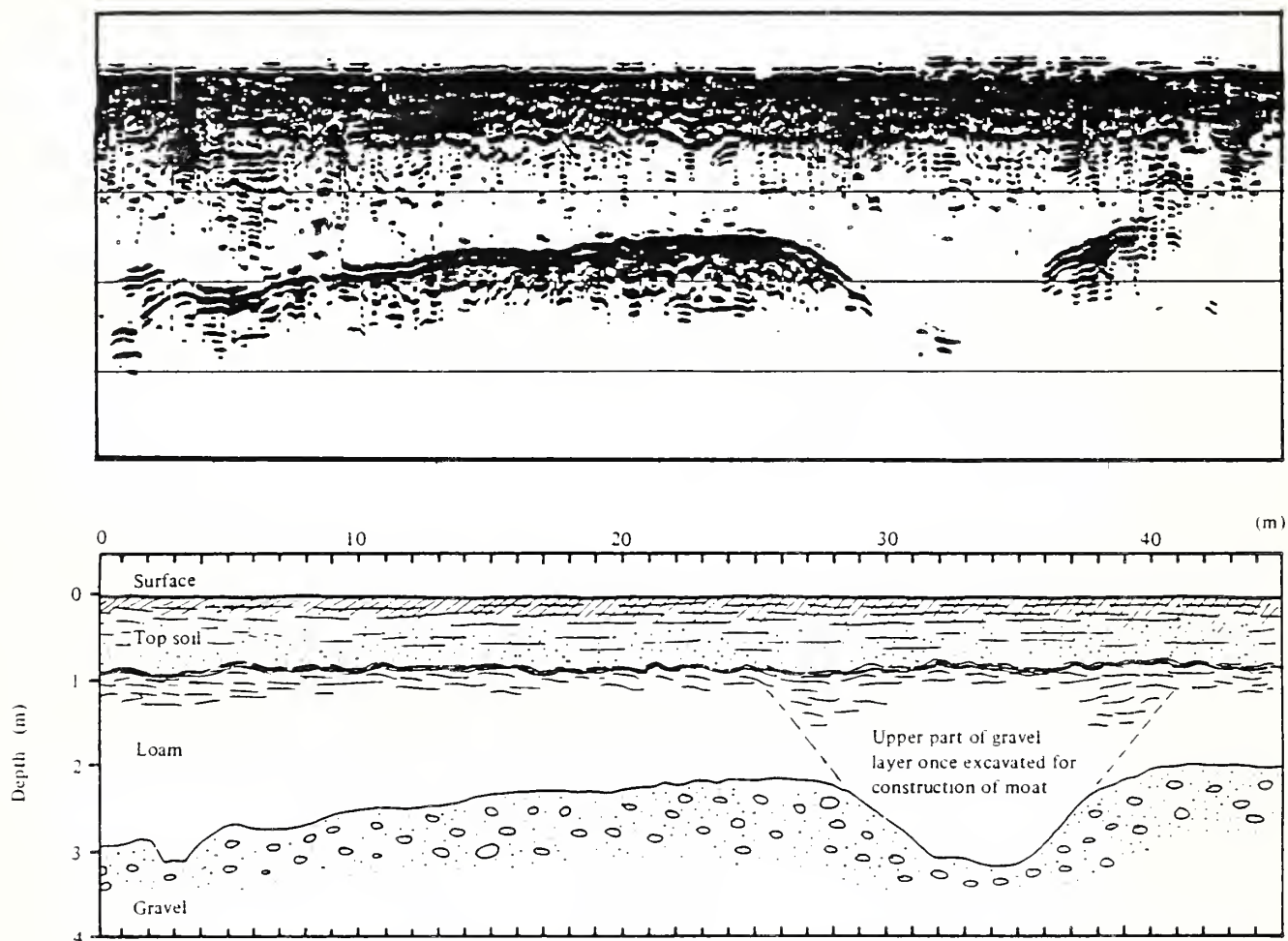


Fig.6 Profile of basal gravel layer, recorded by Georadar- II

TIME DOMAIN ANTENNA ARRAYS FOR USE IN  
GROUND PENETRATING RADAR

BY

SHELDON S. SANDLER\*

Submitted For Presentation  
At

Second International Symposium On  
Geotechnical Applications Of  
Ground Penetrating Radar

March 6-10, 1988

Research for this paper funded by the Army Corps of  
Engineers, technically directed by the Naval Explosive  
Ordnance Disposal Technology Center, and contracted  
by the Naval Research Laboratory

\* Technical advisor to the President, GEO-CENTERS, INC. , Newton  
Centre, MA 02159 and Professor of Electrical and Computer  
Engineering, Northeastern University, Boston, MA 02115

## (1) Antenna Arrays

The purpose of using arrays of sources, arrays of receivers, or both, is two-fold. First, arrays allow the quick acquisition of many signals which can be stacked to enhance the signal-to-noise ratio of a desired pulse and hence improve target detection and discrimination. This is especially useful with low energy sources and noise which is incoherent in both space and time. Second, arrays inherently have a directionality associated with them, and they can, therefore, be oriented to transmit and/or receive the maximum signal in a certain direction. This has the obvious advantage of allowing one to focus on a particular object or direction and to reject noise or unwanted signals from other directions. The directionality or radiation pattern, of an array is a function of the frequency of the transmitted or received energy.

At the simplest level a one-dimensional (1-D) array can be used to detect subsurface features. However, the problem with a 1-D array is that the earth is only being swept in one direction. Although it is possible through computer processing to expand to 2-D through synthetic aperture concepts, a true 2-D array is a better solution. The 2-D array would cover a rectangular area with elements placed on a grid. Note that hard wired connections can be made on this array rather than using time consuming software for a synthetic aperture structure. Arrays offer not only the technical advantages suggested, but also a versatility not possible in a single element GPR (Ground Penetrating Radar) system.

## (2) Directive Antenna Elements as Sensors

Traditional antennas used for GPR are bow tie type dipoles. These have an almost omni-directional radiation pattern and a low front-to-back ratio (meaning they radiate in the air as well as into the earth). GEO-CENTERS, INC. has developed a new type of GPR antenna, a resistively loaded traveling wave antenna configuration, with a narrow radiation pattern, a high front-to-back ratio, and about 50% efficiency. This antenna can be used to increase the overall system gain by increasing the antenna gain parameters  $G_r$  (receiver gain) and  $G_t$  (transmitter gain) through improved directionality. Additionally, the power can be increased through the use of recently available high power pulser electronics by feeding each dipole element with its own pulse instead of the traditional single pulser method.

The resistively loaded traveling wave antenna requires a fabrication material whose resistance cross-section can be varied by changing the physical antenna geometry. To date, antennas have been fabricated from conductive paper and epoxy loaded with graphite. The paper elements work well but are suitable only for building straight antennas. Since curved geometries are necessary to optimize antenna performance, a moldable material such as epoxy is desirable.

The directive time domain antenna developed by GEO-CENTERS is based on the theory of Wu and King (1). The basic design and configuration of the antenna is a resistively loaded dipole which has been folded into a V shape. The optimum taper for these elements is shown to be a linear function of distance. It is proportional to  $(h-|z|)$  where  $h$  is the length of each antenna element and  $z$  is the distance from the driving point.



Note that the current is a pure traveling wave whose amplitude decreases linearly with  $z$ . The traveling wave of current  $I(z)$  is associated with the free space propagation constant,  $k_0$ . Thus, as with any traveling wave antenna, the electrical length determines the cone angle for the main beam radiation. As the electrical length  $k_0 h$  increases, the beamwidth and the main beam cone angle decrease.

The electrical length of the V-antenna is the primary factor controlling the beamwidth. However, the center frequency for time domain operation basically determines the minimum physical length. Thus, the design criterion states that the antenna physical length should correspond to the center frequency electrical length of  $3\lambda$  (i.e.,  $3\lambda = \frac{2\pi h}{\lambda_0}$ ). At 300 MHz, the application of this criterion translates into a V-antenna with elements approximately five feet in length. Since the element lengths for lower center frequencies are impractically long, ways to miniaturize the antennas are needed but not at the expense of increasing the beamwidth. In general, electrically shorter antennas have reduced directivity.

New resistive profiles were considered in order to reduce the size of the V-antenna. A new directive radiating element was designed using software developed to predict the radiation properties of reflectionless antennas. By modeling the radiation properties of the proposed geometry on a finite element basis, a spiraled dipole (Tusk) was found to exhibit the desired directive characteristics. This also places the driving point of the antenna close to the ground for improved coupling of the radar pulse. A drawing of the Tusk antenna and its enclosures is shown in Figure 1.

### (3) Focusing Control Through Time Gating

The major sources of noise and interference for mine detection came from surface effects and clutter. These affects can be minimized by using directive antenna elements, arrays, and focusing. A representative one dimensional array is shown in Figure 2. Time delay sections  $\Delta\tau_1, \Delta\tau_2, \Delta\tau_N$  are preset to focus at a given position in or on the earth. Focusing arrays can also be cascaded to cover a two- or three-dimensional section.

A simple mathematical description of the array can be obtained by considering the output of each antenna as a delta function pulse and the received signal as being perfectly reflected from a buried feature. Thus the signal,  $S$ , received at the sum function of the array of Figure 2, is given by

$$S = \sum_{i=-N}^N \int_{-\infty}^{\infty} \delta \left( t - \frac{2Ri}{v} - \Delta\tau_i \right) dt \quad (1)$$

$$\text{where } \delta(t) = \begin{cases} \infty, & t = 0 \\ 0, & t \neq 0 \end{cases}$$

$$\int_{-\infty}^{\infty} \delta(t) dt = 1$$

Note that by properly adjusting the time delay  $\Delta\tau_i$  such that

$$2Ri/v + \Delta\tau_i = \text{const}, \quad i = 0, \pm 1, \pm 2, \dots, \pm N$$

then  $S$  has a maximum value equal to  $2N+1$ . In practice, earth attenuation, imperfect scattering, and clutter will reduce the idealized focusing effect.

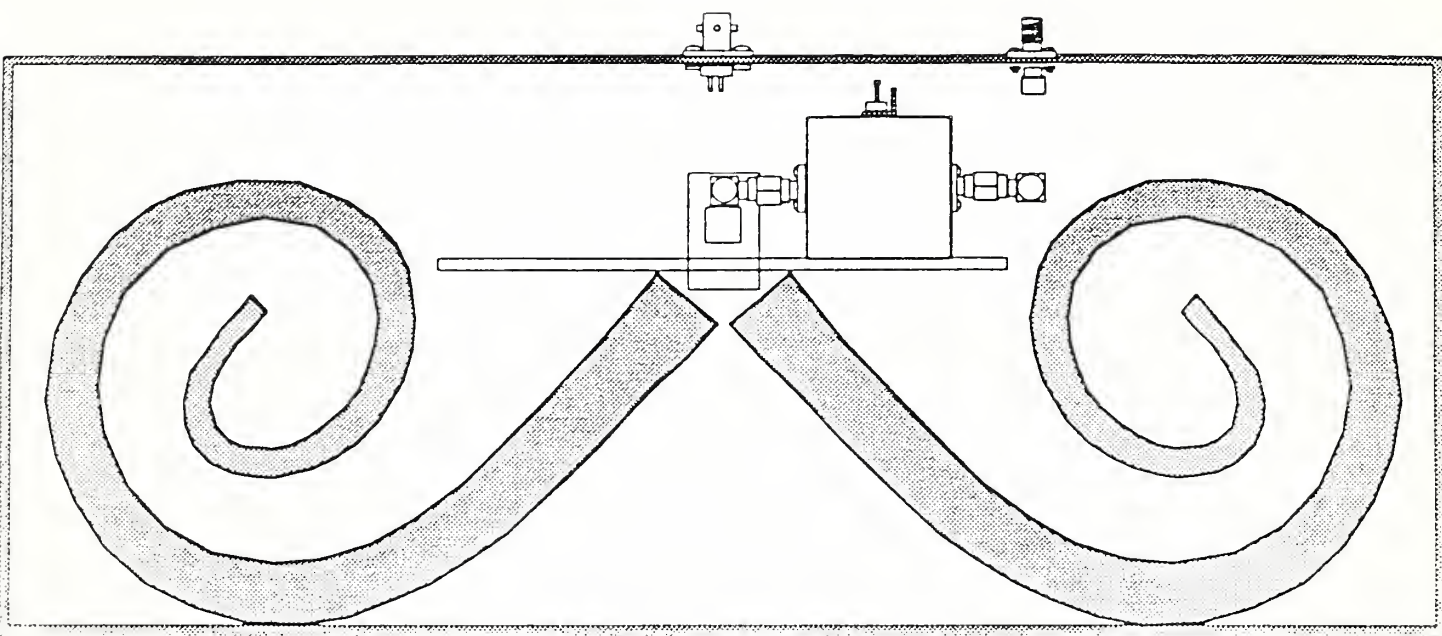


Figure 1. Tusk Antenna with Enclosure

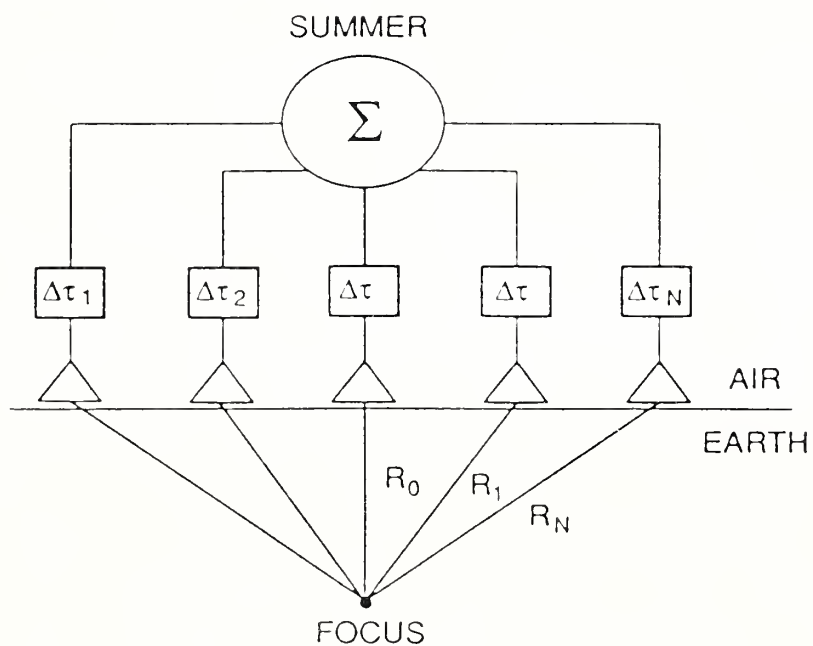


Figure 2. A Focusing Time Domain Array

To give an idea of the appearance of the output of a focused array, an artificial array was modeled. Figure 3 shows a GPR output for a traverse over buried ordnance. Figure 4 shows the output of a five element focused array at different depths A, B, and C. Note that the returns from the radar pulses shown in the marked areas BB and CC in Figure 4 have been focused based on the array outputs of Figure 3.

An alternate approach involves the use of electronic scanning. Here, time delays can be sequenced to move the focusing point along prescribed paths in or on the earth. Examples are scans which are along lines or planes parallel to the earth-air interface. Scanning can also be accomplished using the hard wiring concept. Outputs from a set of pre-focused arrays could be used to give information comparable to that of an electronically scanned system.

Electronic scanning can be accomplished by adjusting the time delays  $\Delta\tau_i$  so that the transmitted pulses add up at a prescribed point in the earth. Figure 5 shows the result of a computer simulation to focus the transmitted pulses along vertical slices in the earth. The returns in the section CC correspond to the similarly marked areas of Figure 3.

#### Acknowledgement

The author would like to acknowledge the help of Michael Benson in programming the array outputs shown in Figures 4 and 5.

#### References

- (1) Wu, T.T. and King, R.W.P., "The cylindrical antenna with non-reflecting resistive coating", IEEE Trans. on Antennas and Prop., Vol AP-13, No 3, pp. 369-373, May 1965.



BSGSS05 (RAW DATA)

HORIZONTAL TRAVEL →

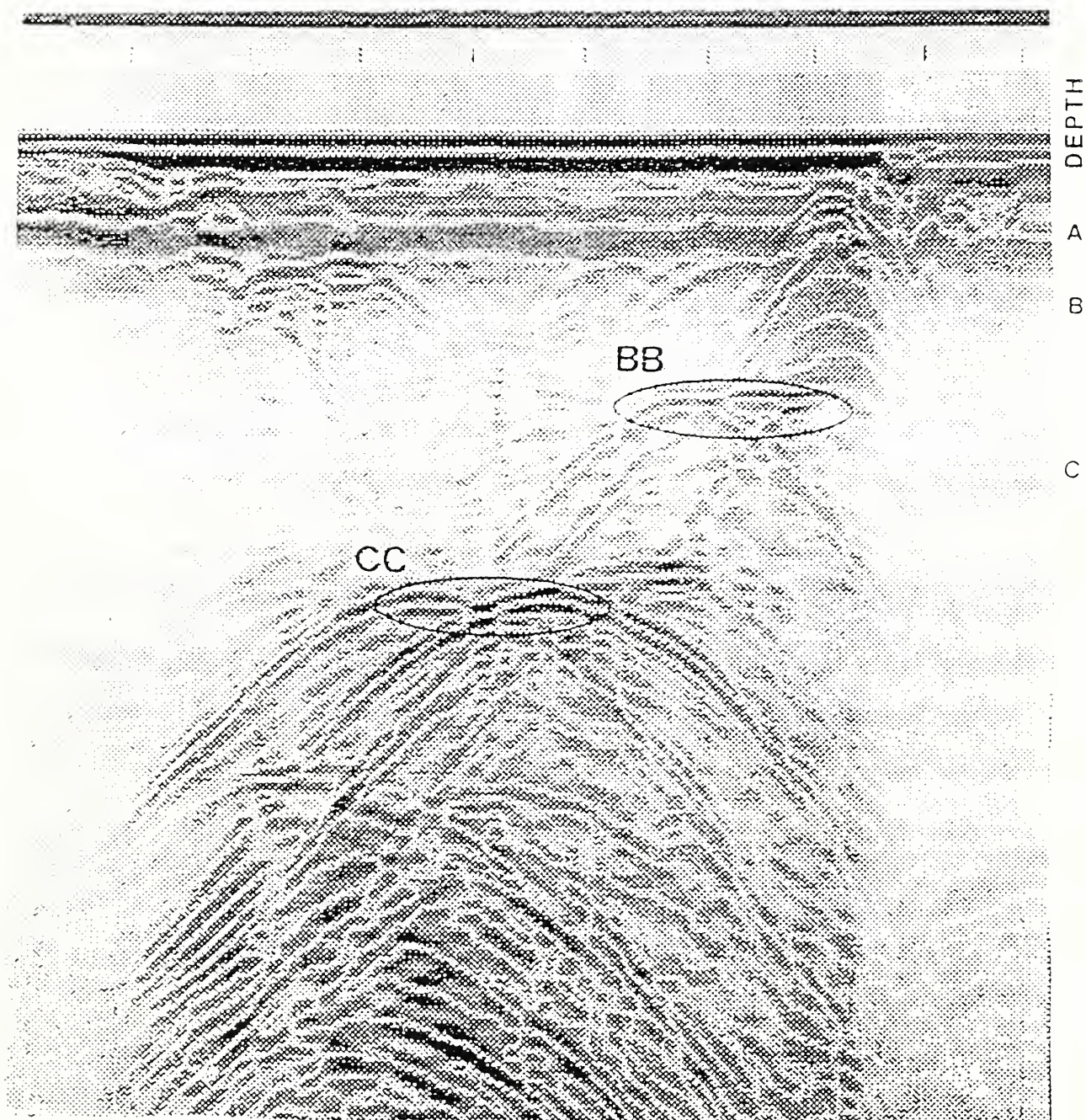


Figure 3. Returns From Buried Ordnance



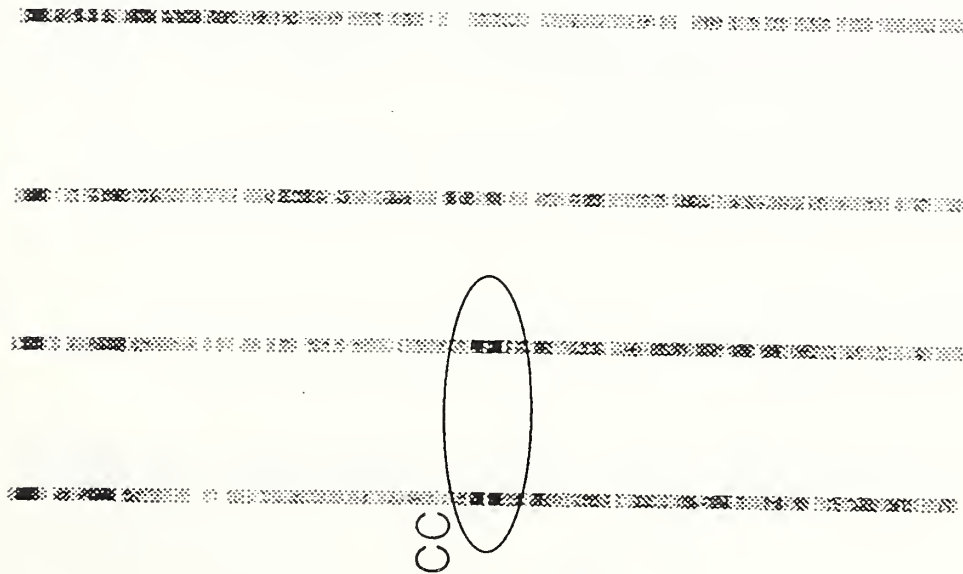


Figure 4. Outputs From an Artificial Array Focused at Different Vertical Depths.

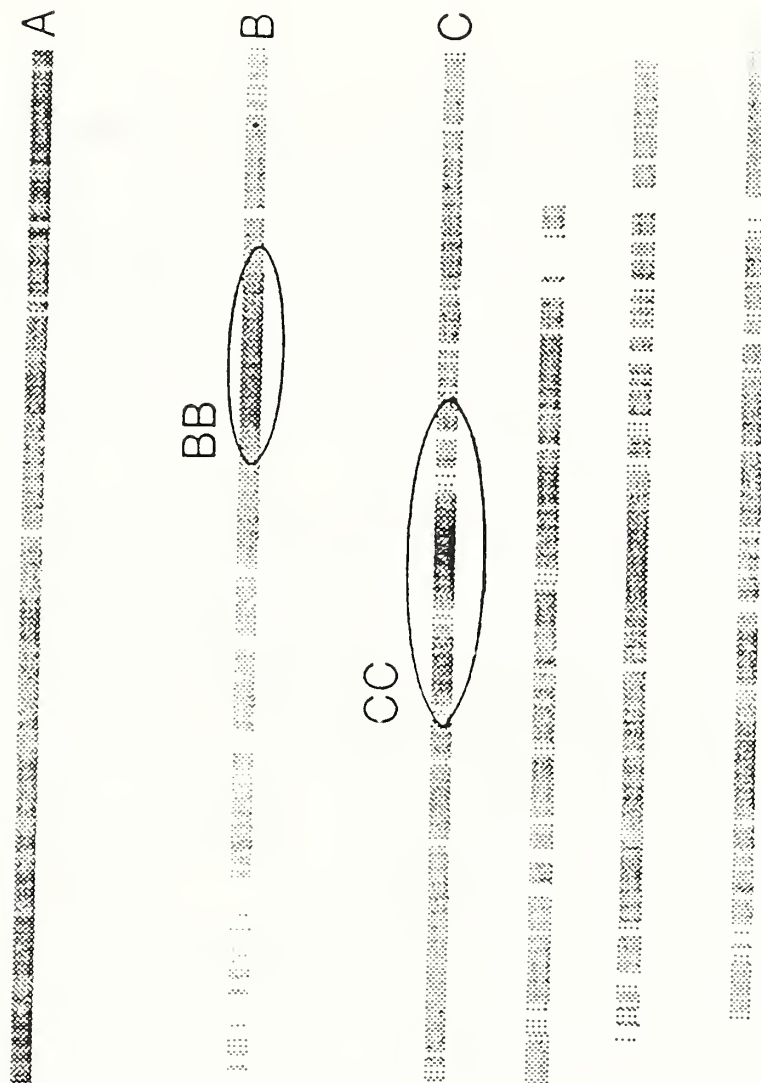


Figure 5. Outputs From an Artificial Array Focused at Different Horizontal Depths.



GEO-CENTERS, INC.

A LARGE AREA, GROUND PENETRATING RADAR SURVEY SYSTEM

BY

ALAN CRANDALL\*

Submitted For Presentation  
At

Second International Symposium On  
Geotechnical Applications Of  
Ground Penetrating Radar

March 6-10, 1988

ACKNOWLEDGEMENT

Research for this paper funded by the Army Corps of  
Engineers, technically directed by the Naval Explosive  
Ordnance Disposal Technology Center, and contracted  
by the Naval Research Laboratory

\* Senior Engineer, GEO-CENTERS, INC., Newton Centre, MA 02159

## A LARGE AREA, GROUND PENETRATING RADAR SURVEY SYSTEM

### 1.0 INTRODUCTION

The U.S. Congress through Public Law 98-212 charged the Department of Defense to institute a remedial action program to clear ranges and areas contaminated with hazardous explosive materials and ordnance. As a part of the response, the Naval Explosive Ordnance Disposal Technology Center (NAVEODTECHCEN) has been tasked by the U.S. Army Corps of Engineers to develop and demonstrate systems capable of detecting, locating, and categorizing shallow buried unexploded ordnance.

An advanced development program using Ground Penetrating Radar (GPR) to detect shallow buried ordnance was undertaken. The thrust of the effort was directed to the application of near term technology. Critical issues and technological risks relative to operational goals were explored through parallel efforts on sensor equipment, field surveys, and data processing. The validity of the GPR technique as an effective survey tool for shallow, buried ordnance was established and documented in a technology validation report.

The program has moved on to the design, development, and delivery of an operational prototype system. This paper describes the design concept of the towed, GPR system being developed. A conceptual drawing is shown in Figure 1.



FIGURE 1. CONCEPTUAL DRAWING OF A WIDE AREA GPR SURVEY SYSTEM

## 2.0 DESIGN GOALS

Three major design goals were established for the system being developed. The first is to detect, locate, and categorize the following buried ordnance.

- 155 mm Projectile at a Nominal Depth of 1.5m (5ft.)
- MK81 (250 lb.) Bomb at a Nominal Depth of 3m (10ft.)
- MK82 (500 lb.) Bomb at a Nominal Depth of 4.5m (15ft.)

The second is to conduct area surveys of contaminated areas at the nominal rate of 30 Acres per day, and the third goal is for the system to generate hard copy target maps for subsequent area clean-up.

## 3.0 SENSOR SELECTION

The first task in the design process was to select the GPR sensor or sensors and a configuration for those sensors that would meet the design goals. Due to the constraint of utilizing near term technology, the key decision was made to use existing, commercially available GPR antennas. Several of these antennas could be combined for wide area coverage in a single pass to achieve the desire survey rate of 30 acres per day. Table 1 lists the available GPR antennas by frequency with comments on their suitability for this application.



Table 1 - GPR Antenna Summary

FREQUENCY	AVAILABLE ANTENNAS	COMMENT
LOW	80, 120 MHz	questionable near surface performance insufficient resolution
MEDIUM	300, 500 MHz	acceptable resolution and penetration for 300 MHz data base available for 300 MHz antenna
HIGH	900, 1000 MHz	insufficient depth penetration

We note from Table 1 that the high frequency antenna propagation distances are not sufficient in most soils to detect the larger, deeply buried ordnance. Energy from low frequency antennas may leave near surface "blind zones" due to unpredictable, near field performance. There is also insufficient resolution to detect targets in aspects other than optimum orientation.

Complicating the selection of an appropriate sensor were numerous adjustable system parameters (summarized in Table 2) that had to be considered. Realizing that no single frequency antenna could provide optimum detection from just below the surface down to 4.5m (15ft.), it was decided to base the design on the requirement to detect a 155mm projectile between 1 and 1.5m (3 and 5 feet) and larger targets deeper. The program would concentrate on detection of the larger, deeper targets foremost and provide an option for changing to higher frequency antennas to enhance near surface capability.

## TABLE 2 - SENSOR SELECTION

### ADJUSTABLE PARAMETERS

<u>Parameter</u>	<u>Range</u>	<u>Considerations</u>
Antenna Frequency	80,120,300,500, 900,1000 MHz	<ul style="list-style-type: none"> <li>• Deeper Penetration at Lower Frequencies</li> <li>• Near Surface Target Detection is Better for Higher Antenna Frequencies</li> <li>• Reduced Target Resolution at Lower Frequencies</li> <li>• Effective Footprint is Larger at Lower Antenna Frequencies</li> </ul>
Pulse Repetition Rate	up to 100KHz	<ul style="list-style-type: none"> <li>• Higher Repetition Rate Yields More Samples</li> </ul>
Number of Antennas	1-8	<ul style="list-style-type: none"> <li>• More Antennas Increase Data Volume</li> <li>• Number of Antennas Increase with Frequency</li> </ul>
Stack Factors	1, 2, 4, 8, 16	<ul style="list-style-type: none"> <li>• Signal-to-Noise of Data Improves by Approximately the Square Root of the Stack Factor</li> <li>• Larger Stack Factor Reduces Data Volume</li> </ul>
Points per Trace	128, 256, 512	<ul style="list-style-type: none"> <li>• Better Vertical Resolution with More Points</li> <li>• More Points Per Trace Increase Data Volume</li> </ul>
Maximum Trace Spacing	1.3 to 15.2 cm (1/2 to 6 inches)	<ul style="list-style-type: none"> <li>• Closer Spacing Increases Data Volume</li> <li>• Closer Spacing Yields Better Target Resolution along the Track</li> </ul>
Storage System	Record Rate up to 100 Kbytes/sec Storage Capacity up to 400 Mbyte/medium	<ul style="list-style-type: none"> <li>• Storage Capacity and Record Rate Determine the Maximum Data Rate and Time Between Media Changes</li> </ul>
Processing Time	_____	<ul style="list-style-type: none"> <li>• Multi Trace Algorithms Take Longer</li> <li>• Larger Recorded Data Volume per Area Increases Processing Time</li> </ul>
Vehicle Speed	1/2 to 6 MPH	<ul style="list-style-type: none"> <li>• Lower Speed Decreases Trace Spacing and Increases Data Volume per Area</li> </ul>



GEO-CENTERS, INC.

Our baseline design using four 300MHz GPR antennas is presented in Table 3. A high frequency option using eight 900 MHz antennas is presented in Table 4.

Once the sensors had been selected, system design objectives were established. These objectives are summarized in Table 5 with the environmental design objectives listed in Table 6.

An overall GPR SYSTEM Block diagram is presented in Figure 2. The system is comprised of two major subsystems, the Tow Vehicle and Platform, and a separate Command Center.

The Tow Vehicle and Platform form a complete field survey subsystem and can operate (collect and store survey data) without the support of the Command Center. The Tow Vehicle is an air conditioned, four wheel drive, Ram Charger class vehicle and the Platform is a custom trailer built to support four 300MHz GPR antennas (or eight 900MHz GPR antennas) either at fixed heights (1 to 12 inches) above ground or in an independent terrain following mode. The operational characteristics for the Tow Vehicle and Platform are highlighted in Table 7.

The Command Center is also a self contained subsystem capable of being transported (towed) to a survey site or left at a central data processing point. Its operational characteristics are summarized in Table 8.

## TABLE 3 - BASELINE DESIGN

Antenna Frequency:	300 MHz
Pulse Repetition Rate:	75 KHz / antenna
Number of Antennas:	4
Stack Factor:	8
Points per Trace:	256
Maximum Trace Spacing:	7.6 cm (3 inches)
Storage System:	400 Mbyte optical disk 80 min / side (38 Kbyte / sec) 160 min / disk
Processing Time:	Goal 1 acre / hour
Vehicle Speed:	1/2 - 6 MPH



GEO-CENTERS, INC.

## TABLE 4 - BASELINE OPTION

Antenna Frequency:	900 MHz
Pulse Repetition Rate:	37.5 KHz / antenna
Number of Antennas	8
Stack Factor:	4
Points per Trace:	128
Maximum Trace Spacing:	3.8 cm (1.5 inches)
Storage System:	400 Mbyte optical disk 40 min / side (75 Kbyte / sec) 80 min / disk
Processing Time:	approximately 4x baseline design *
Vehicle Speed:	1/2 - 6 MPH

\* Assumes no further algorithm development



## TABLE 5 - GPR SYSTEM DESIGN OBJECTIVES

- Survey up to Five Acres Per Hour
- Post Processing of Survey Data
- Operational Evaluation Within CONUS Under Nominal Conditions
- Operational Personnel to be Skilled in Ordnance Surveying and Trained in GPR Operation
- Operational Use in Conjunction with EOD Personnel
- Field Maintenance Limited to Modular Replacement
- Depot Maintenance to be by Geo-Centers Personnel
- User Documentation Consistent with the Above (Commercial Style Manual)
- Design/Fabrication Documentation Suitable for Depot Maintenance
- Provide Hardware and Software "Hooks" for Operation with Complementary Sensor Arrays



GEO-CENTERS, INC.

## TABLE 6 - GPR ENVIRONMENTAL DESIGN OBJECTIVES

- **STORAGE**
  - Temperature of -10°C (14°F) to 50°C (122°F)
  - Humidity <95% Non-condensing
  - Archive Storage Media Limited
- **OPERATION INTERIOR TO TOW VEHICLE AND COMMAND CENTER**
  - Temperature of 4°C (40°F) to 32°C (90°F)
  - Humidity of < 90% Non-Condensing
- **TRANSPORTATION**
  - Temperature of -10°C (14°F) to 50°C (122°F)
  - Humidity <95% Non-condensing
  - Altitude to 10,000 Feet
  - Shock and Vibration of Heavy Equipment Loading/Unloading and Transport by Trailer or Air



GEO-CENTERS, INC.

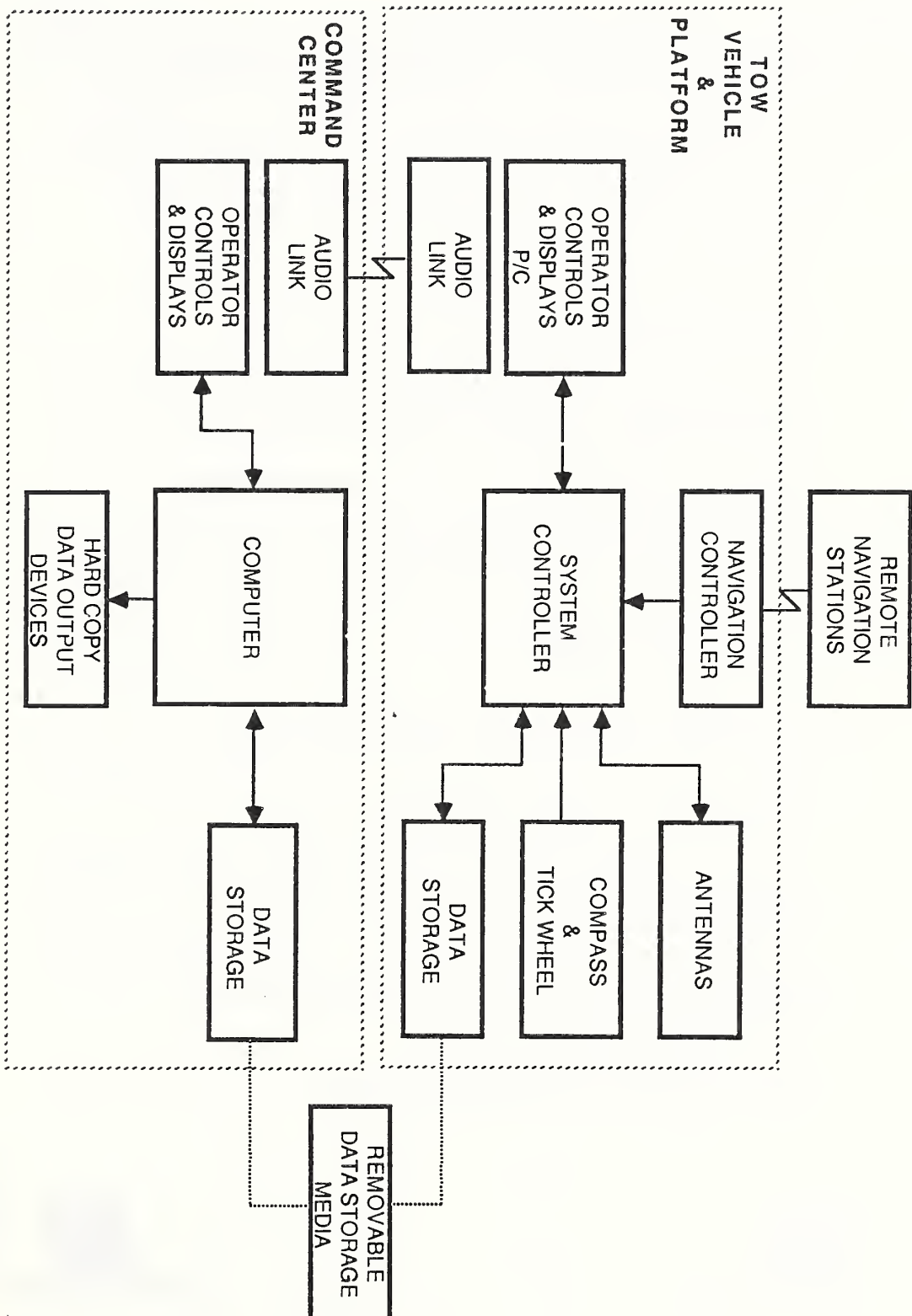


FIGURE 2. GPR SYSTEM BLOCK DIAGRAM

## TABLE 7 - GPR TOW VEHICLE & PLATFORM OPERATIONAL CHARACTERISTICS

- Survey Speed of up to 6 MPH Based on Terrain
- Swath of 3 Meters (10 ft.)
- Data Storage Capacity of 160 Min. / Disk
- Operational Use of Eight Hours Without Logistic Support
- Terrain Capability as Limited by Tow Vehicle & Platform
- Transportable by Air or Ground
- Two Man Operation
- On Board Status Indication for Operators
- Set-Up Time of Less Than Four Hours
- Will Acquire and Record Sampled Sensor Data in Real Time
- Data to be Transferred to Command Center by Removable Optical Disk
- Will Meet Environmental Objectives



GEO-CENTERS, INC.

## **TABLE 8 - GPR COMMAND CENTER OPERATIONAL CHARACTERISTICS**

- Processing Rate of at Least One Acre Per Hour
- Target Location Estimate is  $\pm 1$  Meter on the Ground and  $\pm 1/3$  Meter in Depth
- Target Categorization
- Processed Location Output to be Available with Variable Scaling
- One Man Operation
- Menu Driven Processing
- Transportable by Air or Ground
- Set-Up Time of Less Than Four Hours
- Will Serve as the Field Office



GEO-CENTERS, INC.



A more detailed block diagram for the Tow Vehicle and Platform is presented in Figure 3. The GPR System operator interfaces through the Operator Control and Display Computer. This computer is a ruggedized AT personal computer with a high resolution (512 x 400 x 8 bit) monochrome graphics monitor mounted on a 19 inch rack. This computer steps the operator through the survey set-up sequence, displays real-time radar data, allows operator control of the Radar Controller and Data Acquisition Controller, and monitors and displays system status.

The Data Acquisition Controller is a custom, single board computer whose primary function is to integrate all data into standard record formats for storage on the Real-Time Data Storage device. This controller also passes Operator commands to the Radar Controller, and the Navigation Control and Measurement Unit (CMU) and passes information to display to the Operator Control and Display Computer.

The storage device is a 400Mbyte optical disk capable of handling the higher data transfer rates (up to 100Kbytes per sec.) if eight 900 MHz antennas were present. This high capacity allows ample survey time between media changes (80 min. per side for the baseline design and 40 min. per side for the 900 MHz antenna option).

The radar controller is a custom unit designed by GEO-CENTERS. It accepts Operator control for time window, trace position, and range gain for each antenna. It addresses each antenna separately and is currently configured to transmit and sample each antenna sequentially. The controller filters, applies the range gain and stacks each sample for output. The controller also monitors and outputs the status of each radar channel.

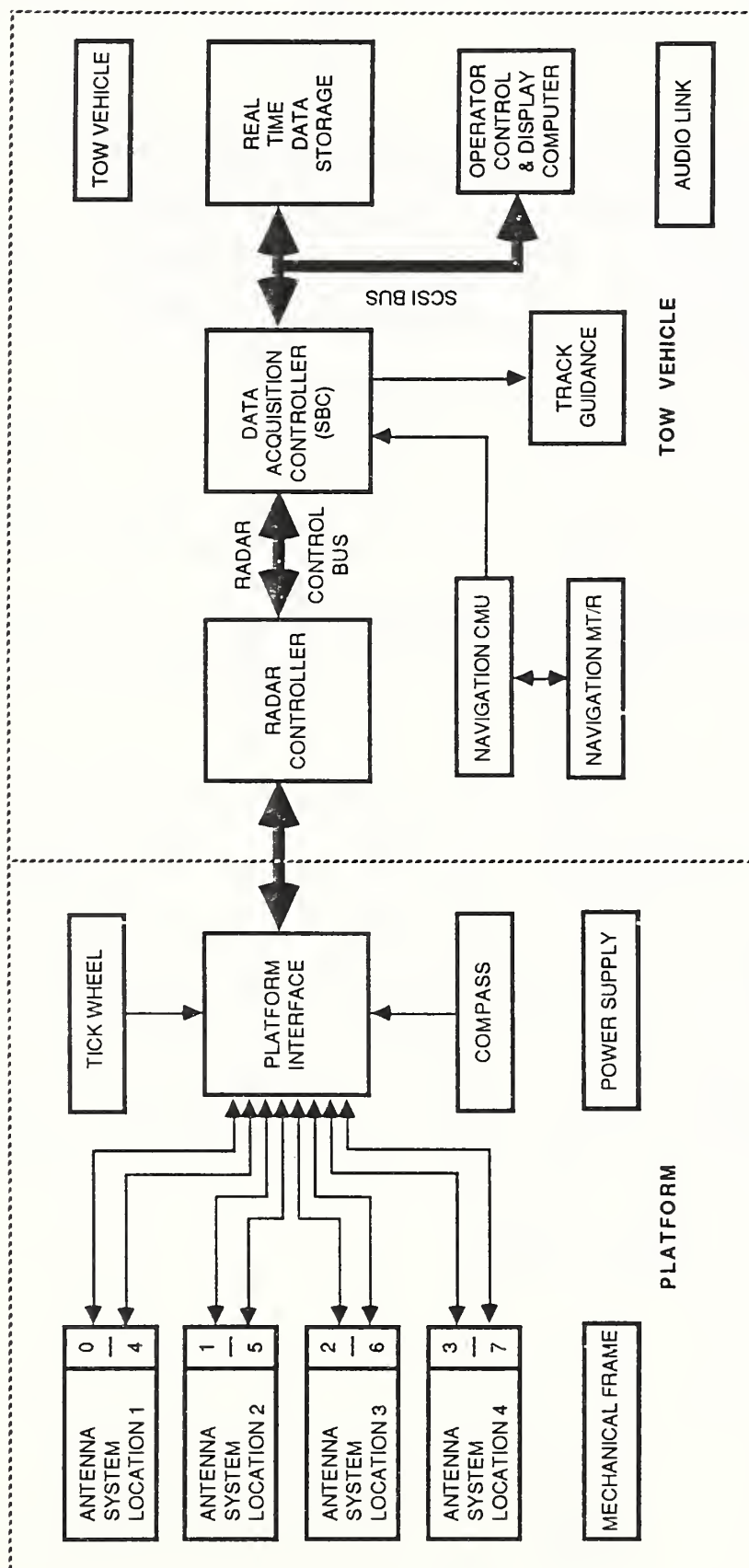


FIGURE 3. GPR TOW VEHICLE &amp; PLATFORM



GEO-CENTERS, INC.

Survey navigation is provided by a microwave positioning system. Using four remote reference stations and a mobile station mounted on the tow vehicle, this line-of-sight system provides very accurate ( $\pm 1$  meter) guidance for systematic surveys conducted in a series of parallel lines optimally configured/oriented to match the area being surveyed. In addition to providing survey guidance, the navigation (X,Y) position information is stored along with the Platform compass and tick wheel information for calculating exact sensor positions used for determining target (X,Y) locations.

Track guidance information is displayed to the tow vehicle operator on a Left/Right meter indicating vehicle position relative to the desired track. Also displayed are distance along the track, distance to end of track and navigation system status.

An audio link is provided for communication with the Command Center and to a remote support group whose primary function is to maintain the remote navigation stations.

The platform is towed by the tow vehicle and is electrically connected via the Platform bus. The mechanical frame shown in Figure 4 is made of lightweight, channel aluminum using standard trailer wheels and suspension. The frame supports each of the four 300 MHz Antenna (or eight 900MHz antennas) from a pair of swing arms that allow a terrain following capability. The swing arms are damped by pneumatic shock absorbers designed to allow easy motion at the beginning of travel but stiffening as the shock absorber reaches its maximum travel. The pneumatic system is also used to raise the antennas to their full-up, transport position.

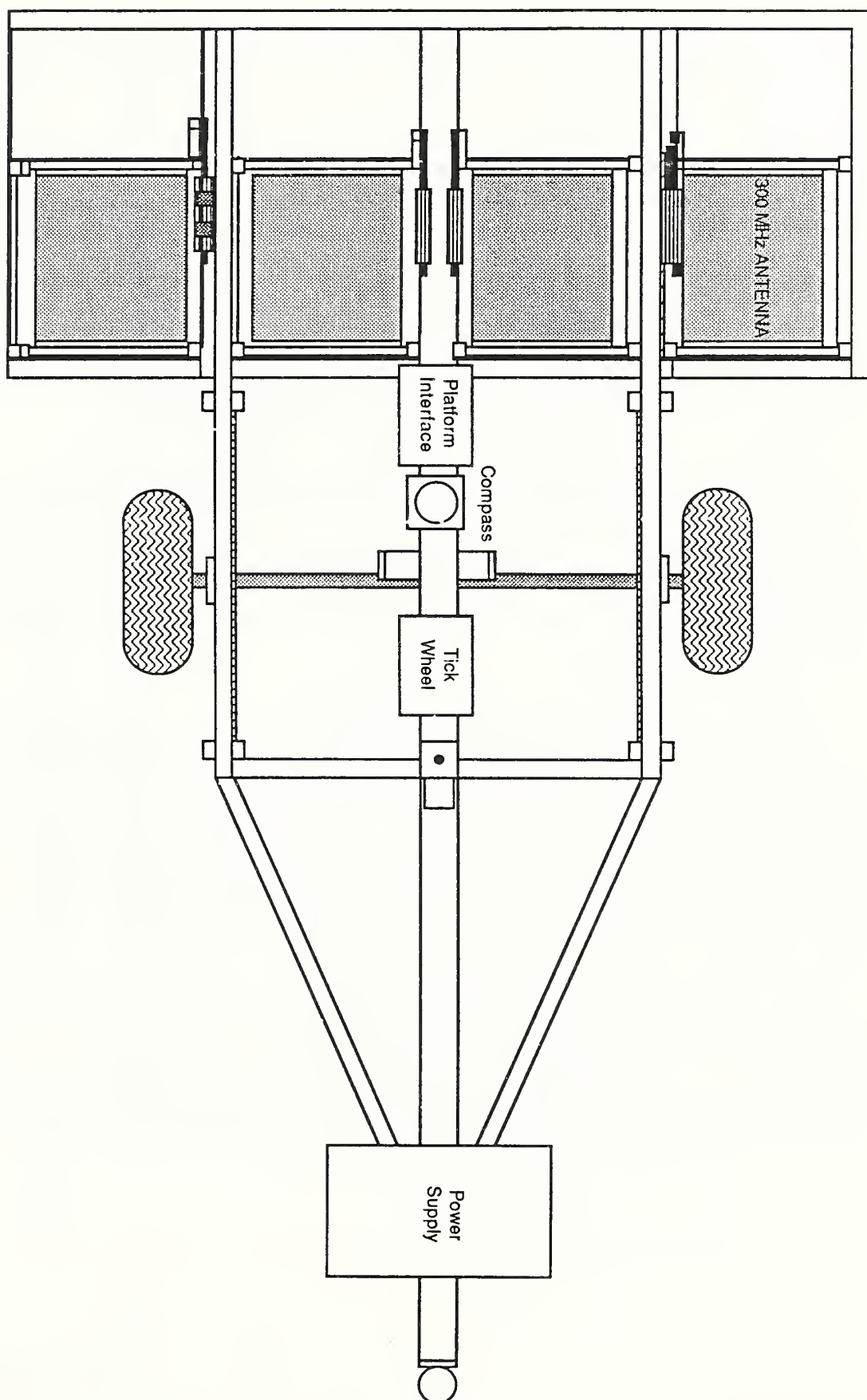


FIGURE 4. GPR PLATFORM CONCEPTUAL DRAWING  
MECHANICAL FRAME



GEO-CENTERS, INC.

The Platform Interface interfaces the platform functions with the controlling circuits located in the Tow Vehicle. The Platform Interface demultiplexes control signals from the Radar Controller, routes them to the GPR antennas, and multiplexes the resulting radar return data back to the Radar Controller. The compass input, used for monitoring the heading of the platform relative to the desired track heading, is passed to the tow vehicle. The tick wheel uses an optical shaft encoder to provide a very accurate measure of the distance traveled. This information is stored and used in the command center to normalize the GPR data to a uniform (3 inch) trace spacing.

Also mounted on the Platform is a gasoline generator that supplies electrical power to the tow Vehicle and Platform. The raw AC power passes through a power line conditioner and power monitor located in the tow vehicle prior to distribution. The generator is also used to charge the remote navigation batteries when not surveying.

A more detailed block diagram of the Command Center is shown in Figure 5. The design concept for the trailer mounted enclosure is shown in Figure 6. The enclosure provides heating, ventilation and air conditioning as required, all powered by a dedicated generator. An additional generator supplies system operating power through a powerline conditioner and power monitor.

The heart of the Command Center is a Motorola 68020 microprocessor in a FORCE, INC. VME System operating in a Uniflex environment. Peripherals include an optical disk for inputting field survey data, and operator control terminal for set-up and



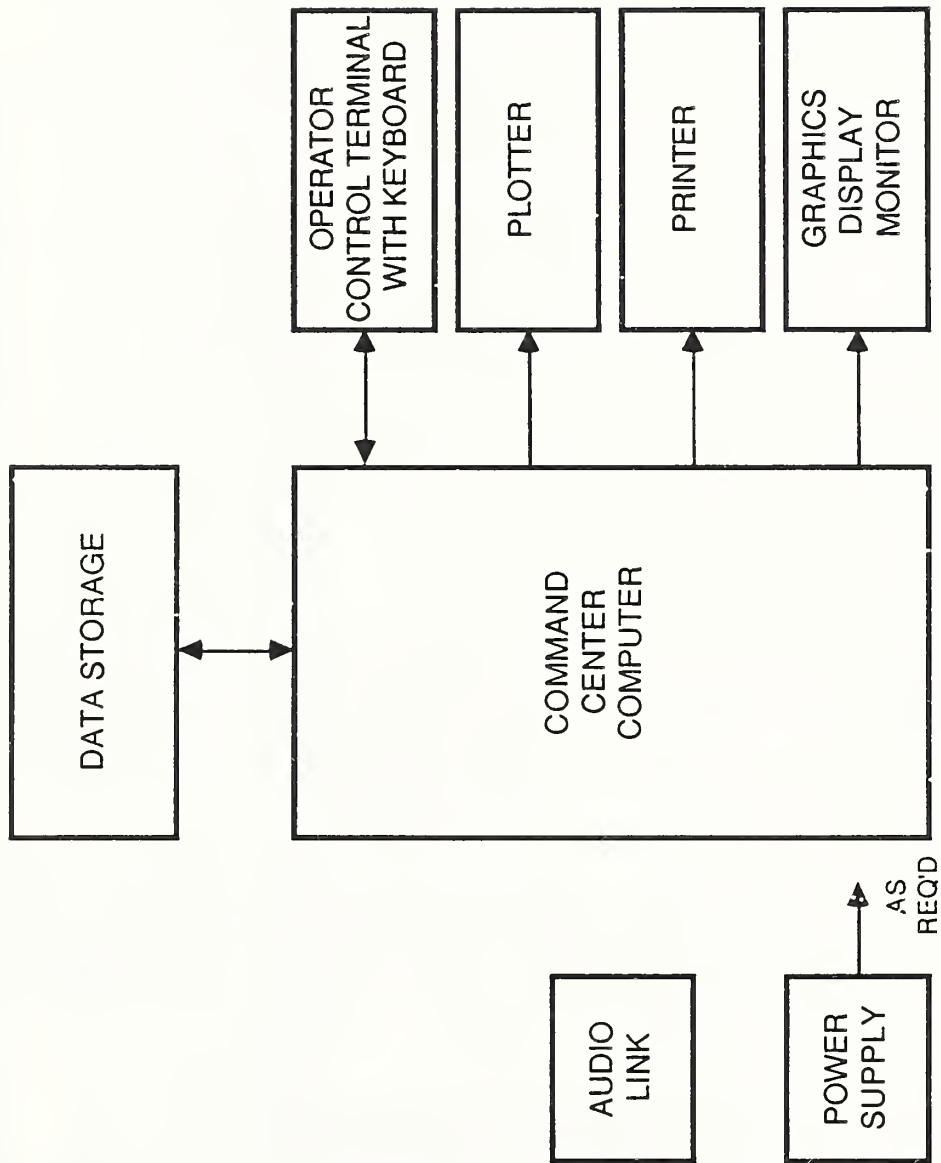
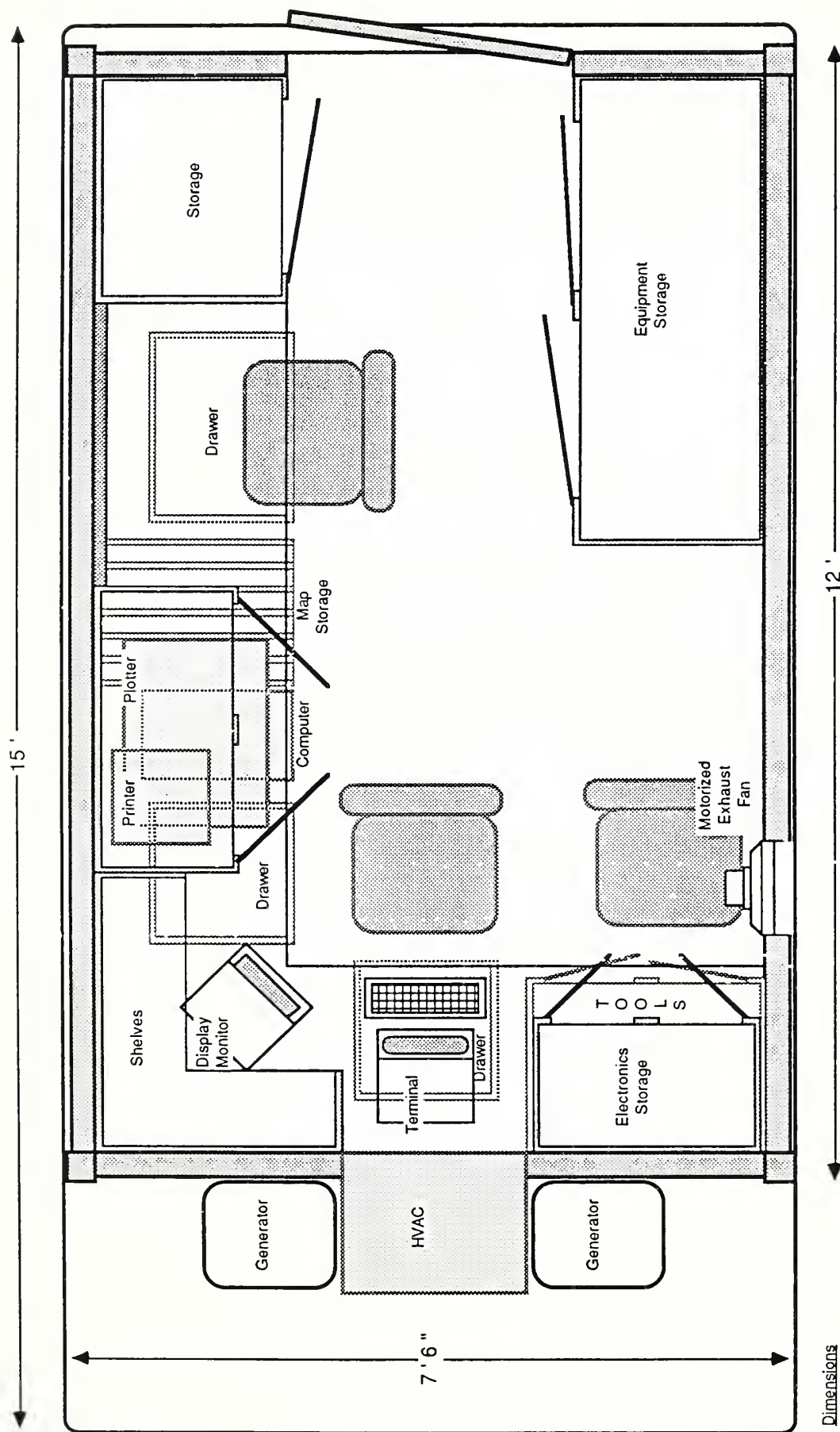


FIGURE 5. COMMAND CENTER



GEO-CENTERS, INC.



Dimensions	
HVAC	H2' W2' D1'6"
Shelves	H2' W3' D2'6"
Printer	H4' W1' D1'
Plotter	H6' W2' D1'6"
Computer Drawer	H4' W1'6" D1'6"
Terminal Drawer	H4' W1'6" D1'6"
Computer Storage	H2' W3' D1'6"
Electronics Storage	H2'6" W2'6" D1'6"
Tool Storage	H2'6" W2'6" D1'6"
Map Drawer	H4' W1'6" D1'6"
Map Storage	H2'6" W1'6" D2'
Computer Storage	H2' W1'7" D2'
Equipment Storage	H7'6" W2'6" D2'
	H7'6" W5' D2'

FIGURE 6. TOP VIEW TRAILER MOUNTED ENCLOSURE WITH  
WORK STATION DIMENSIONS

system operation, a Graphics Display Monitor for displaying raw and processed GPR data and a printer and plotter for outputting and presenting survey information.

An audio link is provided for communication with the field survey team as well as remote support personnel.

The Command Center processing of the field survey data is graphically shown in Figure 7. Field data is transferred on Optical disk and is processed one line (GPR channel) at a time. Data is first preprocessed, which includes sensor (X,Y) positioning, trace space normalization and filtering, and is then stored on hard disk (Mbyte). The Command Center Operator then selectively reviews the pre-processed data and selects certain targets for GPR velocity analysis. This interactive process continues until a satisfactory GPR velocity map of the survey area is stored for subsequent data processing. Data analysis then proceeds automatically using a suite of detection algorithms to detect, locate and categorize targets on a line by line basis and then correlate this line data for storage and final output. Target logs are printed out and a variety of operator selected site maps are generated. Figure 8 is an example of a site plot showing field boundaries, survey quadrants that have been surveyed, and those with targets.

To support pre-processing and data analysis algorithm development, a single channel prototype was built to collect a field database over a range of targets. This prototype, shown in Figure 9, used a 300 MHz antenna supported by wooden swing arms attached to a metal boat trailer, a high resolution tick wheel for normalizing radar trace spacing, a 1.8 KW generator, a GSSI radar controller and power supply and a custom GEO-CENTERS integrating data acquisition system inside the Bronco - II tow vehicle.

This Wide Area GPR Survey System is currently in detailed design and is scheduled for delivery in January, 1989.

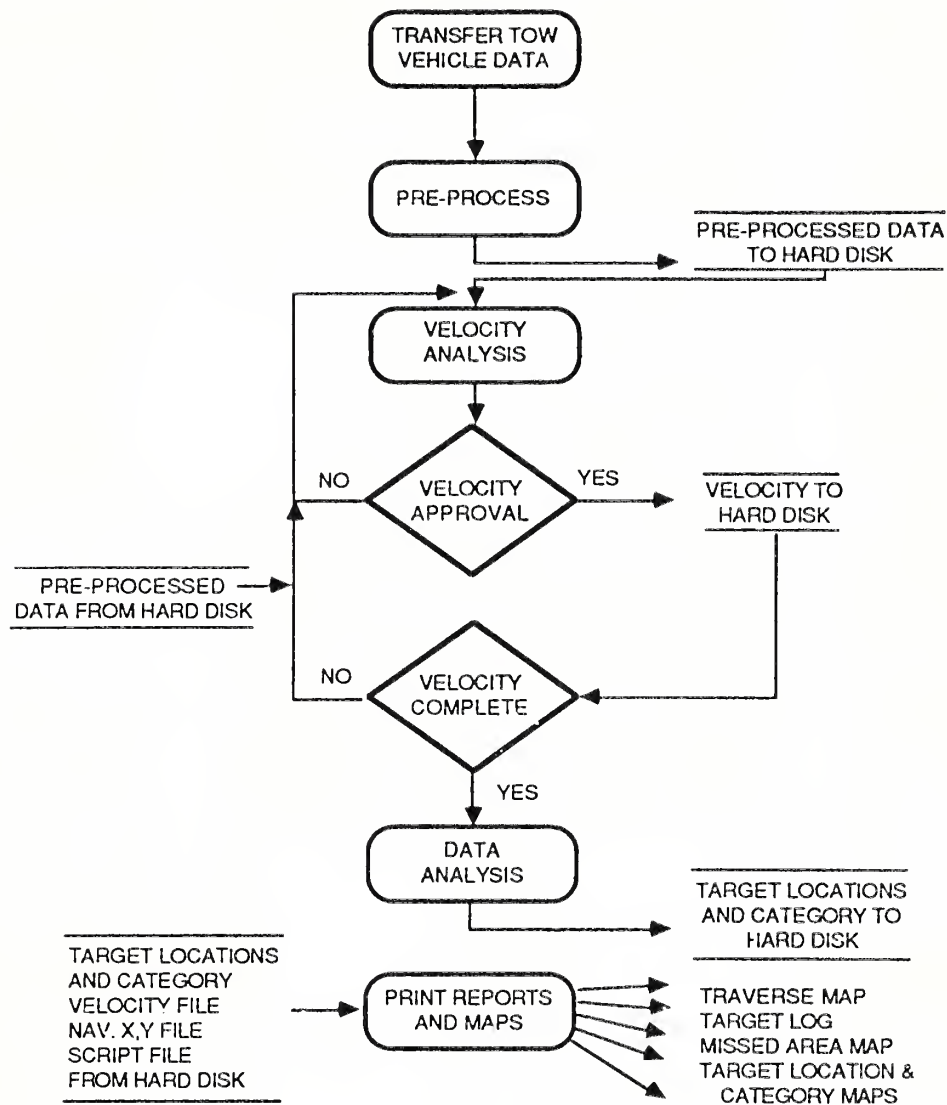
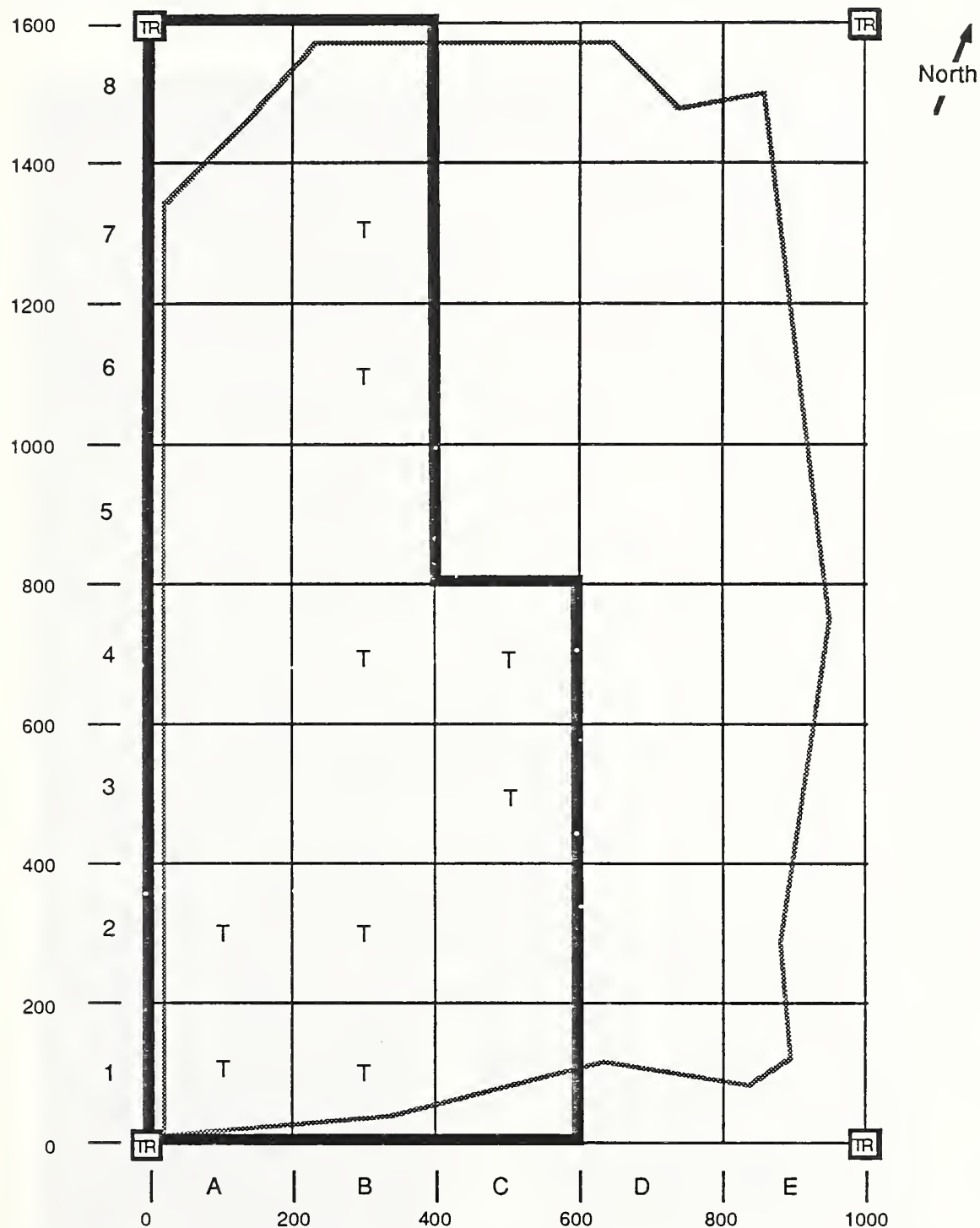


FIGURE 7 - COMMAND CENTER DATA FLOW

Date:  
 Site:  
 Operator:  
 Quadrants: A1 - E8



(Map shows field boundaries, quadrants that have been surveyed, and those with targets.)

FIGURE 8 - FIELD MAP WITH PROCESSING



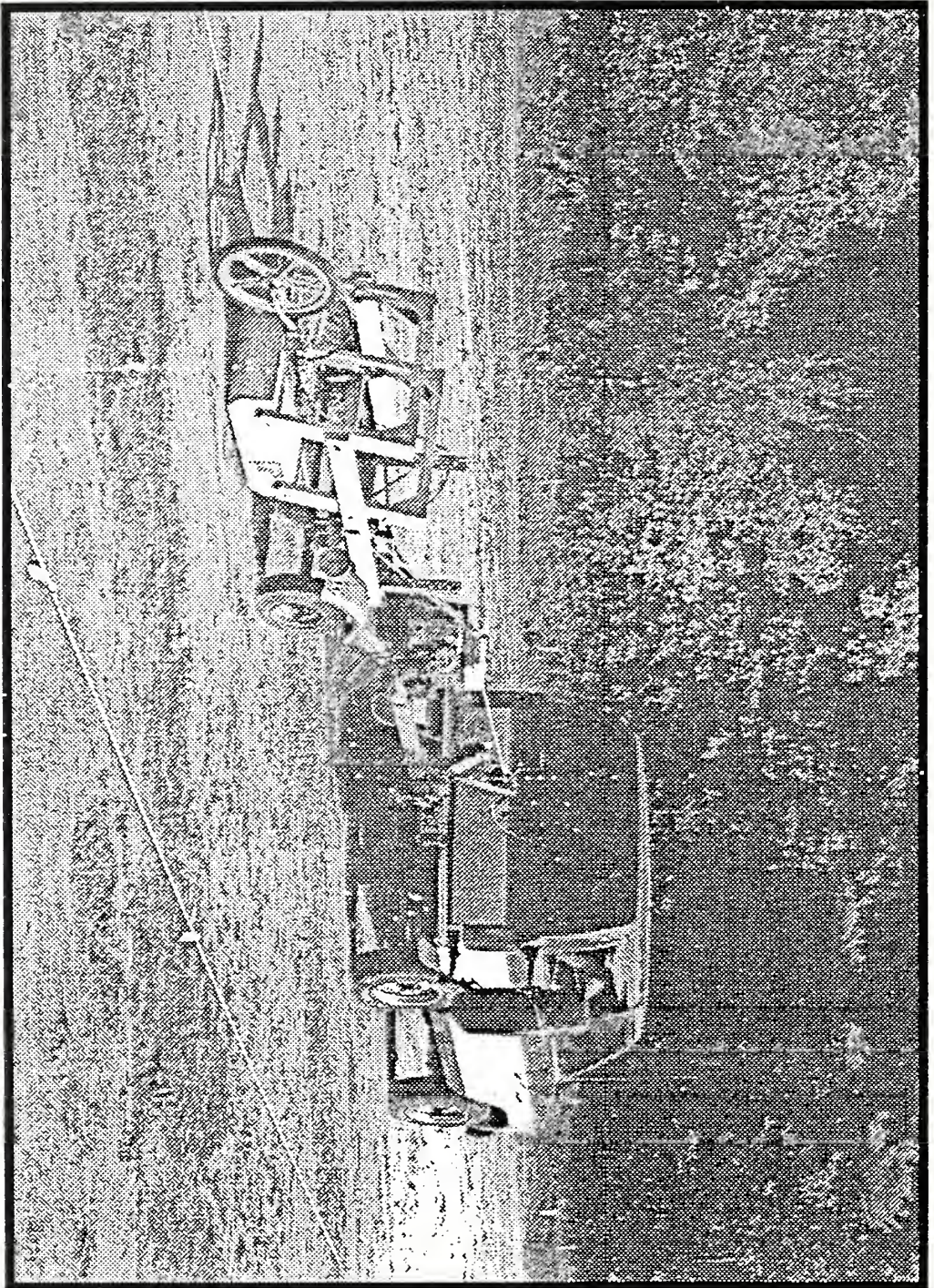


Figure 9. Geo-Centers Prototype GPR System  
Developed for the Government

Data acquisition and processing systems are integrated in the specially modified all terrain vehicle. Suspended antenna follows ground contour.





MIGRATION OF GROUND PENETRATING RADAR DATA:  
A TECHNIQUE FOR LOCATING SUBSURFACE TARGETS

BY

GREGORY HOGAN\*

Submitted For Presentation  
At

Second International Symposium On  
Geotechnical Applications Of  
Ground Penetrating Radar

March 6-10, 1988

ACKNOWLEDGEMENT

Research for this paper funded by the Army Corps of  
Engineers, technically directed by the Naval Explosive  
Ordnance Disposal Technology Center, and contracted  
by the Naval Research Laboratory

\* Senior Scientist, GEO-CENTERS, INC., Newton Centre, MA 02159

# MIGRATION OF GROUND PENETRATING RADAR DATA: A TECHNIQUE FOR LOCATING SUBSURFACE TARGETS

## INTRODUCTION

Migration is a method of processing data to image targets in the subsurface correctly and thus greatly increase target detectability. The technique was first developed in the 1940's by the oil industry to image geologic formations in the earth for the identification of potential oil bearing structures. Migration has enjoyed wide success and is now employed extensively in acoustic (seismic) data reduction. (See for example ref.1). The similarities between acoustic and electromagnetic wave propagation and reflection in the earth encourage application of migration processing to ground penetrating radar (GPR) data.

This paper describes the application of migration processing to the data obtained by ground penetrating radar in automated search for buried ordnance. These targets, buried at depths of 6 inches to 14 feet, range in size from a 155 mm projectile to a 500 lb bomb, and are generally non-resolved point targets for the radar frequencies employed. Although our discussion is limited to the application of migration processing to data from these point targets, the technique is obviously applicable to non-point targets such as the geologic formations mentioned above. We present the results of the application of migration processing to the data. The mathematical derivation of the model is also given.

## APPLICATION OF MIGRATION PROCESSING TO GPR DATA

In a typical GPR survey a radar transmitting and receiving antenna configuration is translated along a straight line across the ground. For a point target in the subsurface, the returning

energy is dispersed along a characteristic hyperbolic curve (or diffraction curve) as shown in Figure 1. These data were taken on targets buried in a specially prepared "sand" pit. The arrangement of the targets is shown in Figure 2.

The shapes of the hyperbolas are determined both by the depth to the targets and the electromagnetic wave propagation velocity profile in the earth. The lateral extent of each curve is many times greater than the correct representation of the physical size of the target. The detection of buried ordnance is also made difficult by the presence of noise, overlapping hyperbolas, geologic structure, and ringing, as shown in Figure 3 which highlights some distinguishing features of Figure 2.

The migration process integrates the energy values over the hyperbolic curve and focuses the resultant sum at the apex of the curve, greatly increasing target detectability. The process is illustrated in Figure 4. In practice, because target locations are unknown, migration processing is conducted for ALL points in the area being surveyed. At each point a summation is performed along the calculated hyperbolic curve. If the apex of the curve does not lie on a target, then the radar energy samples in the migration integral consist of a set of random noise signals which sum to statistically small amplitude. In contrast, if the migration integral is computed over a hyperbolic target signature, then the radar energy signals are correlated and the summation produces a large amplitude result signifying a target.

Figure 5 shows the same GPR data of Figure 1, after being processed by the migration algorithm. The targets are clearly shown. The energy focused at target locations allows discrimination between buried ordnance items and geologic structures using spatial extent criteria. Note that noise and ringing energy does not focus.

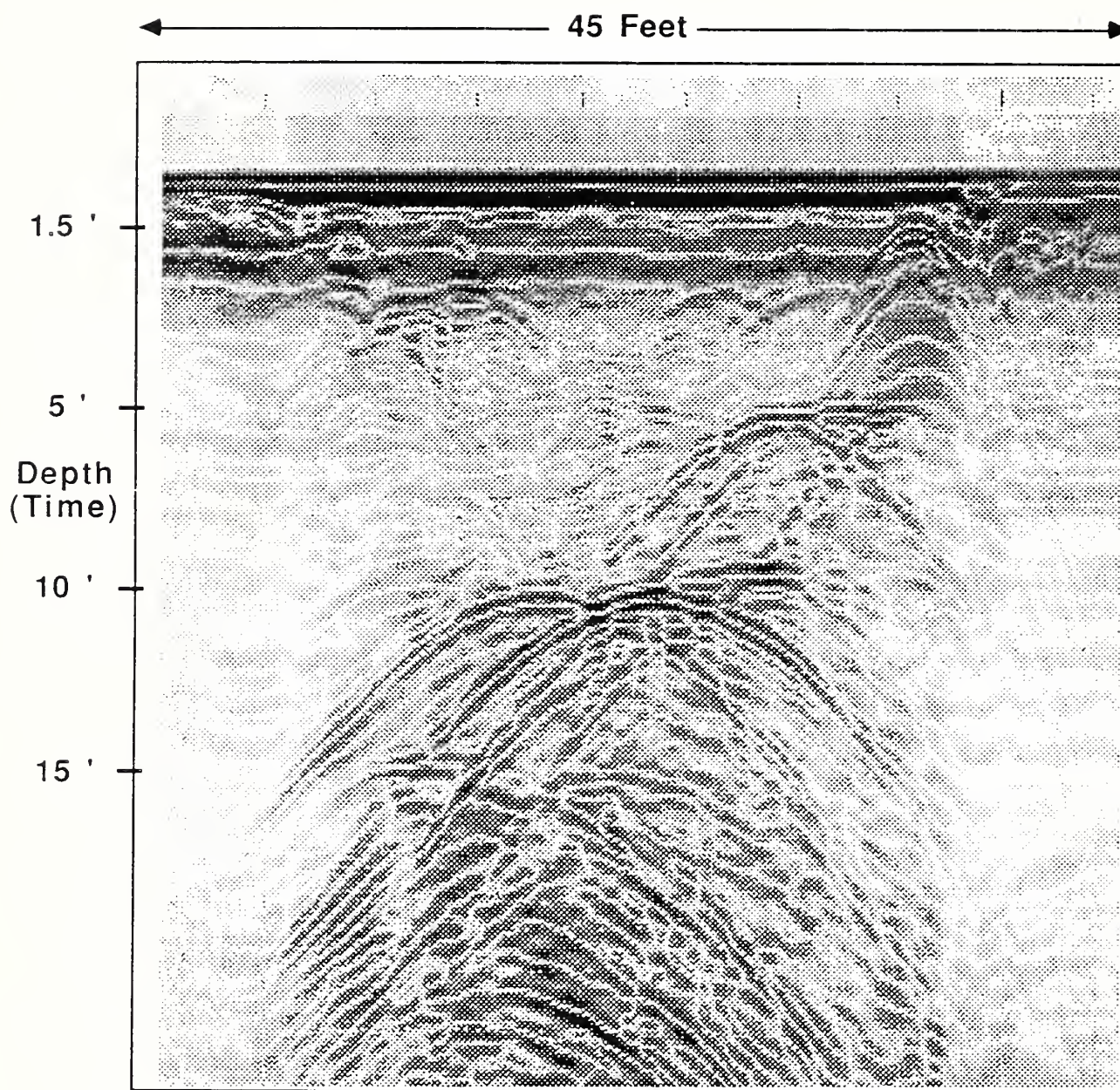


Fig. 1 Digitized ground penetrating radar (GPR) data from test range at Indian Head, Maryland. Hyperbolas indicate "targets".





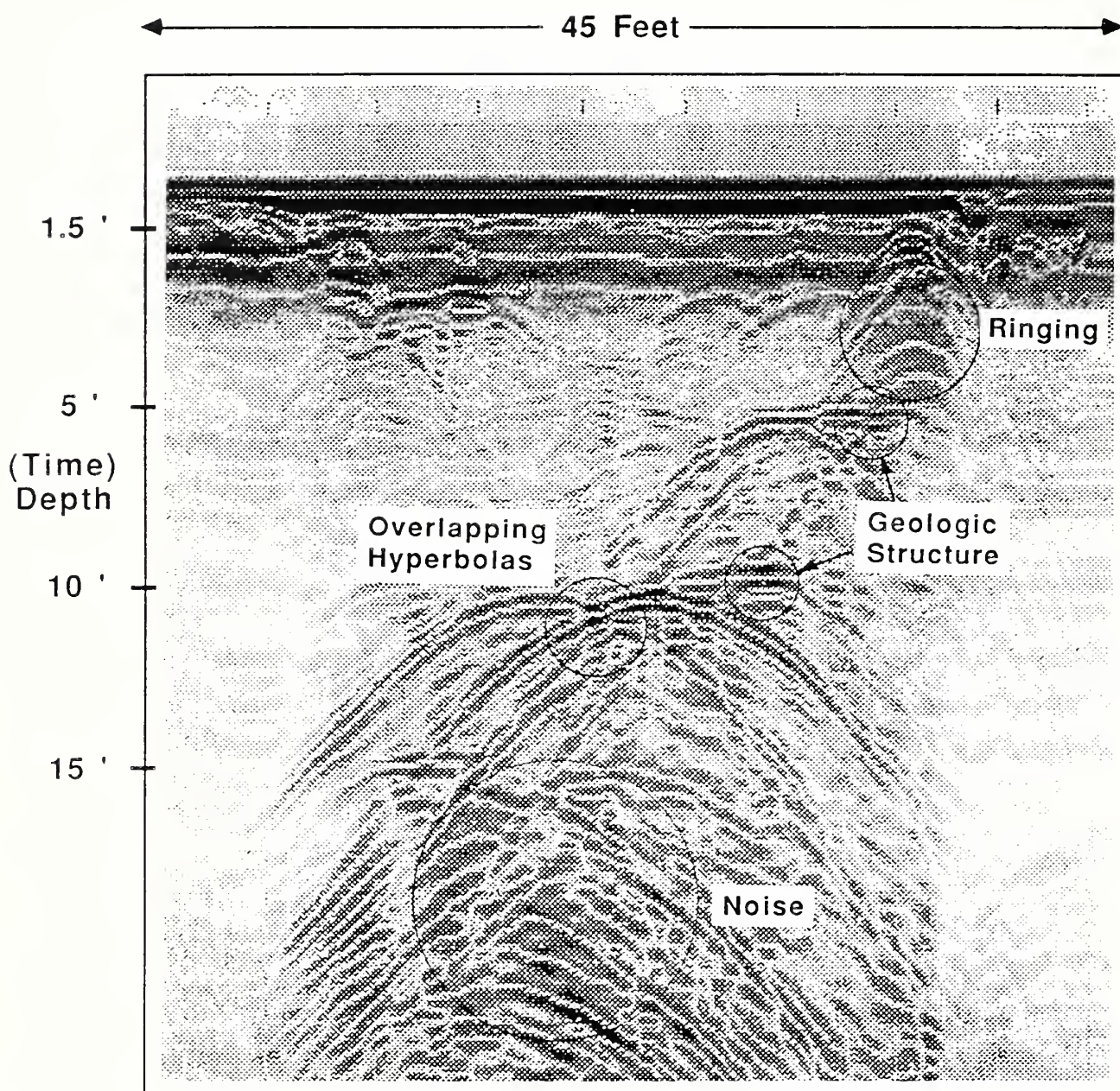


Fig. 3 Digitized ground penetrating radar (GPR) data from test range at Indian Head, Maryland. Detection of buried ordnance is made difficult by the presence of noise, overlapping hyperbolas, geologic structure, and ringing.



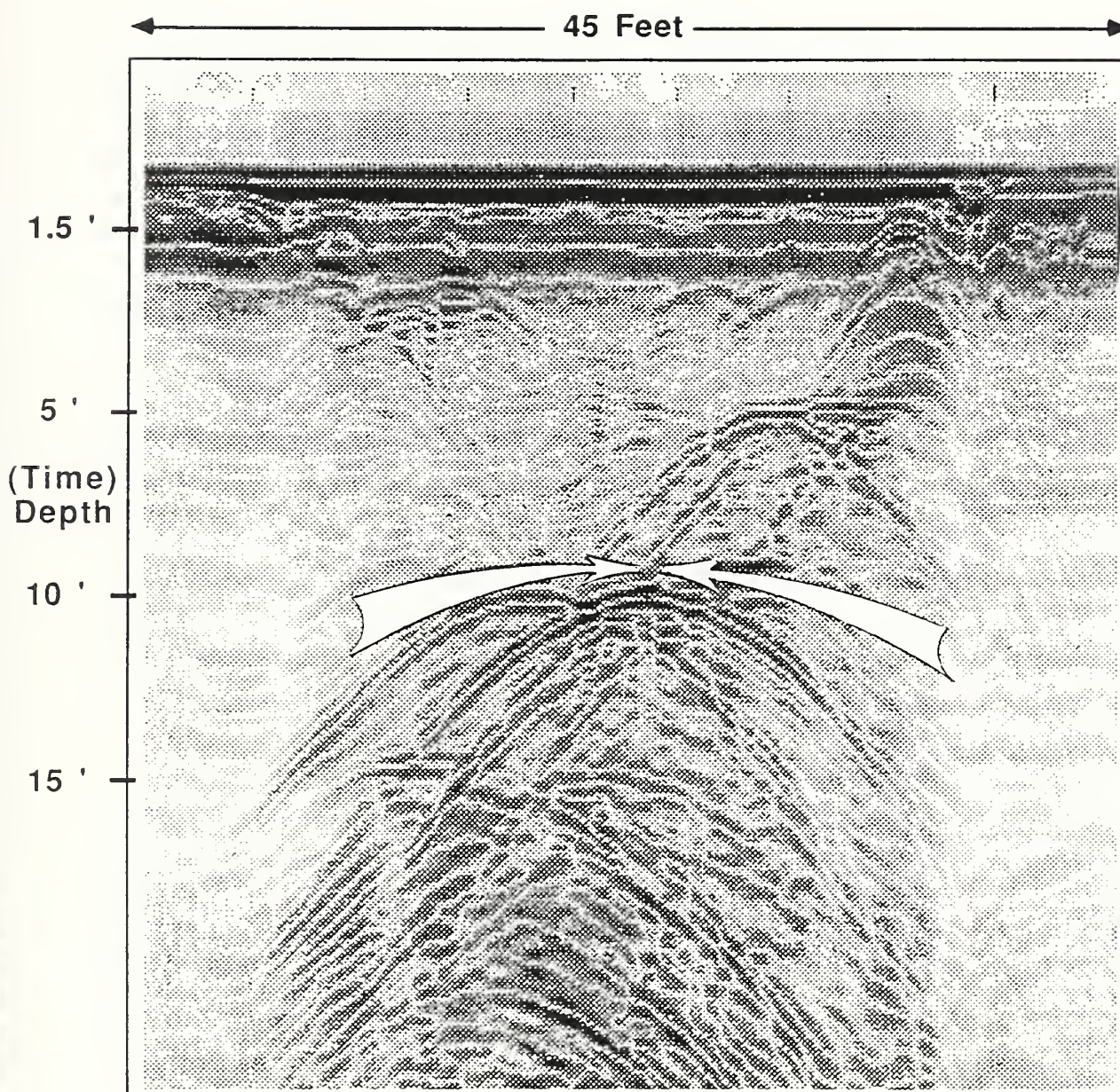


Fig. 4 Migration process focuses hyperbolic energy to the apex, enhancing detectability of buried ordnance



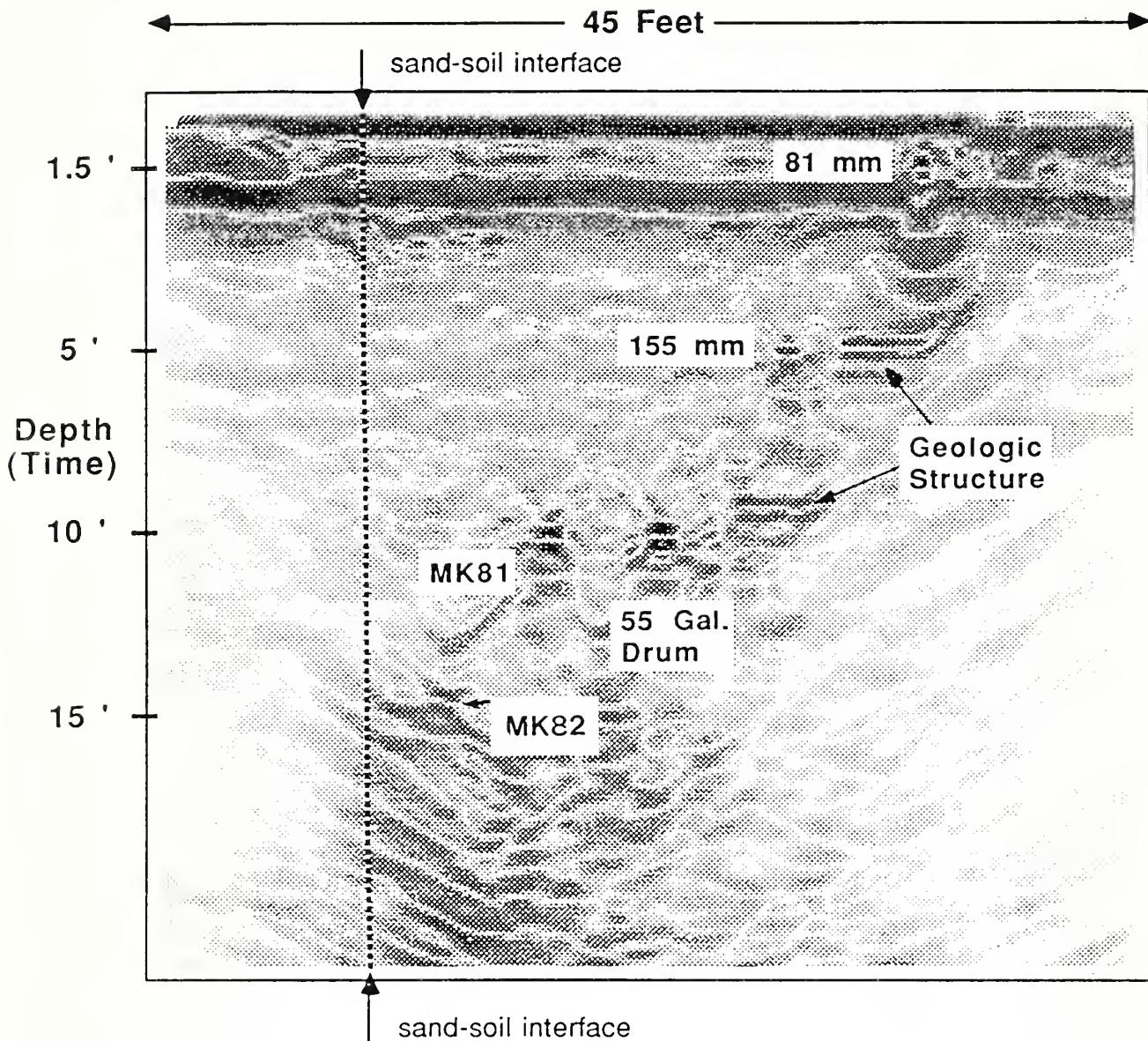


Fig. 5 Migrated GPR data. Energy focused at target locations allows discrimination between buried ordnance items and geologic structures using spatial extent criteria. Note that noise and ringing energy do not focus. 60 mm target of Fig. 2 is not in the sensor field of view. MK 82 target is not well focused due to its proximity to the test range edge.

The migration technique can also be successfully applied to the detection of ordnance buried in ordinary soil. Preliminary analysis of data taken over targets at a test range at Ft. Devens, Massachusetts indicates that use of migration processing enhances target detectivity in a manner similar to the results shown here.

#### KIRCHOFF MIGRATION THEORY

Kirchoff migration images reflectors such that their true locations in the subsurface can be determined. According to the reflection model, the total reflected wave is a sum of reflections from each point on each reflector. Therefore, proper migration of data from any point reflector allows for proper migration of any structure. This section describes the mathematical derivation of the Kirchoff migration method. (Additional information on migration methods can be found in reference 2 and 3).

Consider radar data arising from a point reflector at location  $x, z$ . The result is a radar wavelet along a travel time or diffraction curve  $T_D(x', x, z)$ . The unprimed parameters indicate position in the earth and the primed parameters indicate position along the diffraction curve. The construction of the curve  $T_D$  is shown in Figure 6. The travel time curve can be calculated if the geometry and electromagnetic velocity,  $V$ , are known. The travel time, or diffraction curve is:

$$T_D(x', x, z) = 2 \left[ (T_0/2)^2 + ((x-x')/V)^2 \right]^{1/2} \quad (1)$$

This is the characteristic hyperbolic signature seen in unmigrated radar data generated from point diffractors in the earth.



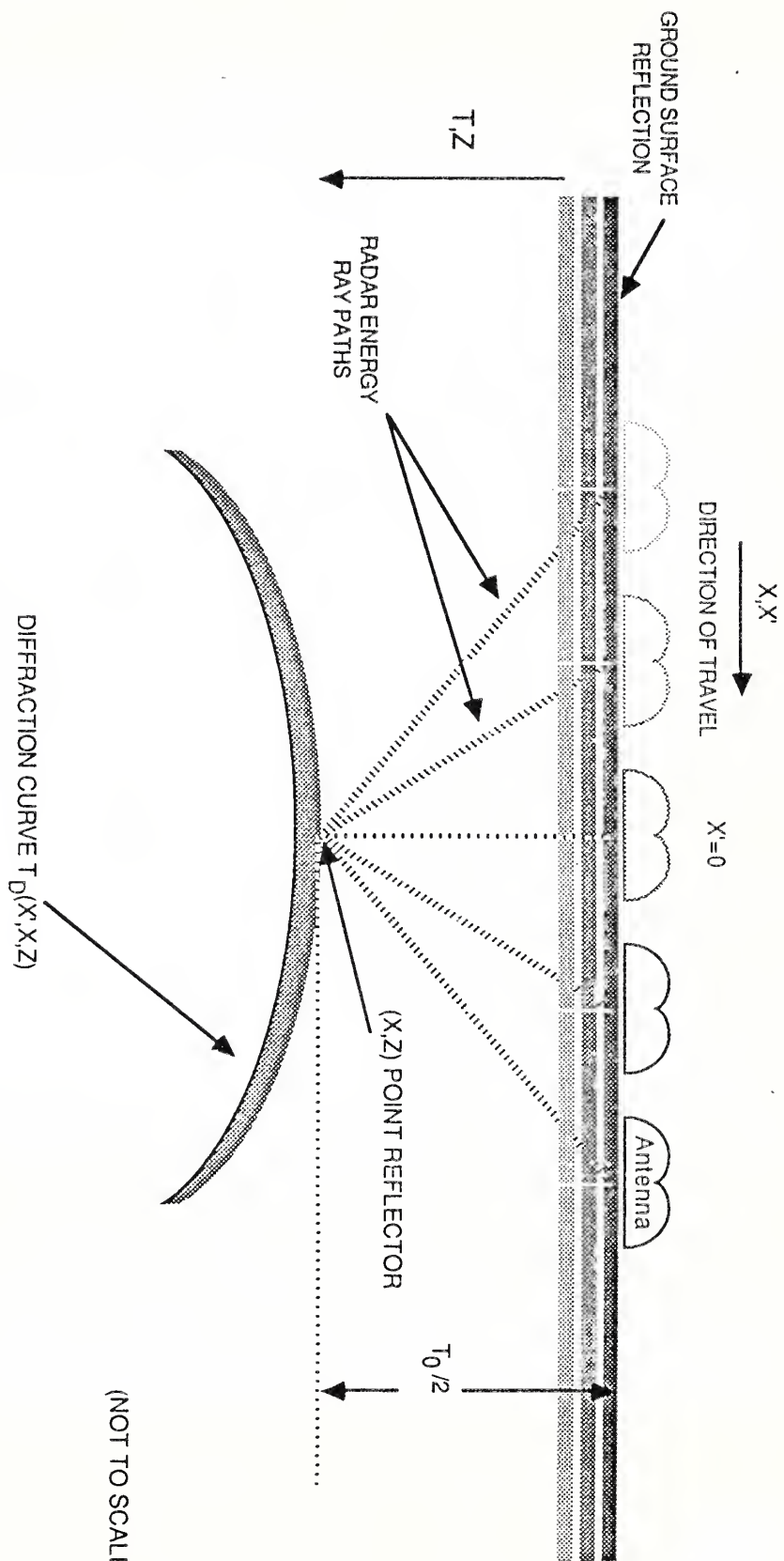


Fig. 6: Diffraction curve arising from a point reflector in a uniform velocity medium

To create an image of the reflection point  $x, z$ , all of the data samples along the diffraction curve are summed, so that all of the data add up in phase, i.e.

$$M(x, z) = \int dx' D(x', T=T_D(x', x, z)) \quad (2)$$

where  $M(x, z)$  is the migrated data at point  $x, z$ , and  $D(x', T)$  is the data at distance  $x'$  and time  $T$ . The contributions from other reflection points will not add up in phase, and will therefore make only a minor contribution to  $M(x, z)$ . By performing this operation for all  $x$  and  $z$ , a complete image of the reflectors is obtained.

Depending on the application, it may be important that the migration algorithm preserve the shape and amplitude of the radar reflection waveform. Although the coherent summation of eq. 1 will image reflections at their proper positions, modifications to the equation are needed to preserve waveform and amplitude.

Consider the case of a continuous reflector whose travel time curve is  $T_E(x)$ . Since migration operates on all reflectors (both point and continuous) this derivation is applicable for the migration of point targets. If the radar wavelet is  $W$ , the observed data will be

$$D(x, T) = W(T - T_E(x)) \quad (3)$$

The migration of the event using equation 2 yields:

$$M(x, T_0) = \int dx' D(x', T_D(x, x', T_0)) = \int dx' W(T_D(x', x, T_0) - T_E(x')) \quad (4)$$

Geometrically, the output of migration is dominated by the point at which the data is tangent to the diffraction curve, because this is where the data add coherently in the Kirchoff integral. A mathematical examination of this point is as follows. Writing the input wavelet as a Fourier transform

$$W(T) = \int d\omega \exp\{i\omega(T_D(x', x, T_0) - T_E(x'))\} \tilde{W}(\omega) \quad (5)$$

We note that at  $x'$  for which the exponent is varying, the oscillations of the exponential cancel, giving a negligible result. The integral is therefore dominated by a small region around the input trace distance  $x'_0$  at which the exponent has no derivative, (principle of stationary phase), i.e.,

$$[\partial/\partial x' (T_D - T_E)]_{x'=x'_0} = 0$$

Since the integral is dominated by  $x' = x'_0$ , a Taylor expansion of  $T_D - T_E$  with respect to  $x'$  about  $x'_0$  can be performed

$$\begin{aligned} T_D - T_E &\approx [T_D - T_E]_0 + [\partial/\partial x' (T_D - T_E)]_0 (x' - x'_0) \\ &\quad + 1/2 [\partial^2/\partial x'^2 (T_D - T_E)]_0 (x' - x'_0)^2 \\ &\text{subscript 0} \rightarrow \text{evaluate at } x' = x'_0 \end{aligned}$$

Equation 4 can now be written as

$$M(x, T_0) \approx \int d\omega \exp\{i\omega(T_D - T_E)_0\} \tilde{W}(\omega) \int dx' \exp\{i\alpha(x' - x'_0)^2/2\} \quad (6)$$

where

$$\alpha = \omega [\partial^2/\partial x'^2 (T_D - T_E)]_0$$

The  $x'$  integral can be performed analytically

$$\int \exp[i\alpha(x'-x'_0)^2/2] dx' = (2\pi/i\alpha)^{1/2}$$

Substituting this result into equation 6 yields

$$M(x, T_0) = (2\pi)^{1/2} [(i\omega)^{-1/2} * W] \{T_D(x', x, T_0) - T_E(x'_0)\} \cdot \left[ \partial^2 / \partial x'^2 (T_D - T_E) \right]_0^{-1/2} \quad (7)$$

The corrections to this result are of the order  $(\lambda/z)^2$  where  $\lambda$  is the radar wavelength and  $z$  is the depth.

Migration has taken the data from distance  $x'_0$  and time  $T_E(x'_0)$  to time  $T_0$  and distance  $x$  determined by the conditions

$$\begin{aligned} T_E(x'_0) &= T_D(x'_0, x, T_0) \\ [\partial / \partial x' (T_D - T_E)]_{x'=x'_0} &= 0 \end{aligned} \quad (8)$$

i.e., the diffraction curve for the image point  $x, T_0$  must be tangent to the data at point  $x'_0$ .

As a result of the summation process, the wavelet has been distorted:

1. The wavelet is distorted in phase by convolution with a filter  $(i\omega)^{-1/2}$

2. The amplitude of the event has been altered by a factor of

$$(2\pi)^{1/2} \left[ \partial^2 / \partial x'^2 (T_D - T_E) \right]_0^{-1/2}$$

3. The wavelet itself is stretched by a factor of  $[\partial T_D / \partial T_0]_0^{-1}$

A discussion of the effects of these distortions and their impact on migration of point targets is given below.

If minimal phase distortion in the resulting wavelet is an important criterion (such as in stratagraphic analysis), it can be compensated for by applying a filter  $(i\omega)^{1/2}$  to the input data. It is implemented by transforming each input trace to frequency, multiplying by  $(i\omega)^{1/2}$ , then inverting the Fourier transform. For the application described in this paper no phase correction is necessary.

The amplitude distortion can be corrected so that reflectors on the migrated image have the same amplitude as they did on the unmigrated image. This is achieved by setting

$$\partial^2 / \partial x'^2 (T_D - T_E) = \partial^2 T_D / \partial x'^2$$

and including the factor  $(\partial^2 T_D / \partial x'^2)^{1/2}$  in the Kirchoff integral. (the migration shown in this paper has included this amplitude correction.)

The stretch effect cannot be eliminated but can be controlled. It is due to the fact that migration treats an event with a wavelet on it as a series of parallel events with a spread in time equal to the duration of the wavelet. From eq. 8 it is seen that a wavelet of duration  $\tau$  gives rise to a vertical travel time thickness of  $\tau (\partial T_D / \partial T_0)^{-1}$ . Since  $\partial T_D / \partial T_0$  is not a constant, the travel time stretching of the wavelet that occurs increases with lateral distance from the center of the diffraction curve. If the stretch factor,  $(\partial T_D / \partial T_0)^{-1}$ , is too great, then the resulting migration summation is distorted. A limit can be set on the allowable stretch by limiting distance along the hyperbola on which migration is performed.



Thus the final form for Kirchhoff integral migration is

$$M(x, T_0) = (2\pi)^{-1/2} \int dx' [(i\omega)^{1/2} * D](x', T_D(x', x, T_0)) \left[ \partial^2 T_D / \partial x'^2 \right]^{1/2} \quad (9)$$

For discretely sampled data, this becomes

$$M(x, T_0) = (2\pi)^{-1/2} \sum_x 2(x-x') [(i\omega)^{1/2} * D](x', T_D(x', x, T_0)) \left[ \partial^2 T_D / \partial x'^2 \right]^{1/2} \quad (10)$$

## CONCLUSION

The application of migration processing to data obtained by ground penetrating radar on buried ordnance clearly results in enhanced target detectivity. Use of the migration algorithm to focus energy at target locations allows discrimination between buried ordnance items and geologic structures. Effects of noise and ringing energy which do not focus are suppressed.

## REFERENCES

1. Gardner, G.H.F., (Editor) Migration of Seismic Data, Society of Exploration Geophysicists: Geophysics reprint series No. 4.
2. Hatton, L., Worthington, M.H., Makin, J. Seismic Data Processing Theory and Practice, Blackwell Scientific Publications, 1986. Chapter 4.
3. Waters, K.H. Reflection Seismology, John Wiley & Sons, Inc. 1981. Chapter 9.

Summary : Interpretation of ground probing radar : migration techniques.

In the conception of a ground probing radar, which is optimised for the detection of underground pipes and cables, BLIS has chosen for a new approach.

In building a ground probing radar, one has to distinguish three elements : - the antenna.

- the interpretation station,

- the expert system.

For each of the elements one has to develop the best solution and then combine them.

The choice of antenna is strongly dependent on the kind of targets one wants to detect.

As BLIS is interested in detecting linear targets, the antenna will be designed to emit circularly polarised signals.

The interpretation station, which performs the digitalisation of the signals and produces a comprehensible presentation of the measurements, is compatible with every type of antenna. The algorithms used are based on migration techniques.

The combination of these two high-technological developments will ensure the detection of, metallic and non-metallic, linear targets with high accuracy.

GROUND-PENETRATING RADAR (GPR) SURVEY  
AT TELL HALIF, ISRAEL

JAMES A. DOOLITTLE  
Introduction

Archaeologists are becoming increasingly aware of the advantages of using geophysical techniques for reconnaissance and pre-excavation surveys. These techniques are being used to facilitate excavation strategies, decrease field time and costs, and pinpoint the location of buried artifacts. Geophysical techniques compliment conventional methods of archaeological investigation. Compared with conventional methods, geophysical techniques are faster, provide greater areal coverage per unit time and cost, and are non-destructive. These techniques help to minimize the number of unsuccessful exploratory excavations and to reduce unnecessary or unproductive expenditures of time and effort.

Geophysical techniques used by archaeologists include electromagnetics (EM), ground-penetrating radar (GPR), magnetometer, and resistivity. Ground-penetrating radar (GPR) techniques have been used to locate buried artifacts in various areas of the world (Batey, 1987; Berg and Bruch, 1982; Bevan, 1977, 1984a and 1984b; Bevan and Kenyon, 1975; Bevan et al., 1984; Grossman, 1979; Kenyon, 1977; Parrington, 1979; Vaughan, 1986; Vickers and Dolphin, 1975; Vickers et al., 1976; and Weymouth and Bevan, 1983). These

studies document the nondestructive efficiency of using GPR methods to pinpoint buried artifacts, facilitate excavation planning, and aid site interpretations.

The GPR field study at Tell Halif, Israel provided a unique opportunity to improve field procedures and develop search strategies and interpretative skills.

## Ground-Penetrating Radar

### Principles of Operation

Ground-penetrating radar is a broad band, impulse radar system that has been designed to penetrate earthen materials. Relatively high frequency (10 to 1000 MHZ), short-duration pulses of electromagnetic energy are radiated into the ground from an antenna. When a pulse encounters an interface separating layers of differing dielectric properties, a portion of the pulse's energy is reflected back to the antenna. The radar's receiving unit samples and amplifies the reflected energy and converts it into the audio frequency range. The processed reflected signals are displayed on a graphic recorder or recorded and stored on magnetic tape.

A continuous profile of the subsurface is developed on the graphic recorder as the antenna is towed along the ground surface. As electrosensitive paper moves under the revolving styli of the graphic recorder, images of subsurface features and conditions are "burned" onto the paper to create a graphic profile. Each scan of a stylus draws a line across the paper in the direction of increasing signal travel time (depth). The intensity of the image printed is dependent upon the amplitude of the reflected signal.

#### Ground-penetrating Radar System

The GPR used at Tell Halif is the SIR (Subsurface Interface Radar) System-8 manufactured by Geophysical Survey Systems, Inc.<sup>1</sup>. The SIR System-8 consists of a control unit, a graphic recorder, a digital tape recorder, and a program control unit (microprocessor). The microprocessor did not significantly improve interpretations and was used with limited success. The system was powered by a 12-volt vehicular battery. A 60 meter transmission cable was used to connect the control unit with the antenna. The antenna was hand-towed along survey lines at an average speed of 2.0 km h<sup>-1</sup>. Detailed techniques for using GPR in the field have

---

1. Trade names have been used to provide specific information. Their mention does not constitute endorsement.



been described by Morey (1974), and Shih and Doolittle (1984).

The 120 and 500 MHz antennas were used in this field study. The lower frequency 120 MHz antenna has greater powers of radiation, longer pulse widths, and emits signals that are less rapidly attenuated by earthen materials than the signals emitted from the higher frequency, 500 MHz antenna.

Each antenna has a fairly broad radiation pattern. Theoretically, the radar pattern is conical with the apex of the cone at the center of the antenna. The antennas have a 90 degree inclusive angle. Reflections from an interface are a composite of returns from within the area of radiation.

#### Factors Affecting the Radar's Performance

The performance of the GPR is highly site specific and soil dependent. The GPR does not perform equally well in all soils.

The maximum probing depth of the GPR is, to a large degree, determined by the electrical conductivity of soils. Soils having high conductivities rapidly dissipate the radar's

energy and restrict its probing depth. The principal factors influencing the conductivity of soils are: (i) degree of water saturation, (ii) amount and type of salts in solution, and (iii) amount and type of clays.

Moisture content is the primary determiner of conductivity. Electromagnetic conductivity is essentially an electrolytic process that takes place through moisture filled pores. Tell Halif is in a xeric moisture regime (Soil Survey Staff, 1975). The average annual precipitation of 25 to 35 cm with a pronounced winter maximum. The survey was conducted during the dry month of July. However, in arid and semi-arid regions, small amounts of moisture can significantly increase the conductivity of soils and substantially attenuate the radar signals (Vickers et al., 1976). Signal attenuation is significantly increased in some soils (Jesch, 1978) when the moisture content is changed from 5 to 10 percent.

Electrical conductivity is directly related to the concentration of dissolved salts in the soil solution. In unirrigated areas, the concentration of dissolved salts in the soil profile and the probing depth of the GPR are influenced by parent material and climatic parameters. Soils formed in sediments weathered from chalk, marl, and limestone, as at Tell Halif, generally contain more salts in solution than soils developed in felsic crystalline rocks.

In general, most soluble salts are leached rapidly from soil profiles in humid regions. However, in semi-arid and arid regions, soluble salts of potassium and sodium and less soluble carbonates of calcium and magnesium accumulate in the soil profile; the depth of accumulation being a function of precipitation. The soils of Tell Halif are calcareous.

The electrical properties of many soils are strongly influenced by the amount and type of clay minerals present. At Tell Halif, moderately-fine textured (18-34 percent clay) soils have formed in residuum, colluvium, and fill materials overlying marl and limestone bedrock. Ions absorbed on clay particles can undergo exchange reaction with ions in the soil solution and thereby contribute to the electrical conductivity of soils. The concentration of ions in the soil solution is dependent upon the clay minerals present, the pH of the soil solution, the degree of water filled porosity, the nature of the ions in solution, and the relative proportion of ions on exchange sites. Smectitic and vermiculitic clays have higher cation exchange capacity (CEC) than kaolinitic and oxidic clays, and under similar soil moisture conditions, are more conductive.

At Tell Halif, unfavorable electromagnetic characteristics of soils, debris or fill material, and buried artifacts limit the radar's probing depth. The moderately deep (50 - 100 cm) and deep (>100 cm), moderately-fine textured,

calcareous soils rapidly attenuated the radar energy and limited the penetration of the 120 MHz antenna to depths of 1.0 to 1.5 meters in most areas. In areas of shallow soils (<50 cm) overlying marl or limestone bedrock, attenuation was less severe and depths of 3 to 4 meters were achieved.

The earthen materials of Tell Halif rapidly attenuated the energy radiated from the 500 MHz antenna and restricted its penetration to depths of less than 50 cm. After limited field trials, use of the 500 MHz antenna was discontinued.

The depth of penetration is also limited by buried artifacts. Buried artifacts cause partial absorption, reflection, and scattering of the electromagnetic energy. The high clay content of mud brick walls and the calcareous nature of debris and fill materials absorbed and dissipated some of the radiated energy. Successive, closely spaced layers of fill, debris, and rubble cause partial reflection and scattering of the energy, thereby, further restricting the profiling depth.

In spite of these limitations, the GPR was successful at Tell Halif as a large number of artifacts were not deeply buried and occurred within the effective profiling depth of the GPR. In most areas, the GPR provided sufficient resolution and penetration to detect artifacts within depths of 0.5 to 1.5 meters.

## Interpreting the Graphic Profiles

Reliable interpretations are developed through experience. Interpretation of radar imagery is best accomplished in the field, through a joint effort of radar technicians and archaeologists, with some ground truth observations to verify the data.

All areas surveyed with the GPR were selected by field supervisors. Archaeologist familiar with the subsurface stratigraphy and history of the site provided invaluable information concerning the distribution and identity of subsurface images. Field supervisors directed the excavation of all ground truth observation sites used to verify the graphic imagery.

Interpretations should be made in the field to relate subsurface anomalies to surface features or expressions. Surface features, such as rock fragments, tree limbs, or metallic reflectors, can introduce unwanted background noise on the radar profiles which if not properly identified, can lead to false conclusions. In Figure 1, overhanging tree limbs (C1) and utility lines (C2) produced undesired background noise on the graphic profile. These undesired



images could be confused with or interpreted as subsurface layers.

Interpretations require a limited number of ground truth observations to correlate the radar imagery with observed features and to determine what features were and were not detected. During the course of this survey, nine exploratory pits were excavated to confirm the presence of buried artifacts and to improve interpretations.

The enclosed graphic profiles (Figures 1 to 3) are representative of traverse conducted in areas having verified subsurface features. They have been included in this report to clarify the interpretation process and to summarize some of limitations of radar surveys.

Figure 1 is a graphic profile from a GPR traverse conducted between excavated areas P5 and O5 in Site 301. The horizontal black lines labelled "A" are reflected images from the ground surface. These lines represent one interface, the air/soil interface. The dark bands represent positive and negative signal amplitudes. The intervening white band is the zero or neutral crossing between the positive and negative signal amplitudes.

The next series of dark bands in Figure 1 (labelled "B") is a composite reflection from several closely spaced, surface

and near surface features. These images overlap and are poorly resolved as a result of the low range and high gain settings used for this traverse. These superimposed images represent changes in surface roughness, soil texture, horizonation, density, organic matter content, coarse fragments, and/or moisture within the upper 40 to 50 cm of the soil profile.

Below surface and near surface images are images from subsurface interfaces. Interfaces are categorized as linear or point reflectors. Soil horizons, geologic strata, and layers of debris or fill having greater horizontal than vertical extent and generally broader than one meter are linear reflectors. When crossed with the antenna parallel with their long axis, foundation walls appear as linear reflectors. Linear reflectors appear as multiple, parallel bands on graphic profiles. In Figure 1, hard, indurated, artificial strata of clay (E), which provide a foundation for outer walls (D), appear as linear reflectors. Also, the false echoes from overhanging tree limbs (C1) and utility lines (C2) appear as linear reflectors.

Small objects, such as stones or boulders, buried artifacts or foundation walls (when crossed perpendicular to their long axis) having limited horizontal extent, will appear as point reflectors. Point reflectors produce hyperbolic patterns similar to the images designated by the letter "D"

in Figure 1 and "A" in Figure 2. Hyperbolic patterns are caused by the antenna's conical radiation pattern. The antenna receives reflections before and after it passes over a subsurface anomaly. The hyperbolic patterns result from range changes as the antenna approaches, passes over, and goes beyond subsurface anomalies.

In Figure 1, the profiled depth is 2.85 meters. However, the effective depth of penetration is only 1.2 meters. Below this depth the radar energy has been so absorbed and dissipated that reflected images from subsurface anomalies are indistinct and partially or completely omitted from interpretations. The potential for errors of omission should be a major concern when determining the radar's effective depth of penetration. The examples published in the literature are mostly from areas in which the radar has performed exceptionally well. Often, it is uncertain whether many of the reported depths were consistently achieved and provided complete and interpretable imagery. Some reported depths may represent the lone and most significant exception to an otherwise more restricted trend in observable depths.

Figure 2 is a graphic profile from the perimeter of the tell in Field IV. The graphic profile depicts and is representative of an area of high "cultural noise". Areas depicted with similar concentrations of subsurface anomalies

represent prime sites for future archaeological investigations. The point reflector appearing in Figure 2 represents buried foundation walls and columns. In Figure 2, variations in the shape of the hyperbola are caused by variations in: (1) the angle at which the feature was crossed, (2) the speed of antenna advance across the top of the feature, (3) the velocity of pulse propagation, and (4) the size, shape, orientation, composition, and number of buried objects.

In Figure 2, a near surface metallic object produced a distinguishing hyperbolic image (A). When passed over with the antenna, metallic objects such as surveying pins or barbed wire cause excessive reverberations or "ringing" of the reflected signal. Signal reverberations produce repetitious, vertical patterns of similar images across the profile. Signal reverberations limit the ability of the radar to discriminate subadjacent anomalies.

While the GPR detects subsurface anomalies, it does not identify subsurface features. Unless sufficient ground-truth observations are made, few images can be correctly identified with a high degree of confidence on radar profiles. With experience and sufficient ground truth observations many subsurface features can be identified by their unique graphic signatures.

The profile in Figure 3 is from a traverse conducted in Field I. The GPR was used at this site to predict the occurrence of artifacts prior to the removal of overlying strata within an excavation site. Subsurface features have been highlighted with a dark line. In this profile two foundation walls (A1 and A2) and three distinct layers of fill (B1 to B3) have been identified. The identity of these features was latter verified. The fill material consisted of layers of ashy detritus.

Each wall in Figure 3 has an identifiable graphic signature and is abruptly terminated by vertical breaks. Rubble and fill materials surrounding foundation walls can complicate the imagery and mask the presence of the walls. In many areas of the tell, it was difficult to isolate walls from rubble. Walls have been segmented by partial destruction and, where intact, are variable in expressions.

The graphic signatures appearing in Figure 3 are based on features which have been produced from unique site histories. Abrupt vertical breaks in the radar imagery are indicative of mans activities, and often, as in Figure 3, separate zones of contrasting site histories. Note the difference in the imagery on either side of wall "A1". The graphic profile is more congested with subsurface reflection to the right of wall "A1" and reflects a different use, and



perhaps, a more complicated history than areas occurring to the left of this wall.

Several layers are superimposed in the upper part of this profile. A large concentration of debris on the surface, "C", produced undesired background noise which interfered with other near surface images.

### Survey Procedures

One of the primary objectives of this study was to evaluate survey procedures for charting the location of buried artifacts within a tell. The most accepted and perhaps efficient method to chart the location of buried artifacts with the GPR is to establish a grid on the area to be surveyed. Generally, rectangular grids are preferred, though Bevan (1977), in a study of subsurface remnants of earthworks, describes traverses radiating outwards like spokes of a wheel from a fort. In addition, "wildcat" surveys have been used by some authors (Berg and Burch, 1982) to quickly locate small areas having large concentrations of buried artifacts within a larger area.

Grid spacing is dependent upon the purpose of the survey, available time, features being identified, local ground

conditions, and desired detection probability. Bevan (1984b) has described three levels of surveying intensities based on the purpose of the investigation. These levels include: (1) locating an archaeological site, (2) defining site boundaries, and (3) charting internal features within a delineated site. The uniqueness and clarity of tells in the Israeli landscape has, in most places, simplified the scope of GPR surveys to charting the internal site features.

Grid spacing is a compromise between detection probability and available time or production rate. Generally, several grids of varying patterns and spacings are constructed within a defined area during the course of a survey. Often, in preliminary or pre-excavation reconnaissance surveys a large grid spacing is used to define the broad or general location of subsurface anomalies. Once the general location of anomalies has been defined, a smaller grid spacing is used. A smaller grid spacing provides more observation points and greater coverage, but, unless antenna positioning and position referencing are more rigidly maintained, does not necessarily insure greater precision. The more closely spaced grid pattern helps to pinpoint the location, define the spatial extent, and perhaps resolve the identity of the subsurface anomalies.

The anticipated size of the buried artifacts being defined or located will dictate grid spacing. In relatively

detailed surveys, grid spacings of 1 meter were used to detect grave sites (Vaughan, 1986), 1.5 to 3 meters to locate buried foundation walls (Bevan, 1979; Bevan et al., 1984; and Grossman, 1979), and 5 meters to define the general location of buried Indian ruins (Vickers et al., 1977). The 5 meter spacing, while satisfactory for defining areas with high concentrations of subsurface anomalies, is too coarse to relate anomalies with any degree of confidence (Vickers et al., 1977). Generally, in studies conducted in the area of the Mediterranean Sea, a 2 meter spacing has been preferred (Batey, 1987; and Fischer et al., 1980).

At many sites, local ground conditions will dictate the survey area as well as the grid spacing. Excessive slope, dense vegetation, irregular rock outcrops, and buildings will hinder or restrict GPR surveys. At Tell Halif, abrupt and precipitous slope breaks or excavation walls often defined the limits of the radar survey. Areas of trees, dense undergrowth, and barbed wire entanglements were generally avoided as these features impeded the movement of the radar antenna, ensnared the transmission cable, and introduced unwanted background noise.

Two reconnaissance surveys were conducted near Site 301 (Fig. 4) to assist the development of excavation strategies. One survey (survey lines A through F) was established to the north and northwest of Site 301 with survey lines spaced at

irregular intervals, parallel with the slope. Reference points were marked at 2.5 meter intervals along each survey line. Survey lines varied in length from 20 to 26 meters.

A second survey area was established to the south of the excavated area at Site 301 (Figure 4). This survey area consisted of an irregularly shaped grid with a 5 meter spacing between each reference point. Survey lines varied in length from 10 to 26 meters.

After the completion of the radar survey, the graphic profiles were examined and annotated in the field. Symbols were used to make the master plot of the grid more interpretable. In Figure 4, only the most readily discernible subsurface anomalies occurring within the upper 1 to 1.5 meters of the soil profile are plotted. Poorly resolved or questionable subsurface features are not depicted on this master plot.

In Figure 4, the more southerly GPR survey area was plotted as having the greatest concentration of subsurface anomalies. The radar profiles disclosed the presence of several buried walls and strata. One exploratory pit was opened along traverse H. This exposure provided ground truth observations which confirmed the presence of a buried structure (a hard indurated layer which was underlain by

stones and pebbles; possibly a wall), and verified the reliability of interpretations.

Radar profiles from the northern GPR survey area revealed fewer subsurface anomalies; in part, a consequence of fewer and more widely spaced traverses. However, the survey did reveal a distribution of subsurface anomalies along the rim of the terrace. It is believed that these anomalies represent major walls and structures. One exploratory pit was dug on traverse line D to confirm the identity of a point object suspected to be a wall. A double row, mud brick interior wall was unearthed at this pit. While this observation confirmed the identity of a subsurface feature, more intensive surveying and further ground truth observations are needed to verify the occurrence of a major wall or the continuation of this wall.

It is generally assumed that linear features, such as buried wall foundations, are easily detect by conducting several parallel traverses with the GPR. According to Bevan (1984), reliable detection of a buried structure requires similar imagery on three to six transects. However, others (Vickers et al., 1976) have noted a "natural tendency" to assume the occurrence of a linear object whenever radar images appear to align. At Tell Halif, foundation walls are not necessarily linear. The 5 meter spacing used at Site 301 was considered too broad to adequately define the



continuation of buried cultural features or the presence of a major wall along this terrace.

A reconnaissance survey was conducted near Field I, on the summit of Tell Halif, in an area latter described as Field IV (Fig. 5). At this site, the presence of fortification walls and domestic structures were inferred from earlier investigations on a similar site (Field III), surface indications, and its location along the perimeter of the tell. A grid was established with a 2.5 meter spacing between reference points. Traverses were conducted along each of the thirty-one survey lines. Survey lines varied in length from 5 to 55 meters.

The preliminary grid at Field IV defined the general location of subsurface anomalies and characterized their distribution. High concentrations of subsurface anomalies appear on graphic profiles from traverses conducted along the western perimeter of the tell. Along the perimeter, two areas of higher cultural noise were identified. The southeast portion of the survey area appears to be relative devoid of subsurface anomalies.

After plotting the distribution of subsurface anomalies detected in the preliminary survey, a more detailed survey was conducted in one area appearing to have a larger concentration of subsurface anomalies (Figure 5). The grid

spacing of the detailed survey was 1 meter. This area adjoins the slope break which defines the outer perimeter of the tell. The 1 meter grid provided a more detailed picture of the area.

In Figure 5, the general distribution of subsurface anomalies appearing on the preliminary survey (2.5 meter spacing) and on the detailed survey (1 meter spacing) correspond. However, the detailed survey discerned more subsurface anomalies as a result of its more intense coverage. Also, some patterns do not appear to agree on the two plots. This is due to slight spatial discrepancies in the placement of survey lines, and imprecise antenna location and position referencing.

Radar surveys were successfully conducted within excavated areas of Field I (Figure 6 and 7) to provide archaeologists with a picture of the underlying strata and artifacts before they were encountered. For each of these surveys, the grid spacing was 1 meter. The intrenched excavation sites proved to be exceptionally tight quarters to operate the GPR. As the antenna approached the enclosing excavation walls, the walls caused some interference and produced background noise which interfered with interpretations.

At Sites A9 and A10 in Field I, traverses varied in length from 2 to 5, providing 3 to 6, equally spaced (1 meter

interval) traverses with the antenna. This spacing proved to be too wide for charting the location of buried foundation walls. Each traverse provides only one image of a wall. With the grid spacing used, images of a wall were spaced at one meter intervals. The presence of rock fragments and debris, which produced undesired point reflections, complicated the tracing of wall patterns within the excavation sites with the grid spacing used. In most areas, a closer, overlapping grid spacing would be desired to accurately anticipate the location of buried foundation walls.

In spite of these limitations, the GPR detected and accurately predicted the location of mud brick and stone walls, and layers of ashy detritus within areas A9 (Figure 6) and A10 (Figure 7) of Field I. Numerical values expressed in these figures are depths to the shallowest, buried subsurface layer detected with the GPR. These plots were developed from radar traverses conducted along all grid lines in Figure 6 and north-south grid lines in Figure 7.

Based on radar surveys at Tell Halif, the following grid spacings are recommended: 2.5 to 5 meter for reconnaissance surveys; 1.0 to 2.5 for general characterization of potential excavation sites; and < 1.0 meter for detailed mapping within an excavation site.

#### Conclusions

The use of ground-penetrating radar for archaeological investigations is in an active stage of growth and development. This trend has been accelerated by the recent growth in its commercialization and by a growing familiarity with its potential uses. However, the use of GPR techniques has been limited because of (i) initial purchase costs, (ii) limited knowledge of performance in various media and geographic locations, (iii) rapid signal attenuation and depth restrictions in certain media, and (iv) results which are often dependent upon the skills and experience of the operator.

At Tell Halif, ground-penetrating radar has proven to be an effective reconnaissance tool for archaeological investigations. Ground-penetrating radar techniques can be successfully applied to tells in Israel. As more archaeologist become familiar with this geophysical technique, its use in Israel will undoubtedly increase.

#### Acknowledgement

The authors wish to express their appreciation to Douglas Barnes, Northeast National Technical Center and to the Public Information Staff, South National Technical Center of the Soil Conservation Service.

## REFERENCES

Batey, Richard A. 1987. Subsurface interface radar at Sepphoris, Israel, 1985. *Journal of Field Archaeology* 14(1):1-8.

Berg, F. and H. Bruch. 1982. Georadar: Archaeological interpretation of soil radar data. Second Nordic Conference on the Application of Scientific Methods in Archaeology. Elsinore, Denmark, 17-19 August 1981. In: *PACT* 7:285-294.

Bevan, Bruce W. 1977. Ground-penetrating radar at Valley Forge. Geophysical Survey Systems, Inc. Hudson, New Hampshire.

Bevan, Bruce W. 1984a. Environmental effects on ground-penetrating radar. In: Abstract, 54th Annual International SEG Meeting, held at Atlanta, GA., Dec. 2-6, 1984, pp. 201-204.

Bevan, Bruce W. 1984b. Looking backward: geophysical location of historic structures. In: *The Scope of Historical Archaeology, Essays in honor of John L. Cotter*. Ed. David G. Orr and Daniel G. Crozier. Temple University, Philadelphia. pp. 285-301.



Bevan, Bruce and Jeffrey Kenyon. 1975. Ground-probing radar for historical archaeology. MASCA (Museum Applied Science Center for Archaeology, University of Pennsylvania, Philadelphia) Newsletter 11(2):2-7.

Bevan, Bruce W., David G. Orr, and Brooke S. Blades. 1984. The discovery of the Taylor House at the Petersburg National Battlefield. *Historical Archaeology* 18:64-74.

Fischer, Peter M., Sven G. W. Follin and Peter Ulriksen. 1980. Subsurface interface radar survey at Hala Sultan Tekke, Cyprus. *Swedish Annual Studies in Mediterranean Archaeology* 63:48-64.

Grossman, Joel W. 1979. Ground-penetrating radar survey at Raritan Landing: an underground map of a buried settlement. Annual Meetings of the Society for American Archaeology, Vancouver, British Columbia. April 23-26, 1979. p.15.

Jesch, R. L. 1978. Dielectric measurements of five different soil textural types as functions of frequency and moisture content. Nat. Bur. Stand., Rep. No. 78-896. pp 1-21.

Kenyon, Jeff L. 1977. Ground-penetrating radar and its historical application to a historical archaeological site. *Historical Archaeology* 2:48-55.

Morey, R. M. 1974. Continuous subsurface profiling by impulse radar. IN: Proceedings, ASCE Engineering Foundation Conference on Subsurface Exploration for Underground Excavations and Heavy Construction, held at Henniker, N.H. Aug. 11-16, 1974. pp 212-232.

Parrington, Michael. 1979. Geophysical and aerial prospecting techniques at Valley Forge National Historical Park, Pennsylvania. *Journal of Field Archaeology* 6(2):193-201.

Shih, S. F., and J. A. Doolittle. 1984. Using radar to investigate organic soil thickness in the Florida Everglades. *Soil Sci. Soc. Am. J.* 48:651-656.

Soil Survey Staff. 1975. *Soil Taxonomy: A basic system of soil classification for making and interpreting soil surveys.* Soil Conserv. Serv., U. S. Dep. Agric. Handb. 436, 754 pp.

Vaughan, C. J. 1986. Ground-penetrating radar survey in archaeological investigations. *Geophysics* 51(3):595-604.

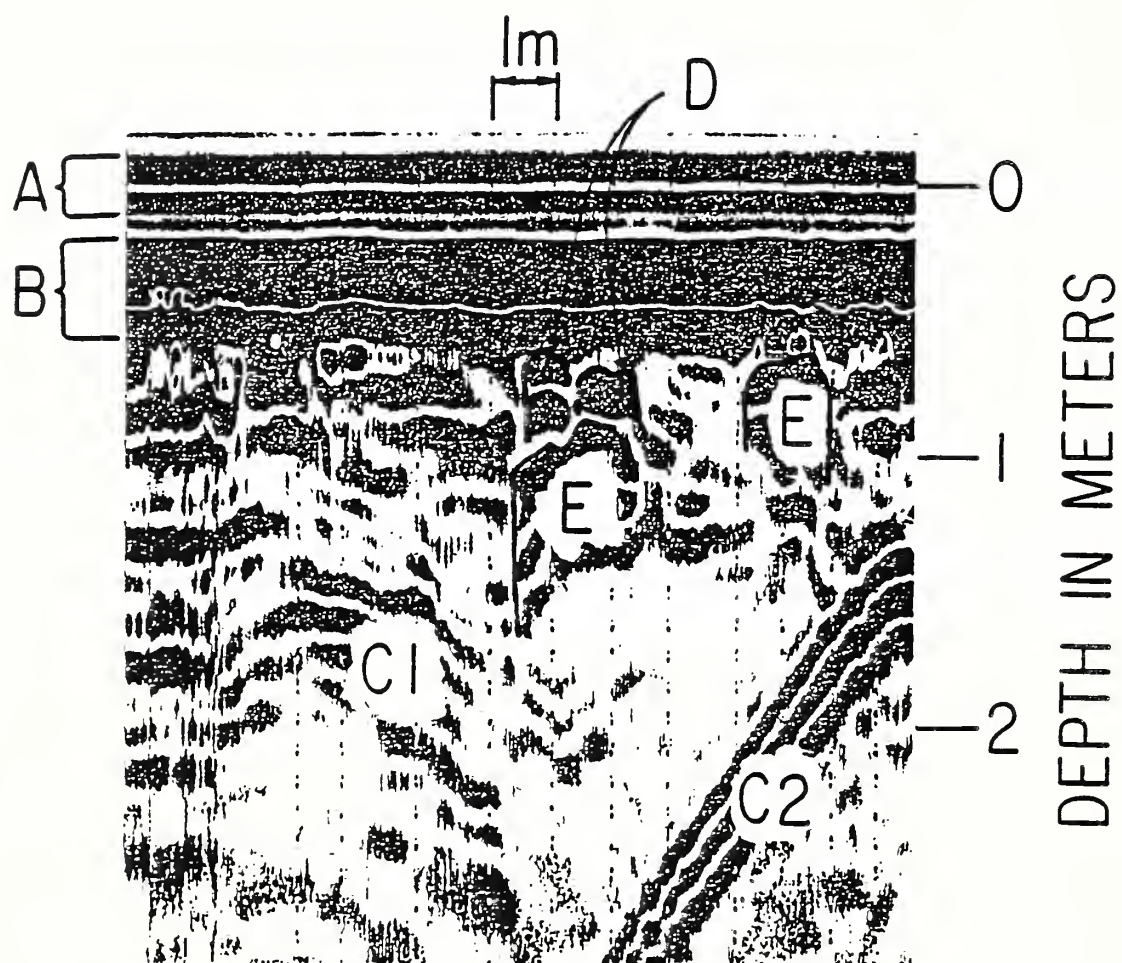
Vickers, Roger S. and Lambert T. Dolphin. 1975. A communication on the archaeological radar experiment at Chaco Canyon, New Mexico. *MASCA Newsletter* 11(1):1-3.

Vickers, Roger, Lambert Dolphin, and David Johnson. 1976. Archaeological investigations at Chaco Canyon using subsurface radar. In: Remote Sensing Experiments in Cultural Resource Studies, assembled by Thomas R. Lyons, Chaco Center, USDI-NPS and University of New Mexico. pp 81-101.

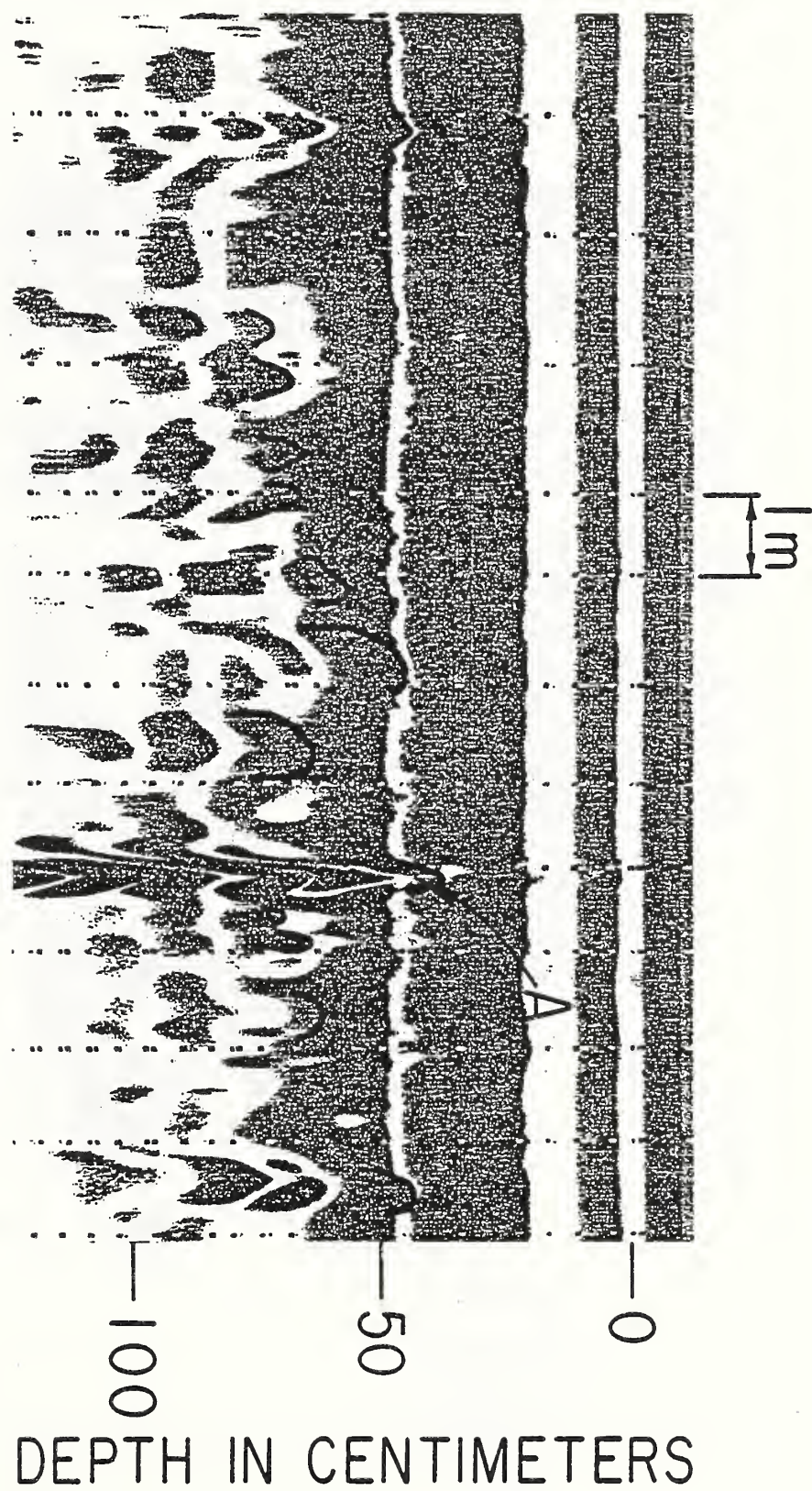
Weymouth, John W. and Bruce W. Bevan. 1983. Combined magnetic and ground penetrating radar survey of an archaeological site in Oklahoma. In: Digest International Geoscience and Remote Sensing Symposium (IGARDD'83') v1, pp 1.1-1.4.

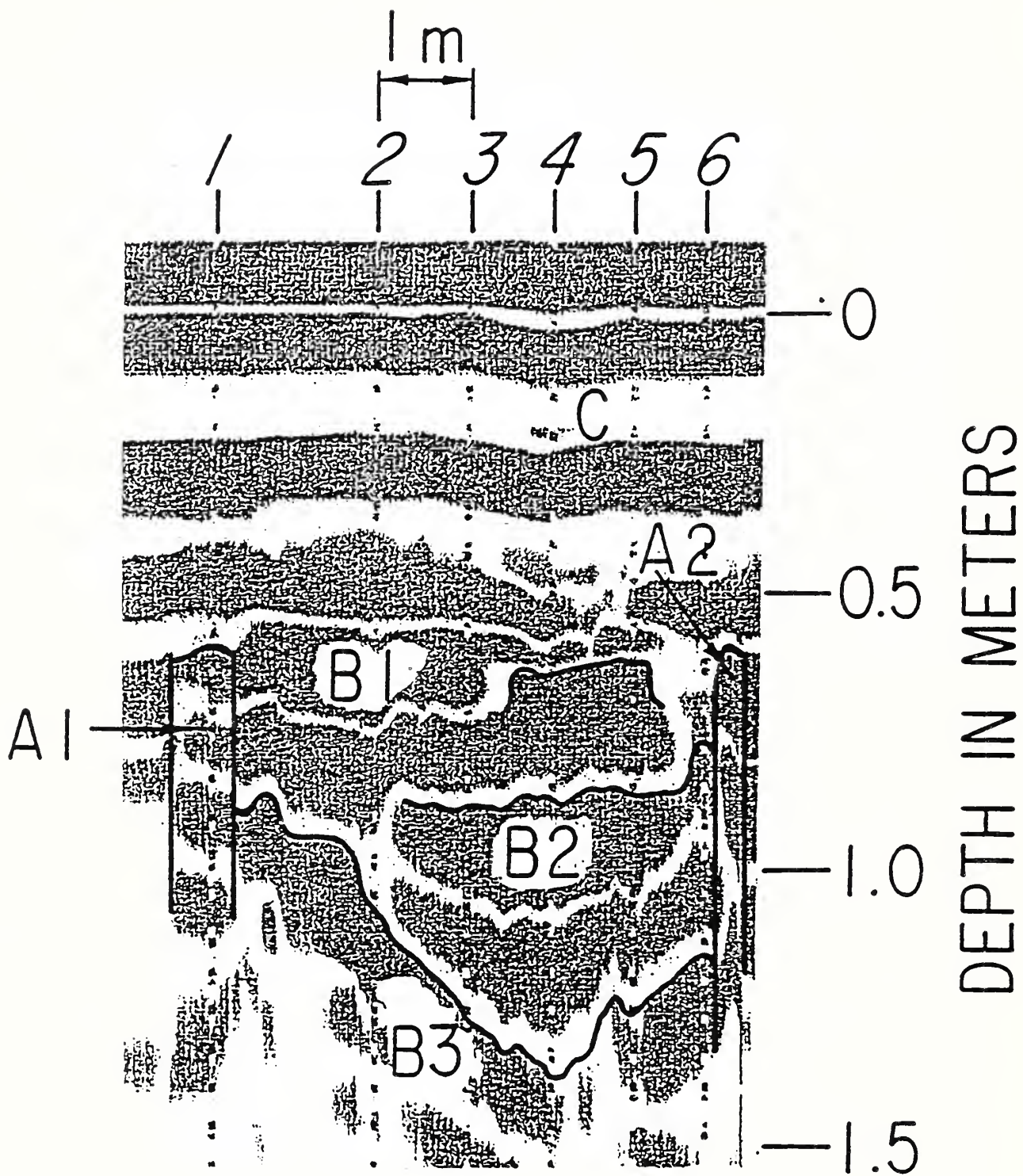
### List of Figures

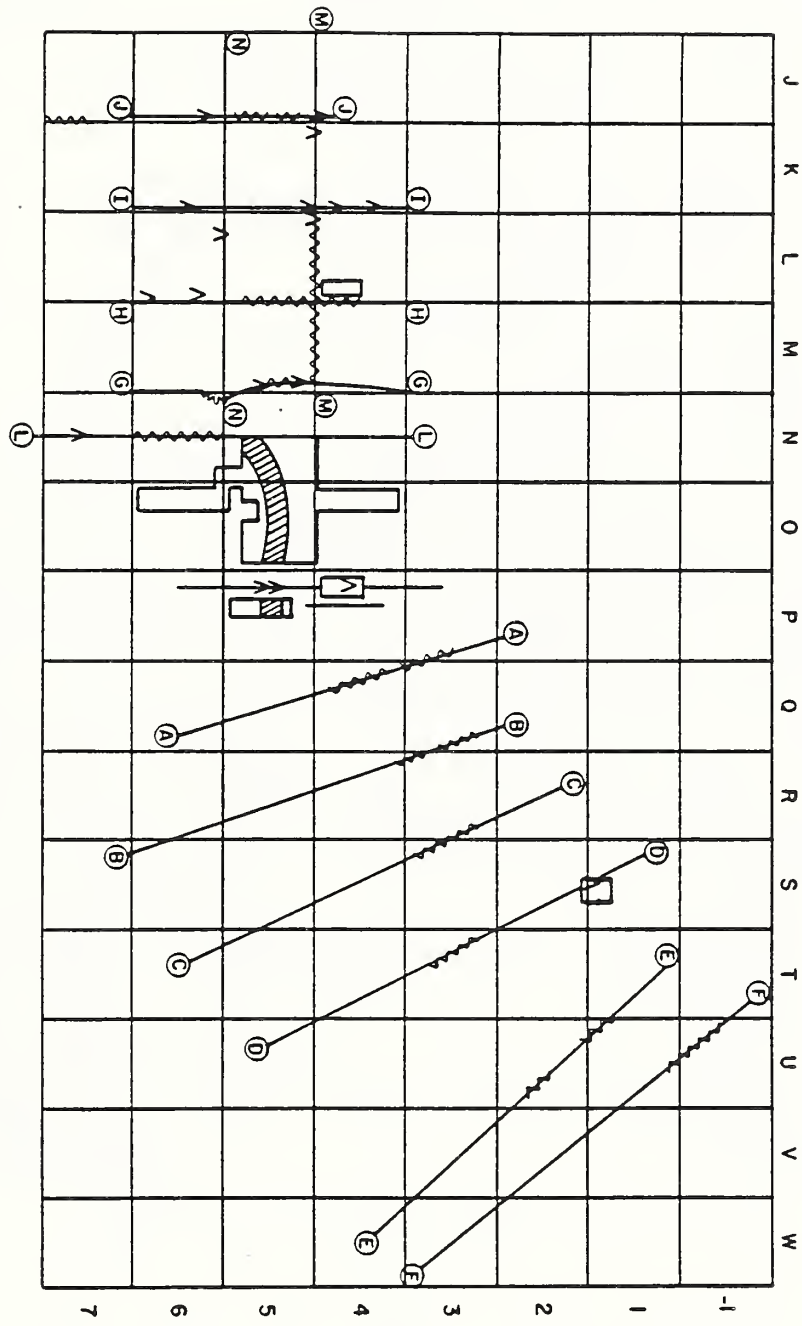
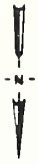
- Figure 1. Radar Profile from Site 301.
- Figure 2. Radar Profile with numerous "point reflectors" from Field IV.
- Figure 3. Radar Profile of detritus layers and foundation walls at Site A9, Field I.
- Figure 4. Plot of radar traverses, Site 301.
- Figure 5. Plots of radar traverses, Field IV.
- Figure 6. Plot of radar traverses, Site A9, Field I.
- Figure 7. Plot of radar traverses, Site A10, Field I.





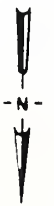
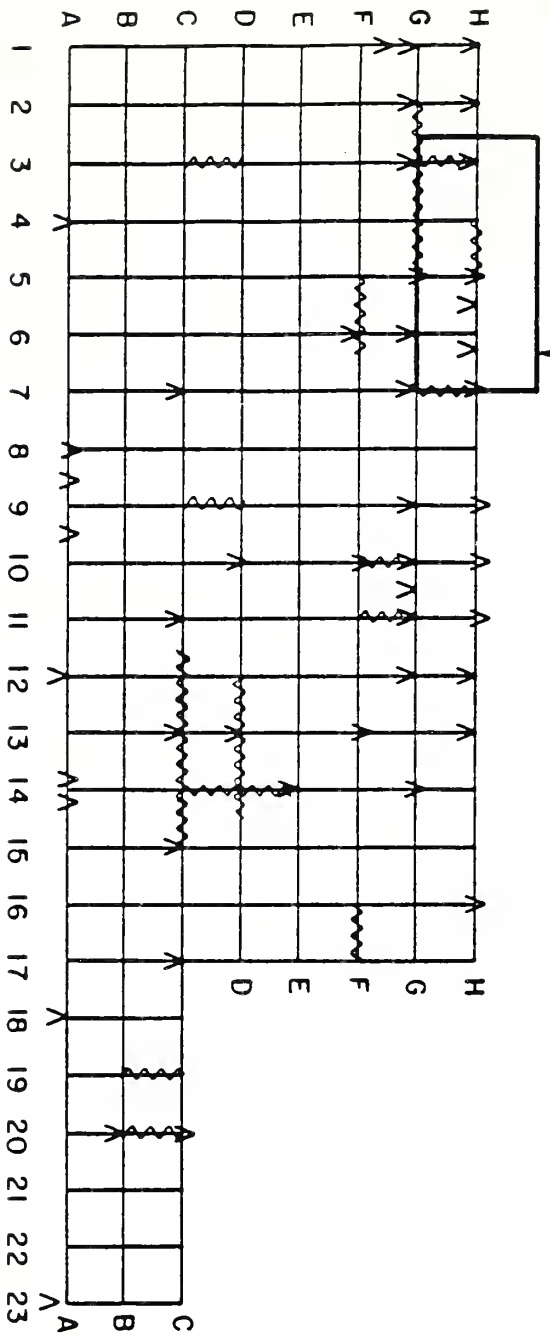
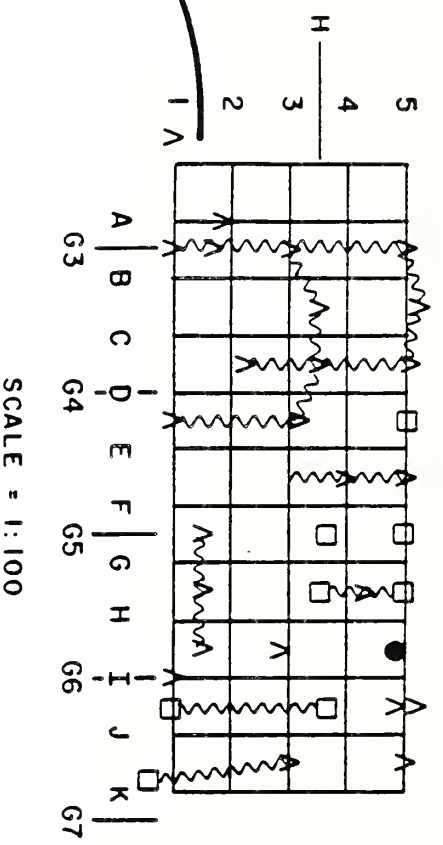






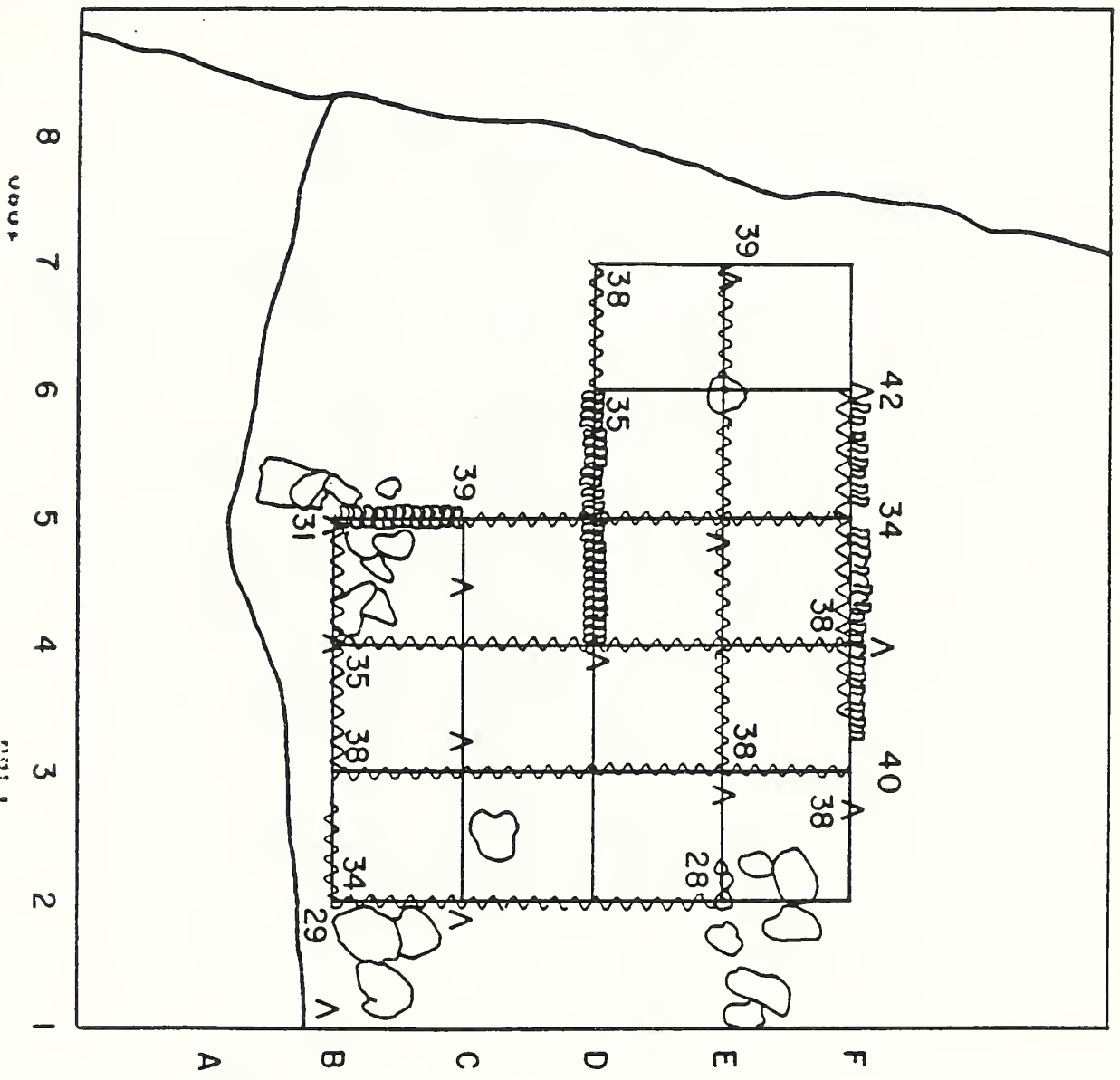
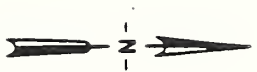
SCALE = 1:50





# LEGEND

- A SINGLE POINT OBJECT
- WALL or SURFACE
- COLUMN
- METALLIC



LEGEND

A SINGLE POINT OBJECT

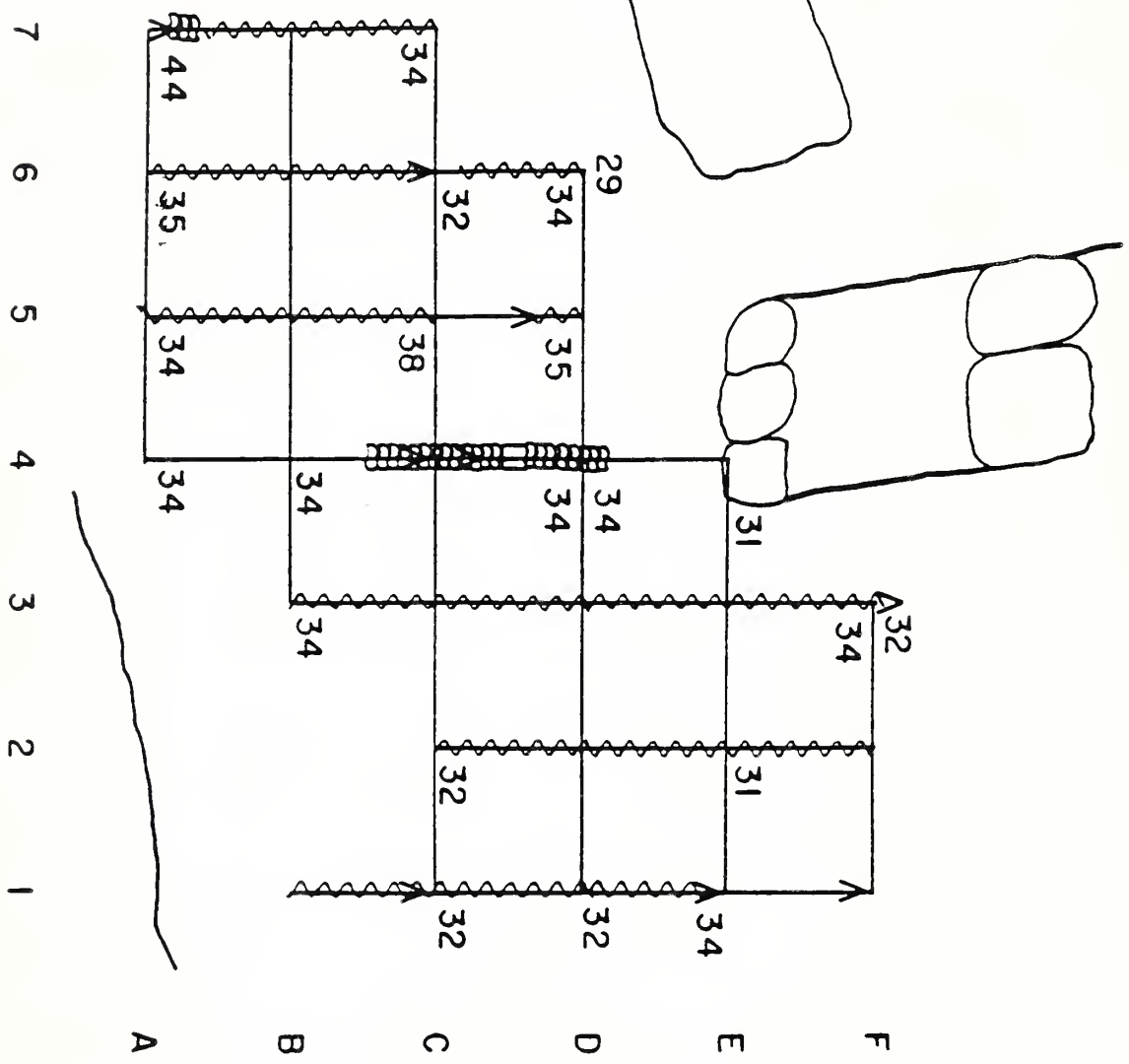
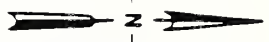
WALL or SURFACE

CULTURAL DEBRIS

SCALE = 1:25

2001





- LEGEND
- A SINGLE POINT OBJECT
  - ~~~~~ WALL or SURFACE
  - ||||| CULTURAL DEBRIS
  - COLUMN

AIRBORNE SURVEYING OF  
ICE COVERS AND WATER BODIES  
USING SHORT PULSE RADAR

by

Kevin O'Neill  
Research Civil Engineer

and

Steven Arcone  
Research Geophysicist

USA  
Cold Regions Research and Engineering Laboratory  
Hanover, NH 03755

February, 1988

## ABSTRACT

Airborne radar surveying offers the possibility of exploring large sections of terrain in relatively short times. Because the antennae are separated from the ground surface, signal processing strategies based on the search for a reliably well defined wavelet are facilitated by the lack of variable impedance loading. In recent exploratory work we have sought to profile ice conditions as well as depth and bottom features of rivers and lakes, using commercially available short pulse radar systems. Antennae were typically mounted on a cantilever off helicopter skids; Alternative arrangements were tried on occasion, such as suspension of the antenna in a cargo net below the helicopter, or the very non-airborne practice of submersion of the antenna from a boat. Recorded returns are generally encouraging in that a variety of features of hydrological interest can be discerned, although significant problems must still be tackled. The short pulse nature of the radiated signal makes it possible to time the delay between echoes from distinct, well separated interfaces, and this often allows reasonably accurate determination of ice layer thicknesses.

The pulse timing approach to layer thickness estimation is limited in part by the finite duration of transmitted pulses. Even with the two higher frequency antennae used (about 600 and 900 MHz center frequencies), we have sometimes experienced overlapping of reflections from upper and lower surfaces of river ice sheets when they are more than about 30 to 50 cm in thickness. For greater thicknesses than that, we employ digital signal processing techniques capable of locating the transmitted pulse, accomodating non-minimum delay wavelets, some wavelet uncertainty, and noise.

For ice thinner than 30 to 50 cm an altogether different approach was developed, utilizing theoretical thin ice reflections together with straight forward cross-correlation operations. The method has been reliably successful in estimating ice thickness from radar records pertaining to ice sheets grown in the lab. The system was able to detect a layer less than 5 cm in

thickness, and also succeeded in distinguishing between layers which differed in thickness by less than 2 cm. Thus the method holds the possibility of increasing resolution by about an order of magnitude, at least under benign conditions. Also, signal processing exercises suggest that this approach may be robust in the face of more diverse field use. In the test case presented below, the method calculates the correct delay between upper and lower surface echoes, despite substantial variations introduced in dielectric constants assumed to surround the layer being investigated. This and other thin ice methods are currently being tested on records obtained from field surveys of rivers in Alaska.

Many challenges are still provided by such phenomena as rough surfaces and rubbly ice, wet surfaces, and the heterogeneous ice-water mixtures which can lead to ice jams. This last item is especially important, because ice jams are a major cause of flooding in seasonally cold regions.

## I. INTRODUCTION

This paper reports some of our activities and recent results in pursuing the long term objective of remote surveying of ice conditions on fresh surface water bodies. Detection of water depth, bottom profile, and related hydrological and geotechnical features is also of interest. Specifically, this investigation used short pulse UHF radar systems to evaluate the possibility of airborne surveying of winter hydrological features over large (multi-km) sections of terrain. Some experiences in unfrozen environments will also be recounted.

In general, past attempts at airborne surveying have utilized systems with pulse center frequencies no greater than about 250 MHz (Dean, 1977; Kovacs and Morey, 1978; Rossiter et al., 1980). In this frequency range it is difficult to distinguish between echoes from top and bottom ice surfaces for sheets less than about 60 cm in thickness. This is unsuitable for many situations of practical interest. In recent years smaller and lighter UHF-frequency antennae have become available commercially, offering the possibility of increased resolution. Successful use in non-airborne surveying (Arcone, 1985; Arcone et al., 1986) have stimulated interest in testing these systems when the antennae are mounted on a helicopter. While airborne surveying can cover large portions of terrain rapidly, one must contend with coherent clutter from aircraft and ground surface, and also with very large amounts of data that result. Questions of lateral resolution, effects of air speed and altitude, scattering and signal strength losses arise. We will review our experiences in addressing some of these items below, and will offer suggestions for future directions.

Both familiar and currently developing signal processing methods show promise for extracting meaningful information from field records. Short pulse radar antennae located on the ground will experience ground loading. That is, unavoidable response by the ground surface will influence currents in the antenna, lowering the overall frequency content and changing the pulse shape. The specifics of this alteration will depend upon the particular characteristics of the ground at hand (under foot). The ground also



causes odd lobing in the radiation pattern (Engheta et al., 1982). When the antenna is airborne it radiates a single broad lobe of minimum pulse duration, although it does so over a large beamwidth. Relatively greater reliability of pulse shapes from airborne antennae greatly facilitates deconvolution and interpretation of records.

## II. FIELD SURVEYS

### Methods and Paraphenalia

When resolution of surface ice layers has been the main concern, relatively high frequency antennae were used. These consisted of GSSI model 3102 and model 101C antennae, with center frequencies of about 600 and 900 MHz and manufacturers peak radiated power ratings of 8 and 2.1 W, respectively. Each of these could be mounted on struts extending approximately 1.5 m from the body of a helicopter, as shown in Figure 1. The system was controlled by a Xadar Electromagnetic Reflection Profiling System (Model 1316) carried inside the helicopter. The resulting pulses resemble that shown on the left in Figure 2, being similar in shape for both antennae though differing in frequency. Duration of the pulse from the 3102 antenna is about 6 ns, with a length in ice of about 1 m, while the 101C pulse is about half that long. The waveform on the right in Figure 2 is from an A<sup>3</sup> Pulse Ekko system, operating at about 50 MHz center frequency. This antenna was suspended beneath the helicopter as shown in Figure 3 but was not used as much in our surveying due to its lack of shielding.

Operating at a pulse repetition frequency of about 50 kHz, the Xadar unit compiles the signals it receives into 8 scans per second. Ultimately the scans are recorded in analog form on cassette magnetic tape, having been sampled and converted to an audio-frequency facsimile before compilation. See the paper by Arcone and Delany (1987) and its references for a more complete description of the system's operation. Under ordinary airborne surveying conditions, digitization of the records must be accomplished later. Handling and digitization of data represents a substantial task,

given that a helicopter speed of 2 m/sec and a digitization rate of 25 ks/sec produces about 12.5 MB of data per km of survey.

These antennae have been designed in such a way that they sacrifice the advantages of high gain and low sidelobes in order to produce a short pulse. The GSSI 3102 and 101C are geometrically similar and both have a 3 dB beam-width of  $70^{\circ}$  in both planes (Arcone et al., 1986). Arcone and Delany (1987) present formulae and a table showing the area of ice bottom illuminated as a function of elevation, ice thickness, and air speed. For 1 m of ice, the area can range from about  $8.4 \text{ m}^2$  at a helicopter altitude of 1.5 m and air speed of 1.5 m/sec, to about  $192 \text{ m}^2$  at 9.0 m and 9.0 m/sec. Thus spatial resolution and waveform coherence can vary due to changes in altitude and direction.

## Results

In this section we provide a representative sampling of previously reported results, to provide an impression of the character, successes, and problems in this sort of surveying. Figure 4 (Arcone, 1988) shows a profile of the ice on Birch Lake, southeast of Fairbanks, Alaska, with indications of principal features. The horizontal bands of coherent clutter represent helicopter and internal system noise; Fortunately the altitude, signal strength, and regularity of the clutter are all such that one can easily distinguish meaningful returns. This ice layer was quite level and uniform in character, thus the separation of lighter (weaker) top and darker (stronger) bottom echoes is approximately constant, while changes in altitude cause the appearance of a wavy surface. A ghostly multiple within the ice is visible below the dark return from the ice bottom. This survey was conducted as something of a dry run, and is marked by the coherence of the echoes. The presence of thin white lines within the main echoes, indicating amplitude zero crossings, means that successive traces show about the same pulse character and do not suffer from a chaotic overlay of echoes from across the entire beamwidth. Returns are being received from a rather small area directly beneath the antenna.

Figures 5a and 5b (Arcone and Delany, 1987) show two profiles of a cross section of the Tanana River in Alaska, both obtained using the 3102 antenna. In the ground survey in Figure 5a, the dark band at the top is antenna direct coupling superposed on the ice surface echo. These two features are widely separated in results from the airborne survey shown in Figure 5b. Figure 6 (Arcone and Delany, 1987) shows a comparison of ice thickness measurements from ground, airborne, and drilling surveys of two river cross sections, including the one depicted in Figure 5 (top of Figure 6). Agreement is good, illustrating the fact that, at least under reasonably friendly conditions, airborne surveying can replace or supplement more laborious measurement on the surface.

Some impression of the character of returns under other more general river ice conditions is provided by Figure 7, which shows part of a 3102 profile of the Yukon River in Alaska (Arcone and Delany, 1987). We note the clear delineation of the top and bottom of the ice on the right and left sides of the figure. In the center is a rubble channel, containing angular chunks of ice frozen in place, protruding on the order of 1 m with typical separations of about 3 m. This produces a degeneration in coherence in both the upper and lower returns. A loss of coherence due to the rough upper surface is necessarily incorporated in the return from the bottom surface, even if the latter is smooth. In this case the character of the lower portion of the record in the rubble channel is typical of what we see in many surveys involving heterogeneous subsurface accretions. These may consist of watery agglomerations of small discoid or spicule "frazil" particles, as well as mixtures of other varied ice fragments (Ashton, 1986). Such accumulations can represent a substantially greater presence of ice mass than one would infer from surface features. Heterogeneity of a jumbled ice deposit under the solid ice cover compounds the degeneration of coherence initiated at the rough upper surface. Subsurface ice accumulations like this have practical importance in that excess ice mass can contribute ultimately to ice jams, which are a major cause of flooding and damage to man made structures.

From the point of view of radar surveying, frazil ice accumulations are problematical in that they may be high in water content thereby causing severe attenuation. In addition, heterogeneities on the order of a significant fraction of the incident wavelength in water will cause substantial scattering. This means that, at the frequencies where we are operating, the scale of heterogeneities is frequently too large for us to swallow them up by treating the medium as an equivalent homogeneous mixture, tantamount to a continuous dielectric medium. They are also too small for us to resolve distinctly.

To the extent that we want to ignore the frazil accumulations, we prefer a higher frequency antenna which is better able to highlight the bottom of the solid ice and which will deliver little response from the watery submerged material. The higher frequencies are scattered more effectively by the distinct pieces of ice; The destructive interference from randomly arrayed scatterers is greater for higher frequencies, and attenuation due to dielectric dispersion in the water is greater. A lower frequency antenna will produce returns which survive scattering better and which suffer less attenuation by the water. Overall, the character of the reflected signals from these and other submerged media is determined by the combination of antenna, flight speed, altitude, specific medium composition and temperature. Other things being equal, lower altitudes and slower air speeds illuminate a smaller area per scan, and thereby increase resolution and decrease incoherence. A narrower sampling of a rough domain allows fewer irregularities away from the area directly beneath the aircraft to contribute to the ultimate mix which the antenna receives. Arcone and Delany (1987) illustrate the different quality of records obtained over irregular ice conditions depending on the frequency range and manner in which the survey is conducted.

The attenuation of radio waves in water due to dielectric dispersion is a very significant factor in the sort of surveying of interest here. Figure 8 (Arcone, 1988) shows the attenuation in dB/m in water at 0° and 20° C, as a function of frequency, assuming that the resistivity of the water is 100

ohm-m (a typical value for an only moderately polluted river). The loss increases drastically with frequency above 100 MHz, and the greater loss at 0 is due to the temperature sensitivity of the dielectric dispersion mechanisms. Dielectric dispersion is responsible for by far the major part of the loss as one approaches 1,000 MHz in any case. This has important implications for the surveying of submerged ice accumulations as well as river and lake bottoms. Higher power, lower frequency antennas (less than 100 MHz) will maximize penetration, but will also mean an overall loss in resolution of ice, bottom features, and submerged objects.

Figure 9 (Arcone, 1988) shows the pleasingly sharp results of a river bottom survey near the Buckley Bridge in Hartford, Connecticut. A GSSI model 3307 "V" antenna was used with a nominal center frequency in air of about 250 MHz. These results were achieved by submerging the antenna in the water and dragging it with a small boat. Ignoring any frequency shift due to interaction with the water, we estimate the center wavelength to be about 13 cm. This small wavelength contributes to the keen resolution of the pattern of scour holes as well as the detail in subsurface sedimentation. Unfortunately such appealing quality in results is not reproduced in some recent airborne attempts to use higher power, lower frequency antennae. An airborne attempt to profile the bottom of a shallow reservoir using a GSSI 3107 antenna (center frequency about 250 MHz) produced results dominated by unwanted reflections and multiples between helicopter, water, and antenna (Arcone, 1988). This occurred despite shielding around the transmit and receive antennae, which were suspended in a cargo net beneath the aircraft. Figure 10 illustrates schematically the various modes in which unwanted reflections can find their way into the results of this sort of survey.

### III. DECONVOLUTION AND THIN ICE LAYERS

Interpretation of data from geophysical exploration systems is frequently based on a presumed pattern of response by a smoothly layered earth model to some impinging energy. We are relatively fortunate in our focus on cold regions in that laterally extensive layers of ice, water, frozen and



unfrozen ground often provide a reasonable approximation of the models postulated. In what follows we sketch briefly some common knowledge on the response of an ideally smooth and piecewise homogeneous layered system to an incident wavelet; This illuminates the methods we have chosen to distinguish echoes from well separated interfaces as well those which we apply to more problematical cases of thin layers. Whether a layer is to be considered thin or not depends upon the combination of its thickness, the wave velocity within it, and the duration of the incident pulse. If these factors come together such that reflection off the bottom of the layer and subsequent multiples interfere with the reflection from the top, then for discrimination purposes we consider the layer to be thin.

As long as we remain with impulse radar of the sort discussed here, it is difficult to make the thin layer problem go away. In some cases one can achieve improved resolution of a relatively thin surface ice layer by resorting to a higher frequency antenna which produces a shorter pulse. However many of the layers we wish to detect lie beneath or consist of media which attenuate higher frequencies severely, as discussed above. If we resort to lower frequencies to enhance penetration we will end up with longer pulses, relative to which the layer of interest may be quite thin. In what follows we describe preliminary results of our attempts to develop signal processing techniques which enhance resolution by approximately an order of magnitude. They do this by distinguishing the different delay structures in different waveforms consisting of superposed wavelets.

Figure 11 shows schematically the impulse response of an ice layer over a perfect reflector, assuming normal incidence. Any layer will produce a similar response pattern, with the signs and magnitudes of the sequential reflections  $R_i$  depending on the dielectric constant contrasts. In the example shown we assume that the system is piecewise homogeneous, consisting of air (dielectric constant  $\epsilon = 1$ ) underlain by ice ( $\epsilon = 3.2$ ) over a perfect reflector. The dielectric constant of water at 0°C is 88, and the impulse response sequence for an air-ice-water system consists of a set of  $R_i$  with the same signs as those shown but with less contrast between the magnitudes of the surface reflection  $R_0$  and the bottom echo  $R_1$ . In the notation below,

we refer to the material above the ice layer as medium 1, that in the layer as medium 2, and that below as medium 3.

The complete echo for the system shown will consist of the convolution of an incident wavelet with the impulse response series illustrated. That is, the response  $x_t$  to the wavelet  $s_t$  will be

$$x_t = R_0 s_t + R_1 s_{t-\tau} + R_2 s_{t-2\tau} + \dots \quad (1)$$

where the subscript  $t$  is a discrete time index and  $\tau$  is the length of time required (in the same units as  $t$ ) for the wavelet to traverse the layer and return. For the most part, it is  $\tau$  that we are trying to determine. Knowing it, we can calculate the layer's thickness from  $\epsilon_2$ , or vica versa. The response coefficients  $R_i$  can be calculated from reflection and transmission coefficients for the various interfaces:

$$G_{jm} = \frac{\eta_m - \eta_j}{\eta_m + \eta_j} \quad (2)$$

$$T_{jm} = \frac{2 \eta_m}{\eta_m + \eta_j}$$

where  $G_{jm}$  ( $T_{jm}$ ) is the reflection (transmission) coefficient for a signal propagating from the material of layer  $j$  to layer  $m$ , and  $\eta_j$  is the impedance of any  $j^{\text{th}}$  material. In these terms, the response coefficients are

$$R_0 = G_{12}$$

$$R_1 = T_{12} G_{23} T_{21}$$

(3)

$$R_i = R_1 (G_{21} G_{32})^{i-1} \quad \text{for } i > 1$$

Under conditions common in our frequency range and survey environments, the reflection and transmission coefficients may be regarded as essentially independent of frequency. Thus we may evaluate the coefficients  $R_i$  as far out into the sequence as we like, and then use equation (1) to construct the overall response  $x_t$  for our wavelet  $s_t$ . An alternative and generally more informative approach is to construct a complex, frequency dependent reflection coefficient  $G_\ell$  for the entire layer system by using an impedance transformation (Cheng, 1983).

$$G_\ell(f) = \frac{Z - \eta_1}{Z + \eta_1} \quad (4)$$

where we have replaced  $\eta_2$  in equation (2) with a complex impedance,  $Z$ , for the combined medium 2 - medium 3 portion of the system.  $Z$  is defined as

$$Z(f) = \eta_2 \frac{\eta_3 \cos(kd) + \iota \eta_2 \sin(kd)}{\eta_2 \cos(kd) + \iota \eta_3 \sin(kd)} \quad (5)$$

where  $\iota$  denotes the square root of minus one,  $k$  is the wavenumber in medium 2, and  $d$  is the thickness of the layer (medium 2). The expression  $G_\ell$  may be used as a transfer function for the layer to construct  $x_t$ :

$$x_t = \int_{f_1}^{f_2} G_\ell(f) S(f) e^{2\pi \iota f t} df \quad (6)$$

where  $S(f)$  is the Fourier transform of the wavelet. Thus in theory we could take the transform of any return  $x_t$  and divide it by  $S(f)$  to obtain the transfer function, which in turn could be inverted to produce a spike train such as appears in Figure 11.

Figure 12 displays  $G_\ell$  for two different systems, consisting of air (medium 1), ice (medium 2), and underlayers with  $\epsilon_3 = 22$  in one case and  $\epsilon_3 = 352$  in the other. The dielectric constant of water at  $0^\circ\text{C}$  is 88, thus these plots show the effect of doubling or halving the square root of  $(\epsilon_2/\epsilon_3)$  relative to an air-ice-water system. Increasing the value of  $\epsilon_3$  raises the magnitude of reflections over all frequencies but has little effect on the overall shape of the magnitude and phase curves of the transfer function. In other words, the structure of the delays between different components of the total return is unchanged, and that is reflected in the similarity in pattern in the two transfer functions.

### Well Separated Echoes

To avoid problems in dividing the transform of a signal by  $S(f)$ , which may have zeroes or areas of low magnitude, it is common practice to use digital inverse filters in the time domain. When the  $R_i$  series contains well separated echoes, one can apply a filter designed to respond to the wavelet itself. The by now classical approach to design such filters is the Wiener least squares wave shaping system. While this filter system has the advantage of a thorough mathematical basis based on optimization of results, one must employ special devices to deal with its sensitivity to noise and pulse distortion (e.g. Treitel and Robinson, 1966; Cooper and McGillen, 1986; Walden, 1988). Instead we choose here to operate directly in the frequency domain, limiting our computations to the band in which the magnitude of  $S(f)$  is most significant and noise is least important. Dividing the transform of an entire signal by a band limited  $S(f)$  has resulted in loss of resolution on some occasions when the signal was much longer than the wavelet itself. Thus we operate on a succession of overlapping segments of the original signal, each the same length as the wavelet.

To proceed, we excise a segment  $\chi_\sigma$  from the original signal, where

$$\chi_\sigma = x_t, \quad n \leq t \leq n + M, \quad \sigma = t - n \quad (7)$$

where  $n$  is any particular point in (discrete, denumerative) time and  $M$  is the wavelet length. Thus  $\chi_\sigma$  contains a segment of  $x_t$  beginning at  $t=n$ , and encompassing the next  $M$  points. As the method proceeds, all time points are taken in succession to be  $n$ . The transform of  $\chi_\sigma$  is calculated, and we test it for similarity to the wavelet spectrum by examining the inverse of the function  $U(f)$ .

$$U(f) = X(f)/S(f) \quad (8)$$

where  $X(f)$  is the transform of  $\chi_\sigma$ . This corresponds to a filtering operation in the time domain producing  $u_\sigma$ :

$$u_\sigma = \int_{f_1}^{f_2} U(f) e^{2\pi i f \sigma} df \quad (8)$$

where  $(f_1, f_2)$  is the frequency band chosen on the basis of  $S(f)$ . If  $\chi_\sigma$  consists of a wavelet, then  $U(f)$  should be a constant with zero phase, and  $u_\sigma$  should consist of a spike at  $\sigma = 0$ .



To construct the filtered signal  $y_n$  in the time domain, we only determine the value of  $u_\sigma$  at  $\sigma = 0$ , to see the maximum response where a spike should be, and insert that value in  $y$  at time point  $n$ .

$$y_n = u_0 = \sum_{f_1}^{f_2} U(f) \quad (9)$$

This means that the filtered signal is constructed simply by summing the transform values of segments of  $x_t$  as they are calculated at each frequency.

In practice we introduce one further modification. To compensate for the loss of optimality relative to the Wiener filter in our band limited calculations, and to further suppress unwanted responses of the filtering operations, we also apply a time dependent weighting factor. This factor can have a variety of forms, the primary requirement being that it equal 1 when (similarly scaled)  $S(f)$  and  $X(f)$  agree and that it decline rapidly when they do not. One successful weight used is

$$w_n = \text{avg} \left( \frac{\exp [-2|\phi_x - \phi_s|/2\pi]}{1 + |1 - A_x/A_s|} \right)^3 \quad (10)$$

where "avg" denotes an average over the frequency band  $(f_1, f_2)$  of the cubed quantity in brackets, and the variables are defined by the expressions for the scaled spectra:

$$U(f) = A_x(f)e^{i\phi_x(f)} \quad (11)$$

$$S(f) = A_s(f)e^{i\phi_s(f)}$$

Thus equation (9) becomes

$$y_n = w_n u_0 \quad (12)$$

One can sharpen or loosen the system by playing with the exponent in equation (10); A value of 3 seems to suppress unwanted responses thoroughly without being unduly sensitive to small differences between the spectra being compared.

This overall approach has worked well in preliminary tests. The upper curve in Figure 13 (O'Neill, 1988) shows a portion of a record obtained over a river ice sheet with the 3102 antenna. The lower curve is  $y_n$ , the result obtained with this filtering system. On the basis of the time separation between the spikes and an assumed ice dielectric constant of 3.2, the estimated ice thickness is about 48 cm, which is within about 10% of values measured in the field in the vicinity of the radar readings. The system appears to be quite robust in the presence of noise (O'Neill, 1988). More extensive testing of this system is underway, as we apply it to field records with representative selections of both common and challenging cases.

#### Thin Ice Layers

When the ice is thin relative to the length of the wavelet in ice, an altogether different approach must be employed. In thin ice returns, members of the  $R_i$  series are superposed, and results from a system designed to recognize separated wavelets will deteriorate. This case is of practical importance because a good deal of ice in seasonally cold areas either remains thin through the cold season or in any case is thin at least during the early part of the season. In such instances safety, scientific, or engineering investigations may be frustrated when the thicknesses are too small to be distinguished with ordinary time domain filtering methods.

To test approaches to signal processing for thin ice we carried out a laboratory program in which a thin sheet of ice was grown on top of a foil sheet. Its thickness was gradually increased by adding water to its surface. After each addition was frozen solid we used the Xadar - 101C system to record pulse reflections. The ice was greater than 4 m square, with the antenna about 1 m above the ice, thus the sheet was large enough horizontally to avoid interference from container sides, antenna supports, etc. The foil underneath prevented the appearance of responses from structural materials in the container and building floor. Because the antenna was immobile, cantilevered out over the center of the ice, it was possible to operate the system in digital mode, stacking 16 scans over about 2 seconds for each record. This offered the convenience of providing digitized data immediately and may also have enhanced the clarity of the records. In the field this direct, digital mode would rarely be advantageous when the antennae are mounted on moving vehicles or aircraft. Fixed mountings on bridge piers or whatever might duplicate the lab test conditions.

We address the signal processing of these thin ice returns by constructing a library of synthetic echoes, each corresponding to a given delay between members of the  $R_i$  series. These echoes were obtained easily using the general formula for  $G_\ell(f)$  evaluated for any chosen  $d$ , together with a reference wavelet. Figure 14 shows a variety of waveforms corresponding to various real and synthetic echoes, where all "real" echoes were obtained from the ice sheet in the lab. Example (a) at the bottom of the figure is a return from bare foil, and it provided the reference wavelet and the  $S(f)$

used in equation (6) to compute all synthetic return shapes. As the ice increases in thickness (bottom to the top of the figure), one sees  $R_0$  and  $R_2$  gradually move away from the larger central reflection  $R_1$ . (Note the magnitudes of the successive spikes in Figure 11). Synthetic example (f) at the top corresponds to 24 cm of ice, and one sees that it is just about at the thickness where  $R_0$ ,  $R_1$ , and  $R_2$  become completely distinct. It is clear that the real and synthetic signals in the figure agree quite well, as they did at a variety of other thicknesses between 0 and about 17 cm of thickness.

Given any real signal to be processed, one performs a cross-correlation with each member of the synthetic library of possible matches. For each possible thickness  $d$ , the correlation function  $c_t$  is examined, and the value of its peak noted. These peak values are assembled into a maximum correlation value function  $a(d)$ , and the value of  $d$  for which  $a(d)$  itself is a maximum constitutes the best estimate of  $d$  for the real signal. This procedure assumes that all synthetic echoes have been scaled to have the same total energy, which is automatically the case when  $G_\ell(f, d)$  is constructed for an air-ice-foil system. Because material 3 is a perfect reflector, all incident energy must eventually return in one form or another. This also assumes essentially 1-D plane wave propagation back and forth between the layer system and the antenna, an assumption which would be compromised by an uneven surface and higher antenna elevation.

Spelling out the above in terms of equations, we first construct synthetic echoes  $g_t$  for each  $d$ :

$$g_t(d) = \int_{f_1}^{f_2} G_\ell(f, d) S(f) e^{2\pi i f t} df \quad (13)$$

We then compute the cross-correlation  $c_t$  of each of these with the real signal to be analyzed,  $x_t$ :

$$c_t(d) = \sum_{j=-\infty}^{\infty} g(d) x_j \quad (14)$$

The maximum value of  $c_t$  is recorded in  $a(d)$  for each  $d$ :

$$a(d) = \max_{\text{over } t} \{ c_t(d) \} \quad (15)$$

and the peak in  $a(d)$  should identify the  $d$  value for which an autocorrelation with zero time shift has been obtained.

Figure 15 shows  $a(d)$  for the two real returns shown in Figure 14 corresponding to 7.3 and 17.1 cm. In each case, the peak in  $a(d)$  is in the right locale, although the maximum in the lower (7.3 cm) curve is barely above the next highest peak. Figure 16 shows the  $d$  values for which  $a(d)$  was a maximum, as a function of measured thickness. That is, the best estimates of ice thickness based on the processing system are plotted on the vertical axis, versus the actual  $d$  values applying in each case. Perfect agreement would place all points on the 45 line. Clearly the level of discrimination is quite good. This represents an order of magnitude improvement over the level of estimation possible on the basis of the raw data or obtainable from conventional time domain deconvolution.

Some signal processing exercises were also performed to gain some feel for the robustness of the method. Figure 17 shows three synthetic returns for a hypothetical 17 cm ice sheet with air above and medium 3 underneath having  $\epsilon_3 = 1, 12, \text{ and } 352$ . Thus the cases cover an  $\epsilon_3/\epsilon_2$  ratio both less than and greater than 1, and both less than and greater than what would occur in ice over water. Each curve is scaled relative to its peak amplitude, producing a relative rise in prominence of the center  $R_1$  component in the



progression from the bottom to the top of the figure. Signals at various intermediate values of  $\epsilon_3/\epsilon_2$  were also constructed, and in all cases some artificial noise was thrown in, for a whiff of realism.

Each of these signals was then processed in the manner described above, using the library developed for the air-ice-foil system. Figure 18 shows the results of this exercise, indicating that the method correctly estimated 17 cm as the subject signal thickness whenever there is a substantial contrast between  $\epsilon_2$  and  $\epsilon_3$ , with less success where they are comparable ( $\log 3.2 = 0.5$ ). Going back to Figure 12, we note that the amplitude curve of the layer system transfer function for the air-ice-foil system represents the limiting case for an increase in  $\epsilon_3$ , and is flat at a value of 1. The shape of the phase curve however is similar to those shown. Thus, despite alteration of the returns caused by variation of dielectric properties, this processing scheme appears to react adequately to information on differential phase shift (delay) which is inherently present in the layer system response. The performance shown in Figure 18 may be a worst case, with better results expected when more reasonable dielectric properties are used for construction of the synthetic library. The method is currently being tested on field records from river ice surveys including heterogeneous ice accumulations under solid ice covers. This will help determine whether the processing system can distinguish the ice sheet when dielectric properties of the sublayer are complex and uncertain.

#### OBSERVATIONS AND WISH LIST

Our recent experiences with and observations on the use of airborne short pulse radar surveying are summarized below. Our primary focus centers on cold regions problems, with additional concern for the general problems in the profiling of rivers, lakes, and other geophysical features.

Airborne surveying is most successful in terms of both data collection and interpretation when smooth, extensive horizontal layers are present,

with low electrical conductivity and reasonably (piecewise) homogeneous permittivity. Exposed rock or dry soil strata and clean ice layers are ideal. Uncluttered upper ground or ice surface with low reflectivity also helps. Superior results are often obtained when antennas are shielded and when low altitude and air speed can be maintained.

Both established and developing signal processing techniques should be able to help interpret records from cleanly layered ice (and perhaps other) strata, even for quite thin layers. Wet and rough surfaces and heterogeneous ice-water mixtures still pose many interesting challenges. A new direction is represented by the use of pulse code modulation, such as has been developed at CRREL (Wills, 1987). In this promising approach, one cross correlates a transmitted pulse code with a stored complementary code, ideally producing compressed pulse returns with enhanced penetration at low power.

A variety of future developments would increase the ease and overall feasibility of this kind of surveying. Built-in, rapid digitization and storage of signals is highly desirable, as is a flexible built-in capability for various deconvolution and signal processing activities. Ideally a system would allow one to select or program a deconvolution strategy to suit local conditions, the results of which would be recorded and also displayed in real time. Faster and better graphical and display capabilities are needed overall, especially in light of the large amounts of data recorded during a single survey. A helicopter speed of 2 m/sec produces about 12.5 MB of data per km of survey, assuming a digitization rate of 25 ks/sec.

Ideally satellite positioning systems should be integrated into the enhanced processing and display capabilities. This should be done so that flight paths and positions within them can be identified accurately during both real time and subsequent examination of data.

More agreeable designs for higher power, lower frequency short pulse antennas are required for situations in which penetration is of greater importance. Preferably these systems should feature center frequencies as low

as the sub 50 MHz range, and should weigh no more than about 50 kg. Substantial weight can be accommodated by a sling arrangement beneath a helicopter. However extensive shielding and flight safety considerations limit one's options, especially when high power work requires separate transmit and receive antennas.

Extensive shielding might be avoided by the use of filtering and polarization techniques. The effectiveness of filtering strategies is likely to be compromised by the variety of waveforms in reflections from the helicopter itself. In cross polarization techniques one receives at an angle orthogonal to that of the transmitted signal. Because smooth flat surfaces do not rotate the polarization on reflection, this would diminish reflections and losses from smooth surfaces and allow greater attention to rough surfaces, volume inhomogeneities, and reflective 3-D objects. Such schemes must await serious improvements in the signal to noise ratio of short pulse radar systems, which are now limited by sampling noise in the receiver. Circular polarization would enhance detection of surfaces. The rotational sense of the transmitted wave would be reversed by the air-water interface, but not by the water-bottom interface, thus allowing these to be distinguished by alternative receive modes. Experiments are now underway at CRREL, using broadband logarithmic spiral antennas, excited by pulse type waveforms.

#### IV REFERENCES

Arcone, S.A. (1985). Radar Profiling of Ice Thickness, Cold Regions Technical Digest 85-1, USACRREL, Hanover, NH.

Arcone, S.A. (1988). Some airborne applications of subsurface radar, presented at TRB 67th Annual Mtg, Jan 1988, Wash. D.C.

Arcone, S.A. and A.J. Delany (1987). Airborne River-ice thickness profiling with helicopter-borne UHF short-pulse radar, J. Glaciol., 33:1-11.

Arcone, S.A., A.J. Delany, and R. Perham (1986). Short Pulse Radar Investigations of Fresh Water Ice Sheets and Brash Ice, CRREL Report 86-6.

Ashton, G.D. ed-author (1986). River and Lake Ice Engineering, Water Resources Publications, Littleton, Col.

Cheng, D.K. (1983). Field and Wave Electromagnetics, Addison-Wesley, Reading, Mass.

Cooper, G.R. and C.D. McGillen (1986). Modern Communications and Spread Spectrum, McGraw-Hill, New York.

Dean A.M. jr (1977). Remote Sensing of Accumulated Frazil and Brash Ice in the St. Lawrence River, CRREL Report 77-8.

Engheta, N., C.H. Papas, and C. Elachi (1982). Radiation patterns of interfacial dipole antennas, Radio Sci., 17:1557-1566.

Kovacs, A. and R.M. Morey (1978). Remote detection of water under ice-covered lakes on the North Slope of Alaska, Arctic, 31:448-458.

O'Neill, K. (1988). On thin ice: radar identification of thin and not so thin layers in hydrological media, Proc. 7th Intl. Conf. Comp. Meth. Wat. Resour., Cambridge, Mass., in press.

Rossiter, J., J. Snellen, K. Butt, and T. Ridings (1980). Multi-year ice thickness distribution in the Beaufort Sea determined by airborne impulse radar, C-CORE publ. No. 80-11, C-CORE, Memorial University, St. John's, Newfoundland.

Treitel, S. and E.A. Robinson (1966). The design of high resolution digital filters, IEEE Trans. Geosci. Electronics, GE-4:25-38.

Walden, A.T. (1988). Robust deconvolution by modified Wiener filtering, Geophys., 53:186-191.

Wills, R.H. (1987). A digital phase coded ground probing radar, Ph.D. Thesis, Dartmouth College, Hanover, NH.



a

Figure 1. GSSI 3102 short pulse radar antenna mounted on a Bell Jet Ranger 206 helicopter.

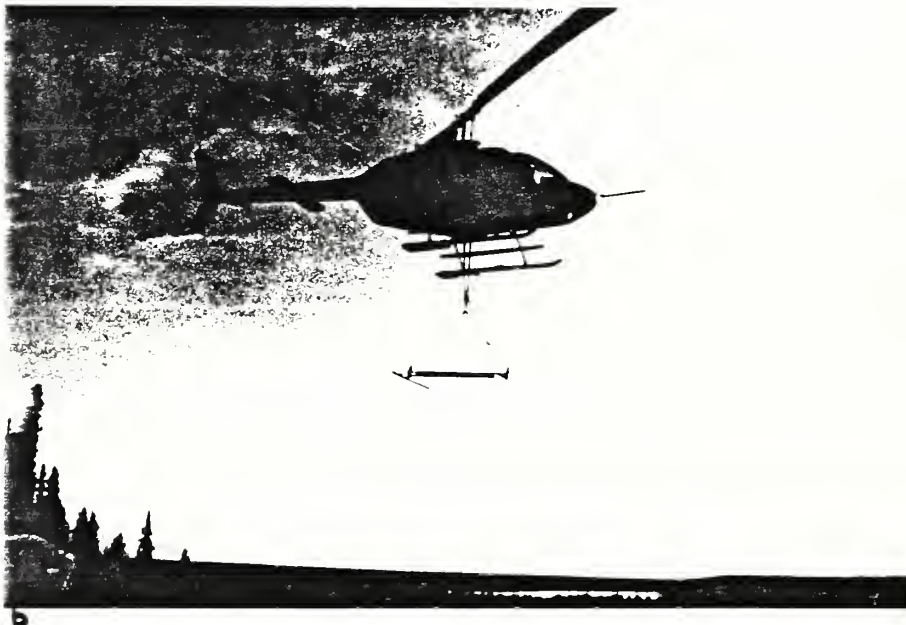


Figure 3. A-Cubed pulse ekko antenna, suspended below Bell Jet Ranger 206.



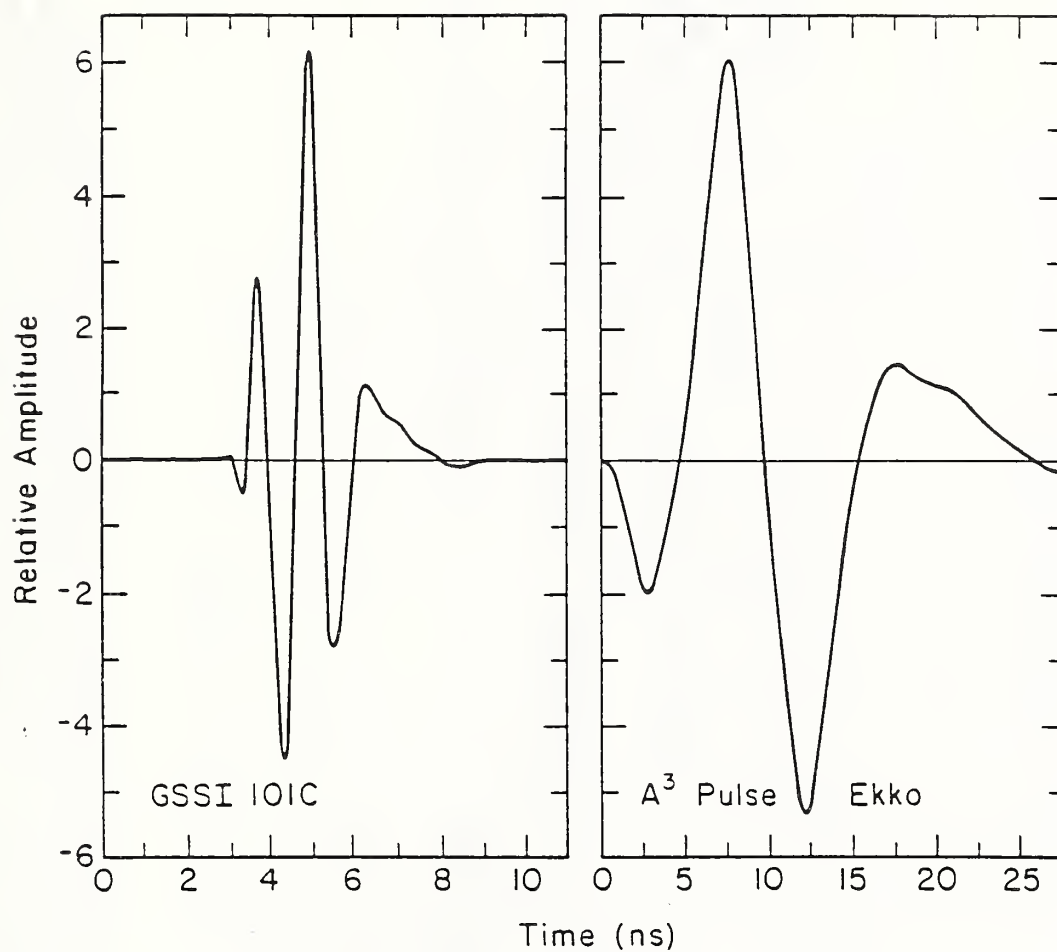


Figure 2. Waveform examples in short pulse radar. Left: GSSI model 101C resistively loaded dipole, vintage 1979. Right: A-Cubed "pulse ekko" low frequency folded dipole, vintage 1985. The waveforms have been modified slightly by filters of a control unit.

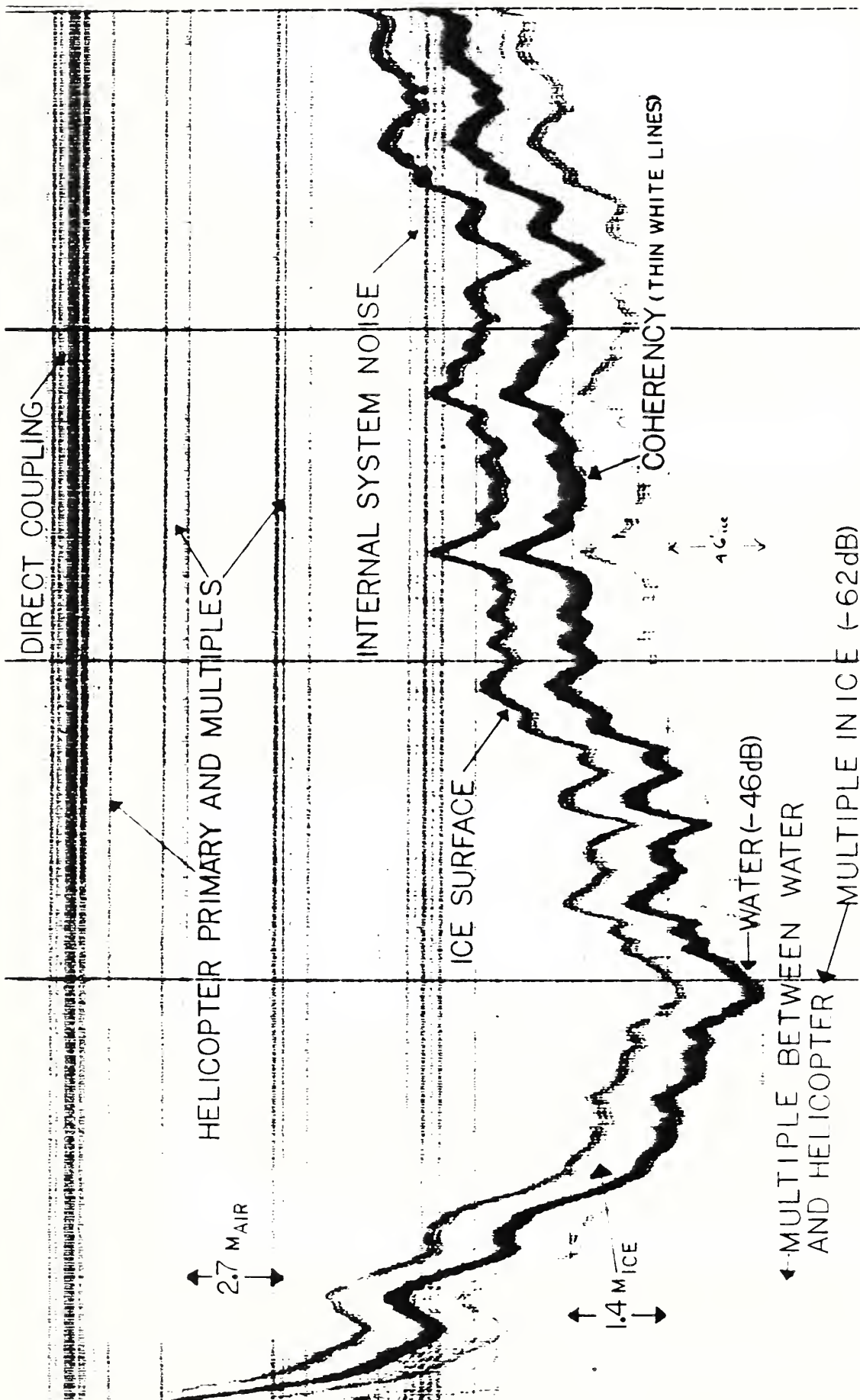


Figure 4. Antenna model 3102 profile of ice thickness over Birch Lake, Alaska, with various events in the record identified. The vertical ice thickness scale applies only within the first two reflections. The decibel values given in parentheses refer to the round trip propagation loss for the water and ice multiple events at the points indicated. Portions of some events may not be visible in the reproduction because the figure was made light enough to view the signal zero crossings (thin white lines) in the stronger events.

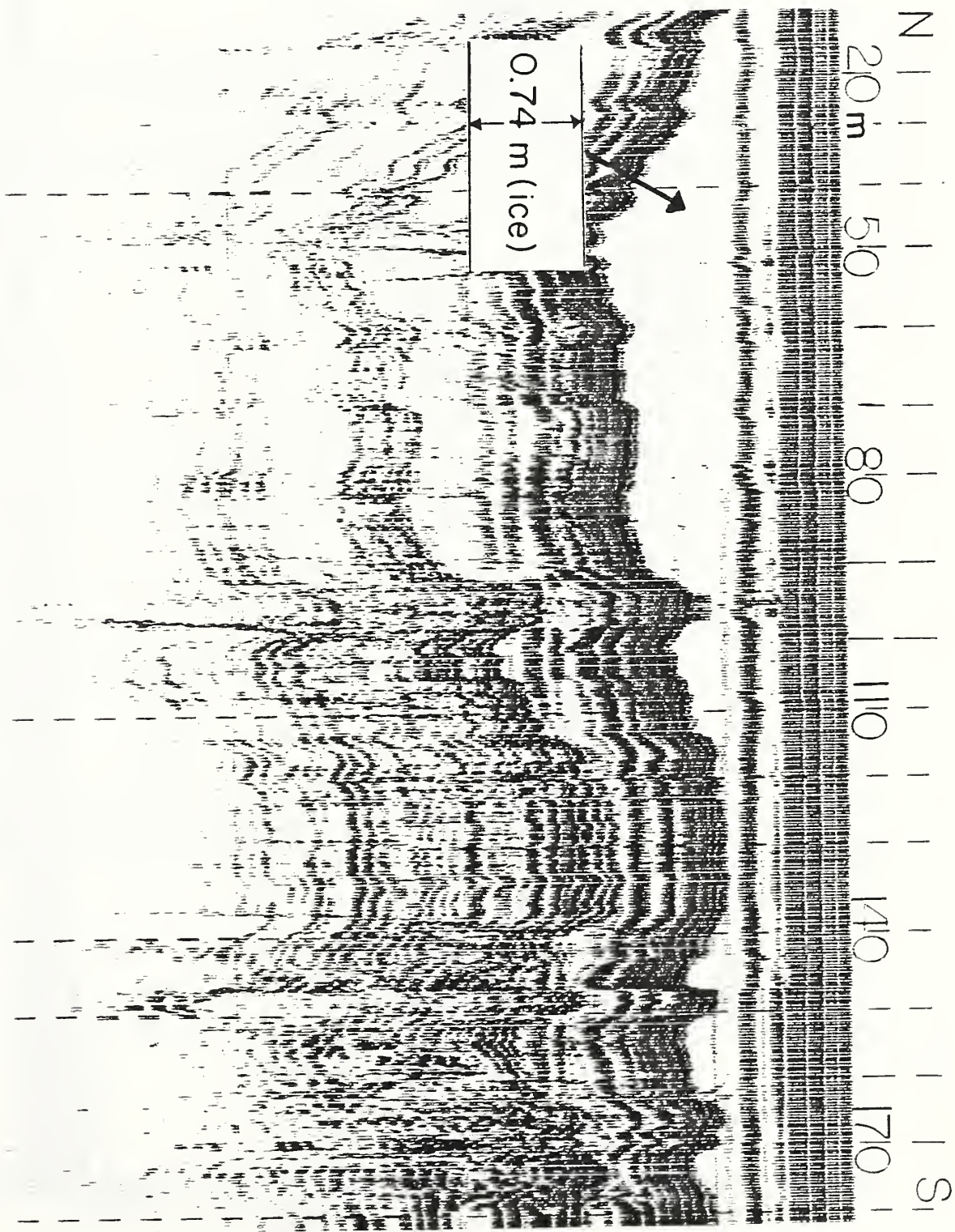
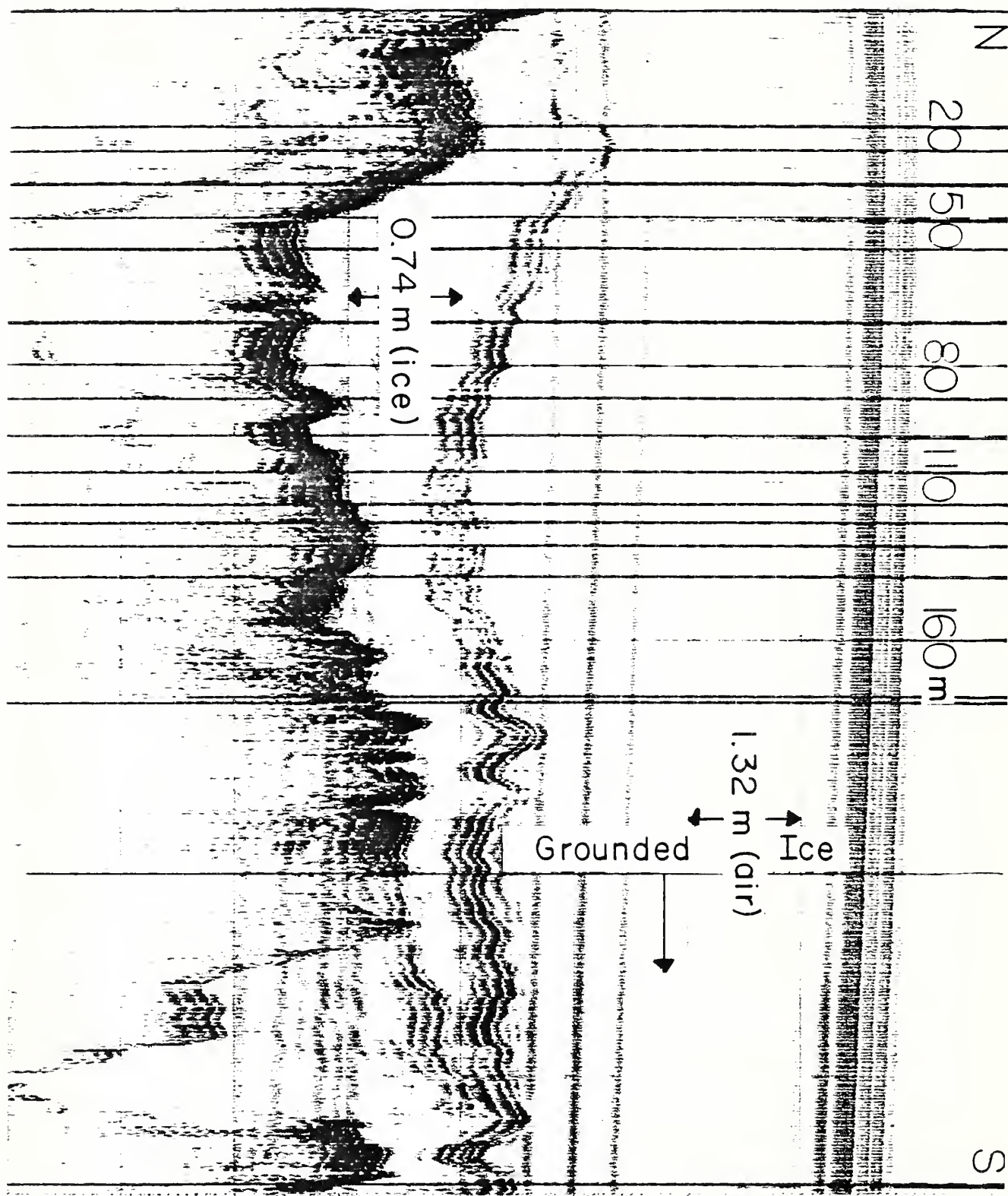


Figure 5a. Ground survey of a cross section of the Tanana River in Alaska.





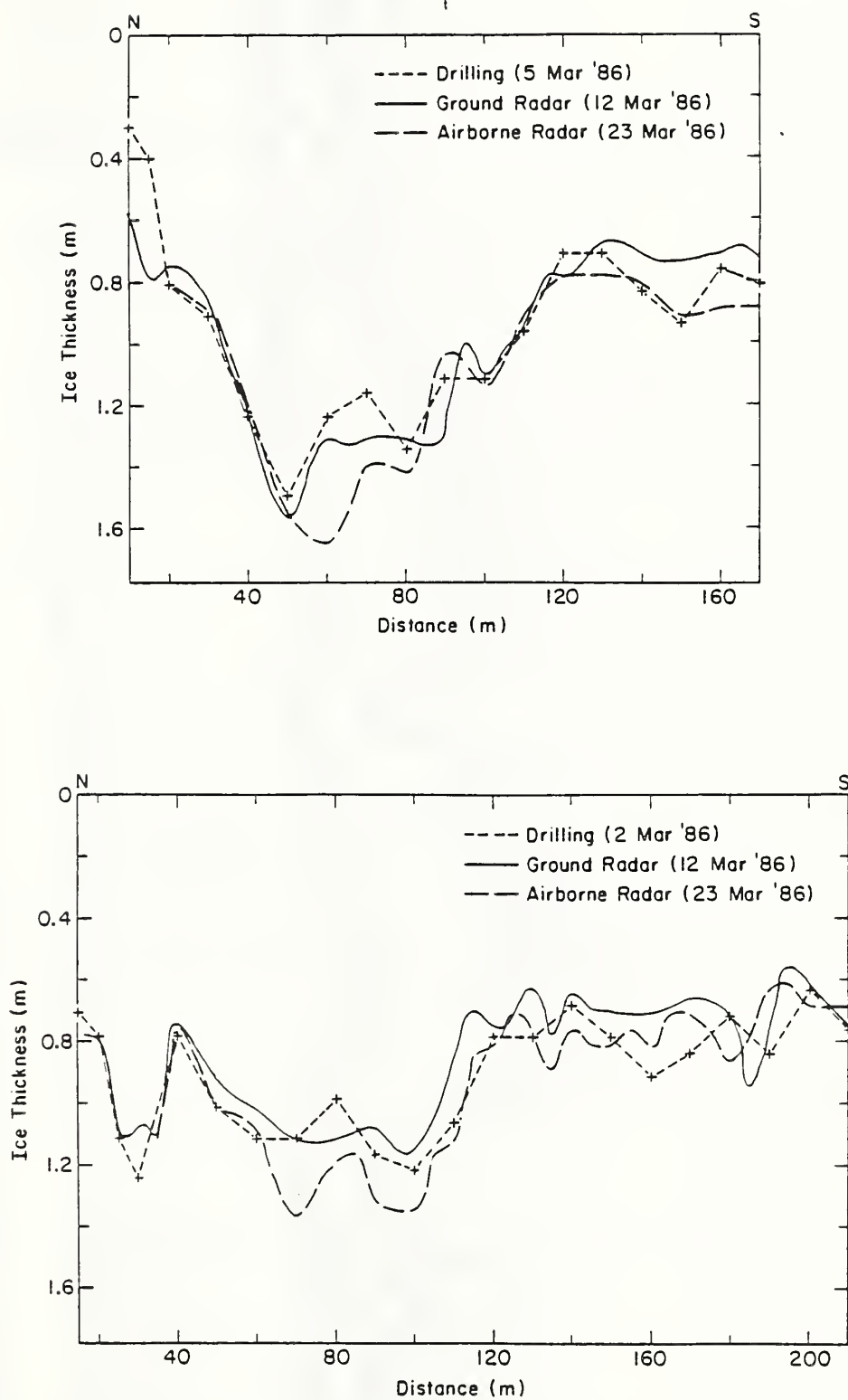


Figure 6. Ice thickness measurements by ground and airborne radar measurement and by drilling. Figure 5 shows a portion of X6.



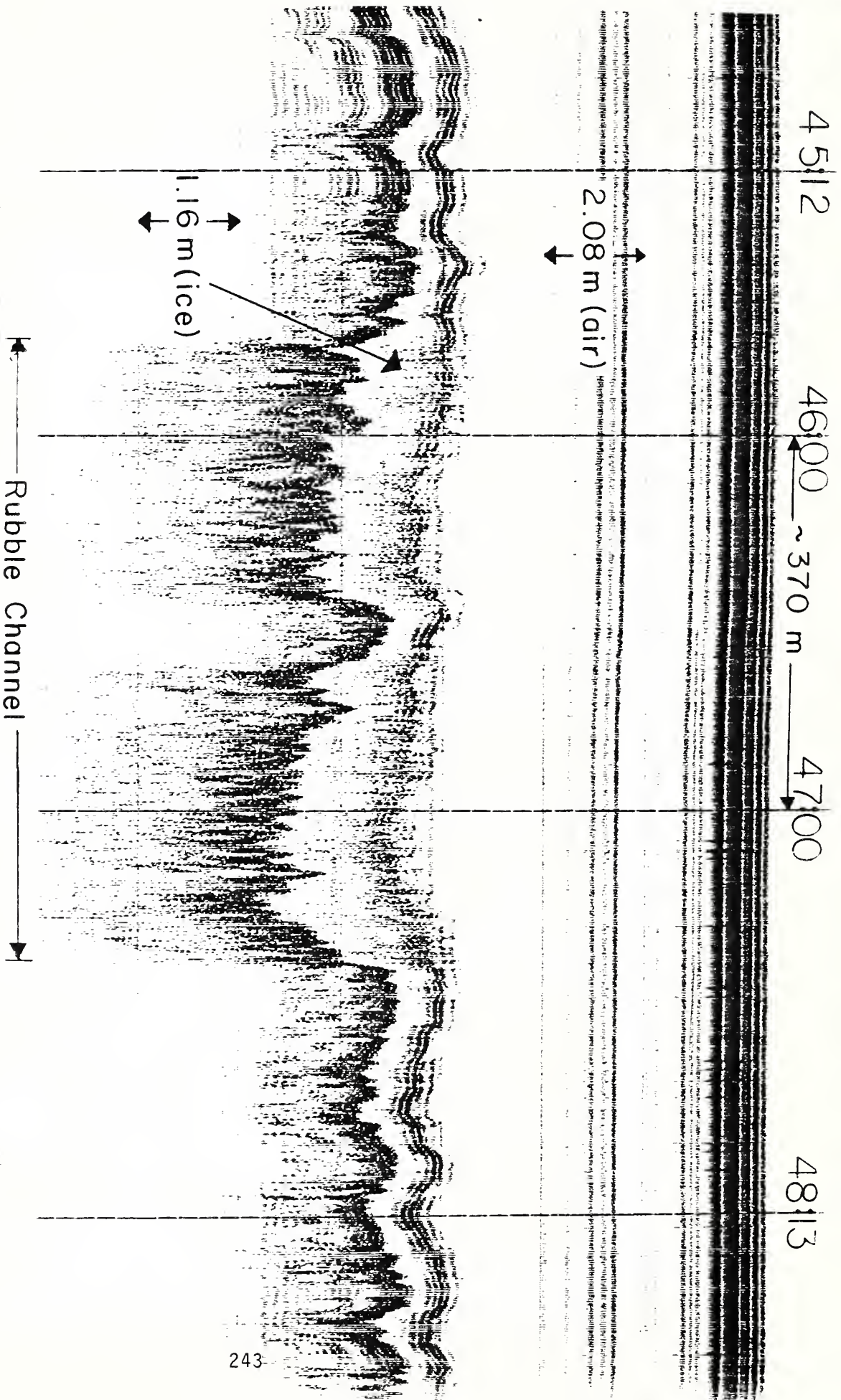


Figure 7. A section of the Yukon River profiled with the 3102 antenna showing part of an ice rubble channel.

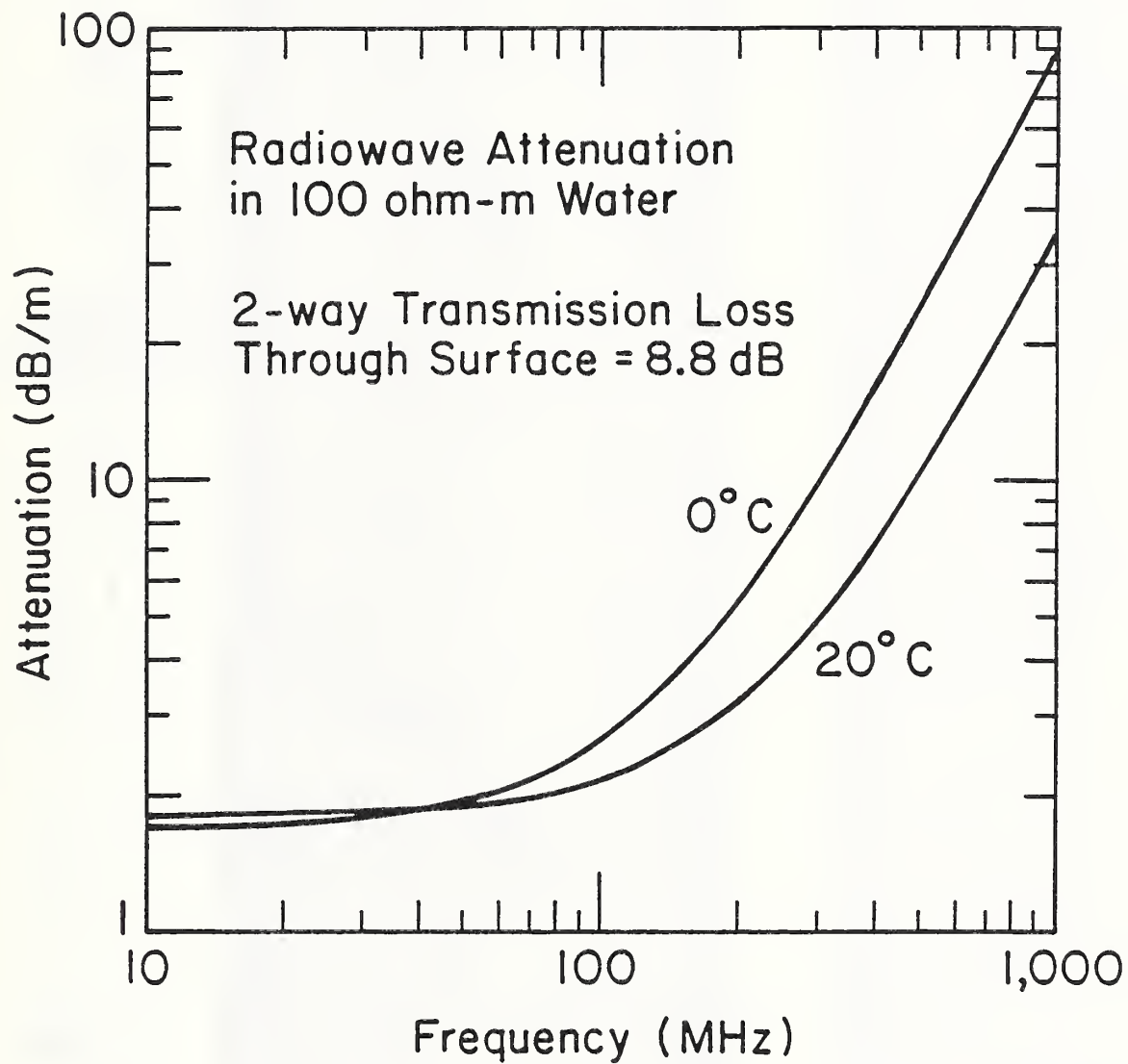


Figure 8. Attenuation rate of radiowaves in fresh water as a function of frequency at a conductivity of 0.01 S/m (100 ohm-m resistivity).



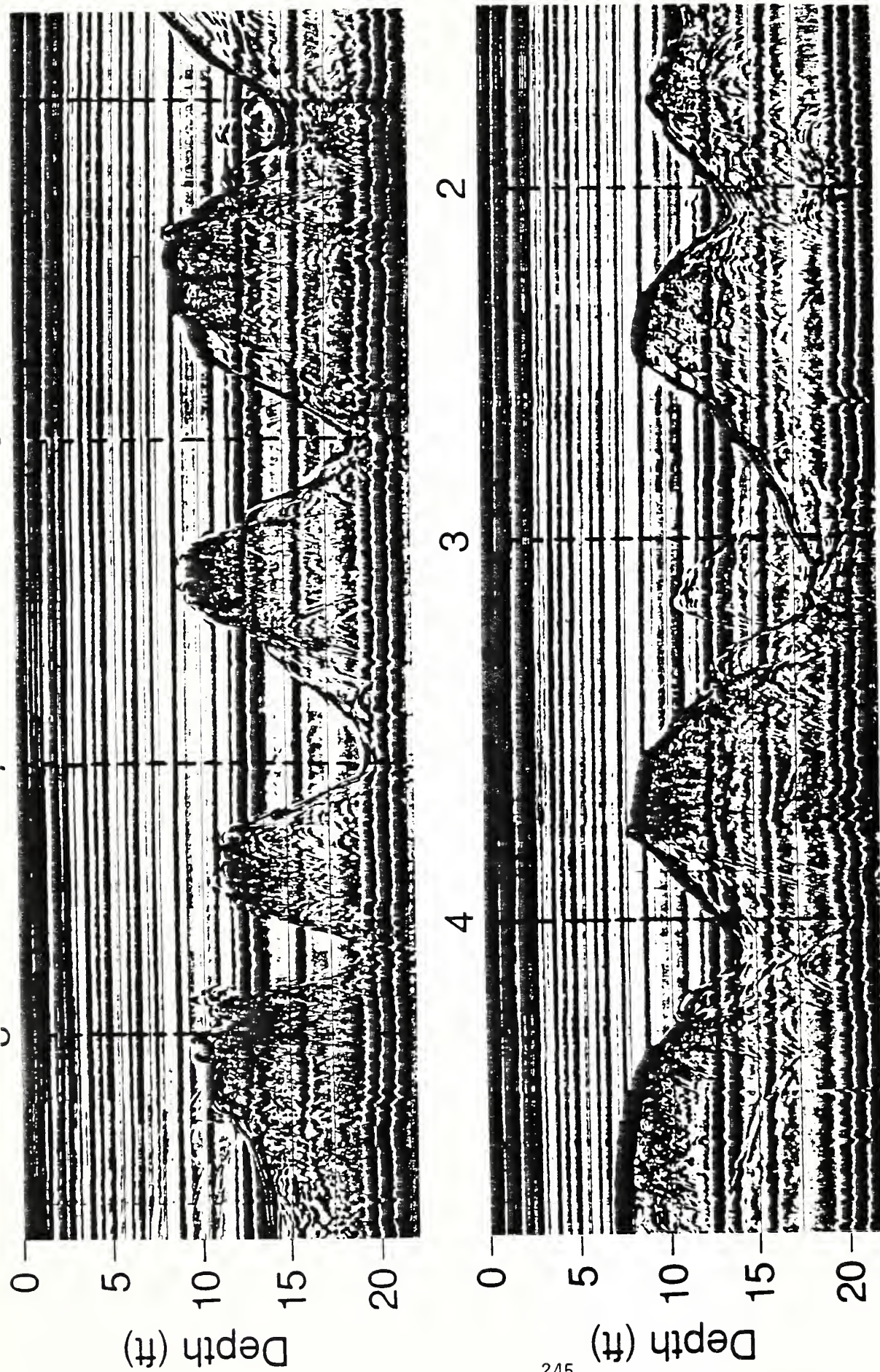


Figure 9. Surface radar profile of scour holes on the upstream side of the Buckley Bridge (Hartford, Conn.). Numbered vertical demarcations indicate the positions of the piers. Note the sharp pulse defining the bottom and the amount of subsurface information.

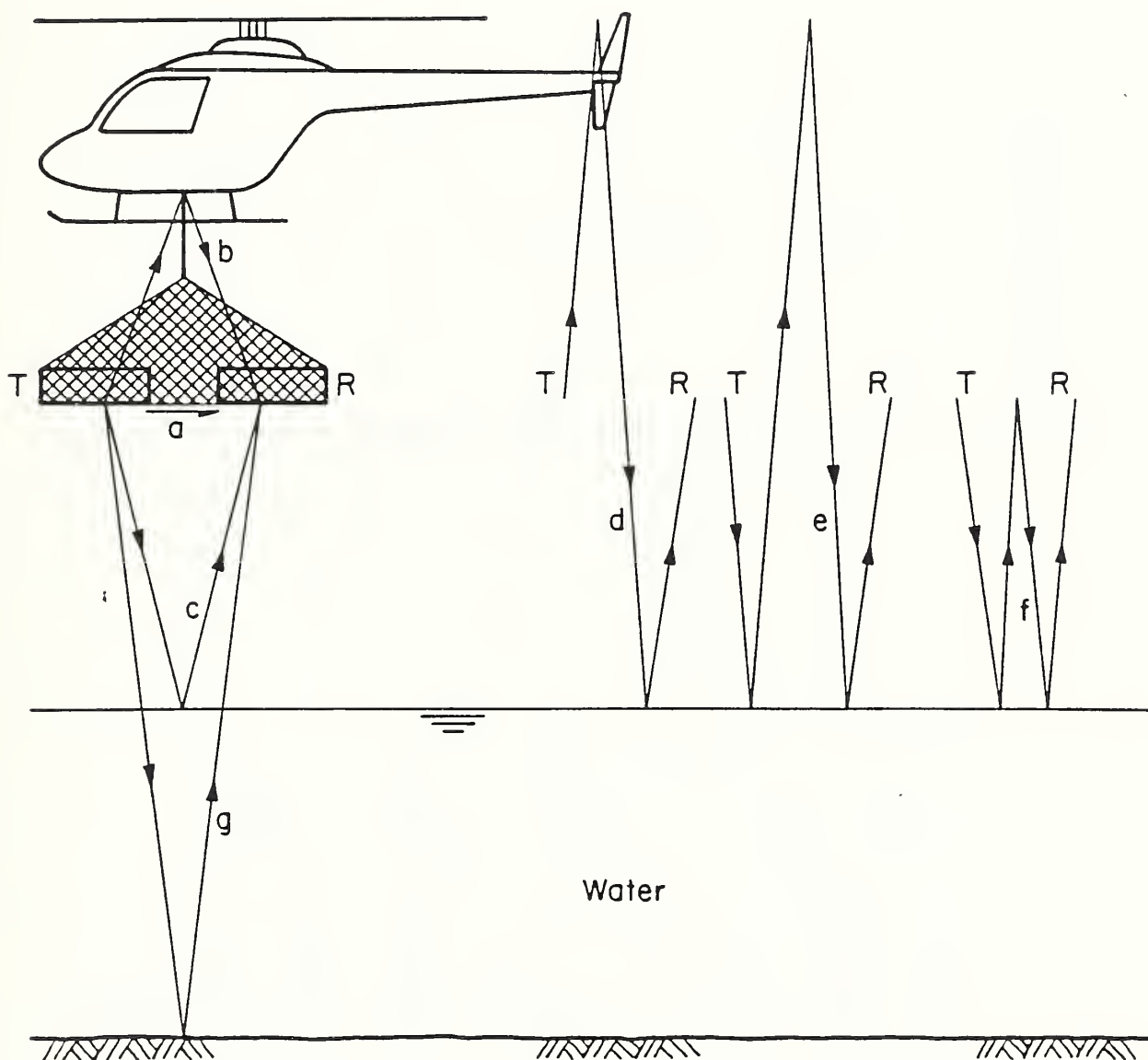


Figure 10. Illustration of the various modes by which clutter can be generated during helicopter surveying

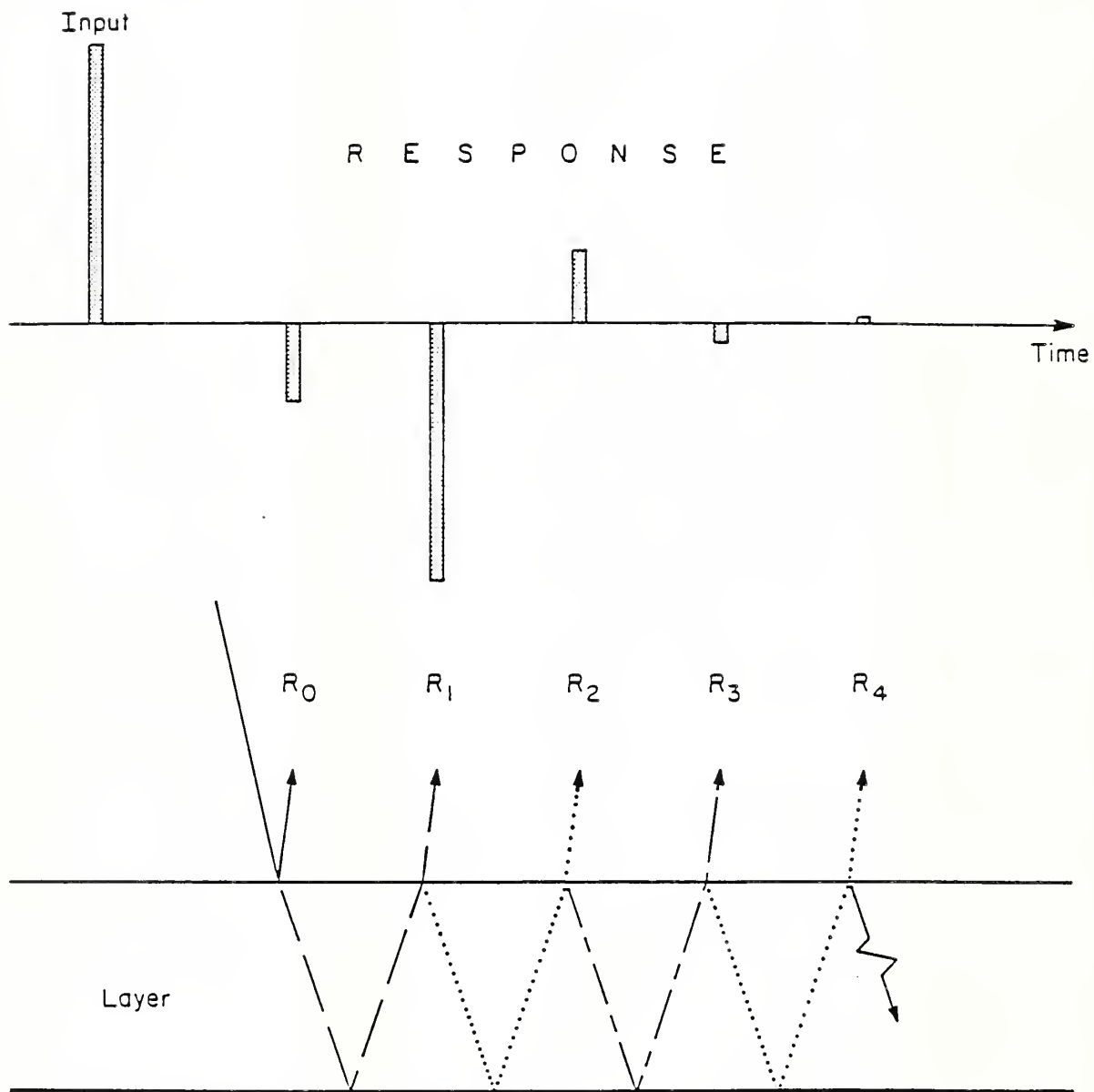


Figure 11. Impulse response by ice layer over perfect reflector.



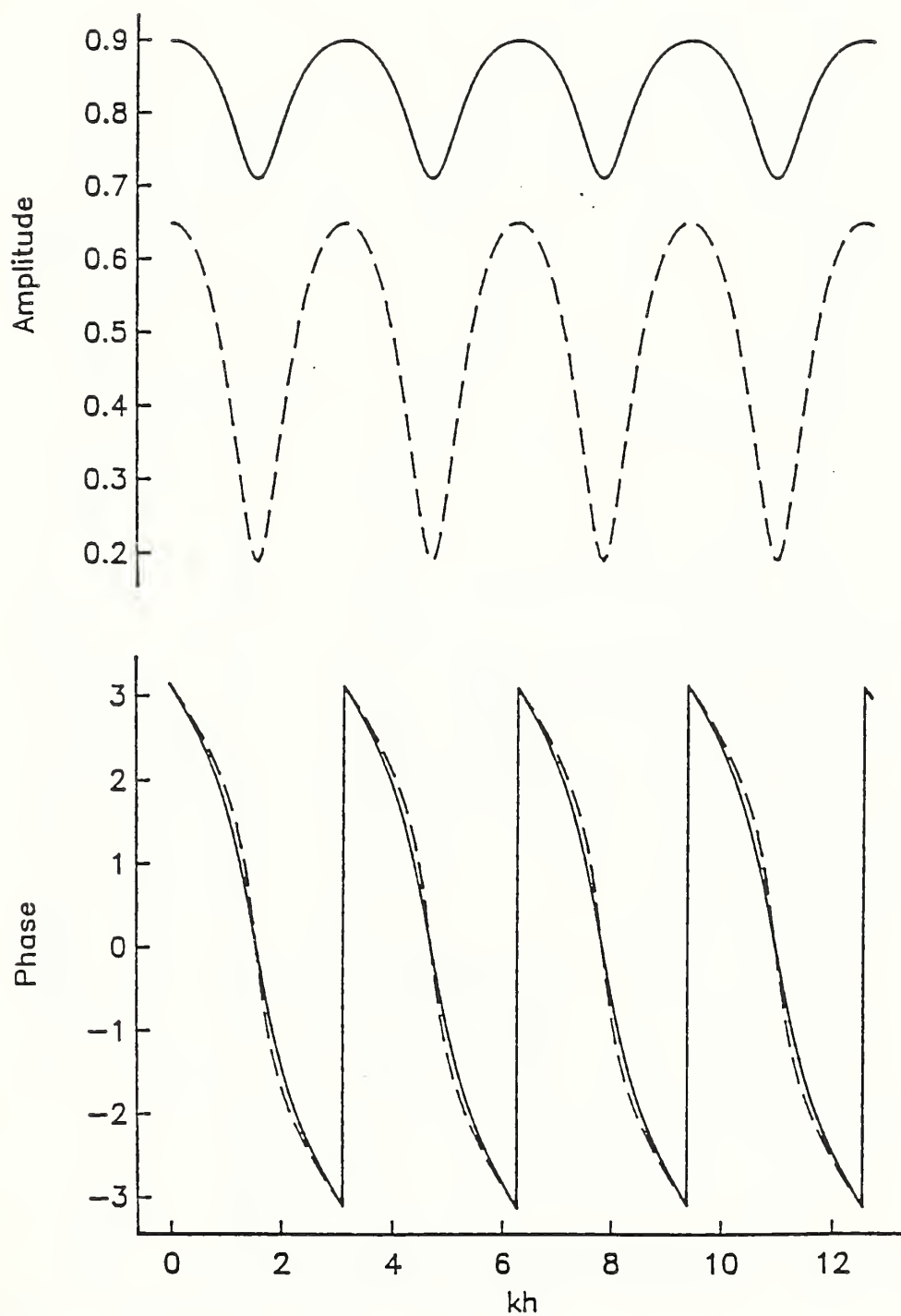


Figure 12. Transfer function for combination of media 2 and 3, as a function of wavenumber times layer thickness.

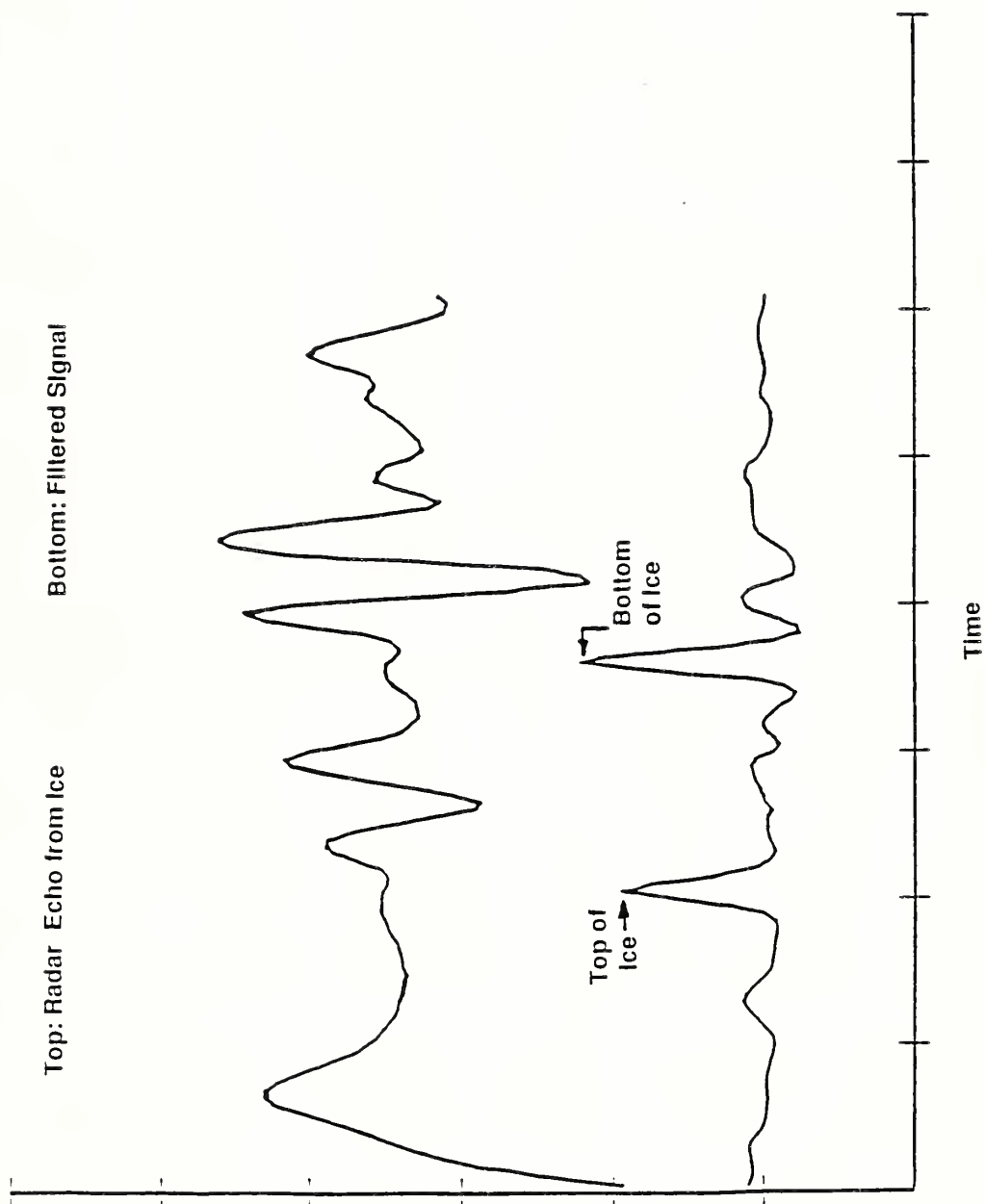


Figure 13. Portion of a record from a field survey using the 3102 antenna and a processed version of the same.

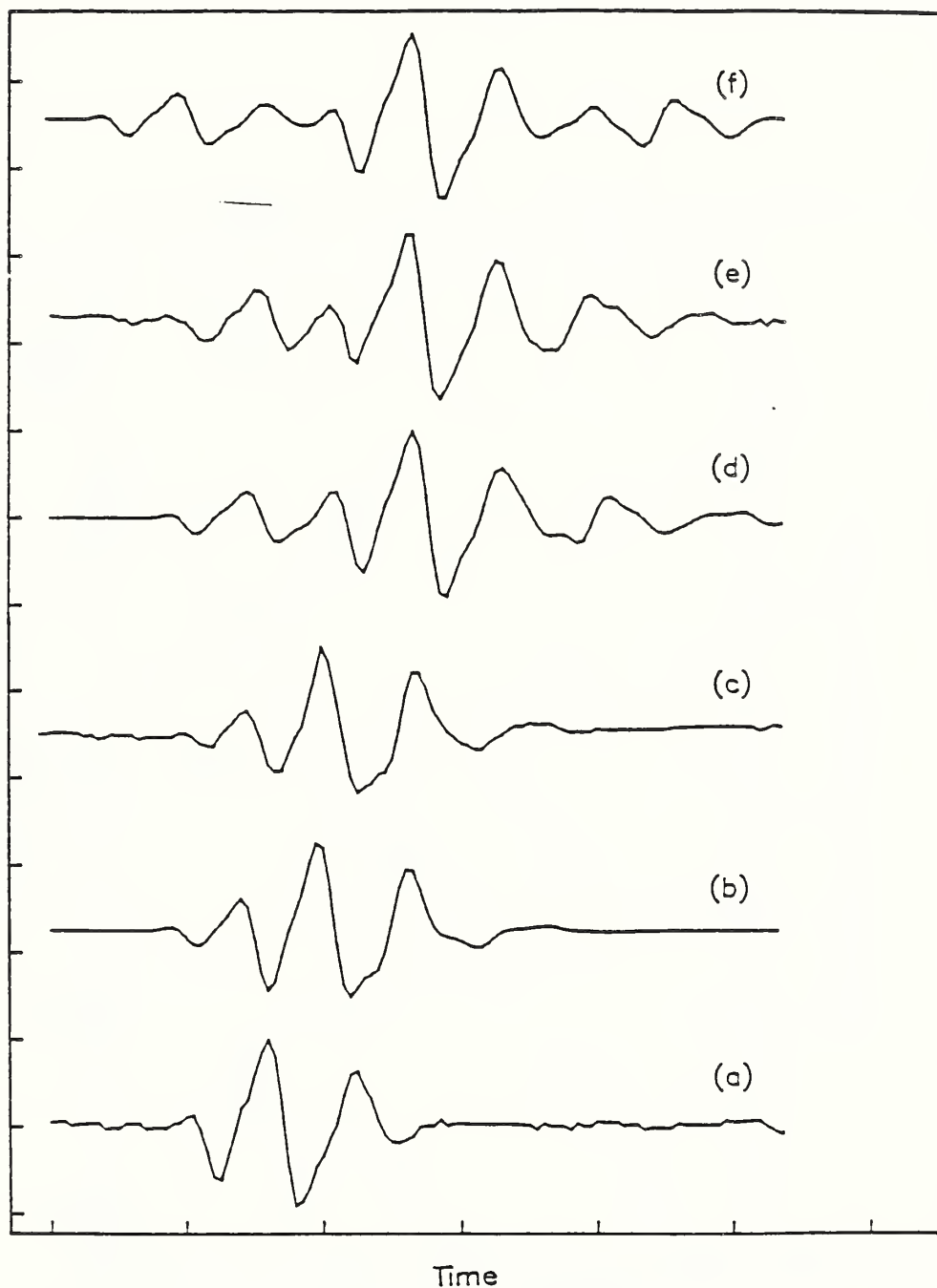


Figure 14. Real and synthetic waveforms for reflections from ice over foil. (a) real echo from bare foil; (b) synthetic echo for 7.0 cm thick ice sheet; (c) real echo from 7.3 cm sheet; (d) synthetic echo for 17.0 cm sheet; (e) real echo from 17.1 cm sheet; (f) synthetic echo for 24 cm sheet.

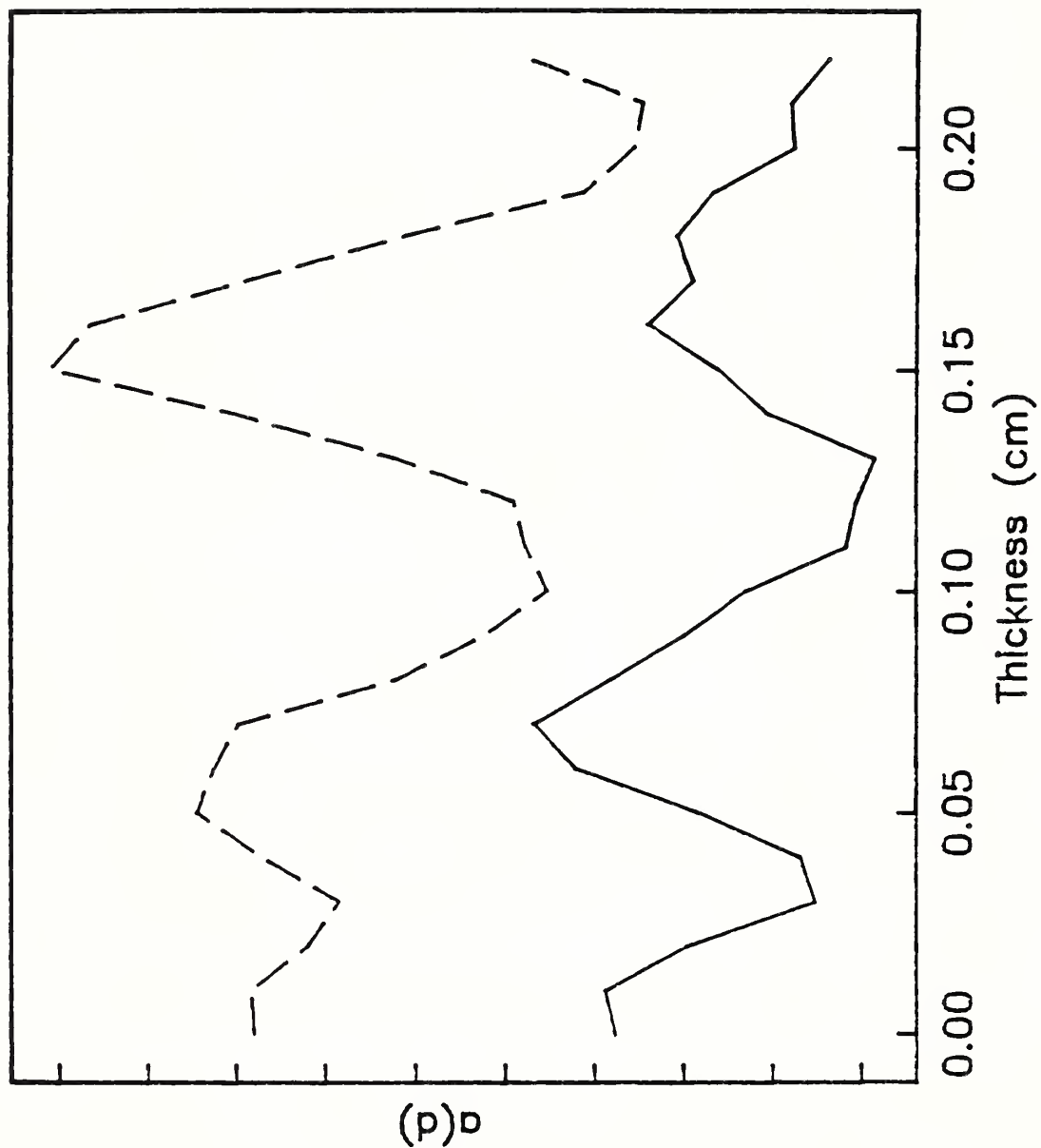


Figure 15. Correlation maxima function  $a(d)$  for 17.1 cm ice sheet (dashed) and for 7.3 cm sheet (solid line).

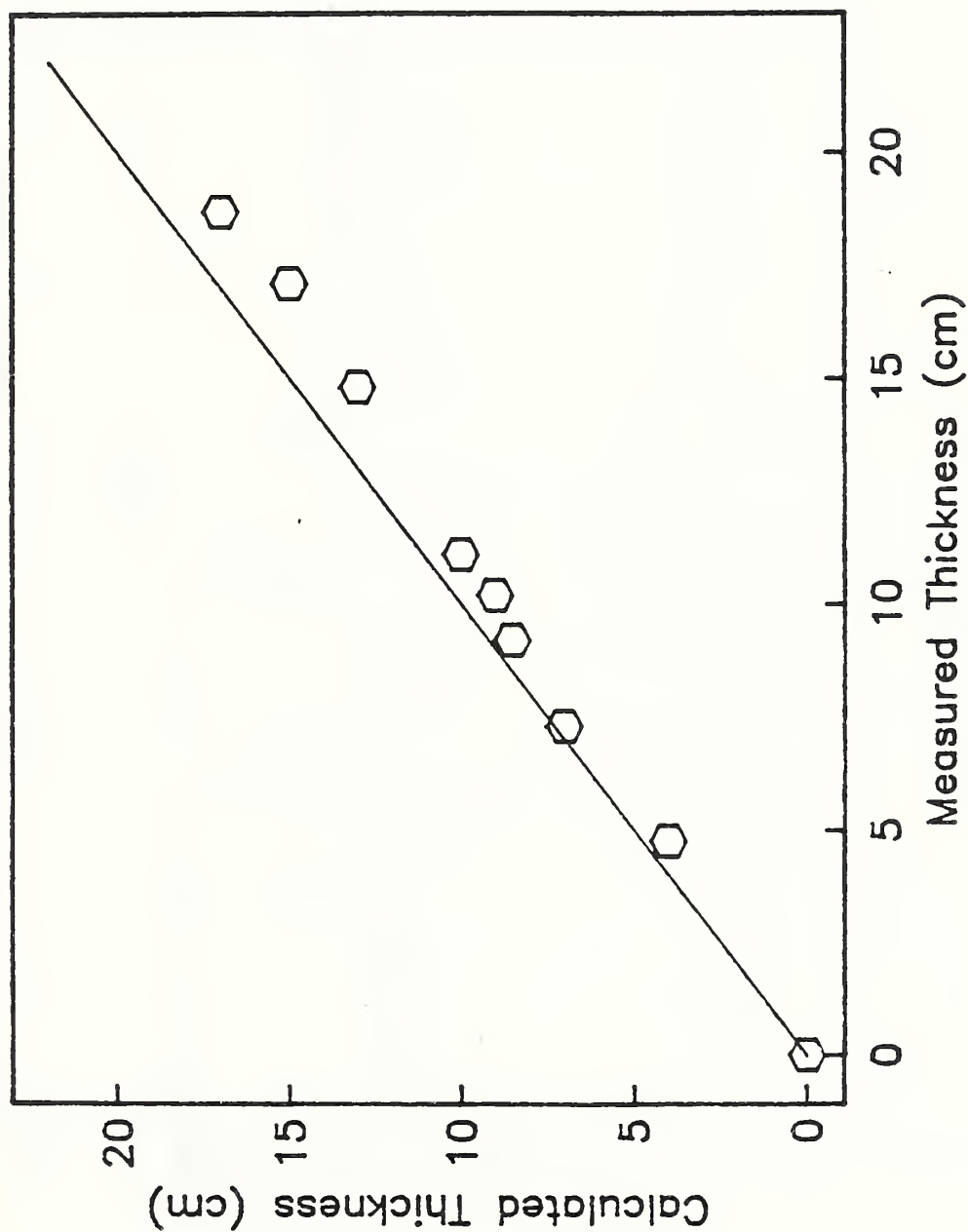


Figure 16. Thin ice sheet thickness as determined from signal processing (peak locations in  $a(d)$  function) versus actual thicknesses of lab ice sheets from which reflections were recorded.



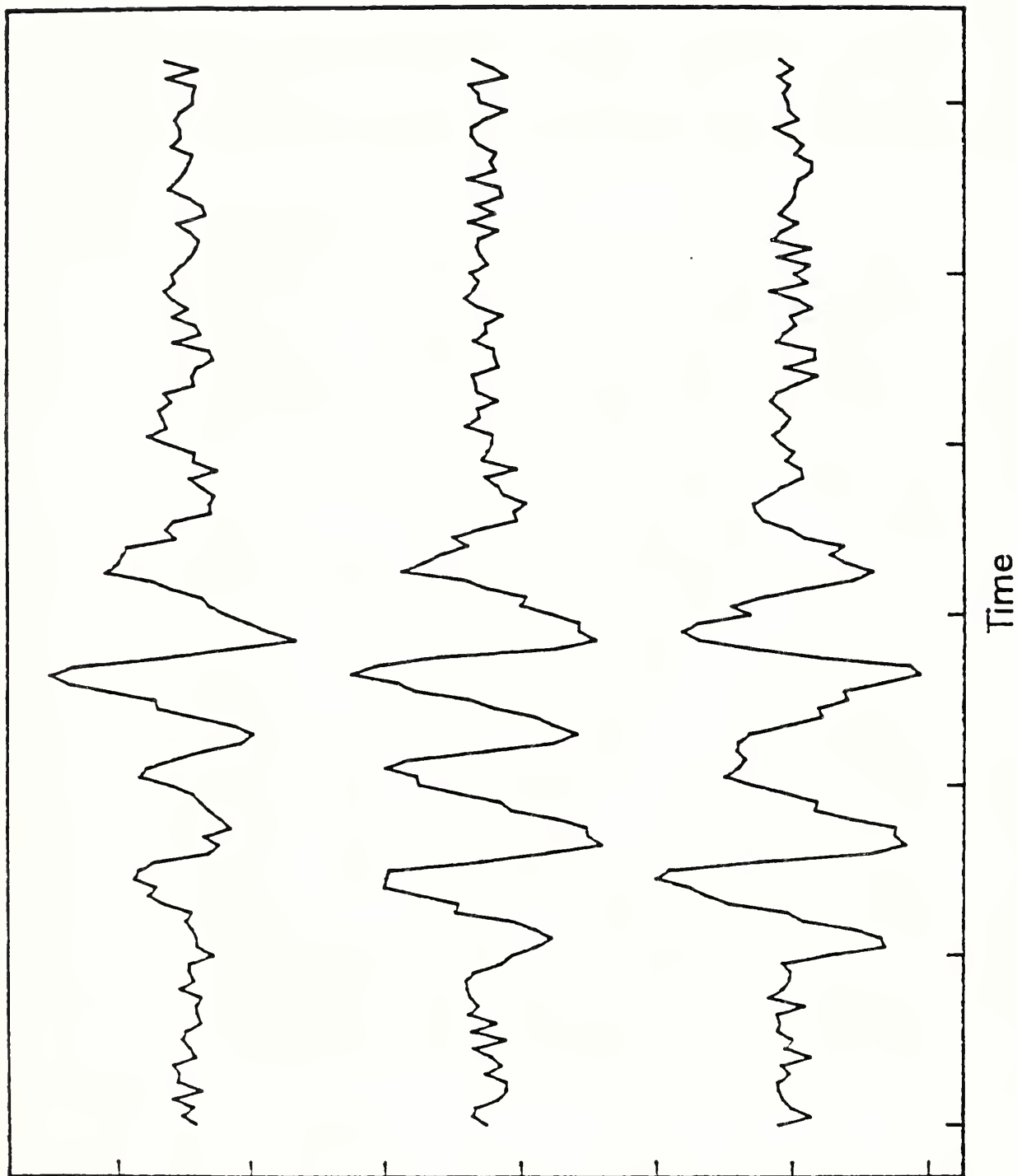


Figure 17. Synthetic echoes with added noise for 17 cm thick ice layer, when  $\epsilon_3 = 1.0$  (bottom),  $\epsilon_3 = 12$  (middle),  $\epsilon_3 = 352$  (top).

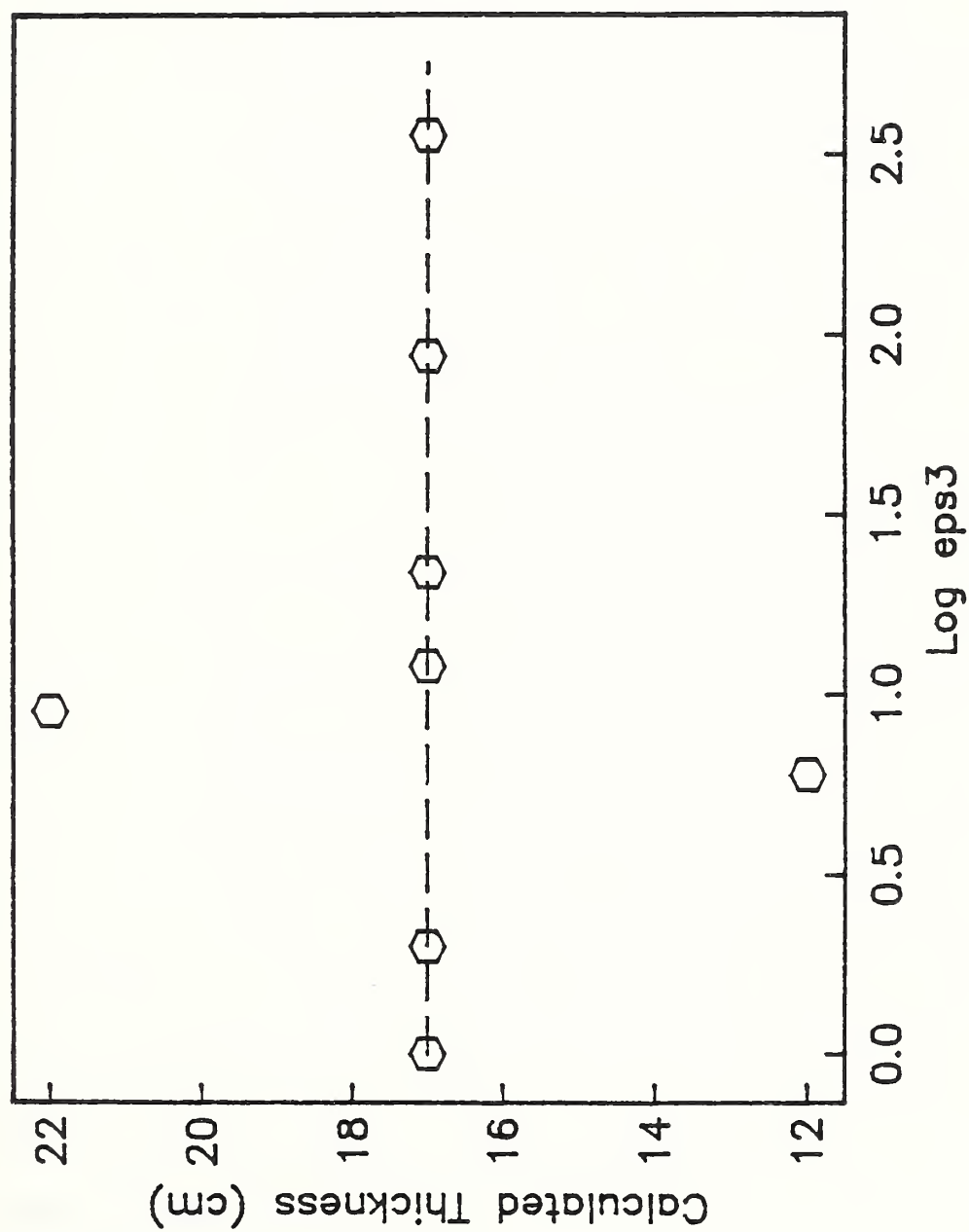


Figure 18. Thickness calculated for various 17 cm layer systems with  $\epsilon_3$  varied. Log 3.2 = 0.5.



## INVESTIGATION OF THE SURFICIAL MATERIALS OF NORTHERN DELAWARE

C.G. Olson and J.A. Doolittle

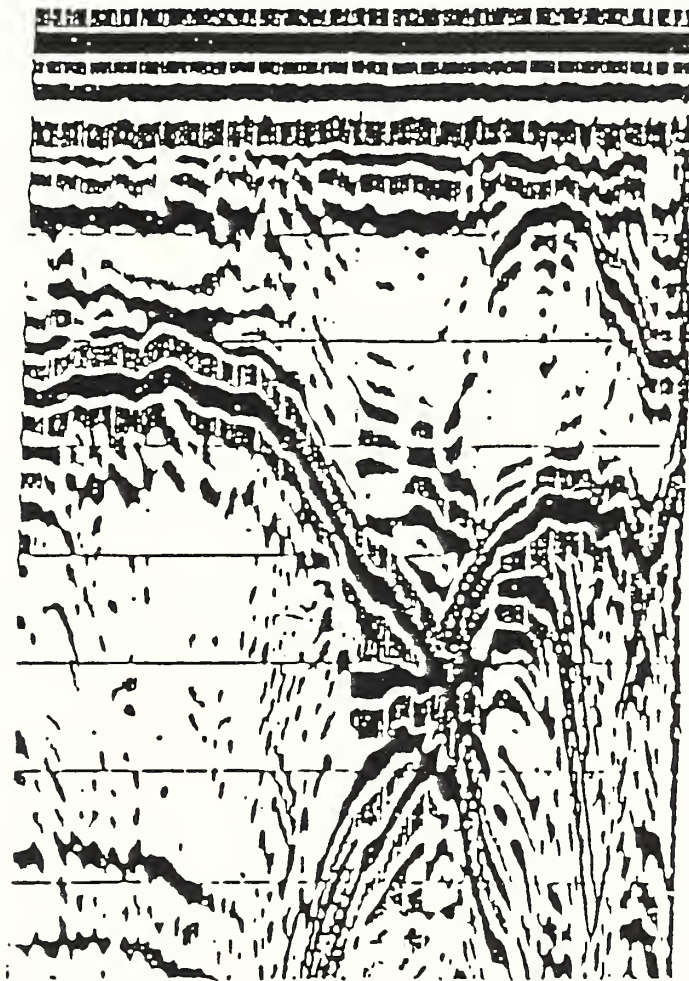
U.S. Geological Survey, Reston, Virginia and Soil Conservation Service,  
Chester, Pennsylvania

The Delmarva Peninsula is a part of the Coastal Plain physiographic province and is underlain by unconsolidated Cretaceous-age and younger sediments that range in thickness from 0 to 2438 m (8000 ft). This sequence is unconformably overlain by a water-table aquifer that is the main source of recharge to the Coastal Plain sediments below. This surficial aquifer is generally less than 60 m (200 ft) thick and consists of a series of loamy sands and feldspathic deposits called the Pensauken Formation. It is overlain by eolian sands and silts. The eolian material characteristically grades downward into the Pensauken Formation but is often abruptly terminated by a gravel line at the contact. To better understand the relationship of the surficial aquifer to infiltration and recharge of the underlying sediments, the distribution and extent of the eolian mantle was investigated. A reconnaissance study using ground-penetrating radar (GPR) was developed to provide a rapid means of mapping the eolian materials. A small watershed in northern Delaware was chosen in which a series of transects were set up perpendicular to major drainageways. Preliminary results indicate that GPR is a reliable tool for distinguishing thick silts from underlying coarser materials particularly where an abrupt boundary is present. A strong contrasting GPR image occurs. Where silts are  $\leq 36$  cm (14 in) thick, the image is not clear and the results become interpretive. The presence of a plow layer from 0-25 cm (10 in) causes additional disturbance in this zone. If there is a transition or gritty layer in which silts are admixed with coarser sands and gravel at the base of the silt mantle, the radar image becomes lighter and less intense.

The signal is quickly attenuated in the sediments of the underlying Pensauken Formation. This attenuation is attributed to the high percentage of muscovite mica present in these materials.



Abstracts for  
Second International Symposium on Geotechnical  
Applications of Ground-penetrating Radar



MARCH 6-10, 1988

Holiday-Inn West Gainesville, Florida



U.S. Department of Agriculture  
Soil Conservation Service  
and  
Institute of Food and Agricultural Sciences  
University of Florida





## Table of Contents

Sunday, March 6

P.M.

Poster Session..... 1

Monday, March 7

A.M.

SESSION I: GEOLOGICAL/HYDROGEOLOGIC  
APPLICATIONS..... 4

P.M.

SESSION II: SOIL INVESTIGATIONS.....13

Tuesday, March 8

A.M

SESSION III: ENVIRONMENTAL DAMAGE ASSESSMENT.....26

P.M.

SESSION IV: NEW TECHNIQUES, APPLICATIONS, AND  
EQUIPMENT.....36



## **POSTER SESSION**





## TITLE SUMMARY

Name James A. Doolittle and Mary E. Collins

Affiliation/Title USDA-SCS and University of Florida

Presentation Title Mapping the Depth to Bedrock with Ground-penetrating Radar

### Summary

In many upland areas, it is exceedingly difficult to examine soil profiles and determine the depth to bedrock. Rock fragments and irregular or weathered bedrock boundaries limit the effectiveness of surface probe techniques. Ground-penetrating radar was used to map the depth to bedrock within two study sites in Maine. Data were used to compare the depth to bedrock collected by GPR and by conventional surface probe methods, to determine the variability of the depth to bedrock within similar delineated areas of a map unit, and to produce computer generated three-dimensional surface net diagrams and two-dimensional contour maps depicting the distribution of soils in the landscape based upon the depth to bedrock.

FOR POSTER PRESENTATION

---

---

Paper available at registration? :

Yes

No

Radar Signatures of Subsurface Features on Karst in West Central Florida. W.E. Puckett, M.E. Collins, and G.W. Schellentrager, Univ of FL. and USDA-SCS.

The ground penetrating-radar (GPR) was used to survey a 4 ha area located on the Chiefland Limestone Plain. The study was conducted to determine the relationships between subsurface stratigraphy and radar images on karst landscapes. The study area was transected on a 10 m interval grid. The GPR images were then grouped into seven major signature categories. The signature categories were established based on depth, thickness, continuity and density of the radar images. Seven soils were sampled within the study area which were representative of the signature categories. The coefficient of determination between field measured depths and estimated depths of radar interfaces was 0.95. Radar signatures were observed for calcitic and phosphatic bedrock, argillic horizons (both with low and high clay percentages), solution pipes and quartz sand. Various combinations of these features made up the seven signature categories observed within the study area. Subsurface-net diagrams were used to study the spatial distributions of the seven signature categories.

**SESSION I**  
**GEOLOGICAL/HYDROGEOLOGIC  
APPLICATIONS**





GROUND-PENETRATING RADAR INVESTIGATIONS OF SURFICIAL  
MATERIALS IN NORTHERN DELAWARE. C. G. Olson and  
J. A. Doolittle, United States Geological Survey and  
Soil Conservation Service, Reston, VA. and Chester, PA.

# TITLE SUMMARY

Name Toshihiko Sakayama, Masaki Osada, <sup>\*</sup>Takashi Kanemori  
Affiliation/Title OYO Corporation, Japan. <sup>\*</sup>OYO Corporation USA  
Presentation Title A Geophysical Experiment to Cross-Adits Rock Investigation :  
Radar Tomography

## Summary

In the civil engineering field, many adits are excavated for investigating rock structures, in the case of construction of dam, nuclear site, etc. Geological features are observed and studied from walls in adit. However, precise studies on rock formation or fault systems are very difficult based only on simple extrapolation of these observed features in each adit. So that, geophysical methods are utilized to investigate detailed rock structures between adits. Electromagnetic wave (radar) tomography technique is one of the most attractive methods, so numerous efforts are paying to study and develop this technique in many countries. We conducted a field experiment on radar tomography by using impulse radar equipment with two antennas, transmitting and receiving antenna, respectively. Test field is located at rhyolite zone in central Japan. In this experiment, we focused our attention on two points, especially. First was the probing distance of EM pulses in high attenuative, low resistivity rock. Another point was the detectability of faults or fracture zone from their reflections. In this paper, we will discuss on these two points based on actual records and analyzed results. We will also mention present state of the art in radar tomography technique to apply rock investigation, in some general.

Paper available at registration? :

Yes

No

NAMES: James S. Mellett\*, Edwin Karp\*, and Robert E. Loeb\*\*

AFFILIATION: \*Department of Biology, New York University,  
New York, NY 10003, \*\* Department of Biology, Penn State  
University, Altoona, PA 16603.

TITLE: A ground-penetrating radar survey of Quaternary  
sediments in and near Washington Square Park, New York, NY.

Geologists attempting to do stratigraphy in urbanized areas lack the fundamental data base of outcrops. But during building construction, excavations expose a variety of horizons. In downtown Manhattan, near Washington Square Park during construction of university buildings, foundation excavations went down about 25 feet (7.7 m) below street level and a stratigraphic section including sands, silts, and clays, some of which bore organic materials, was exposed. The organic material yielded four radiocarbon dates of about 13,000 BP, the first and oldest inland radiocarbon dates from Manhattan Island (AMQUA Abstr., Jun 86:141). Cores and drilling logs from surrounding sites have shown that Manhattan Schist bedrock may lie about 40-75 feet (12.3-23 m) below street level. The local water table lies nearly 20 feet (6.2 m) below the street. To the north in Washington Square Park a former stream channel (Minetta Brook) flowed SW toward the Hudson River, and its original course may have lain about 15 feet (4.6 m) below park level. Extensive filling brought the valley up to its present level of 24-37 feet (7.4-11.4 m) above mean sea level. Over a span of about 200 years, the area served as farmland, became a potter's field in the late 18th century, a military parade ground by 1828, and subsequently a park. Using 300 MHz and 80 MHz antennas, scans will be made in and around the park to locate bedrock, the old stream channel, and the stratigraphic horizons found in the building excavations. Difficulties in obtaining clear radar records in urban locations include extensive cover (asphalt, concrete, and paving stones), road salt contamination below and in the paving material, and extensive background noise from reinforcing bars, as well as the large and abundant buried gas, water, steam, and electric utility lines.

PAPER WILL BE AVAILABLE AT REGISTRATION

## TITLE SUMMARY

Name S.F. Shih, Jim A. Doolittle, Don L. Myhre, and Gregg W. Schellentrager  
Univ. of Fla - Professor - USDA, SCS      Univ. of Fla      USDA, SCS  
Affiliation/Title Soil Scientist - Professor      Soil Scientist  
Presentation Title Ground-Penetrating Radar in Water-Table Investigation

### Summary

The feasibility of using ground-penetrating radar (GPR) to determine the depth of water table was demonstrated in separated studies in Massachusetts and Florida. In Massachusetts, two sites were chosen to demonstrate the application of GPR techniques for water-table depth investigation in a topographically diverse setting. In Florida, a site was selected to demonstrate the accuracy of measurement made from GPR to estimate the depth and the spatial distribution of the water table. An evaluation of results indicated that the GPR proved to be an effective and efficient tool for investigating the depth of water tables. The coefficient of determination ( $r^2$ ) between the well and the radar was 0.90. The radar imagery was used to map the water-table distribution over a study area. Results indicated that about 3 transects are needed to determine the water-table depth at 90% level of statistical accuracy; whereas, about 8 transects are needed at 95% level and two transects at 80% level. A non-linear relationship exists between sample size and statistical accuracy. Areas having more irregular distribution of water-table depth or shallower depth of water table require more sample sizes or vice versa.

Paper available at registration? :

Yes

No

September 10, 1987

Doug Hearn  
Staff Hydrogeologist  
Michael D. Sims & Associates, Inc.  
4780 North Orange Blossom Trail  
Orlando, Florida 32790

Presentation    APPLICATION OF GROUND PENETRATING RADAR IN A  
Title:           KARST TERRAIN - CENTRAL PASCO COUNTY, FLORIDA.

A characteristic set of landforms--sinkholes, deranged drainage, poljes, and uvalas--collectively describe a terrain defined as karst, associated with the occurrence of soluble rock types. Ground penetrating radar can provide information on karst landforms, as they appear to be forming as well as after they have ceased activity. These features are difficult to detect by traditional means if not expressed at the surface. They are of interest to geologists because they may serve as sites of surficial and hydrologic instability. This study investigates these features on a site-specific basis and the ability of GPR to detect them.

A 640 acre site was investigated by traditional methods, (auger borings) and then by GPR. In the study area, a surficial blanket of sand overlies a thin bed of clayey sediments, which in turn overlie a series of limestones - which comprise the upper zone of the Floridan aquifer. The clay unit is areally extensive but has been breached by solution created voids, such as soil pipes, etc.

The GPR profiles were examined with specific interest into the nature of the confining clay bed on-site. Where the clay unit appeared to be breached by solution pipes, or underlain by cavity-like features these features were noted on the graphic profile. Specific sites that were representative of these features were relocated with a second GPR investigation and auger borings made into these anomalies.

Correlation of the boring logs to the GPR data allowed specific interfaces to be traced throughout the site. This correlation also allowed inferences to be made as to the nature of the anomalous features observed on the GPR profiles. The GPR extensively increased the subsurface information available for this site providing a cost-effective means for enhancing the results of a costly drilling programs.



# SYNTHETIC GPR PROFILES GENERATED BY RAY-TRACE ANALYSIS AND APPLICATIONS FOR INTERPRETING KARST FEATURES

by Barry F. Beck and William L. Wilson

Director and Research Assistant in Geology, respectively, Florida Sinkhole  
Research Institute, University of Central Florida, Orlando

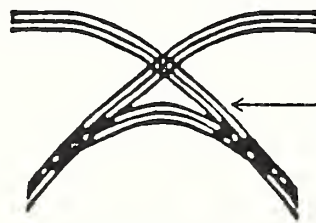
The most commonly used ground penetrating radar (GPR) antennas have an included beam angle of 90 degrees in the direction of travel. Only subsurface features which are perpendicular to some portion of the radiated signal reflect waves back to the antenna. However, the geometry of some curving subsurface interfaces may cause three reflections to be received from different portions of a single interface. Reception of lateral reflections (those that do not originate directly below the antenna) complicates interpretation of the radar profile. As an aid for interpretation, synthetic GPR profiles were generated by ray-trace analysis for hypothetical interfaces representing idealized karst features such as buried paleosinkholes and bedrock pinnacles. Profiles of three features are shown in the accompanying figure. The types of profiles obtained by ray-trace analysis are analogous to those that are widely known from seismic interpretation. A basic understanding of the laterally migrated reflections is crucial for correct interpretation of the steep-sided, compound-curving features detected by radar. Simple bowl-shaped depressions in a subsurface interface yield three reflections, none of which are parallel to the interface. The upper two lateral reflectors cross in the middle forming a signature analogous to the classical "bow tie" seen on seismic records. The lowest lateral reflection forms one sheet of an upward pointing hyperbola. The apex of the hyperbola matches the bottom of the depression. For depressions that are wider than they are deep, the limbs of the hyperbola merge with the descending limbs of the "bow tie". When the depression is deeper than it is wide, then the hyperbola appears below, and separate from, the lower limbs of the "bow tie". Some workers have interpreted such hyperbolas as representing soil cavities beneath sediment-filled paleosinkholes. Such an interpretation may be erroneous and must be confirmed by drilling. Drilling confirmation requires a freefall drop of the drill pipe rather than merely a loss of circulation which is very common in the porous limestone of the Gulf Coastal Plain. Limestone pinnacles have three laterally migrated reflections. The upper reflection is one sheet of an upward pointing hyperbola, the apex of which matches the summit of the pinnacle. The width of the hyperbola exceeds the width of the pinnacle. The two lower lateral reflections begin at the base of the pinnacle, with one reflection on either side, and drop below and away from the pinnacle. Synthetic GPR profiles generated by ray-trace analysis are a form of forward modelling that allow prediction of the signatures on radar profiles from subsurface features. Continued use of synthetic profiles will improve the accuracy of GPR interpretation.

---

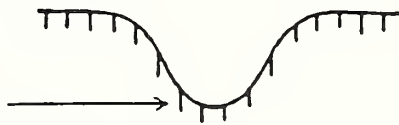
RADAR PROFILE

---

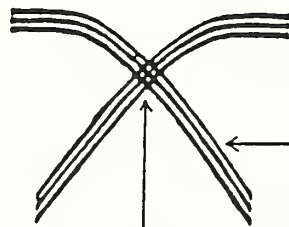
INTERFACE GEOMETRY



Bottom

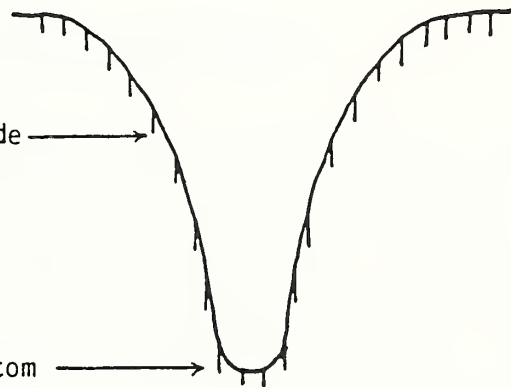


U-shaped depression,  
width greater than depth



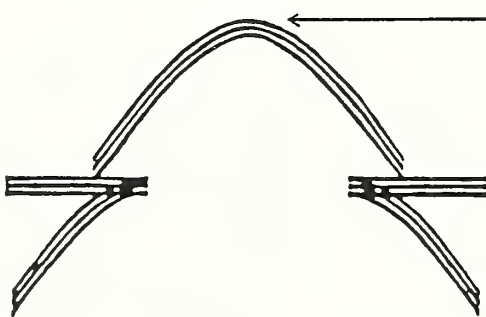
"Bow Tie"

Side

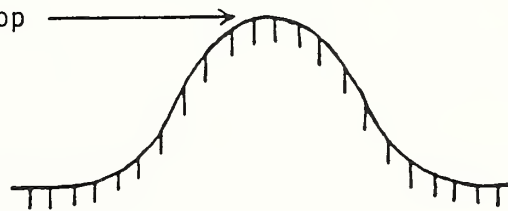


Bottom

Depression, width less than depth



Top



Pinnacle

---

Synthetic radar profiles (left) for idealized subsurface interfaces with compound curves (right). Generated by ray-trace analysis by B.F. Beck, W.L. Wilson and B. Barfus, Florida Sinkhole Research Institute, 1987.

AN ABSTRACT SUBMITTED TO THE SECOND INTERNATIONAL  
SYMPOSIUM ON GEOTECHNICAL APPLICATIONS  
OF GROUND PENETRATION RADAR

TITLE: CAPABILITIES OF GROUND PENETRATING RADAR  
FOR STUDYING SINKHOLE CAVITY IN FLORIDA

BY

S.S. KUO, PH.D., P.E.

Associate Professor of Engineering  
Department of Civil Engineering  
and Environmental Sciences  
University of Central Florida  
Orlando, Florida

ABSTRACT

The Florida peninsula is underlain by limestone undergoing a continuous solution process resulting in subsurface cavity formation. The overburden soil deposits can be washed down into the cavities and cause subsurface and surface subsidence and eventually lead to sinkhole collapse. Sinkhole activity in Florida has become a serious problem in recent years. The recently developed electromagnetic ground penetrating radar (GPR) has demonstrated the capability to provide a rapid, non-destructive method for detecting and profiling the subsurface cavities. To test the ability of GPR the model cavities of varying size, shape, and content were buried above and below the water table at a test site. Strong reflecting signals were received from the roofs of each model.

On field investigation from various locations in Central Florida, the GPR has shown the capability of identifying the subsurface cavities and caves within the limestone. GPR survey conducted at an 11-acre site of housing development in Oak Run, Florida showed the penetration in excess of 70 feet in some areas. Strong hyperbolic reflections were detected indicating the presence of a large cavity. A drilling truck used to identify the cavity lost drilling mud at a depth of 43 feet, while eleven cubic yards of concrete mix were grouted into the void. A radar survey over a 200-acre pasture in Apopka Blue Sink, Florida showed that some areas exhibit a definite subsiding which indicates a vavelling of overburden soils into subsurface voids. Several large cavities were detected in this site. A distinct large cavity at depth of 40 feet with sharply depressed subsurface collapsed about six months after the survey, verifying the prediction of collapsing cavity.

**SESSION II**  
**SOIL INVESTIGATIONS**





# TITLE SUMMARY

Name Toshihiko Sakayama, Masaki Osada, \*Takashi Kanamori, \*Satoru Ohya  
Affiliation/Title OYO Corporation, Japan. \*OYO Corporation USA  
Presentation Title Electromagnetic Wave Velocity and its Application to  
Civil Engineering Investigation of Soil Layer

## Summary

The soil with high water content ratio is inappropriate for the material of earth works, such as embankment. If wet soil is embedded and layered, embankment will be more instable. Wetter soil is, electromagnetic wave velocity in soil is considerably lower. So that, if we will be able to observe the velocity structure precisely, we will obtain valuable information to investigate the stability of embankment. From the point of view cited above, we took place a field experiment for in-situ EM velocity estimation by using ground probing radar. Equipment used is impulse radar system with center frequency about 100MHz, with two antennas, transmitting and receiving antenna, respectively. Wide angle reflection and refraction (WARR) measurements were carried out along the observation line at every 1 m. Observed data were A/D converted, and processed. After undergoing digital signal processing such as bandpass filtering and deconvolution, velocities were analyzed by constant velocity scan method, or velocity spectra method, including the dip correction. Velocities and stacked profile section show up fine velocity structure in embankment. Especially, a thin layer with very low velocity is found markedly at the depth of 2.5~3.0m beneath. Observations at cutting show that wet and loose loam layer correspond to this low velocity zone.

Paper available at registration? :

☒ Yes

☐ No

PROPAGATION OF GROUND PENETRATING RADAR SIGNALS IN SOILS

BY

DAVID V. SMITH\*

Submitted For Presentation  
At

Second International Symposium On  
Geotechnical Applications Of  
Ground Penetrating Radar

March 6-10, 1988

(a paper will be available at the Symposium)

\* Group Supervisor, GEO-CENTERS, INC., Newton Centre, MA 02159



*GEO-CENTERS, INC.*

## PROPAGATION OF GROUND PENETRATING RADAR SIGNALS IN SOILS

The interpretation of ground penetrating radar (GPR) data and the development of automated data processing methods require an understanding of electromagnetic propagation through the earth. Accurate depths to subsurface reflectors can be deduced from the standard two-way travel-time output plots once the velocity of radar pulse propagation in the subsurface is determined. Easily measured soil properties provide velocity estimates and information on the maximum attainable probing depth for available antenna frequencies.

A theoretical background describing electromagnetic properties of soils and rocks is presented. Following a brief discussion of these properties on GPR pulse propagation in the earth, different soil models are examined and related to GPR data.



*GEO-CENTERS, INC.*

## TITLE SUMMARY

Name R. K. Hubbard, L. E. Asmussen, H. F. Perkins and H. L. Allison

Affiliation/Title USDA, ARS, Southeast Watershed Research Laboratory, Tifton, GA 31793

Presentation Title "Application of Ground-Penetrating Radar to Coastal Plain Soils  
with Variable Texture and Clay Mineralogy"

### Summary

A study was conducted to determine the applicability and effectiveness of Ground-Penetrating Radar (GPR) on Coastal Plain soils. Soil series were selected encompassing a range of surface textures from loamy sand to sandy clay loam, and subsoil clay mineralogies from kaolinite to montmorillonite. Soils series selected included Greenville, Red Bay, Americus, Susquehanna, Gritney, Megget, and Faceville. Where possible, three sites were selected for each soil series, and GPR transects of 50 ft were made using the 120 and 500 MHZ antennas at different power settings. Clay mineralogy, particle size distribution, saturated hydraulic conductivity, and soil moisture retention were determined on surface and subsoil samples from each site. The study showed the effectiveness of GPR as a geotechnical tool for Coastal Plain soils relative to soil texture and clay mineralogy.

Paper available at registration? :

<u>          </u>	<u>          </u>
Yes	No

## TITLE SUMMARY

Name S. F. Shih, J.A. Doolittle, & G.W. Schellentrager

Affiliation/Title Univ. of Fla./Professor, USDA, SCS/Soil Scientists,  
USDA, SCS/Soil Scientist

Presentation Title Sampling Design for Ground-Penetrating Radar Application

### Summary

The feasibility of using the ground-penetrating radar (GPR) to study the thickness of organic soils in the Everglades Agricultural Area (EAA) has been established. Several questions pertaining to sampling design remain from earlier studies, in particular, the number and length of GPR transects required to determine the average thickness of organic soil within a management unit, and the number of ground-truth observations required to scale the radar imagery. A 16-ha vegetable field was intensively studied with the GPR to gain insight into the optimal sampling required to define the average thickness of organic soils. Soil depths were normally distributed within the management unit (i.e., 16-ha field). Results indicate that, at 90% level of confidence, about 3 calibration sites are required to scale the radar imagery, and about 3 transects are needed to determine the thickness of the organic soil. There exists a nonlinear relationship between the increase of sample size and the improvement of statistical accuracy. Areas having more irregular bedrock surfaces or shallower layers of organic soil require a larger sample size. Consequently, as the subsidence continues in the EAA, a corresponding increase in the sample size will be needed.

Paper available at registration? :

Yes

No



## TITLE SUMMARY

Name Dr. Carolyn G. Olson

Affiliation/Title Research Geologist - U.S. Geological Survey

Presentation Title A Comparison of Two Geophysical Techniques for Soils Investigations in Steep Terrain

### Summary

Two geophysical techniques, ground-penetrating radar (GPR) and seismic refraction, were compared to evaluate their reliability for reconnaissance determinations of soil thickness and depth to bedrock in steep, forested terrain of western Virginia. Each technique has advantages. GPR is a continuous-profiling technique with good depth penetration in nonclayey materials. Irregularities in water table and bedrock surfaces as well as the presence of fractures, lenses of differing material, rock fragments and the thickness of weathered material above bedrock, are visible on GPR profiles. In some cases, soil horizons may be observed. Seismic refraction, a discontinuous recording method requiring multiple, overlapping field lines, produces an overall record of thickness of surficial material and depth to bedrock. Results obtained from seismic refraction are expressed in velocities rather than in electromagnetic pulse frequencies as obtained from GPR. Because the seismic velocities of most materials are known, seismic refraction provides information on the general composition of the material as well as its location in the stratigraphic section. This technique has lesser attenuation in clayey materials than does GPR and will generally penetrate to bedrock. In the study area, GPR had the best near-surface resolution in the upper 2m of the profile. Rock fragments and argillic horizons could be determined. Where thick clayey or shaley colluvium blankets side slopes, the GPR could not consistently define the bedrock interfaces. The seismic-refraction technique provided water-table information and depth to bedrock regardless of the thickness of overlying materials but could not distinguish soil-profile characteristics. GPR is the preferred method for differentiation of soil horizons and near-surface discontinuities in this study. Although both methods can provide adequate information for reconnaissance purposes, these techniques have a greater probability of success in areas where some prior subsurface information is known.

Paper available at registration? :

X  
Yes

        
No

AN ABSTRACT SUBMITTED TO  
THE SECOND INTERNATIONAL SYMPOSIUM ON  
GEOTECHNICAL APPLICATIONS OF GROUND PENETRATING RADAR

TITLE: COMPARISON OF SUBSURFACE CAVITY INVESTIGATIONS USING  
GROUND PENETRATING RADAR, ELECTRICAL RESISTIVITY, AND  
SEISMOGRAPH

By

Dennis Filler Graduate Assistant  
S.S. Kuo, Ph.D., P.E. Associate Professor  
Department of Civil Engineering & Environmental Sciences  
University of Central Florida

This research study compares the effectiveness of ground penetrating radar (GPR), electrical resistivity, and seismograph in detecting subsurface cavities. Tests were conducted at two sites: the test site at the University of Central Florida, Orlando, and a natural site near Apopka, Florida.

At the test site, a 300MHZ antenna successfully located all the buried model cavities, clearly delineating the air-filled cavities. A DC resistivity instrument also located all the shallow cavities, distinguishing air-filled from water-filled and yielding approximate dimensions. A multi-channel seismograph detected only the two largest cavities but was not able to determine their size.

An 80MHZ radar antenna initially located five cavities from a subsurface investigation at the Apopka site. GPR clearly displayed the hyperbolic signature analogous to cavities, defining depth to and lateral dimensions of cavity upper portions. Low resistivity values defined all of the limestone cavities to be water-filled. Cavity delineation was possible but to a lesser extent than GPR. Seismic surveys clearly detected limestone pinnacles often masking the presence of underlying cavities. Only seismic data produced details of the detected cavities lower portions.

It is concluded that both GPR and resistivity methods exhibit excellent capabilities in the detection of cavities in sandy soils and underlying limestones. GPR can quickly and clearly detect cavities to 100 feet deep. Resistivity can penetrate deeper, yet surveys are time consuming. Preliminary interpretations of field data can be made during GPR and resistivity surveys. Seismic surveys failed to detect smaller cavities but can provide more information regarding subsurface stratification.

Ground-Penetrating Radar Applications in Northeastern  
Palm Beach County, Florida

By Gary M Russell, Wesley L. Miller and Cathleen J. Peterson 1

ABSTRACT

Ground-penetrating radar was used by the U.S. Geological Survey to determine the continuity and depth below land surface of near-surface marl units in northeastern Palm Beach County. Ground-penetrating radar was used because marl units are known to attenuate the radar signals. An 80-megahertz center-frequency antenna, equipped with wheels was towed at 5 to 15 miles per hour 30-meters behind a 4-wheel drive vehicle. Record of signal return was obtained on graphic strip charts and magnetic tape. Continuous ground-penetrating radar profiles for about 35 miles were obtained within the 323-square-mile study area.

The study area is generally flat, containing extensive unpaved dirt roads with minimal traffic and utilities. The area is frequently inundated due to poor surface drainage and to marl units, which retard rainfall infiltration. Scarcely populated at present, increasing developmental pressures indicate 15,000 to 20,000 homes served by private wells and septic tanks will be in existence by the year 2000. It is believed that percolation of septic tank drainfields would be adversely affected by the marl units.

Results from the radar profiles indicate that from 0 to 15 feet below land surface a continuous marl unit exist throughout the study area. Marl units occur at increasing depths and smaller vertical extent toward the east. The eight radar profiles through the study area proved to be an excellent method to substantiate and extend knowledge gained through direct-current resistivity soundings and well logs.

1) Respectively, Hydrologist, U.S. Geological Survey, Stuart and Miami FL; and Hydrologic Technician, U. S. Geological Survey, Stuart, FL.

## TITLE SUMMARY

Name D.L. Myhre, S.F. Shih, and S. Ploetz

Affiliation/Title Univ. of Fla., Professors; USDA-SCS Soil Scientist

Presentation Title Application of Ground-Penetrating Radar to Soil  
~~Variability Investigations in Citrus Grove~~

### Summary

Ten soil orders and over 400 soil series are present in Florida. Citrus is grown on many of these inherently diverse soils. Also, soil compaction occurs as a result of bed formation, hedging, harvesting, and other cultural operations. The main objective of this study was to use a ground-penetrating radar (GPR) system as a reconnaissance tool to provide characterization information at lower soil depths. This study was conducted in the Coca Cola (Cloud) grove near Ft. Pierce, FL because of its apparent soil variability and non-random distribution of trees with citrus blight. Two GPR transects, each 400 m, between the two middle rows of a 4-row bed were conducted using either a 300 or 120 MHz antenna. Borings at 11 sampling points were made to establish ground truth for characteristic target signatures from certain horizons. Soils were described to a depth of 200 cm and soil penetrometer resistance (SPR) was measured continuously in the top 90 cm. Four soil orders (Alfisols, Entisols, Histosols, and Millisols) and six soil series (Boca, Chobee, Hallandale, Kaliga, Nittaw, and Winder) were identified in the 400-m transect. The SPR mean values in the top 55 cm were  $< 0.5$  MPa for Nittaw and Chobee and  $> 2.5$  MPa for Hallandale and Winder series. The GPR images provided a graphical "picture" of the land forms which are useful in showing the existence, depth, transition, and lateral extent of many soil horizons. The subsurface features were poorly delineated with the 300 MHz antenna. Resolution was improved using the 120 MHz antenna. Much work remains to be done to improve interpretation of GPR images for correlative purposes with soil properties.

Paper available at registration? :

Yes

No

## TITLE SUMMARY

Name James A. Doolittle

Affiliation/Title Soil Specialist USDA-SCS

Presentation Title Application of Ground-penetrating Radar to Archaeological Studies

### Summary

Ground-penetrating radar (GPR) provides a rapid, cost effective, and nondestructive method for detecting the presence and pinpointing the location of buried artifacts. The GPR is being increasingly used for routine reconnaissance and pre-excavation surveys of archaeological sites. Procedures for conducting radar surveys of archaeological sites are similar to those used in other investigations. Search strategies represent compromises between available resources and the desired level or probability of detection.

Paper available at registration? :

Yes

No



TITLE SUMMARY

Name Toshihiko Sakayama, Masaki Osada, Kouichi Tamura  
Affiliation/Title Geotechnical Institute, OYO Corporation, Japan  
Presentation Title Some Examples of Archaeological Investigations  
Using Ground-Probing Radar

Summary

Recently, there have been many attempts to apply ground-probing radar surveys to archaeological investigations. We also have used ground-probing radar in archaeological investigations.

The depth at archaeological sites in Japan where cultural treasures are buried has been shallow in such range of 1 to 2 meters, which has been offering the favorite condition for ground-probing radar surveys. The relics that ground-probing radar can capture are those of relatively large scale such as the remains of ancient dwellings, ancient moat, ancient water course etc. Kitchen middens and burial mounds also make the objects of exploration.

This paper refers to the examples proving the effective utilization of archaeological investigations by means of ground-probing radar and tries to compare those examples with the results from the actual excavations.

Paper available at registration? :

Yes

No

APPLICATION OF GPR AT THE SOLAR BOAT CHAMBER, PYRAMID OF CHEOPS, GIZA, EGYPT

T. Fenner, GSSI, Hudson New Hampshire

M. Blackey, Weston Geophysical Corporation, Westboro, Massachusetts

V. J. Murphy, Weston Geophysical Corporation, Westboro, Massachusetts

In order to assess the possibility/probability of the existence of a 2nd Solar Boat at the Great Pyramid of Cheops in Giza, Egypt, ground penetrating radar (GPR) profiles were operated and augmented with resistivity measurements, and sonic/seismic velocity profiling.

The existence of a 2nd Solar Boat is postulated following excavation of an area southerly of the Great Pyramid which disclosed the 1st Solar Boat. This world treasure was subsequently exhumed, reassembled, and placed in a museum type building adjacent to the pyramid structure.

These suites of geophysical data were also used for planning of drill hole/video inspection and photography of the internal section of this large chamber which extends for 33 meters in length and is about 2.5 meters wide.

As an essential part of our program, containment blocks from the 1st Solar Boat chamber were used as an outdoor laboratory/calibration site by performing the various geophysical measurements on individual blocks of different sizes. These data were then used to establish the plan and conduct profiling of the buried 2nd Boat chamber.

## **SESSION III**

# **ENVIRONMENTAL DAMAGE ASSESSMENT**



# Use of ground penetrating radar techniques to aid in site selection for land application sites

HERBERT G. STANGI AND P. L. Adamson & Associates, Inc., Orlando, Fla., USA  
SHOU SAN KHO P. L., College of Engineering, University of Central Florida, Orlando, USA

## ABSTRACT

Ground Penetrating Radar (GPR) has been used as an effective hydrogeologic tool in the selection of cost-effective site(s) for land application systems in karst areas in Central Florida. Favorable land application sites in Central Florida typically have a thick permeable sand aquifer with a deep existing water table and good recharge rates to the artesian aquifer such as the Floridan aquifer. This type of land is ideal for development and is costly when it is near urban areas. Consequently, the smallest parcel required is most cost-effective. Furthermore, the land application systems should not be located over paleosinks or where there could be a short circuit of treated wastewater to the Floridan aquifer, according to the rules and regulations of the Florida Department of Environmental Regulation.

GPR surveys were conducted on approximately 70.8 hectares in Central Florida. A 15- to 30.5-meter grid spacing was used for the survey. The grid spacing depends upon the sinkhole characteristics in the area and the physical dimensions of the area.

The radar profile identified areas where thin sand layers overlie relatively impermeable clayey soils and potentially active sinkhole areas. The remaining areas were considered suitable for further study in selecting cost-effective land application areas. These latter areas would provide relatively good hydraulic capacity with low potential for direct connection to the artesian aquifer. A boring program was performed to calibrate the radar information.

## Introduction

This paper emphasizes the results of a Seminole County survey where ground penetrating radar (GPR) was used in evaluating sites as potential rapid rate Land Application System (LAS) sites. Hydrogeologically, these sites have a thick permeable sand aquifer with a deep existing water table and good recharge rates to the artesian aquifer, the Floridan Aquifer. These LAS sites typically are also ideal for land development when they are near urban areas. Consequently, the land is costly for purchase as a land application site and, therefore, the smallest possible parcel is typically considered. A rapid rate LAS site utilizes the highest application rates possible and the smallest land area. A rapid rate system has an application rate on the order of several centimeters per day while a slow rate system has an application rate of about 1.3 to 1.5 centimeters per week.

The Florida Department of Environmental Regulation (FDER) does not favorably consider rapid rate land application systems located over paleosinks or where there could be a short circuit of treated wastewater effluent to the Floridan aquifer.

Figure 1 shows the potential for sinkhole development in Florida. The collapse, solution and erosion sinks are three distinct types of sinkholes in these sinkhole prone areas. The GPR is generally most useful for detecting an erosion type sink in the following geologic and groundwater setting:

- Limestones overlain by relatively pervious unconsolidated sediment
- Cavity systems in the limestone
- A water table higher than the potentiometric surface in the underlying limestone.
- A breach of the limestone into the cavernous zone creating a point of high recharge to the lower aquifer.

GPR was used in this survey and in other surveys in Central Florida as an effective hydrogeological tool in the selection of cost-effective LAS sites.



SUBSURFACE CHARACTERIZATION OF HAZARDOUS WASTE  
SITES USING GROUND PENETRATING RADAR

BY

GEORGE MARKT\*

Submitted For Presentation  
At

Second International Symposium On  
Geotechnical Applications Of  
Ground Penetrating Radar

March 6-10, 1988

(a paper will be available at the Symposium)

\* Scientist, GEO-CENTERS, INC., Newton Centre, MA 02159



*GEO-CENTERS, INC.*

## SUMMARY

### SUBSURFACE CHARACTERIZATION OF HAZARDOUS WASTE SITES USING GROUND PENETRATING RADAR

Ground penetrating radar (GPR) has been successfully applied to the subsurface characterization of hazardous waste sites (HWS). The technique provides a quick, cost effective means of HWS hydrogeologic site assessment. This paper summarizes GPR field investigations conducted by GEO-CENTERS, INC. at three separate and geologically distinct HWS: a search of a 50 acre lake for metal drums believed to have been disposed of in the lake; an investigation to detect areas of possible buried coal tars near a former coal gasification plant, and a survey to detect underground fiberglass gasoline storage tanks and associated piping at the site of a former gasoline station. Examples of field data are presented along with interpretive maps detailing the successful results of each investigation.



*GEO-CENTERS, INC.*

# TITLE SUMMARY

Name Akio Tanaka, Kouichi Tamura, Tetsuma Toshioka, <sup>\*</sup>Satoru Ohya  
Affiliation/Title OYO Corporation, Japan. \*OYO Corporation USA  
Presentation Title Surveys of Cavity and Burried Object by  
Ground-Probing Radar

## Summary

The maximum probing depth of ground-probing radar is about 3 to 5m in usual soil ground in Japan. Accordingly, in many cases, ground-probing radar has been used for high resolution survey of underground shallow range.

The survey for the maintenance of structures, detecting cavities under pavements, old burried pipes and cavities adjacent to the lining of tunnel, is one of effective surveys for ground-probing radar.

Especially, large cavities often occur and underlie the pavement along shoreline or the pavement beneath which waterworks and/or sewerage pipes have been installed by shield driving method. Such occurrence of cavities is extremely hazardous, as it tends to cause the abrupt collapse of the pavement. For the safety management of road, whether paved or unpaved, recent trend has been indicating the increasing demand for cavity survey.

This paper refers to some examples of surveys actually done by using ground-probing radar.

Paper available at registration? :

Yes

No

AN ABSTRACT SUBMITTED TO  
THE SECOND INTERNATIONAL SYMPOSIUM ON  
GEOTECHNICAL APPLICATIONS OF GROUND PENETRATING RADAR

TITLE: A RAPID EVALUATION OF CONCRETE PAVEMENTS USING GROUND  
PENETRATING RADAR

By

S.S. Kuo, Ph.D., P.E.

Associate Professor of Engineering  
Department of Civil Engineering &  
Environmental Sciences  
University of Central Florida  
Orlando, Florida

ABSTRACT

Periodic evaluation of concrete pavements are required for maintenance and repairs. Voids and deteriorations that exist within and under the pavements must be detected early before the slab fails. The conventional method to investigate the concrete pavements and the underlying subsurface materials is usually of drilling the test holes and examining the core samples. Ground Penetrating Radar (GPR) system can provide a graphic record of subsurface features without disturbing the materials being probed and identify subsurface features by distinguishing media with different dielectric constants and electrical conductivities. These electrical constitutive parameters of the medium can be determined from the reflected pulse.

In order to test the capability of GPR system, a model concrete pavement with 4.5 ft. width by 15 ft. length, and a thickness ranging from 5 to 6 inches, was built at a test site for an experiment. Pipes, rebars, voids, and coarse aggregate base were artificially constructed within and beneath the concrete pavement, respectively, in four sections. The results from this study show that the electromagnetic pulse from GPR can penetrate the concrete pavement components, identify the thickness of the slab, and detect the voids and features such as pipes, rebars, and aggregate base. These identified pavement thickness and subsurface features are valuable factors in the evaluation of pavement strength. In the field test a two-mile section of concrete pavement was studied with GPR antenna being hung behind a vehicle. From the test it was found that GPR system can detect the pavement changes and identify the pavement surface, base, and subgrade interfaces. The result of the study indicates that GPR system would be a feasible tool for nondestructive, quick and economical evaluation of concrete pavements.

## ABSTRACT

### Ground Penetrating Radar Investigations in the Tri-State Mining District, Kansas

by

Raye Lahti and Pieter Hoekstra, PhD  
Blackhawk Geosciences, Inc.  
Golden, Colorado

As part of a Remedial Investigation and Feasibility Study at the Cherokee County Superfund Site, Galena, Kansas, CH2M Hill contracted for a Ground Penetrating Radar (GPR) survey. The objective of the GPR survey was to delineate unexposed mine workings, so that an estimate of the percentage void space under the site could be made.

Firstly, a GPR test survey was undertaken over areas with ground truth. Important purposes of the test survey were to determine

- ° optimum survey parameters, such as monostatic versus bistatic antennae, antennae frequency, and antennae separation
- ° maximum depth of void detectability
- ° influence of geologic noise.

From the test survey it was determined that voids could be detected to a depth of 30 ft to 40 ft. A major reason for this good exploration depth was that over most of the site overburden was shallow and mainly coarse grained.

Secondly, a production survey was run over accessible areas covering approximately 46,525 linear feet. It was found that approximately 8 percent of this linear distance was underlain by void spaces.



## TITLE SUMMARY

Name Ma Buzhou

Affiliation/Title Inst. of Soil & Fertilizer, Hebei Academy of Agri. & Forestry  
Sci., China.

Presentation Title \_\_\_\_\_

### Summary

Using the Subsurface Interface Radar made by Geophysical Survey Systems INC., the author conducted an experiment for sounding Ustalf ( calcic Brown earth ) and ochrept ( fluvisol ) in Hebei Province of China in 1987.

For ustalf soil, SIR can sound the Argillic B Horizon of 40-80 cm deep. As for ochrept soil, It can distinguish the fluvial layers of diferent texture within 1 meter deep. Two kinds of transducers, 120 & 500, were used. Besides, Using SIR to sound the ~~level of~~ groundwater has also achived a desirable result. The level of ground water of 3 meters deep can be sounded clearly.

3 m

Clay layer

Water table

A.

Paper available at registra

Yes

No

DETECTION AND STABILIZATION OF POTENTIAL SINKHOLE SITES AT A  
LANDFILL IN ALACHUA COUNTY, FLORIDA

By William L. Wilson

Research Assistant, Florida Sinkhole Research Institute, University of Central Florida.

Ground penetrating radar was used to locate potential sites of sinkhole development on the floor of a landfill near Gainesville, in Alachua County, Florida. The newly excavated landfill cell was 370 feet wide and 715 feet long. An SIR-3 GPR control unit and 120 megahertz transducer, manufactured by Geophysical Survey Systems, Inc., were used to obtain radar profiles. The area was covered by 73 traverses, from west to east and 9 traverses from north to south. The average spacing between profiles was 5 feet. The radar profiles covered a linear ground distance of approximately 56,250 feet (10.65 miles). Geologic materials at the landfill consisted of 10 to 30 feet of silty sand, 1 to 4 feet of clay, and limestone with a highly irregular top, solutionally modified by paleokarren. Thirty radar anomalies were identified that represented suspect sites where unstable conditions might occur. The anomalies had U- or V-shaped reflections representing subsided soil layers, and narrow, vertical stacks of deeply penetrating reflections that represent sand-filled, vertical solution shafts in the limestone. The shafts ranged from 10 to 27 feet wide and averaged 17 feet wide. Each anomaly was drilled using the standard penetration testing method to determine the type of sediment-fill and strength of the in-filling material. Fourteen of the sites were filled dominantly with medium dense sand and were judged to be stable. The remaining 16 sites were filled with light brown, loose or very loose sand which was thought to be of recent or Pleistocene age. These sites were considered to be potentially unstable. All potentially unstable sites were pressure grouted with concrete to plug the limestone shafts through which unconsolidated sediment could pass to cause sinkhole development. A minimum of 6.1 and a maximum of 90.2 cubic yards of grout were used to plug the shafts. On average, 31.1 cubic yards of grout were used per shaft. The maximum grout pressure used was 600 psi although most pumping was done at pressures of less than 200 psi to avoid heaving the sand on the landfill floor. The initial site investigation with GPR accurately characterized the site conditions and allowed accurate estimation of grout volumes. Subsequent to stabilization of the landfill floor, the cell was lined with clay and geofabrics designed to stretch and fill any sinkhole up to seven feet wide. The liner and a clay cap on the landfill prevent vadose seepage and greatly reduce the possibility of future sinkhole development.

AIRBORNE SUBSURFACE EXPLORATION AND  
DETECTION OF THIN LAYERS USING  
SHORT PULSE RADAR

by

Kevin O'Neill  
Research Civil Engineer

and

Steven Arcone  
Research Geophysicist

USA  
Cold Regions Research and Engineering Laboratory  
Hanover, NH 03755

Airborne radar surveying offers the possibility of exploring large sections of terrain in relatively short times. In recent work we have sought to profile surface ice conditions as well as river and lake bottoms, using short pulse radar. Such systems are suited to the detection of surface and subsurface layering. Given the electromagnetic wave velocity within each layer, one can determine layer thicknesses by timing the separations between echoes.

This approach is limited in part by the finite duration of the radiated pulses. Using some currently available radar systems, we experience overlapping of reflections from upper and lower surfaces of river ice sheets when they are up to about 30 to 50 cm in thickness. A new signal processing system has been developed which utilizes theoretical thin ice reflections, together with straightforward cross-correlation operations. When applied to radar records for a range of thin ice samples, the method has been uniformly successful in determining thickness down to less than 5 cm. Many challenging problems are still provided by such phenomena as rough surfaces, wet surfaces, and the heterogeneous ice-water mixtures which can lead to ice jams. This last item is especially important, because ice jams are a major cause of flooding.



## **SESSION IV**

# **NEW TECHNIQUES, APPLICATIONS, AND EQUIPMENT**





Applications and Limitations of Computer-Processed  
Ground-Penetrating Radar Data

by Gary R. Olhoeft  
U.S. Geological Survey  
P.O.Box 25046 DFC MS964  
Denver, CO 80225

Summary

Most of the time, ground penetrating radar either works well or not at all. Roughly ten percent of the time, ground penetrating radar can only solve a geotechnical problem through computer processing or modeling of the data. Such computer processing may include direct computer manipulation of the data such as background removal, rubber-sheeting to correct for variations in antenna traverse speed, topographic correction, reduction to true geometry and scale, adaptive deconvolution, contrast stretching, migration, statistical scattering determination, and conversion to velocity, attenuation and dispersion. Indirect and direct modeling of the data for ray tracing and inversion, diffraction, multipathing, ringing, interference, and target signature may also be useful. Not all radar data can be improved by processing, but when necessary, there are no alternatives. Examples from ground water, toxic waste, dam safety, and tunnel detection will illustrate the use of computer processing to solve problems with ground penetrating radar.

TITLE SUMMARY

Name Tetsuo Hara, Toshihiko Sakayama, \*Tsutomu Suzuki, \*Ikuo Arai  
 Affiliation/Title OYO Corporation, \*The University of Electro-  
Communications  
 Presentation Title Synthetic Aperture Processing applied to  
Georadar Records

Summary

Georadar is the instrument for the survey of underground structure through emission of electromagnetic pulse wave towards underground and through capture of reflected waves from layer boundary or target.

While this survey method is admitted to be effective for the survey of shallow underground structure, further functional enhancement has been pointed out in respects of expansion of its exploration depth, its capability of determination on specific variety of the target etc.

For the solution of these tasks, the proper software plays an important role, not to mention the hardware. This paper is intended to take up the signal processing related to georadar record, particularly "Synthetic Aperture Processing" applied to pulse radar, thereby clarifying the same serves to enhance horizontal resolution and S/N ratio with georadar record.

In addition, this paper refers to the flow chart of the processing by the software pack developed by us, authors, accompanied by its detailed function along with its processig examples.

Paper available at registration? : 38

Yes

No

TITLE SUMMARY

Name Toshihiko Sakayama, Yukio Kanezaki, Tetsuma Toshioka  
 Affiliation/Title OYO Corporation  
 Presentation Title Development of Georadar System and Basic Experiment

Summary

Pulse radar of surface type is an effective method for the exploration of the shallow underground structure. To further enhance practical effect of georadar as the method for underground exploration, the development of georadar system with following four improvements involved, has been carried out.

- 1) Realization of multi-antenna system to achieve efficiency of measurement job as well as enhancement of exploration performance:
- 2) Improvement of data output speed through achievement of higher speed and higher density with sampling:
- 3) Elimination of interference between antenna and enhancement of quality aptitude with the record:
- 4) Development of antenna suited for the exploration purposes:

Reference is made as follows to the basic characteristics for the developed system and to the results of basic experiments through its utilization.

Paper available at registration? :

Yes

No

REAL TIME KIRCHOFF MIGRATION ON GROUND PENETRATING RADAR DATA

BY

JAMES MacARTHUR\*

Submitted For Presentation  
At

Second International Symposium On  
Geotechnical Applications Of  
Ground Penetrating Radar

March 6-10, 1988

(a paper will be available at the Symposium)

\* Engineer, GEO-CENTERS, INC., Newton Centre, MA 02159



## SUMMARY

### REAL TIME KIRCHOFF MIGRATION ON GROUND PENETRATING RADAR DATA

Migration is a widely used technique for focusing dispersed energy from subsurface reflectors; however, it is extremely computation intensive. The time to process Ground Penetrating Radar (GPR) data using the Kirchhoff migration algorithm on a MicroVAX II is approximately two orders of magnitude greater than the acquisition time. By recasting the algorithm onto a special purpose coprocessor board, it is possible to achieve real time migration, even on a microcomputer. This paper describes the design of the coprocessor, and discusses the steps taken to restructure the migration algorithm in a form suitable for digital signal processing hardware. GPR data migrated by conventional software and simulated coprocessing are compared.



*GEO-CENTERS, INC.*

TIME DOMAIN ANTENNA ARRAYS FOR USE IN  
GROUND PENETRATING RADAR

BY

SHELDON S. SANDLER\*

Submitted For Presentation  
At

Second International Symposium On  
Geotechnical Applications Of  
Ground Penetrating Radar

March 6-10, 1988

(a paper will be available at the Symposium)

\* Technical advisor to the President, GEO-CENTERS, INC., Newton  
Centre, MA 02159 and Professor of Electronics and Computer  
Engineering, Northeastern University, Boston, MA 02115



*GEO-CENTERS, INC.*

## SUMMARY

The purpose of using arrays of sources, arrays of receivers, or both, is two-fold. First, arrays allow the quick acquisition of many signals which can be stacked to enhance the signal-to-noise ratio of a desired pulse and, hence, improve target detection and discrimination. This is especially useful with low energy sources and noise which is incoherent in both space and time. Second, arrays inherently have a directionality associated with them, and they can, therefore, be oriented to transmit and/or receive the maximum signal in a certain direction. This has the obvious advantage of allowing one to focus on a particular object or direction and to reject noise or unwanted signals from other directions.

The major sources of noise and interference come from surface effects and clutter. These affects can be minimized by using directive antenna elements, arrays, and focusing. The focusing concept involves time delay sections between the elements and a summing element preset to focus energy at a given position in or on the earth. Focusing arrays can also be cascaded to cover a one- or two-dimensional slice.

An alternate approach involves the use of electronic scanning. Here, time delays can be sequenced to move the focusing point along prescribed paths in or on the earth. Examples are scans which are along lines or planes parallel to the earth-air interface. Outputs from a set of fixed pre-focused arrays could also be used to give information comparable to that of an electronically scanned system.



*GEO-CENTERS, INC.*

A LARGE AREA, GROUND PENETRATING RADAR SURVEY SYSTEM

BY

ALAN CRANDALL\*

Submitted For Presentation  
At

Second International Symposium On  
Geotechnical Applications Of  
Ground Penetrating Radar

March 6-10, 1988

(a paper will be available at the Symposium)

\* Senior Engineer, GEO-CENTERS, INC., Newton Centre, MA 02159



*GEO-CENTERS, INC.*

## SUMMARY

### A LARGE AREA, GROUND PENETRATING RADAR SURVEY SYSTEM

Searching large areas with existing Ground Penetrating Radar (GPR) systems is both time and labor intensive. This paper describes the design concept of a towed GPR system being developed to survey up to 30 acres per day with the aid of a radio navigation system. A short, metal trailer with an array of 4 (low frequency) or 8 (high frequency) terrain following GPR antennas is used to obtain 3 meter coverage. A 4 wheel drive tow vehicle houses a single radar controller and operator control and display unit. A precise microwave navigation system is used to automate systematic surveys and provide information for mapping detected targets. An integrating data acquisition system, including a 400 Mbyte optical disk drive, is used to record high volume field data for subsequent processing and analysis. Criteria for antenna frequency selection, radar control and processing techniques, data integration and storage capability are discussed.



*GEO-CENTERS, INC.*



MIGRATION OF GROUND PENETRATING RADAR DATA:  
A TECHNIQUE FOR LOCATING SUBSURFACE TARGETS

BY

GREGORY HOGAN\*

Submitted For Presentation  
At

Second International Symposium On  
Geotechnical Applications Of  
Ground Penetrating Radar

March 6-10, 1988

(a paper will be available at the Symposium)

\* Senior Scientist, GEO-CENTERS, INC., Newton Centre, MA 02159



*GEO-CENTERS, INC.*

## SUMMARY

### MIGRATION OF GROUND PENETRATING RADAR DATA: A TECHNIQUE FOR LOCATING SUBSURFACE TARGETS

Migration is a method of processing radar data which focuses dispersed energy at the apex of the characteristic hyperbolic return. Not only does this correctly position subsurface reflectors, but also increases signal-to-noise ratio, greatly enhancing target detection and location. While this technique is employed extensively in the oil industry to process seismic information, little attention has been directed towards ground penetrating radar (GPR) applications. This paper presents the theory of Kirchhoff migration as applied to electromagnetic wave propagation in the earth. Factors affecting the migration process such as medium velocity, dielectric discontinuities, and geologic inhomogeneities are considered. Examples of migrated GPR data with subsurface targets are presented and discussed.



*GEO-CENTERS, INC.*

VARIABILITY OF RADAR VELOCITY IN A PLIO-PLEISTOCENE DUNE SAND,  
POLK COUNTY, FLORIDA

by William L. Wilson

Research Assistant in Geology, Florida Sinkhole Research Institute, University  
of Central Florida, Orlando, Florida 32816

An SIR-3 ground penetrating radar unit and a 120 megahertz transducer were used to investigate the variability of radar velocity in a Plio-Pleistocene dune sand. The study area was located on the east side of Lake Leonore (Lake Patrick), along the eastern margin of the Lake Wales Ridge, in southeastern Polk County, Florida. The sand in the area was thought to be relatively clean and homogeneous. The major soil unit developed in the area was the Astatula Sand. Radar profiles of the water table were obtained along 12.8 miles of transect. The depth to the water table was precisely known at seven monitoring wells located along the profiles. The depth ranged from 7.9 to 28.6 feet. Radar velocities were calculated for the unsaturated sand at the monitoring wells. The radar velocity, based on two-way travel time, ranged from 0.24 to 0.31 ft/nsec. The mean velocity was 0.27 ft/nsec and the standard deviation was 0.026 ft/nsec, which amounts to 9.6 percent of the mean. Radar velocity was observed to decrease with increasing two-way travel time. A linear regression of the data yielded the equation  $y = 0.323 - 0.000809x$  where  $y$  is the velocity in ft/nsec and  $x$  is the two-way travel time in nsec. The coefficient of correlation ( $r^2$ ) equals 0.904 for the regression. The equation probably should not be extrapolated beyond the observed points. The variability of the radar velocity has important implications for the precision of quantitative information derived from the radar profiles. Quantitative radar investigations should be based on a statistically significant number of radar velocity tests, and the standard estimate of error should always be specified.

INTERPRETATION OF GROUND PROBING RADAR: MIGRATION  
TECHNIQUES. D. DeBock, Bles, Inc., Belgium.





NATIONAL AGRICULTURAL LIBRARY



1022255216

\* NATIONAL AGRICULTURAL LIBRARY



1022255216